# *The Synthesis of Branched, Vinyl Functional Polyacids via CCTP & Their Application to Dual-Cure Dental Materials*

*A thesis submitted in partial fulfilment of the requirements for the degree of*

*Doctor of Philosophy in Chemistry*

*Department of Chemistry*

*University of Warwick*

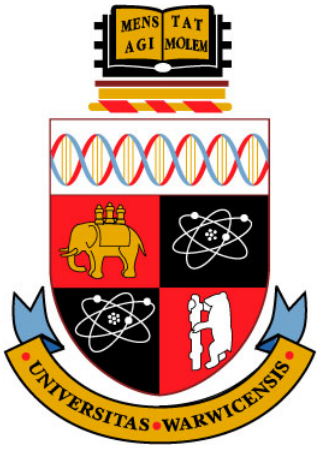


*September 2014*

**LIST OF FIGURES**

**LIST OF TABLES**

## *Abbreviations*

| | |
|---|---|
| \|η*\| | Complex viscosity |
| (+)-TA | (+)-tartaric acid |
| AA | Acrylic acid |
| AIBN | 2,2'-azobis(isobutyrylnitrile) |
| AMU | Atomic mass unit |
| ATR | Attenuated total reflectance |
| ATRP | Atom transfer radical polymerization |
| BI | Bromine Index |
| BPO | Benzyl peroxide |
| CCT | Catalytic chain transfer |
| CCTA | Catalytic chain transfer agent |
| CCTP | Catalytic chain transfer polymerization |
| CoBF | Co(II) dimethylglyoxime-difluoroboryl |
| Co(III)-H | Co(III) hydride |
| CQ | Camphorquinone |
| CRP | Controlled radical polymerization |
| $C_s$ | Chain transfer constant |
| CS | Compressive strength |
| *Đ* | Dispersity |
| DDMA | Dodecyl methacrylate |

| | |
|---|---|
| DDT | Dodecanethiol |
| DMSO | Dimethyl sulfoxide |
| DP | Degree of polymerization |
| DPIC | Diphenyl iodinium chloride |
| DRI | Differential refractive index |
| DSC | Differential scanning calorimetry |
| DVB | Divinyl benzene |
| EGDMA | Ethylene glycol dimethacrylate |
| ESI—MS | Electrospray ionization mass spectroscopy |
| FAS | Fluoroaluminosilicate (glass) |
| FTIR | Fourier transform infrared spectroscopy |
| FRP | Free radical polymerization |
| GC-FID | Gas chromatography, flame ionization detection |
| G’ | Storage modulus |
| G’’ | Loss modulus |
| GIC | Glass ionomer cement |
| GMA | Glycidyl methacrylate |
| GPC | Gel permeation chromatography |
| HEMA | Hydroyethyl methacrylate |
| IEM | 2-isocyanatoethyl methacrylate |
| IV | Intrinsic viscosity |

| | |
|---|---|
| LCST | Lower critical solution temperature |
| log M | log molecular weight |
| MALDI-ToF | Matrix assisted laser desorption ionisaton – time of flight |
| MALS | Multi angle light scattering |
| MAA | Methacrylic acid |
| $Me_6$Tren | Tris[2-(dimethylamino)ethyl]amine |
| MMA | Methyl methacrylate |
| $M_n$ | Number average molecular weight |
| $M_p$ | peak molecular weight |
| $M_w$ | weight average molecular weight |
| MW | Molecular weight |
| MWD | Molecular weight distribution |
| NMP | Nitroxide mediated polymerization |
| NMR | Nuclear magnetic resonance (spectroscopy) |
| PEG | Poly(ethylene glycol) |
| PEGDMA | Poly(ethylene glycol) dimethacrylate |
| PEO | Poly(ethylene oxide) |
| PMMA | Poly(methyl methacrylate) |
| ppm | Parts per million |
| PS | Polystyrene |
| RAFT | Reversible addition fragmentation chain transfer (polymerization) |

| | |
|---|---|
| RI | Refractive index |
| RMGIC | Resin modifed glass ionomer cement |
| SD | Standard deviation |
| SEC | Size exclusion chromatograhy |
| SCVP | Self condensing vinyl polymerization |
| TEGDMA | Tri(ethylene glycol) dimethacrylate |
| *t*-BA | *Tertiary*-butyl acrylate |
| $T_g$ | Glass transition temperature |
| TFP | 2,3-Tetrafluoropropan-1-ol |
| THF | Tetrahydrofuran |
| TMA | *N,N,N',N'*-tetramethyl aniline |
| TMPTMA | Trimethylopropane trimethylacrylate |
| TMS | trimethyl silane |
| UV | Ultraviolet |
| VA-044 | 2,2'-Azobis[2-(2-imidazolin-2-yl)propane]dihydrochloride |
| $V_h$ | Hydrodynamic volume |
| VISC | Viscometry detector |
| $V_R$ | Retention volume |

## *Acknowledgments*

Firstly, my thanks must go to Dave for the opportunity to work in this research group – it has been one of the best decisions of my life. Thanks for the guidance and support, the generosity, the conference trips and sending me to Melbourne for 3 months! Dave has been a great boss, and his "just do it" attitude and enthusiasm for my "free radical with magic dust" project was ~~always~~ usually appreciated. If I'm ever asked about working in the Haddleton Group, I will have nothing but the strongest recommendation to offer.

I need to thank everyone from the Haddleton group and further afield who helped me out, answered a (probably stupid) question or contributed to anything I've worked on. The "old" Haddleton crew who helped me out when I joined the group and became some of my best friends are amazing: Mat, Stacy, Ant, George, Kay (Team CCTP!!), James and Jay. I'll never forget the gigs/festivals/sport/food/drinks and look forward to visiting you all where ever you are now! Thanks as well to the newer guys, Jenny, Jenny, Claudia, Chris, Vasiliki and Athina.

Thanks to the post-docs for all their contributions, Ronan, Flo, Gabit and Olivier, but especially Paul for being the go-to guy for just about everyone, including me, even when it's not your job (at least I didn't make you read this, mate). Special thanks go to Tara and Wayne at Monash. I'm so grateful that you and Dave made that trip happen, I learned so much and could never have taken this project so far without you guys! Thanks also to Nancy for the support, perspective and direction.

Outside of the lab (but not outside of chemistry) I have to thank my housemates Holly, Ed, Dave and Alex. Thanks for the risotto, lifts, listening to me moan; and for the music recommendations, drinks and trips around the country to gigs; and for a French perspective on rugby, beer, wine, AA and MAA. Thanks as well to the sporting guys: to UWRFC for making the first year of my PhD so difficult, and to the Chemistry cricket team, who made the last year of my PhD so bearable (champions 2014!).

Lastly, I should thank my family. Mum and Dad: you've supported me through everything I've done, and giving me both the opportunity to achieve something and the sense of ambition to know I should take it. To Hannah and Daniel: for being there when life is fun and being at the other end of the phone when it isn't, thanks for everything.

## *Declaration*

Experimental work contained in this thesis is original research carried out by the author, in the Department of Chemistry at the University of Warwick between October 2010 and August 2014, and at the Department of Materials Engineering at Monash University between January and March 2013.

Results from other authors are referenced throughout in the usual manner.

**Date:**

**Jamie Godfrey**

## *Abstract*

This thesis details the synthesis of non-linear, acid functional polymers and their application to photo-curable polymer-inorganic dental composites. Many polyacids containing photo-polymerizable groups used in current materials require multi-step synthesis and purification, due to the toxic solvents and reagents used. This work describes the synthesis of non-linear polyacids containing vinyl functionality that can be synthesized in a one step process, using non-toxic, aqueous media, as well as their subsequent testing in glass ionomer cements.

Initial work in Chapter 2 set out to investigate the feasibility of synthesizing low molecular weight linear poly(methacrylic acid) (PMAA) *via* Catalytic Chain Transfer Polymerization (CCTP). The process was found to proceed efficiently, with good control over the molecular weight achieved by varying concentration of the chain transfer agent (CTA). Work then moved toward the incorporation of the less CCT-active acidic monomer, acrylic acid. It was found that the monomer reactivity ratios for the CCT copolymerization led to substantial compositional drift during the reaction and the formation of high molecular weight species. Additionally, multi-detector size exclusion chromatography (SEC) analysis revealed the formation of non-linear polymer architectures, likely due to the CCT-derived vinyl group participating in propagation leading to an extent of grafting.

The copolymerization of MAA with the difunctional monomer ethylene glycol dimethacrylate (EGDMA) was then investigated in two aqueous solvent systems. It was found that conducting the copolymerization in water led to a biphasic system at the outset of polymerization. This solvent system yielded a branched polymer of higher molecular weight and dispersity than analogous products synthesized in homogeneous solutions in water/IPA. The presence of a high level of vinyl functionality was confirmed using a bromination-titration methodology and the branched architecture revealed by multi-detector SEC.

In Chapter 3, the linear and branched polyacids synthesized were then applied to dual-cure glass ionomer cements (GICs), a class of polymer-inorganic composite materials. A model photo-polymerizable GIC system was established *via* optimization of a three component, camphorquinone based photo-initiating system and investigation of the effect of additives and polymer concentration on the curing of the cement. This model system was used to investigate the influence of the polymer component on the final cement, with polymers of higher molecular weight generally leading to cements with greater compressive strengths. The

resulting materials were characterized using a range of online monitoring techniques, including photo-DSC, photo-rheology and *in situ* FTIR, and the final cements' compressive strength tested.

Several methacrylate-modified PAAs were also synthesized in order to investigate the effect of photo-polymerizable functionality, and their properties compared to those of the linear and branched PMAA-based materials. It was found that the acrylic polymers led to cements with substantially higher compressive strengths than both the linear and branched methacrylic systems. However, the methacrylate-modified PAAs were found to give compressive strengths of similar magnitude to commercial materials, verifying that the relatively simple materials developed were an appropriate model system for this investigation.

# 1 Introduction; the synthesis of branched polymers via radical approaches and the use of polyacids in dental glass ionomer restoratives.

As work in this thesis describes the synthesis of branched polyacids and their application to photo-curable dental composites, areas related to synthetic polymer chemistry and dental materials must be discussed.

Free radical polymerization will be introduced, with particular emphasis on chain transfer reactions and the synthesis of non-linear architectures. As the polymerization method of choice for this work, Catalytic Chain Transfer Polymerization (CCTP) will be discussed, with its mechanism and the evolution of its catalysts given treatment, as well as its use in both academic and industrial fields. The previous reports of its application to the synthesis of branched and highly branched polymers will be reviewed, and the motivation for using CCTP in this work explained.

In order to provide context for the synthetic route chosen for this work, and to discuss some of the merits and disadvantages of the many polymerization techniques that have found use synthesizing branched structures, controlled radical polymerization (CRP) will be discussed briefly. The routes that have been reported to give access to branched and highly-branched structures will again be emphasized, and the techniques evaluated with respect to their suitability for undertaking similar work to that described in this thesis.

The discussion will then turn to the field of polymer-containing dental materials, as the polymers synthesized will be applied in this area. The evolution of dental glass ionomer restoratives since their invention in the 1970s will be discussed, and some of the advantages and drawbacks of these materials highlighted. Dual-cure glass ionomer systems containing polymerizable functionality will be introduced, along with common strategies used in these materials.

## *1.1 Free Radical Polymerization*

Many of the commercial polymers encountered in everyday life are produced by free radical polymerization (FRP). FRP polymers' ubiquity stems from the relative ease of their synthesis compared to other polymerization techniques, such as "living" ionic polymerization and *pseudo-living* CRP strategies. The robust nature of FRP, being tolerant of trace impurities and proceeding at a high rate, make it extremely attractive industrially, but high rates of reaction with no deactivation of the reactive, non-selective radical species will usually lead to poor control of polymer architecture and dispersity.[1-3]

FRP can be thought of as a chain reaction, and requires the introduction of a radical which can react with a monomer unit in an initiation process. In the majority of polymerizations radical species are generated by the decomposition of a small-molecule. This is followed by propagation, where the radicals produced will go on to react with a number of monomer units by opening of the π-bond to form a new radical, which will form long polymer chains with the same repeat unit (in the case of homopolymerization). Finally, the polymer chain stops growing when the radical is quenched by a chain terminating process.

Common types of initiators are azo and peroxide compounds, such as 2,2′-azobis(2-methylpropionitrile) (AIBN) or benzyl peroxide (BPO), which decompose to give two radicals upon heating. Several external stimuli can also be used to initiate polymerization, including heat, irradiation with light of a certain wavelength or by redox reactions, depending on the chemistry employed. However generated, these radicals will add to a monomer unit in the first polymerization step, yielding a radical capable of undergoing propagation (Figure 1.1).

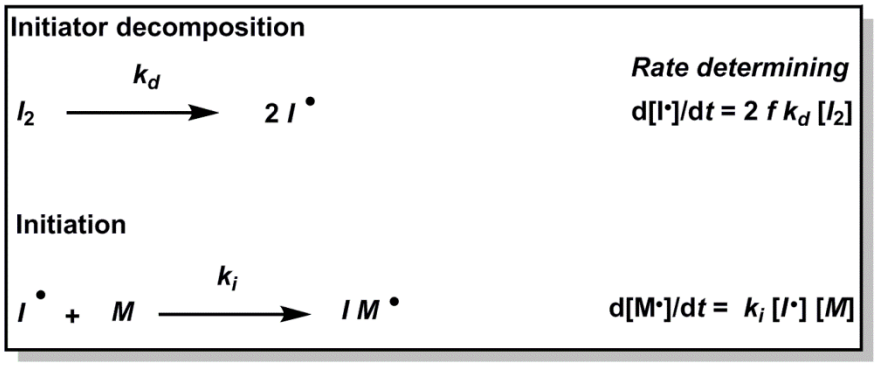


**Figure 1.1: Initiation reactions and rate equations for FRP, where $I_2$ is the initiator, $I$ is the initiator fragment, $M$ is the monomer, $k_d$ and $k_i$ are the rate constants of initiator decomposition and initiation, respectively and $f$ is the initiator efficiency.**

The radical will now propagate by the sequential addition of monomer units to the polymer chain end until either there is no more monomer or the chain is terminated by a competing side reaction. The rate of propagation will largely depend on concentration of radicals, monomer and the rate constant for propagation, $k_p$, which will depend on the monomer used.

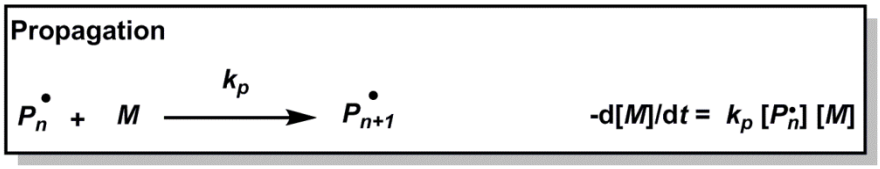


**Figure 1.2: Propagation reaction and it's rate equation for FRP. Where $P_n$ is a polymer chain consisting of $n$ monomer units and $k_p$ is the rate constant of propagation.**

Whilst propagation will not change the concentration of radicals, simply converting one radical to another, termination steps will occur throughout the polymerization, leading to "dead", permanently deactivated polymer chains and a decrease in the radical concentration unless more radicals are produced by initiator decomposition. In many treatments a steady state of radical concentration is assumed, where the rate of formation of radicals equals the rate of removal of radicals *via* termination events. Permanent deactivation of polymer chains can occur by three major routes; combination, disproportionation and chain transfer (Figure 1.3), but the prevalence of each process will depend on the monomer and solvents used, as well as the reaction temperature.

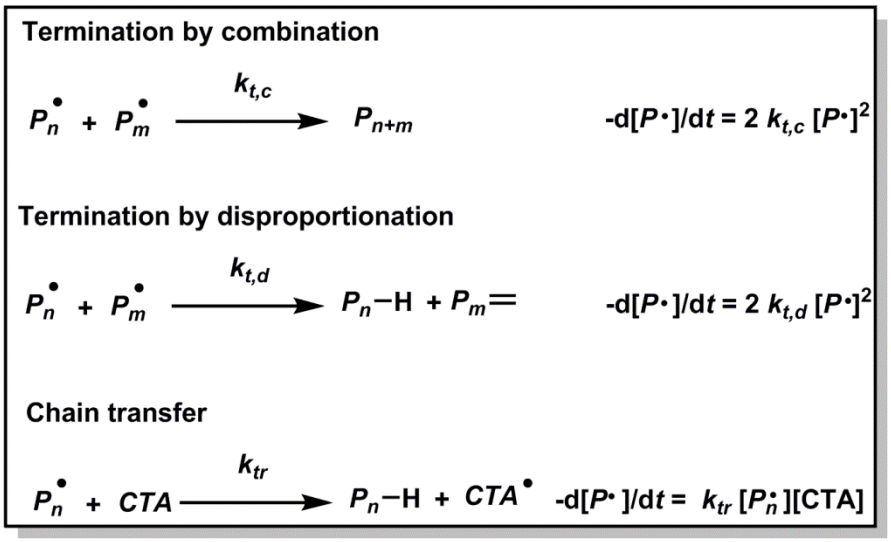


**Figure 1.3: Termination reactions and their rate equations for FRP. Where $P_m$ is a polymer chain consisting of *m* monomer units, $P_{n+m}$ is a terminated polymer chain of *n* + *m* monomer units, $P_n$-H is a polymer chain of *n* units terminated by H, $P_m$= is a polymer chain of *m* units terminated by a double bond, *CTA* is a chain transfer agent (whether monomer, solvent, polymer or an added species), and $k_{t,c}$, $k_{t,d}$ and $k_{tr}$ are the rate constants of termination by combination, termination by disproportionation and chain transfer, respectively.**

Combination is the direct coupling of two radicals, and will lead to a terminated polymer chain with the combined molecular weight (MW) of the two terminated radicals, and thus will often generate species of higher than average MW for the system. Termination by disproportionation is the transfer of a hydrogen atom from one polymeric radical to another, giving terminal unsaturation at the chain-end of one polymer and a terminal hydrogen on the other. Rate constants for termination are usually several orders of magnitude higher than those for propagation, but this does not prevent polymerization as the radical species are at a very low concentration compared to monomer. Following the same reasoning, termination is expected to become more dominant at high conversions when monomer concentration is greatly reduced.

### *1.1.1 Conventional chain transfer in FRP*

Chain transfer is the transfer of an atom (usually hydrogen) from a chain-transfer agent (CTA) to a polymer radical, terminating the polymer chain and producing a radical from the CTA fragment. The CTA can be monomer, solvent, polymer or a species deliberately added to the reaction in order to affect chain transfer. Chain transfer will reduce the overall degree of polymerization ($DP_n$) of a chain growth system, since it will prematurely terminate the polymer

chain before the kinetic chain length has been reached. Chain transfer will usually have no effect on the rate of the polymerization, although specific cases in which the relative rates of propagation, chain transfer and reinitiation lead to a decreased rate of polymerization do exist (Table 1.1).[2]

| $k_p : k_{tr}$ | $k_a : k_p$ | Resulting chain transfer | Effect on $R_p$ | Effect on $DP_n$ |
|---|---|---|---|---|
| $k_p >> k_{tr}$ | $k_a \approx k_p$ | Normal chain transfer | None | Decrease |
| $k_p << k_{tr}$ | $k_a \approx k_p$ | Telomerization | None | Large decrease |
| $k_p >> k_{tr}$ | $k_a < k_p$ | Retardation | Decrease | Decrease |
| $k_p << k_{tr}$ | $k_a > k_p$ | Degradative chain transfer | Large decrease | Large decrease |

**Table 1.1: Outcomes of various $k_p : k_{tr}$ and $k_a : k_p$ ratios in free radical polymerization, where $k_a$ is the rate contant for reinitiation of polymerization from the CTA fragment. Adapted from reference.[2]**

Whilst chain transfer is often a competing side-reaction, it can also be exploited to provide further control of the average $DP_n$, reducing the cost of producing lower MW products (as large amounts of initiator are not required). The most common CTAs used in radical polymerization are thiols (which have amongst the highest chain transfer constant, $C_s$, of conventional CTAs – usually between 1-10 for stabilised monomers), as the hydrogen is readily transferred to the propagating chain.[2-3] This will yield a hydrogen terminated polymer chain as well as a thiyl radical capable of reinitiating polymerization. Therefore, the thiol is often incorporated into the polymer product, which can be used to introduce new functionality but is not always desirable. Stoichiometric levels of thiol have been used to delay gelation in the free radical copolymerization of vinyl monomers with relatively low levels of divinyl monomers, in what is commonly referred to as the "*Strathclyde route*".[4-8] The application of thiol-CTAs to branched structures will be discussed in greater detail in section 1.4.3, below.

## 1.2 Catalytic chain transfer polymerization (CCTP)

### 1.2.1 Introduction & history

Catalytic chain transfer polymerization utilizes the extremely high efficiency of cobalt(II) macrocycles as catalytic chain transfer (CCT) agents in free radical polymerization, and is a convenient method for the synthesis of low molecular weight polymers.[9-12] The technique also provides an uncommonly high (for FRP) level of vinyl end-functionality (which would also result from termination by disproportionation).[13-14] Due to its high chain transfer constant, the Co(II) complex is usually only required in ppm concentrations, which has led to a strong history of industrial use of CCTP.

#### *Discovery and filing of initial patents*

CCTP was developed in Russia in the mid-1970s by Smirnov, Marchenko and Enikolopyan, with later work by Gridnev, while investigating the effect of transition metal porphyrin complexes on FRP. The observation that Co(II) porphyrins appeared to inhibit FRP of methyl methacrylate (MMA) stimulated further investigation, leading to a series of papers and patents in the Russian literature in the late 1970s[12, 15-18] which went largely unnoticed by the general community.

However, apparently as a result of Enikolopyan's visit to DuPont in 1979, interest in CCTP made the jump to the American chemical industry, leading to the filing of early patents by the Glidden paint company (on the parent cobaloxime, note that Glidden was a subsidiary of DuPont at the time)[19-21] and DuPont (covering $BF_2$-bridged cobaloximes with alkyl and phenyl substituents)[22-23]. These initial patents, along with those filed by ICI/Zeneca covering aryl-substituted cobaloximes[24-26], led to industrial exploitation, although dormancy of research in the open academic literature persisted for many years, despite the range of industrial applications developed. However, CCTP experienced something of a resurgence in the academic press in the mid-1990s, and has received modest attention from academic researchers since.

#### *General considerations*

CCTP is an attractive method for the synthesis of low molecular weight polymers since it combines the versatility and robustness of FRP with the molecular weight control and vinyl

functionality imparted by CCT (Figure 1.4), allowing further applications of the products as macro-monomers. It has also been shown that such α-substituted macro-monomers can be made to undergo β-scission, allowing their own use as addition-fragmentation chain transfer agents. This process has been exploited to synthesize telechelics, block copolymers and further macro-monomers, demonstrating further versatility of this chemistry.[22, 27] Industrial use, particularly, has focussed on using macro-monomers and oligomers in functional coatings applications, such as high solids coatings, radiation curable systems and powder coatings.[28] This has been driven by both the efficiency of macro-monomer synthesis and increased demand to remove volatile organic compounds from formulations. Macro-monomers have also found considerable use in the synthesis of graft copolymers, and these systems have been extensively patented.[19, 21, 23-26, 29-30] While the majority of reports have applied CCTP to bulk or solution processes, several examples in patent and academic literature have reported CCTP under emulsion and suspension polymerization conditions.[26-27, 31-37]

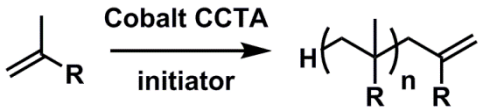


**Figure 1.4: General scheme for the CCTP of a monomer possessing an α-methyl group, leading to the formation of a vinyl terminated polymer chain.**

Generally, efficient CCTP is limited to methacrylates and styrene (although the latter proceeds with a much reduced chain transfer constant[10-11]). Other monomers, such as acrylates, have been studied, but these systems are often complicated by catalyst poisoning by formation of secondary alkyl-Co(III) compounds as well as formation of non-linear structures.[38-39] For this reason, successful CCTP processes will usually have methacrylates (or other α-methyl monomers) as the major part of a copolymerization mixture.

### *1.2.2 Mechanism*

Catalytic chain transfer has been proven to be truly catalytic, as the regenerated cobalt porphyrin has been isolated following polymerization[12, 15-17]. However, while it is clear than re-initiation provides a new propagating chain initiated by H, the mechanism for H transfer is less clear. Three distinct mechanisms have been proposed and are summarized in Figure 1.5, with mechanism (3), involving re-initiation mediated by a Co(III) hydride, the most widely accepted:

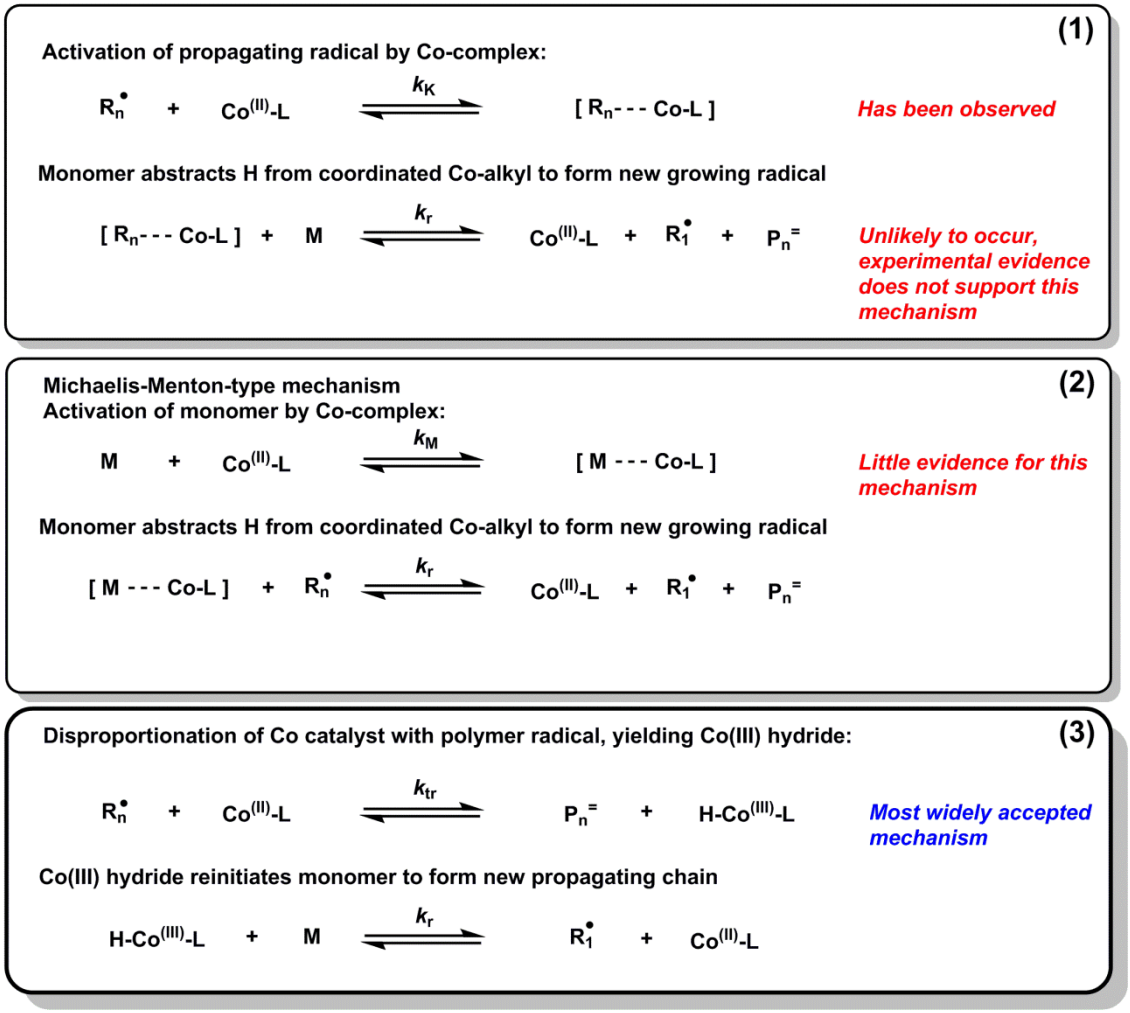


**Figure 1.5: Proposed mechanisms for catalytic chain transfer polymerization. Where $R_n$ and $R_1$ are the polymeric and monomeric radicals, M is the monomer, Co(II)-L is the cobalt chelate CCTA and $P_n^{=}$ is a polymer with an unsaturated chain end. Adapted from reference.[28]**

There is evidence that mechanism (1) is improbable, as it has been demonstrated that the monomer does not directly participate in the hydrogen abstraction step, suggesting the methacrylate does not abstract a H atom.[28, 40] Mechanism (2) suggests that the rate of CCT is dependent on monomer concentration, which has also been disproved.[41] In the case of mechanism (3), the highly reactive H-Co(III)L has yet to be observed, but Smirnov and co-workers have carried out kinetic studies proving the formation of a cobalt hydride. This, along with further evidence provided by O'Driscoll, Gridnev and other researchers has led to general agreement.[9-11, 40, 42-46]

Thus, the Co(II) macrocycle is considered to terminate growing polymer chains by H atom abstraction. CCT differs from conventional chain transfer in that the CTA is recycled and the Co(III)-H complex is capable of reinitiating polymerization. Much like conventional chain transfer, the overall effect is to dramatically reduce the molecular weight of the product without affecting the kinetic chain length or rate of polymerization. The accepted mechanism can be shown as a catalytic cycle[28] (Figure 1.6 – note that complexation reactions of the catalyst with the monomer and polymer are reversible, but are not drawn as equilibria for clarity), but it should be noted that several anomalies have yet to be explained, and as such the mechanism is still not fully understood.

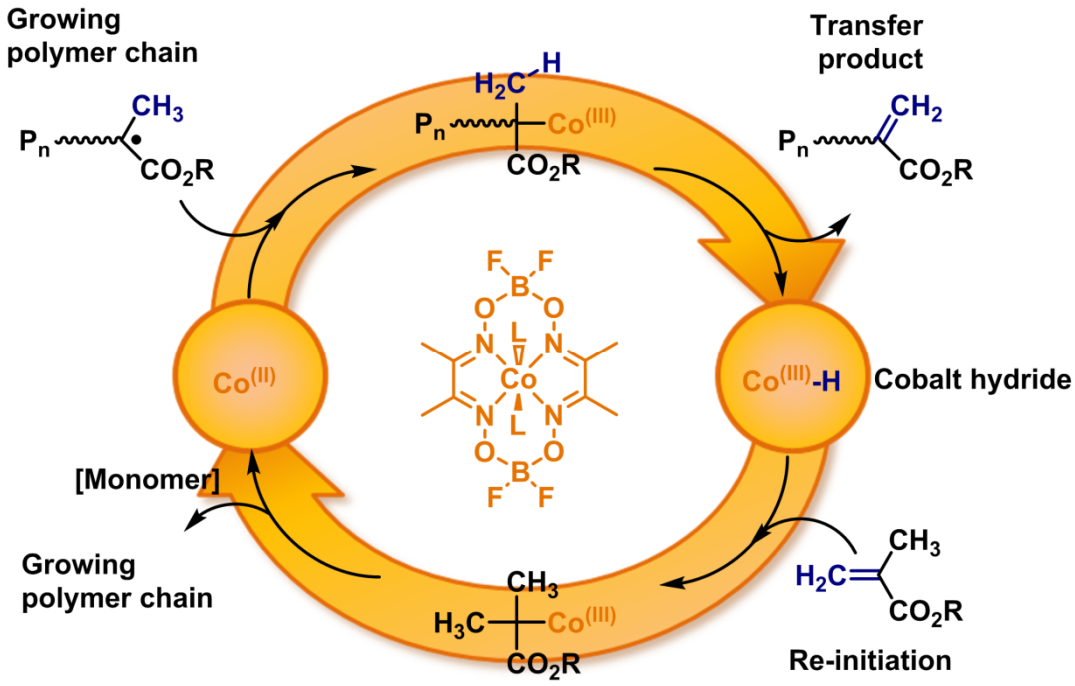


**Figure 1.6: Generally accepted catalytic cycle mechanism for CCTP of methacrylates, where general ligand L can be methanol, pyridine, Cl or a phosphine.**

This lack of certainty is partly due to inherent difficulties in finding analytical methods capable of elucidating the active species during polymerization: the catalyst is paramagnetic - and contains few signals that could be followed by $^{1}$H-NMR anyway – preventing NMR analysis of the complex. However, the possible polymer end groups (which will be identical to those produced in chain transfer and bimolecular termination in FRP) have been investigated by

DuPont, using $^{1}$H- and $^{13}$C-NMR to measure the amount of vinylidene groups per polymer chain[47]. The authors conclude that > 82 % of polymer chains possess vinyl functionality, although numbers of groups terminated by disproportionation or combination are not discussed (this value is similar to the percentage expected for termination by disproportionation for methacrylates[2]). Matrix assisted laser desorption time-of-flight mass spectrometry (MALDI-ToF-MS) has allowed mass spectra of PMMAs of over 15,000 AMUs to be recorded with high resolution, and work by Haddleton *et al.* has found that more than 95 % of polymer chains detected by MALDI-TOF analysis were terminated with vinyl functionality.[13-14]

As with all free radical processes, radicals will be consumed throughout the polymerization by conventional radical coupling reactions, and so a continual supply of radicals is necessary for a successful polymerization. Typically, reactions are carried out in the presence of thermally degradable azo initiators at timescales where a roughly constant radical flux is maintained. However, CCTP is somewhat limited in terms of possible initiators in comparison to FRP, since peroxide or persulfate initiators cannot be used. These oxygen centred radicals have been shown to poison the catalyst, preventing CCT.[48]

### *1.2.3 Catalysts*

#### *Active catalytsts*

Active CCTP catalysts are all low-spin cobalt(II) complexes with octahedral geometry, with a macrocyclic ligand occupying a square planar geometry, leaving two axial coordination sites.[49] Since $d^7$ Co(II) can exist as either low- or high-spin (i.e. one or three unpaired electrons - Figure 1.7), choosing the correct ligand to give a low-spin complex becomes an important facet of catalyst design for a catalytic chain transfer agent (CCTA). However, little empirical reasoning has been found for whether a certain macrocycle with nitrogen or oxygen atoms bonding will give high- or low-spin complexes.

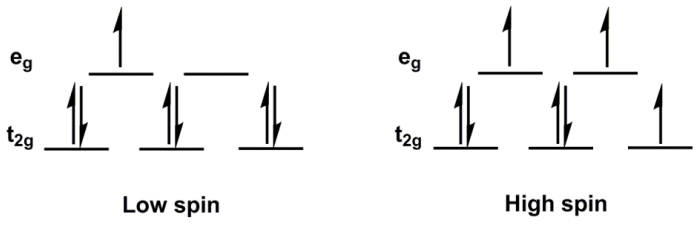


**Figure 1.7: d-electron configurations of d7 Co(II) in low spin (left) and high spin (right) configurations.**

## *Evolution of catalysts*

Early CCTP catalysts were cobalt(II) porphyrin complexes, such as Co(II) hematoporphyrin ether (**1**, Figure 1.8). While these complexes showed relatively high activity ($C_s$ = 2.4 x $10^3$)[50], they were difficult to isolate and therefore too expensive to be considered for industrial applications. This, their high colour and their poor solubility, led to the need for alternative catalysts to be developed.

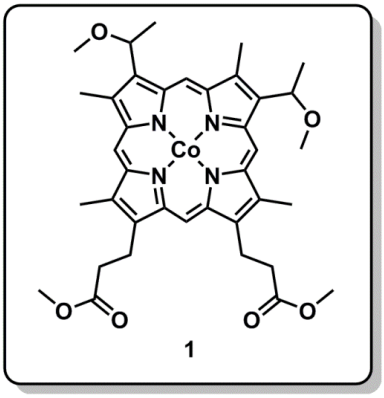


**Figure 1.8: Co(II) hematoporphyrin IX tetramethyl ether, an early first generation CCTA.**

The second generation of Co(II) catalysts were cobaloximes (**2**, Figure 1.9). These show greater activity than their porphyrin analogues ($C_s$ values up to 2 x $10^4$) and are less expensive. Additionally, their solubility and stability can be tuned through variation of axial and equatorial groups, increasing the activity and versatility of the catalysts[11, 36, 43, 51]. However, a significant drawback of cobaloxime catalysts was their susceptibility to hydrolysis and oxidation, leading to the development of a third generation of cobaloximes. These catalysts add a $BF_2$ bridging group between the axial oxygens, which significantly stabilizes the complex in oxygenated and aqueous solution – in particular at low pH – while maintaining high activity ($C_s$ = 4 x $10^4$).[11, 51] These catalysts, which are by far the most widely used presently, are given the general name CoBF, used to describe complexes of general structure **3**.

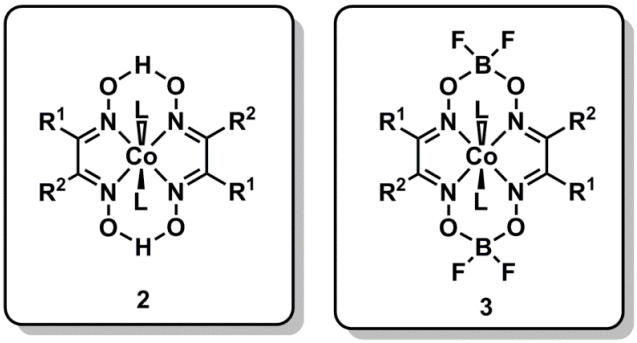


**Figure 1.9: Second and third generation cobaloxime complexes used in CCTP.**

## *Measuring catalyst activity*

Catalyst activity for a specific system (i.e. catalyst, monomer, solvent etc.) is given by the chain transfer constant, $C_s$, which is defined as the ratio of the rate constant for chain transfer to the rate constant for propagation ($k_{tr}/k_p$). Given the relatively few available methods of characterization for these complexes, measurement of $C_s$ is often used as an indicator of catalyst purity by comparison to values for known systems (commonly homopolymerizations of MMA, which give $C_s$ values up to 4 x $10^4$ for CoBF).[52] Conventional CTAs, such as thiols, will usually give $C_s$ values of 1-10 for methacrylates,[2-3] whereas the $C_s$ values for CCTAs for analogous methacrylic systems will often be four orders of magnitude higher. Hence it is clear that dramatically lower concentrations of CCTA are required to give a similar reduction in MW to a conventional CTA. This is a major advantage of CCTP, with the very small quantities required negating the relatively high cost of the catalyst.

$C_s$ values can be measured using the Mayo equation (often referred to as the Mayo method), as described in Equation 1.1: a series of polymerizations are conducted with differing ratio of CTA to monomer and stopped at low conversion (generally < 5 %), so as to avoid changes in monomer concentration and to minimise termination. From this a linear Mayo plot of $1/DP_n$ vs. [S]/[M] can be constructed, with a slope equal to $C_s$ for that polymerization system, whereas $DP_{n0}$ will be given by the intercept.[2]

$$\frac{1}{DP_n} = \frac{1}{DP_{n0}} + C_s \frac{[S]}{[M]}$$

**Equation 1.1: General form of the Mayo equation, where $DP_n$ is the number average degree of polymerization in the presence of the CTA, $DP_{n0}$ is the number average degree of polymerization in the absence of CTA, and [S] and [M] are the concentrations of CTA and monomer, respectively.**

The number average DP can be calculated either from $M_n^{SEC}$, or by division of $M_w^{SEC}$ by two times the monomer mass. Strictly, use of $M_w$ should only be considered for systems dominated by chain transfer, in which the theoretical dispersity will be approximately equal to 2. However, this method has been reported to give greater accuracy that measurements based on $M_n$, due to the weight average's lower susceptibility to baseline deviations in SEC.[53-55]

### *1.2.4 Monomers*

Monomers that have excellent activity in CCTP will invariably have an α-methyl group, and therefore contain a H-atom that is easily abstracted by the CCTA complex. This results in a labile Co(III)-C bond and allows facile formation of a Co(III)-H complex and a vinyl terminated polymer chain.[56] For this reason, methacrylates and other monomers with tertiary propagating radicals, are extensively used in CCTP and provide high chain transfer efficiency. In the case of monomers that lack an α-methyl group and have secondary propagating radicals, such as acrylates, there is no easily abstractable H-atom. This results in the formation of a relatively stable Co(III)-C bond and has the effect of temporarily removing the catalyst from the cycle, reducing the chain transfer constant.[16, 57] This is summarised in Figure 1.10, showing the expected results for active and non-active CCTP monomers. It should be noted that styrene is something of an exception, having moderate activity despite the absence of an abstractable H-atom.

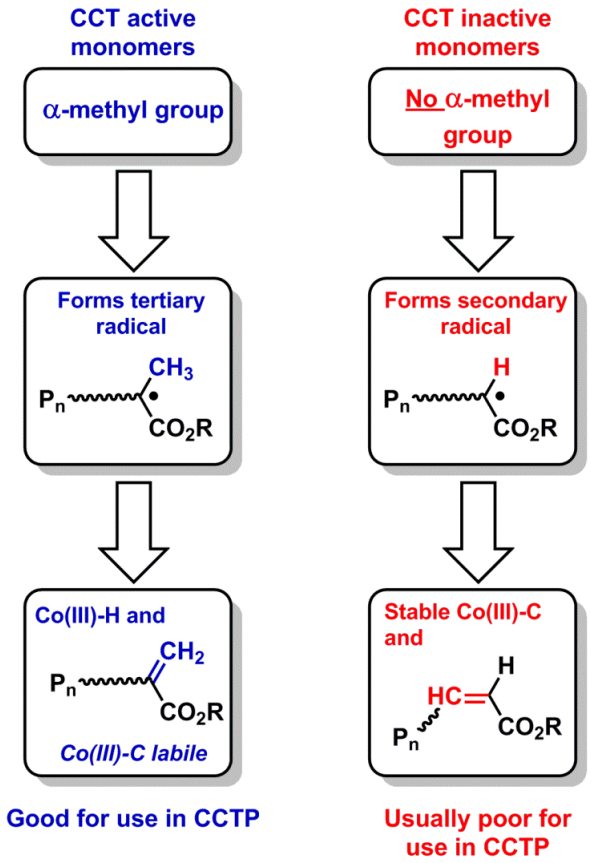


**Figure 1.10: General monomer properties for CCT active and less active monomers.**

## *CCTP of reactive methacrylates*

Many methacrylates have been used in CCT, with MMA and other alkyl methacrylates used most extensively. However, in addition to these, many more exotic monomers with a range of functionalities have been shown to polymerize well under CCT conditions. These have included monomers with reactive functionality, capable of undergoing additional post-polymerization modification, such as glycidyl methacrylate, TMS-protected alkyne methacrylates[58] and allyl methacrylate[59], or monomers possessing functionality interesting in itself, such as sugar-monomers[60-61] or zwitterions[62]. CCTP has been reported to be tolerant of functional groups as diverse and reactive as carboxylic acids[62], epoxides[61], isocyanates and aldehydes, although the latter are published in the patent literature and have yet to be reported academically.[28]

This tolerance of reactive or useful functional groups can be combined with the inherent terminal vinyl group provided in a successful CCTP process, allowing dual functionality.[61] The

vinyl end group has been exploited both as a macro-monomer (see section 1.2.5, below) and for post-polymerization modifications. The α-β-unsaturation lends itself well to conjugate addition of soft nucleophiles, and has as such been shown to often react efficiently and quantitatively with thiols in thio-Michael addition, allowing the introduction of a range of functionalities under mild conditions.[58-59, 63-65] CCTP and thio-Michael addition has also been used to synthesize and modify thermoresponsive[66] and sugar functional polymers for biological applications[58, 60], as well as oil soluble viscosity modifiers based on long chain alkyl methacrylates.[13]

### *CCT copolymerizations with less active monomers*

As discussed above, monomers that have secondary propagating radicals will often have very low activity in CCT, due to the increased stability of the Co(III)-C bond to the polymer chain end.[15, 57, 67] This Co-C complex with the propagating radical has even been observed by MALDI-ToF in the case of acrylates[45]. Several methods have been used in order to weaken this bond, and thereby increase chain transfer frequency, including increasing the reaction temperature or irradiating the reaction mixture with ultraviolet light.[68-69] However, such approaches have been shown to increase the rate of back-biting, leading to a mixture of vinyl-terminated polymers. In any case, the internal double bond formed in such processes will be of limited synthetic use, either for modification or polymerization reactions. For these reasons, homopolymerization of such monomers is rarely attempted by CCTP, as the levels of CCTA required would lead to a costly procedure.

However, copolymerization of less active monomers, such as acrylates, with more reactive CCT monomers has also been extensively studied. It has been found that many secondary radical-forming monomers can be copolymerized with methacrylates, albeit with an associated decrease in the chain transfer constant.[70] However, above a critical concentration of the less active monomer, considerable amounts of grafted architectures can be formed, as the secondary radical is able to add to the CCT-derived vinyl groups (this is very slow in the homopolymerization of methacrylates for steric reasons). This will be discussed further in Chapter 2.

### *1.2.5 Uses of CCTP macro-monomers*

In addition to industrial use of CCTP controlling MW in FRP processes, the macro-monomers produced have also found a variety of uses. It has been reported that CCTP-derived macro-monomers will copolymerize with acrylics and other secondary radical-generating monomer, leading to graft- or comb-like structures[71]. For the case of copolymerizations of macro-monomers with methacrylates, little copolymerization will be seen due to steric hindrance, but macro-monomers have been shown to themselves act as CTAs.[32, 72-73] The CCTP macro-monomers will chain transfer in an addition-fragmentation mechanism *via* β-scission, allowing the formation of low dispersity block copolymers under certain conditions.[27] One example of industrial use of macro-monomers as CTAs is the case of the α-methyl styrene dimer being used to control the MW of polymerizations such as polystyrene[74], as well as to control polymerization temperature in UV curable dental composites[75].

Macro-monomers have also found use in the synthesis of telechelic polymers, taking advantage of the addition-fragmentation mechanism of chain transfer. One such study reports the synthesis of α,ω-dihydroxy telechelic poly(methyl methacrylate) *via* β-scission of 2-hydroxethyl methacrylate (HEMA) dimer used as a CTA, allowing introduction of functional end groups in FRP.[76] This use of macro-monomers as CTAs has been well explored in the academic literature.[73, 76-78]

One example of copolymerizing macro-monomers to give grafted architectures uses RAFT polymerization to give a well defined polymer chain before terminating *via* CCT, to give unsaturated vinyl end-group macro-monomers of unusually low dispersity.[79] The polymers were subsequently copolymerized with acrylic monomers to give comb-like structures. Polymerization of macro-monomers with copolymerizable acrylics has also been used to synthesize star-shaped polymers. Macro-monomers have been copolymerized with a difunctional acrylic monomer, in order to form a crosslinked core that will bind the macro-monomer "arms" together. Such structures have been synthesized using CCTP-derived macro-monomers comprising random blocks of iso-butyl methacrylate, 2-ethylhexyl methacrylate and hydroxyl ethyl methacrylate of molecular weight 4 – 20 kg $mol^{-1}$. These were copolymerized with butanediol diacrylate to yield stars with differing hydrophobicity (depending on ratio of monomers used to make the arms) for use as rheological modifiers.[80]

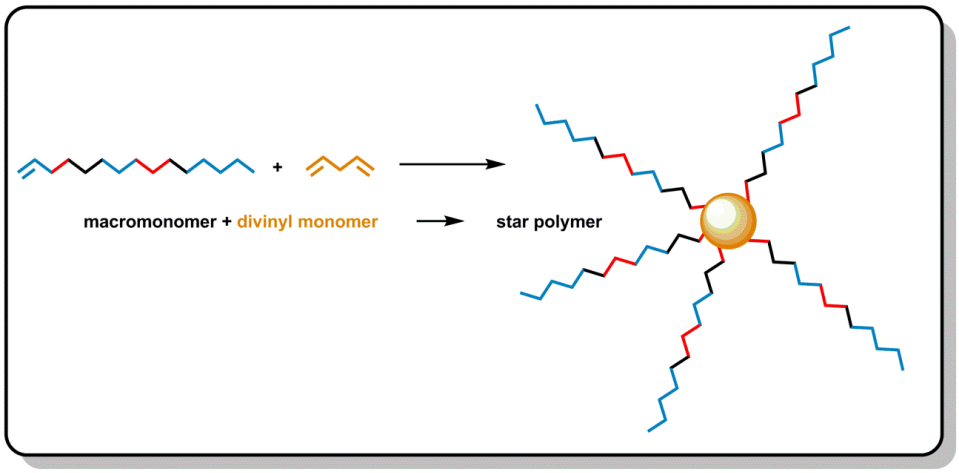


**Figure 1.11: Star polymers through graft-copolymerization of CCTP-dervived macromers.**

## 1.3 Controlled radical polymerization (CRP)

As mentioned above, FRP-derived polymers rarely have well defined architectures, and will often have dispersities greater than 2. However, many of the undesirable side reactions (particularly termination and chain transfer) encountered in radical polymerization can be suppressed by maintaining a low radical concentration.[81] Control of the polymerization is often achieved by reversible termination or deactivation of the propagating radical, increasing the lifetime of radicals (and their *pseudo*-radicals) during polymerization. In such polymerizations, this will reduce termination[82] and allow all polymer chains to continue growing at a similar rate. A successful CRP system will tend towards the desirable characteristics of living anionic polymerization, including:

1. Low dispersity (Đ, $M_w/M_n$), generally ≤ 1.5, but current state-of-the-art will often report ≤ 1.2.
2. Near-quantitative retention of α- and ω-functionality, allowing reinitiation and chain extension by subsequent monomer addition.
3. Control over $DP_n$ by molar ratios of initiator or CTA to monomer at the beginning of polymerization and good agreement between experimental and theoretical MW.
4. Linear evolution of logarithmic conversion with time, indicative of a constant concentration of radicals and suppression of termination by maintaining a low concentration of active species.
5. Linear evolution of number average MW ($M_n$) with conversion.

A number of controlled radical polymerizations have emerged, and in many cases allow the synthesis of well-defined polymers of complex architectures and functionality without the stringent experimental conditions required for living ionic polymerization. As well as providing excellent control and predictable MWs, these techniques have been utilized to synthesize complex functional architectures such as multi-block copolymers and well defined stars. Additionally, the high chain end fidelity of an efficient CRP has led to post-polymerization modification to give polymers with functional end groups.

### *1.3.1 Nitroxide-mediated polymerization (NMP)*

Nitroxide-mediated polymerization was the first controlled radical polymerization technique to find widespread use, and thus represents a major shift in the evolution of polymer science. The technique exploits the stable free radical of nitroxides, which is capable of undergoing a reversible chain-capping reaction, forming a dormant alkoxyamine at the terminus of the propagating chain.[83-84] Like other subsequent CRP strategies, NMP relies upon an equilibrium between the active and dormant species which suppresses bimolecular termination and other undesirable side reactions. The most commonly used controlling agent is 2,2,6,6-tetramethylpiperidynyl-1-oxy (TEMPO), which was first reported to reversibly quench radicals by Moad and Rizzardo in 1985[85], before being used to control the polymerization of styrene by Georges in 1995.[83] However, use of TEMPO and many other nitroxides is largely limited to styrenic monomers, although some acyclic analogues have been shown to increase the scope of the polymerization.[86-88] Further limitations of the technique include the relatively long reaction times, high temperatures used stoichiometric quantities of the controlling agent required.[2]

### *1.3.2 Atom transfer radical polymerization (ATRP)*

Atom transfer radical polymerization was developed independently by Sawamoto[89] and Matyjaszewski[90] in 1995. The systems rely on the exchange of a halogen (either Cl or Br) between a transition metal complex and the propagating chain end, in a redox process that forms an equilibrium between active propagating radicals and halide-capped dormant chains.[91-92] Sawamoto *et al* first reported a ruthenium(II) catalyst controlling the polymerization of MMA in the presence of phosphine ligands and Lewis acids. However, Matyjaszewski used copper(I) complexes of 2,2'-bipyridine to control the polymerization of

acrylates and methacrylates, and it is these Cu-based systems, with a variety of nitrogen-based ligands, that have become very extensively used. ATRP has been shown to give good control over polymerization of acrylates, methacrylates and styrenic monomers, through the use of different nitrogen-based ligands, especially pyridine imines[93] and branched tetradentate ligands, such as tris[2-(dimethylamino)ethyl]amine ($Me_6$Tren)[94-95].

The accepted mechanism for ATRP is shown in Figure 1.12. It can be seen that the process proceeds *via* the abstraction of the halide atom from the initiator or dormant chain by the transition metal complex. This process is reversible, with the catalyst also capable of transferring the halogen to a propagating radical, thereby end-capping the chain. The equilibrium lies far to the dormant state if the polymerization proceeds ideally. Any active chains in the system will propagate by monomer addition to the radical as in FRP, with the rate dependent on $k_p$, and so some termination will occur (albeit at far reduced levels compared to uncontrolled systems).

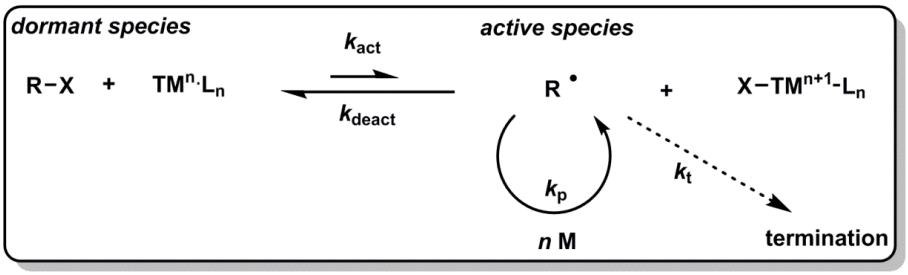


**Figure 1.12: Mechanism of ATRP, where X = halogen, $TM^n$ = transition metal in oxidation state n and L = ligand**

### *1.3.3 Cu(0) mediated CRP*

In 2006, a different methodology for copper-mediated CRP was reported by Percec.[96] Unlike previous work performing Cu-mediated CRP, in which activation of alkyl halides was mediated by Cu(I) complexes, Percec used copper(0)-based systems in the presence of solvents that stabilize Cu(II) and disproportionate Cu(I) in the presence of chelating N-based ligands, regenerating the activating and deactivating species. It was proposed that the polymerization occurred *via* a novel mechanism, which led to the coining of a new term: Single Electron Transfer Living Radical Polymerization (SET-LRP). However, there has been heated debate over the mechanism of the process since its inception, with the Matyjaszewski group, amongst others, arguing that the process in fact is Cu(I) catalysed, and therefore is a subset of the ATRP processes.[97-98] Whatever the true mechanism of the polymerization (which may be very

complex, and subject to many factors depending on experimental conditions), the use of Cu(0) has led to a step-change in the ease of synthesizing well defined polymers rapidly. The technique is now extremely well reported, and has been used to synthesize polymers of excellent "livingness", with dispersities < 1.1 and near quantitative end-group fidelity, even being applied to the synthesis of 10+ blocks in sequential monomer additions.[99-101] The polymerization is extremely well suited to acrylates, but has also been adapted to give well defined poly(acrylamides) in rapid reactions times *via* use of pre-disproportionated Cu(0)/Cu(II) catalysts in water.[102]

### *1.3.4 Reversible addition fragmentation transfer polymerization (RAFT)*

A new CRP technique was developed in 1998 by Thang, Moad and Rizzardo. The technique utilizes a reversible chain transfer mechanism, that allows an equilibrium between active propagating radicals and a dormant macro-RAFT agent.[103] CTAs used in RAFT polymerization are thiocarbonylthio-species (Figure 1.13), with dithioesters (**A**), trithiocarbonates (**B**), xanthates (**C**) and dithiocarbamates (**D**) all extensively used.[104] Key among the advantages of RAFT is that a good choice of CTA will allow polymerization of nearly all common vinylic monomers. For more activated monomers (MAMs), such as (meth)acrylates or styrenics, dithioesters or trithiocarbonates provide good control. Whereas, for more electron-rich less activated monomers (LAMs), xanthates or dithiocarbamates will be used. However, in order to synthesize blocks containing both MAMs and LAMs, universal or switchable RAFT agents have been developed, though levels of control attained are rarely as high as in homopolymerizations using the optimal RAFT group.[105-107]

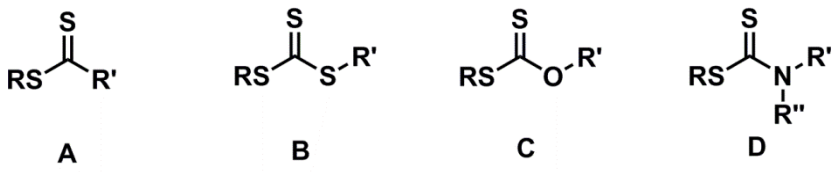


**Figure 1.13: Commonly used RAFT agents.**

The "livingness" of RAFT, that is, levels of termination and end group fidelity, have been substantially improved in the case of acrylamides by Perrier *et al*. Use of monomers with very high $k_p$ allowed the researchers to lower the concentration of radicals while still attaining very

short reaction times. This allowed the synthesis of extremely well defined block copolymers of 4 different monomers, with up to 20 chain extensions, indicating excellent end-group fidelity throughout.[108]

## *1.4 Branched polymers*

Polymer architecture plays an important role in determining the properties of polymers. Branching, and other non-linear architectures, can impart a range of properties to polymer systems, relative to linear counterparts, including; modification of viscosity and rheology, changes in density, reduction of crystallinity or increased solubility.[2, 109-110] Control of such properties is often highly desirable both for the properties of a final product and for ease of processing at some stage of manufacture.

An additional feature of highly-branched polymer structures is their inherently high levels of terminal functionality, leading to applications of dendrimer-like materials in biomedical fields, such as drug delivery vehicles.[111-112] Dendrimers are highly branched macromolecules, ideally being monodisperse, and often have large extents of peripheral functionality. However, synthesis of true dendrimers is extremely demanding, often involving multiple steps, substantial purification and high wastage of reagents due to large excesses, in many cases leading to high cost and limiting application.

Fortunately, several methods have been developed for the relatively facile synthesis of less well defined branched topologies, with dendrimer-like properties at lower cost. These have included branched, hyperbranched and star structures. As this work will focus on the synthesis and application of highly branched materials, synthetic strategies allowing control of branched architecture will be discussed, while star structures are beyond the remit of this thesis and will not be discussed.

### *1.4.1 Synthesis of branched polymers*

Traditionally, branched polymers are synthesized using monomers of Flory's $AB_x$ structure (as in Figure 1.14, wherein A groups can only react with B groups and the reactivity of A and B is equal). As is clear from Figure 1.14, the polymers yielded by self-condensation of such monomers can yield truly hyper-branched polymers, with the addition of each monomer resulting in the formation of a potential branch-point.[113]

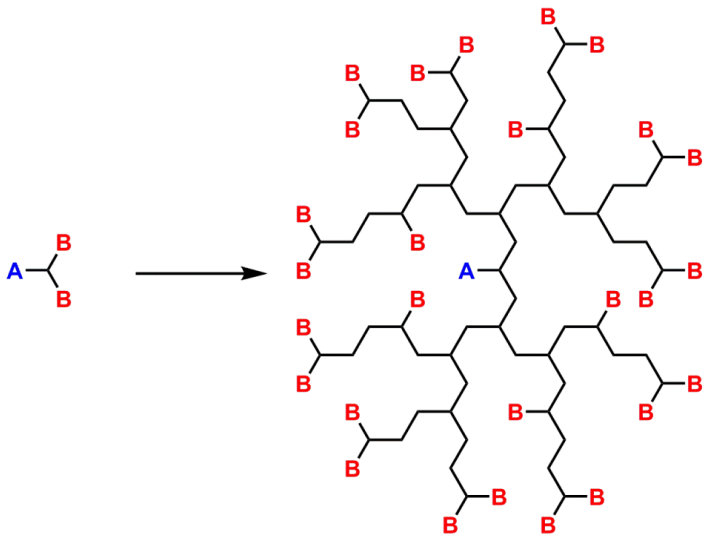

**Figure 1.14: Reaction scheme for general self-condensation of $AB_2$-type monomers**

Condensation of $AB_x$ monomers has a particular advantage over some other (particularly chain growth) strategies for making branched polymers as, if the ideal selectivity where A can only react with B groups holds, crosslinking will be impossible. However, in reality side reactions often occur and can lead to cyclization or undesirable crosslinking of B groups.[114] The $AB_x$ single monomer methodology is limited by the relatively small amount of monomers available that provide this reactivity. Therefore, a double monomer methodology where monomers $AB_x$ and $B_y$ are copolymerized has been introduced, which provides a method tuning the degree of branching of a sample. This will also allow different functionality to be introduced *via* the $B_y$ unit, which will often be a commercially available monomer.

As the work contained in this thesis will involve and be related only to radical polymerization approaches, non-radical methods for the synthesis of branched polymers will not be discussed further. It should be noted that step-growth systems are extensively used and find many applications in industry and academia, but are considered outside the scope of this thesis. Several comprehensive reviews of this chemistry have been published in the last decade or so.[109, 115-125]

### *1.4.2 Crosslinking and network formation*

A key consideration when undertaking the synthesis of branched polymers through the (co)polymerization of multifunctional monomers is the propensity of the material to crosslink, which can result in the formation of an infinite network (i.e. an insoluble gel tending to infinite

MW - Figure 1.15). Network formation can occur both through random crosslinking during polymerization, or by using some chemistry post-polymerization to link pre-formed polymer chains. Both cases have been used to form a range of commercial products. For example, contact lens hydrogels can be produced by radical copolymerization of hydrophilic monomers with multi-functional monomers in a random crosslinking process, whereas materials as diverse as rubber for vehicle tyres, epoxy resins and polymers templates for integrated circuit fabrication are produced industrially by crosslinking pre-formed polymers.[2-3] Both mechanisms of network formation will be relevant to work in this thesis, with prevention of crosslinking during synthesis of highly branched polymers of particular importance for the synthetic work in Chapter 2, and the efficient formation of polymer networks *via* post-polymerization curing a key concept in Chapter 3.

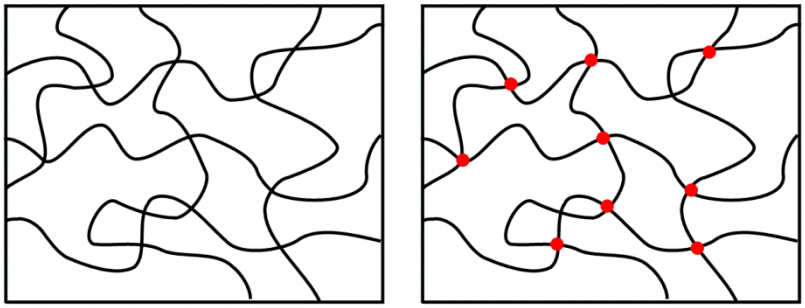

**Figure 1.15: Illustration of an uncrosslinked (*left*) and crosslinked (*right*) polymer system in melt or concentrated solution.**

The crosslinking of difunctional monomers *via* radical polymerization can be considered analogous to step polymerizations of multifunctional reactants.[2] This has been treated mathematically for many years, with key work from Flory[126-128] and Stockmayer[129] providing much of the basis for the theory of network formation. However, this early research was found to give a large discrepancy between theoretical and experimental gel points, partly since cyclization (which will form loops that do not contribute to the network) was not taken into account.

Further investigations have concentrated on specific radical copolymerizations with relatively small amounts of diene – typically < 1 mol. % – with the reactants having varying reactivities. Examples of systems of monomers pairs with approximately equal reactivity ratios (as will be the case in this work) include MMA-EGDMA[130-131], styrene-divinyl benzene[132] and vinyl acetate-divinyl adipate. As reactivity is equal, it can be assumed that, for an A + BB copolymerization,

extent of reaction *p* of A double bonds will equal *p* for B double bonds. It follows that extents of reactions for the respective groups can be written *p*[A] and *p*[B], whereas fully reacted BB units will be $p^2$[BB]. The number of crosslinks is defined simply as the number of BB units fully reacted, $p^2$[BB]. As the critical extent of reaction at the gel point will occur when the number of crosslinks per chain is ½,[2-3] the gel point ($p_c$) will be given by Equation 1.2:

$$p_c = \frac{[A] + [B]}{[B]\bar{X}_w}$$

**Equation 1.2: Gel point, $p_c$ for radical cocopolymerization of monofunctional monomer A, and difunctional monomer BB, where [A] is the concentration of A double bonds, [B] is the concentration of B double bonds and $\bar{X}_w$ is the weight average degree of polymerization.[2]**

As very low amounts of diene are used in such systems, $\bar{X}_w$ will be essentially the weight average degree of polymerization observed in homopolymerization of monomer A. This equation calculates extensive crosslinking during A-BB polymerizations, with gelation in copolymerization of MMA with 0.05 mol. % EGDMA occurring at just 12.5 % conversion[133-134]. However, it has been shown that calculated values increasingly underestimate $p_c$ as concentration of the difunctional species increases, as set out in Table 1.2 for the case of styrene-DVB. As with Flory-Stockmayer theory, underestimation is also caused by cyclization and that pendant functionality on the polymer chain may be less reactive than the free monomer groups[135].

| | Gel point ($p_c$) | |
|---|---|---|
| **mol. % DVB** | **Calculated from Eq. 1.2** | **Observed[132]** |
| 0.004 | 0.21 | 0.16 |
| 0.008 | 0.10 | 0.14 |
| 0.020 | 0.042 | 0.076 |
| 0.032 | 0.026 | 0.074 |
| 0.082 | 0.010 | 0.052 |
| 0.30 | 0.0042 | 0.045 |

**Table 1.2: Crosslinking in the copolymerization of styrene-divinyl benzene.[2]**

Both calculated and observed values for the free radical copolymerizations involving difunctional monomers suggest that insoluble networks will be formed at very low

concentrations of multifunctional monomer, even at very low conversions. This should emphasize the efficiency of the numerous strategies that have been developed allowing the synthesis of soluble, highly branched structures using far greater concentrations of crosslinking agents, as discussed in the coming sections.

### *1.4.3 Chain growth strategies to branched polymers*

By far the most versatile and robust chain growth approach to branched and highly branched polymers is radical polymerization. Strategies employed to give high levels of branching in radical polymerization have ranged from exploiting transfer to monomer or polymer that is inherent in FRP under many conditions – such as the synthesis of branched polyethylene by chain transfer to polymer[136-137] – to designing and synthesizing specialist monomers, initiators, or transfer agents for use in CRP. Several approaches that yield branched architectures will be discussed in these sections, with particular focus on copolymerizations of multi-functional monomers.

#### *Conventional chain transfer reactions*

The simplest method of providing non-linear architectures in FRP is to choose a monomer that provides a propagating radical that will undergo chain transfer to polymer under the conditions applied. This will generally occur with monomers that propagate with non-stabilized radicals, such as vinyl acetate or polyethylene.[110] It should also be noted that chain transfer to monomer and polymer will be significant in the polymerization of many acrylates, despite this being reduced by many CRP methods.[138] However, such transfer will often not occur at a sufficient rate for particularly high levels of branching to be obtained. In such cases, functionality can be introduced that is far more susceptible to chain-transfer, such as thiols, which are ubiquitous when discussing transfer in FRP. Indeed, copolymerization of styrene with vinyl benzyl thiol leads to a highly-branched structure.[139] However, such monomers will be unstable and always likely to undergo self-condensation *via* Michael addition to the electron-poor vinyl group. Another approach, which has been explored extensively by Rimmer and co-workers, is to copolymerize non-stabilized monomers with a co-monomer such as **4** (Figure 1.16) which readily undergoes chain transfer to monomer and polymer. The researchers exploited the transfer by abstraction of a 2-propyl hydrogen to produce highly branched poly(vinyl acetate),[140] poly(*N*-vinyl pyrrolidinone) and poly(1,1-bis(ethoxycarbonyl) vinyl cyclopropane)[141]. While these have given access to highly branched architectures

through robust and economical FRP processes, the method provides little control over polymerization and no control over polymer end groups, the high functionality of which is increasingly important in many applications.

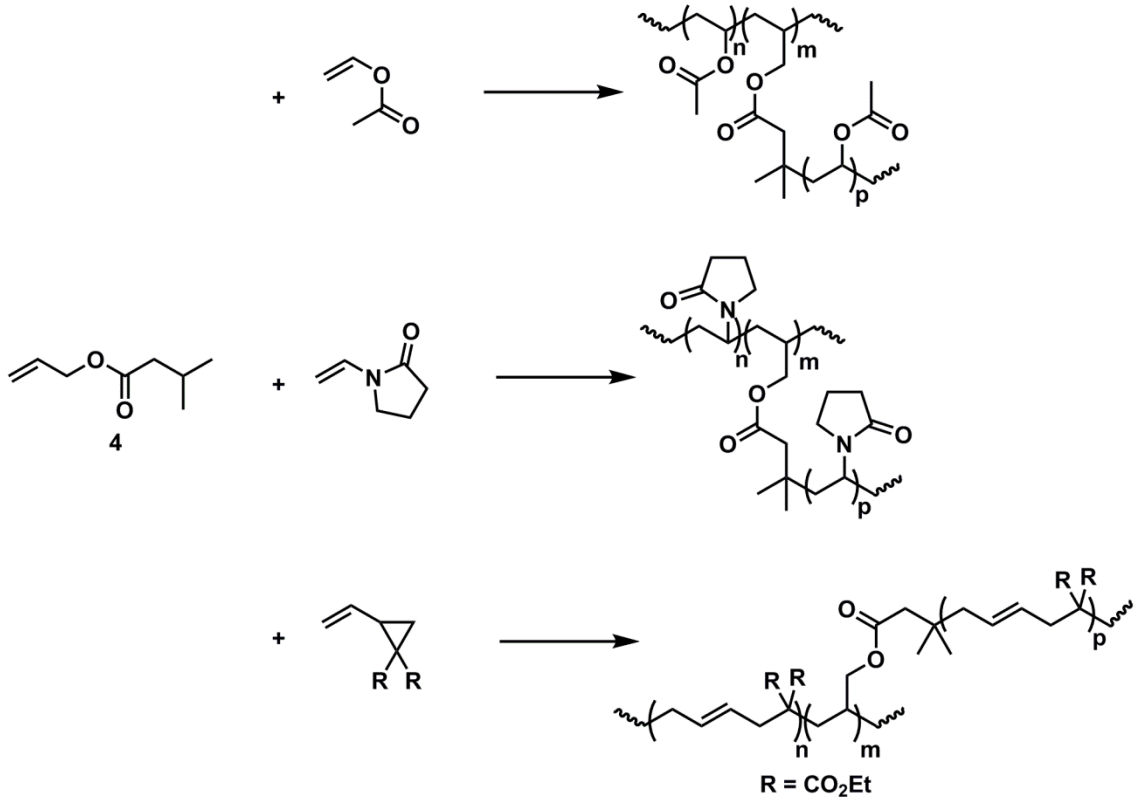


**Figure 1.16: Polymerization with branching comonomer, which transfers *via* abstraction of the 2-propyl hydrogen during polymerization of monomers that propagate with non-stabilized radicals. Adapted from reference.[110]**

## *Polymerization of difunctional monomers in the presence of conventional CTAs*

Clearly, FRP in the presence of a difunctional monomer (e.g. divinyl benzene, ethylene glycol dimethacrylate *etc*.) will quickly give a crosslinked network, leading to irreversible gelation when the number of crosslinks per chain exceeds unity. Even in dilute solutions, polymerization involving such monomers can reach gelation at less than 20 % conversion.[134] However, addition of substantial amounts of thiol CTA has been shown to reduce the primary chain length and delay gelation, leading to a strategy that can be used for the synthesis of highly branched, soluble materials. This approach was introduced by Sherrington in 2000,[4-8] and has since become known as the "*Strathclyde route*", after the institution of its discovery.

The Strathclyde route is a facile, one step, cost-effective way to produce branched polymers using robust FRP techniques. However, relative to many other strategies, the degree of branching is low, with the difunctional monomer usually used in low concentrations with a mono-functional monomer (Figure 1.17). Therefore, truly hyper-branched polymers are not accessible using this method. A range of architectures and functionalities are possible, as the free radical process is tolerant of various monomer functionalities.[4, 6, 8] However, the process is limited to polymerization of electron-deficient,[142] resonance stabilized propagating radicals, as non-stabilized propagating radicals (such as those derived from vinyl acetate or N-vinyl pyrrolidinone) will be quenched by the thiol. Additional functionality will also be imparted by the thiol CTA, although the number of branched chains terminated with this functionality will be low, since each chain transfer event will also terminate a propagating chain with a hydrogen atom.[110] This route has also been used to synthesize branched polymers in emulsion systems, although the choice of suitable CTAs has somewhat limited its scope.[143]

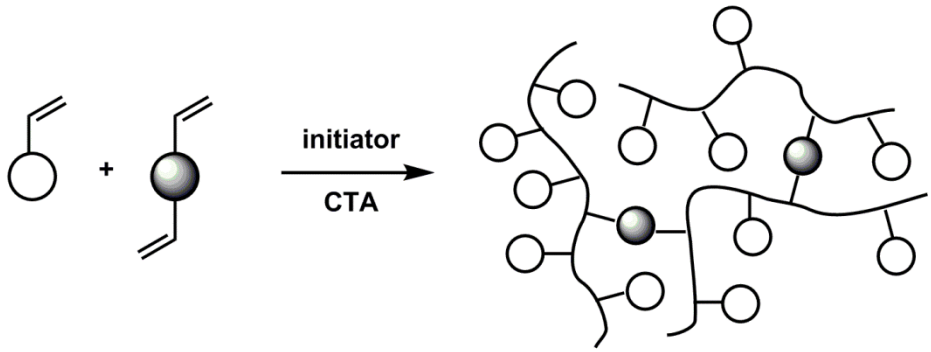


**Figure 1.17: Strathclyde route to branched polymers, by copolymerization of a mono- and di-functional monomer in the presence of a CTA.**

The polymers produced by these systems exhibit poorly defined MWDs and poor control over end-groups, as would be expected for a free-radical system, and suffer from the need to use stoichiometric amounts of toxic and malodorous thiols. Therefore, work in this thesis will aim to use a similar process based on chain transfer in FRP to synthesize branched structures. While levels of control will be similar for the two processes, CCTP will offer far lower CTA loadings (due to its catalytic nature) and far higher end group fidelity, which will prove vital to the final application for polymers synthesized.

## *Self condensing vinyl polymerization*

In order to provide an increased level of control of MW, degree of branching and polymer functionality, there has been much research unto accessing highly branched polymer structures using CRP methodologies. These are often based on the Self Condensing Vinyl Polymerization (SCVP) process, reported by Fréchet *et al* in 1995.[144] SCVP is performed with a vinylic monomer which also contains a group capable of initiating polymerization, leading to the formation of many branch points. Fréchet polymerized 3-(1-chloroethyl)ethenyl benzene, in the presence of $SnCl_4$, to give a branched poly(styrene) type structure. This proceeds *via* a "*pseudo*-living carbocationic" mechanism and produces a high MW product (>100 $kg.mol^{-1}$). However, the process has fairly poor control over the end groups retained after polymerization, with a mixture of secondary alkyl chlorides and methoxy groups (which will have limited usefulness for modification in any case). The process has since been developed and adapted to the controlled polymerization of vinylic monomers by radical mechanisms. In two seminal papers from 1995 and 1996, Hawker and Matyjaszewski applied the newly discovered NMP and ATRP processes to give hyperbranched polymers using an SCVP approach.

The NMP method used a monomer containing both a polymerizable styryl group and reversible propagating/deactivating stable free radical group (Figure 1.18). As with standard NMP and SFRP, the low bond dissociation of the carbon-oxygen bond linking to the nitroxide allows thermal activation of the SCVP process, with control provided by reversible termination by nitroxide species.[145] The process produced branched poly(styrene)s with MWs up to 300 kg $mol^{-1}$ and dispersities from 1.6 - 4.4, demonstrating a level of control absent in previous SCVP work. This work has since been expanded to give branched materials using a number of other polymerizable SFR groups. For example, Tao *et al* have synthesized polymerizable nitroxides that incorporate cleavable nitroxide groups into the polymer structure,[146] allowing thermal decomposition of polymer networks,[147] irreversible cleaving by addition of terminating groups,[148] and the propagation of another monomer, giving access to a range of functionality.

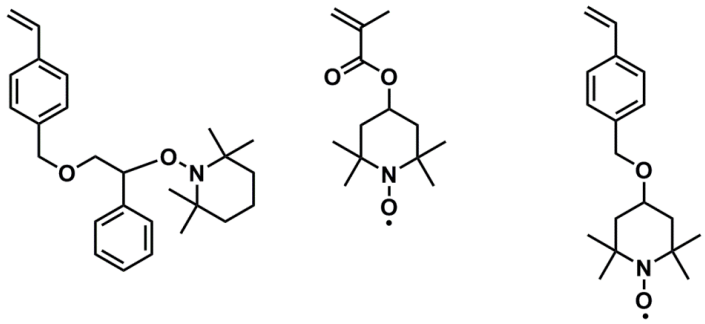

**Figure 1.18: Examples of nitroxide monomers used in SCVP.[110]**

The second major development in controlled radical SCVP strategies came from the Matyjaszewski group,[149] who realized that their newly developed Cu(I)-mediated ATRP could create branched motifs if the vinylic monomer and alkyl halide initiator were combined in a single monomer. This approach used simple ATRP conditions (i.e. CuBr and 2,2'bipyridyl) and *p*(chloromethyl) styrene, which has since often been termed an "inimer". Upon homolysis of the alkyl chloride bond, the inimer will undergo propagation with the styrene groups, with every addition giving the possibility of initiation of a polymer chain from the branch point (Figure 1.19). However, a study published by Weimer, Fréchet and Gitsov found that a relatively low degree of branching had been obtained, with the difference in reactivity of initiating and propagating species leading to formation of predominantly linear structures at modest conversions.[150] A successful ATRP system following ideal SCVP (and giving highly branched polymers throughout the reaction) requires a high initiator to monomer ratio, which will often result in termination and consumption of the Cu(I) activator (as in the persistent radical effect, which is responsible for control in many ATRP systems, giving an excess of Cu(II) species), preventing the reactivation of alkyl halides. This was remedied by Matyjaszewski for acrylate- and methacrylate-inimers by either changing the ligand to 4,4′-di-tert-butyl-2,2′-dipyridyl (for acrylics) or adding Cu(0), which was added to reduce Cu(II)-X species to Cu(I), thereby pushing $K_{ATRP}$ toward activation.[151]

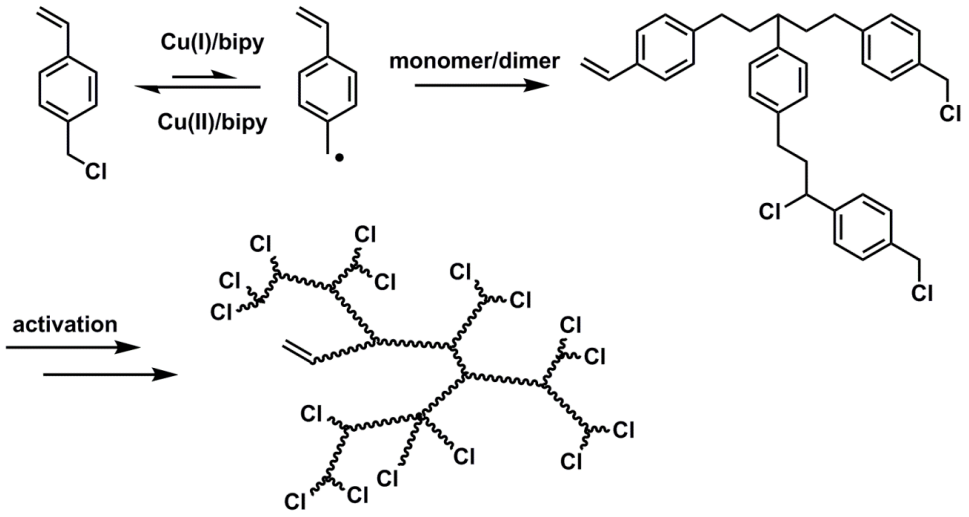


**Figure 1.19: ATRP-SCVP to create highly branched polymers.**

ATRP mediated SCVP has since been used extensively to introduce a range of functionalities to branched polymers, often by using a mono-functional monomer to give longer chain branching. This has been applied to give branched polymers with functionality and structure as diverse as fluorinated polymers[152-153], amphiphilic core-shell structures[154], polyelectrolytes[155] and branched glyco-polymers[156-157]. While these examples demonstrate that such a process is very versatile (indeed, it should be tolerant of the same functional groups as "standard" ATRP, that is, a great many), it should be noted that control over the MWD is not precise, and well defined polymers giving analogous dispersities to linear CRP should not be expected.

Many approaches to well defined topologies have involved sequential steps and protecting group chemistry, which would further increase the difficulty of synthesis and thus the cost. A particularly relevant example would be work published by Xie and Zhao in 2011, detailing the synthesis of hyperbranched poly(acrylic acid)s, their modification with photo-polymerizable functionality and application to dual-cure dental restoratives.[158] While the advantages of accessing a highly branched polymer of this functionality and applying it to dental composites are clear, the process would be unlikely to be viable on an industrial scale. The authors use an ATRP-SCVP method to create highly branched poly(*tert*-butyl acrylate), which is then deprotected to poly(acrylic acid) and modified with vinyl functionality using isocyanate chemistry. This three step synthesis would be very costly on an industrial scale, and indeed the levels of catalyst required for the initial ATRP-SCVP, combined with synthesis of the inimer,

would likely be deemed too costly to be performed industrially for all but the most high-value, non-commodity products.

RAFT-SCVP was introduced by Yang *et al* in 2003, *via* the incorporation of a dithioester RAFT agent into a styrene monomer.[159] However, the monomer design led to a weak dithioester link in the branched chains, limiting the use of the technique to synthesize robust structures. This was overcome by Carter *et al*, who designed similar monomers that would place the RAFT groups at the end of the branched chain ends. This was achieved by polymerization of monomers such as **5** and **6** (Figure 1.20) with NIPAM[160-161]. This synthetic route was further exploited by Rimmer *et al* to give highly branched block copolymer structures[162], and has been expanded to various other monomers containing RAFT groups, including those based on methacrylates and those synthesized using a "click" chemistry approach.[163]

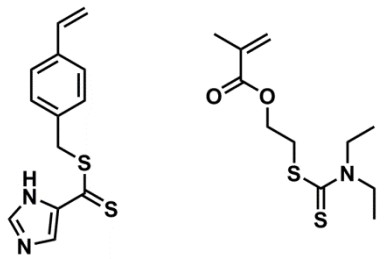


**5** **6**

**Figure 1.20: Examples of monmers containing RAFT functionalities used in RAFT-SCVP.[160, 162]**

Perrier reported a method that would remove and recover all RAFT groups, and could be used to introduce a range of functionalities.[164] An excess of radical initiator was added to the polymer, which upon decomposition will result in bimolecular termination to functionalize the chain end. The functionality imparted on the polymer end groups will depend on the radical initiator employed, and this technique has been further used to add carboxylic acids with the use of 4,4'azobis(4-cyanopentanoic acid).[161]

However, as in the CRP-SCVP strategies discussed above, the custom synthesis of the monomer-RAFT agent would likely preclude this technique from industrial use, even using the RAFT process which has, at the time of writing, been the only CRP method undertaken on a commercial scale.

The above description of various SCVP strategies illustrates that a large range of functional materials can be produced. However, a large driving force for the discovery and development

of radical polymerization methods capable of creating highly functional, branched structures is their ease of synthesis and lower cost relative to truly dendritic materials. As such, in many cases a facile synthesis by an economic process that yields a relatively poorly defined, but highly functional macromolecule, would often be far more desirable than a very well defined analogue produced in an intensive and costly process. So, while SCVP is a very useful process, and can often provide levels of control absent in free radical branching strategies, it requires (in most cases) specialist synthesis of non-commodity monomers, and relatively large amounts of catalyst which must then be removed. For these reasons, the undeniably interesting materials produced by CRP-SCVP approaches are limited in their usefulness outside of academia. Therefore, several approaches that can be used to give functional, highly branched polymers by FRP processes have been considered to be more interesting to the chemical industry generally. The key examples of this are, for the most part, based around the use of a chain transfer methodology.

## *1.5 Branched polymers by CCTP*

Golokov and co-workers were the first to report the synthesis of branched polymers *via* CCTP. The authors polymerized triethylene glycol dimethacrylate (TEGDMA) in the presence of a cobalt(II) hematoporphyrin tetramethyl ester complex CCTA (**1**). Although gelation was prevented in some cases and soluble oligomers were formed, the reactions were inconsistent and the products were not fully characterized.[165] Further work with the same monomer was filed in a patent by Abbey in 1986, using a Co(II) catalyst generated *in situ*, but high levels of catalyst used led to the formation of only very low MW products, and thus the majority of the polymers produced were linear.[166]

A key patent was filed by Guan of E. I. Du Pont Nemours and Company in 1998, describing the CCT homopolymerization of a number of di- and tri-vinyl monomers as well as their copolymerization with several mono-functional monomers containing a range of functionality.[167] Similar work was subsequently published, in part, several years later in the academic literature.[168] The highly branched polymers synthesized by Guan exhibited low solution viscosities and a high level of vinyl functionality, leading the author to mark their potential for automotive coatings and photo-curing applications. The homopolymerizations of dimethacrylates reported was postulated to lead to truly hyper-branched structures, with the levels of CCTA used leading to trimerization and cascade branching (Figure 1.21).

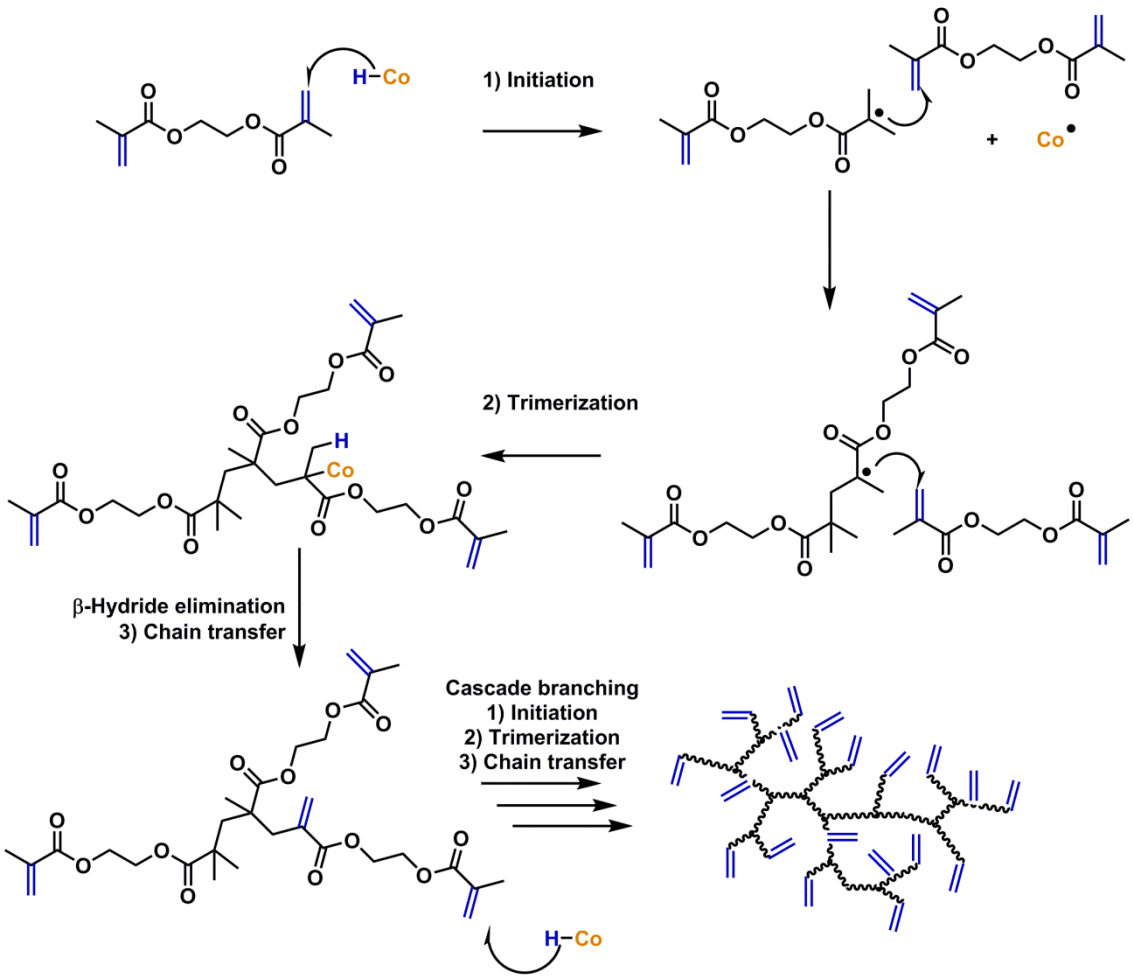


**Figure 1.21: Proposed mechanism for CCTP of EGDMA, with cascade branching leading to the formation of vinyl terminated polymers.[168]**

Through SEC experiments utilizing a viscometry detector, it was found that the branched polymers had significantly lower intrinsic viscosities (IV) than linear counterparts. It was also observed that there was very little dependence of IV on MW, whereas the value of IV increases linearly with MW for linear polymers, following the Mark-Houwink equation.[3] Work by Guan on the homopolymerization of divinyl monomers also allows the synthesis of hyper-branched polymers where MW is directly proportional to the level of branching, providing a tool for controlled polymer topology *via* control of MW.[168-169]

Further work conducted by the University of Strathclyde, Viscotek and Ineos Acrylics investigated the synthesis of branched copolymers of MMA and tripropylene glycol diacrylate (TPGDA) *via* both CCTP and conventional, thiol-mediated chain transfer (i.e. the "Strathclyde route").[5] Around 5 wt. % of the difunctional monomer was incorporated, and the resulting

polymers shown to have high levels of vinyl functionality. As would be expected, levels of branching observed were increased by using higher levels of difunctional monomer and by increasing MW. The authors found that reducing the concentration of the CCTA (CoBF) had little effect on $M_n$, although $M_w$ increased as expected, leading to the conclusion that [CoBF] had little effect on levels of branching. It should be noted that acrylic monomers would be expected to reduce the chain transfer frequency of the catalyst (due to their lack of an easily abstractable α-methyl H)[28], and under certain conditions could lead to the formation of grafted structures.[66, 71, 80] Additionally, commonly observed reactivity ratios for copolymerization of acrylates and methacrylates lead to gradient polymers, with acrylic species consumed predominantly at high conversions[170] – indeed, the authors confirmed this by fractionation experiments. As such, a monomer such as TPGDA would usually be avoided when performing CCTP, with the conventional chain transfer route certainly favoured for copolymerization of acrylic species, despite the large increase in the level of CTA required to delay gelation.

Another publication relating to the use of CCTP to synthesize branched copolymers emerged from the Russian literature, in which Kurmaz *et al* copolymerized styrene with dimethacrylates.[171] It was found that the gel effect was suppressed (compared to a FRP system) through the use of cobalt(II) tetramethyl hematoporphyrin, [$Co^{II}P$]. The authors also investigated the increases in elasticity with branching and MW. The same group carried out further research into related systems by replacing styrene with a long chain alkyl monomer (dodecane methacrylate, DDMA).[172] It was postulated that the bulk of DDMA would prevent interaction of the polymeric radical with pendant (that is, unreacted) vinyl groups, thereby reducing crosslinking and cyclization. However, bulk polymerizations were found to be less controlled, with gelation only delayed. The authors did note that soluble branched polymers with high levels of vinyl functionality could be used as macro-monomers for preparing star, hyper-branched or block copolymer hybrids.

In 2005, Sherrington *et al* published work that disputed the findings of Guan, Kurmaz and others who had reported copolymerizations of di- or trifunctional methacrylates under CCT conditions. Sherrington compared the CCTP route to branched copolymers of EGDMA and MMA (previously reported by Guan) with the analogous system using dodecanethiol as CTA.[173] They reported that, in contrast to work by Guan, soluble polymers were not always obtained. Sherrington and his co-workers postulated that Guan may have observed backbiting cyclization reactions, which would prevent the polymer chains crosslinking. However, the authors

reported that conventional chain transfer approaches to branched polymers (or the "*Strathclyde route"*) gave greater control and suppressed gelation. Additionally, multi-detector SEC was used to measure g' values (a measure of decreased viscosity relative to a linear standard, often indicative of degree of branching between samples, see chapter 2), which suggested a higher degree of branching for 'Strathclyde' polymers, relative to products synthesized *via* CCTP. However, this is unsurprising, as the levels of crosslinker employed in the conventional chain transfer reactions were greater.

The somewhat negative conclusions made relating to CCTPs utility in branched polymer synthesis have been dispelled in recent years. Kurmaz published the homopolymerization of divinyl monomers by CCTP in 2006,[174] but particularly rigorous examples of CCTP's ability to give very highly branched structures were published by Haddleton and McEwan[64] and Smeets *et al*[175]. Haddleton investigated the homopolymerization of difunctional EGDMA and trifunctional trimethylpropane trimethacrylate (TMPTMA), before functionalizing the resulting hyper-branched structures *via* thio-Michael addition.[64] Smeets used a similar process of EGDMA homopolymerization followed by thio-Michael modification and reductive amination to synthesize core-crosslinked micelle analogues, comprising a hyper-branched EGDMA core functionalized with a water-soluble polysaccharide corona.[175] Both bodies of work report detailed multi-detector SEC analysis, and leave little doubt that highly branched systems have been produced.[65] In addition, such work emphasizes that the high levels of vinyl functionality afforded can be invaluable tools for the creation of novel, non-linear architectures though both polymerization and post-polymerization modification.

## *1.6 Introduction to polymer-inorganic dental materials*

### *1.6.1 Glass ionomer cements*

#### *History/Introduction*

Glass-ionomer or -polyalkenoate cements (GICs) were introduced in the early 1970s by Wilson, Kent and Crisp as an aesthetic alternative to traditional amalgam restoratives.[176-183] These materials, along with composite materials[184], were part of a new class of dental restoratives that combined a polymer component with an inorganic filler. Early GICs introduced in the mid 1970s showed slow curing times and high moisture sensitivity, but due to their aesthetic

benefits, and the incremental improvement of their properties in the last 40 years, have become a very important class of dental material.[185-188] No other class of dental restorative has received so much attention in terms of research in the last 15 years.[186-187, 189-194]

The most basic GICs consist of a concentrated (up to 50 w. %)[176-180, 194-197] aqueous solution of poly(acrylic acid) (PAA) which is mixed with a reactive, ion-leachable calcium fluoroaluminosilicate (FAS) glass powder. In the presence of water (which acts as the reaction medium), the acidic polymer attacks the glass powder, with the neutralization reaction releasing calcium and aluminium cations, and forming a silica hydrogel. The calcium and aluminium cations (formally $Ca^{2+}$ and $Al^{3+}$) are then chelated by the polymer carboxylate groups, forming intra- and inter-molecular salt bridges: the system undergoes a gradual setting process, leading to a hard, crosslinked material.[186-187, 194] During this setting time, the ratio of bound (structural water) to un-bound water will increase, along with the mechanical and physical properties. This process is shown in cartoon form in Figure 1.22; however, in reality the ionic setting mechanism is far more complex, and relatively poorly understood despite being the subject of much research over the last 4 decades.

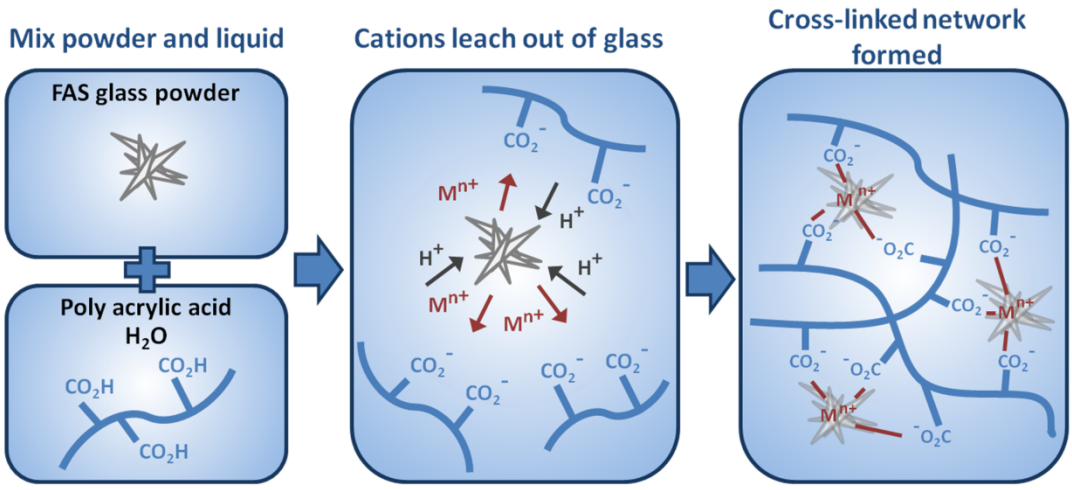


**Figure 1.22: Cartoon of setting process upon mixing of liquid and powder components of GICs.**

## *Acid-base setting reaction*

Most glasses used in GICs are based on either $SiO_2$-$Al_2O_3$-CaO or $SiO_2$-$Al_2O_3$-$CaF_2$, and produced by the fusion of ingredients at 1200-1550 $^{o}$C and shock cooling in water or on a cold metal plate.[177, 180] This produces a coarse frit, which is normally ground further to give a powder with

a particle size < 45 μm for filling grade materials or < 15 μm for a fine luting grade material.[186] The acid degradable properties of the glass arise from the presence of Al and Ca: a simple silicate glass will consist of only $SiO_4$ tetrahedra, and would not be susceptible to acid attack.[198] Presence of the aluminium cation, which is formally 3 coordinate, leaves a net negative charge on the local structure which is balanced by Ca or Na cations.[199] Much research has focused on innovation of the glass component of GICs;[192] however, the glass will not be further discussed in this work, which focuses on the polymer component of the materials.

Several techniques have been developed for characterization of the acid-base setting reaction in glass ionomer cements, including FTIR, $^{13}$C-NMR, electron probe micro-analysis and simply monitoring of the change in pH.[200-207] FTIR has shown that the neutralization reaction does not go to completion, with the stiffness of the material reducing mobility of the carboxylates at high extents of curing. FTIR has been shown to be a powerful technique for characterization of the neutralization reaction since it can distinguish between the two possible metal salts formed (i.e. calcium and aluminium carboxylates). This technique suggests that calcium is released from the glass powder before aluminium, with signals due to calcium salts detected within the first minute of the reaction.[200, 202] However, these finding have been disputed by both Cook and Nicholson, who dissolved the materials in base and acid, respectively, before analysing the solutions. Both groups and techniques suggest that $Al^{3+}$ and $Ca^{2+}$ cations are leached from the glass early in the reaction.[208-209] The role of silicon species in the curing and final cement has also been investigated, with the suggestion that the silica forms a hydrated inorganic gel network of its own, contributing substantially to the strength of the final cement.[210-211]

Several factors will influence the speed of the setting reaction and the strength of the final material. These include the structure of the polymer (i.e. the molecular weight and number and type of acid groups), the concentrations of the polymer solution and the powder/liquid ratio of the cement.[194, 212-214] As would be expected, the mechanical properties (compressive and flexural strengths) of the cured material will increase with the MW of the acidic polymer used.[194] However, there is a balance between the strength of the final material and the viscosity of the mixture before setting, as a polymeric component of too high molecular weight will yield a paste that is too viscous to be workable when applying the restorative. The same will also be true for the powder-liquid ratio of the cements, with the highest ratios giving the strongest materials to the detriment of workability.[186, 189, 215]

By far the most important small molecule additive used in GIC formulations is (+)-tartaric acid ((+)-TA), which has been added to cements at 5-10 w. % concentrations since its introduction in early GIC systems.[216-217] The optically active enantiomers of TA have been shown to modify the initial setting process after mixing of powder and liquid by increasing the working time (i.e. delaying the neutralization and subsequent crosslinking of the polymer) and sharpening the setting of the material.[182, 202, 217] This is favourable for clinicians as GICs without such an additive would require rapid mixing of the cement and placing of the restorative before the material becomes unworkable. Additionally, (+)-TA has been shown to significantly enhance the compressive strength of the final cement.[186-187, 189, 194, 216-217] While the process is not fully understood, most postulated mechanisms for delaying of the working time suggest that (+)-TA chelates $Ca^{2+}$ and $Al^{3+}$ cations more strongly than the polyacid, delaying the initial setting and allowing more homogeneous solutions to be produced.[186, 202] This would give a solution with fewer surface flaws and bulk inhomogenetities, leading to increased overall strength of the material.[218] Interestingly, only the optically active forms of TA have been shown to give either the desirable modification of setting kinetics or the increases in mechanical properties.

## *Advances in polyelectrolyte component of GICs*

### *Tradtional monomer systems*

Original polyacid components consisted of highly viscous PAA solutions, which tend to form a gel over time, reducing the shelf-life of the ionomer solution.[219] In addition to the possibility of gelation, the high solution viscosity frequently resulted in poor mixing and led to materials that were difficult to handle. Some early PAAs incorporated methacrylic acid[197], which has been reported to prevent gelation.[220-221] However, while these materials improved chain-interaction in setting and increased mechanical strength, the chain stiffness leads to increased viscosity and difficulties in handling the cement after mixing.[194] This has clear implications for the work in this thesis incorporating branching PMAA-based polyacids into GICs, however, it is hoped that branching will have the effect of reducing viscosity and allowing the formation of a workable cement, even at high MWs and polymer concentrations.

### *Di- and tri-functional acid monomers*

Several acidic monomers containing two or three acid groups have been successfully incorporated into GICs. This has been explored due to early GIC's high solution viscosity and relatively low mechanical strengths and wear resistance. Polyfunctional monomers include itaconic acid, maleic acid and 2-butene-1,2,3-tricarboxylic acid (Figure 1.23).[186, 194] Acrylic acid

copolymers with itaconic acid were first applied to dental cements in the mid 1970s by Crisp and Wilson, and in several patents relating to GIC chemistry during this time published by Crisp, Kent and Wilson.[176, 178, 182, 197] This was subsequently expanded to copolymers of other difunctional acidic monomers, such as maleic acid.[196, 222-225]

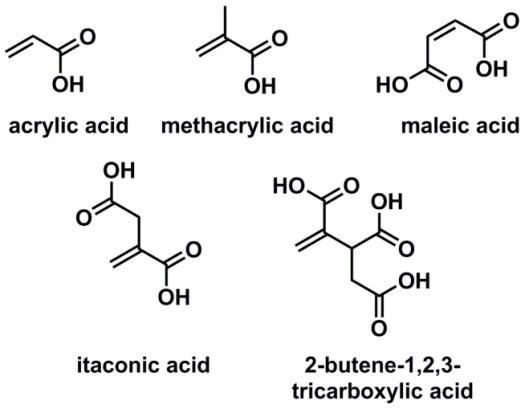


**Figure 1.23: Acidic monomers traditionally used in the polymer component of GICs.**

Acrylic acid/itaconic acid copolymers, P(AA-*co*-IA), have seen particularly widespread use due to their relatively low viscosity (compared to PAA of the same MW) and greater number of acid groups.[214] These copolymers have been reported to have excellent mixing and mechanical properties due to the reduced viscosity, as well as reducing the likelihood of gelation occuring.[219] Acrylic acid/itaconic acid copolymers have also been shown to give similar mechanical properties to PAA cements at lower MWs, due to the increased number of crosslinks they can provide per repeat unit.[181, 220] These copolymers have been extensively reported in the patent literature, and are used in several industry leading commercial GICs.

Acrylic acid copolymers with tri-functional acid monomer 2-butene-1,2,3-tricarboxylic acid have also been reported[226], and incorporation of this monomer has been shown to increase the mechanical strength of the material, while giving a lower viscosity when compared to acrylic acid homopolymers.[194]

## *Advantages of GICs*

GICs have shown competitive mechanical properties, with sufficient compressive and flexural strengths for class II and III applications, as well as providing a hard cement.[186, 189, 219, 227-228] However, glass ionomers have a number of important advantages not related to their mechanical properties.

Common problems arise in the use of *in situ* polymerization in dental cement curing, with free cytotoxic monomer residual in the interior of the filling and shrinkage during polymerization undesirable. GICs exhibit neither of these problems, since the acid-base neutralization reaction hardening the cement requires no monomers and has been shown not to undergo shrinkage during setting.[229] The absence of monomers also contributes to the good biocompatibility displayed by these systems.[186, 230-231]

The same chemistry that leads to the ionic crosslinking and setting reaction in glass-ionomers also gives advantageous adhesion to enamel and dentin, meaning that GIC materials require no adhesive and can be used as luting cements or to attach orthodontics to the tooth.[232-233] GICs have been shown to chelate calcium ions on the surface of enamel and dentin, as well as displacing phosphates from the hydroxyapatite surface. This provides an important advantage over other dental composites, which have no inherent binding to the tooth surface and require the use of adhesives.[186, 189, 219, 234-236] Tooth adhesion also gives the benefit of the tooth surface requiring little pre-treatment and no etching, reducing treatment time.

In all reactive glass powder compositions used in GICs the fluoride content is high, which leads to an important benefit of GICs, as fluoride has anti-cariogenic (disease preventing) properties.[231] Additionally, GICs have been shown to release fluoride over time, resulting in prevention of secondary caries. The calcium-fluoroaluminosilicate glass filler also contributes to the excellent aesthetics relative to traditional dental materials such as amalgam.

### *Problems with GICs*

A major problem with GICs is their moisture sensitivity immediately after application, which is due to the relatively slow setting time.[187] This results in a successful GIC restoration requiring greater care from the dentist and longer time in the chair for patients. This lack of control over setting of the cement also causes problems with low working time and the need for clinicians to mix the cement thoroughly and mould the restoration relatively quickly.

Other drawbacks that reduce the applicability of GICs to more classes of restoration relate to the mechanical properties of the final cement. Conventional GICs provide medium to low mechanical strengths, relative to amalgam or polymeric composite resins, resulting in them being unsuitable for class I and some class II restorations and load bearing areas susceptible to

high masticatory forces. Other problems cited include the materials' resistance to wear and pressure, again relative to amalgam and composite materials.[186-187, 189]

These issues with mechanical properties, moisture sensitivity and control of setting, have lead to the development of glass-ionomer hybrid materials that incorporate a free radical polymerization component. These dual-cure materials are generally known as resin-modified GICs.

### *1.6.2 Resin-modified glass ionomer cements (RMGICs)*

Glass ionomers combining acid-base ionic setting with polymerizable components were introduced by Antonucci *et al* in 1986[237-238], who used a redox system to initiate polymerization of HEMA and poly(ethylene glycol) dimethacrylate (PEGDMA). However, a significant breakthrough, leading to a step change in glass ionomers with polymerizable components, occurred with the report of systems containing pendant polymerizable groups, with polymerization initiated photo-chemically.[224, 239] The system utilizes isocyanate and epoxide chemistry to functionalize a portion of the acid groups with photo-polymerizable methacrylate groups (Figure 1.24), using isocyanatoethyl methacrylate (IEM) and glycidyl methacrylate (GMA), respectively. The patent also describes the synthesis and methacrylate-functionalization of itaconic acid and maleic acid copolymers with acrylic acid. This work has proven seminal in the fields of dual curable glass ionomers, with these materials commercially available as Vitribond (3M)[225] and other materials also developed using similar princples.[228 240]

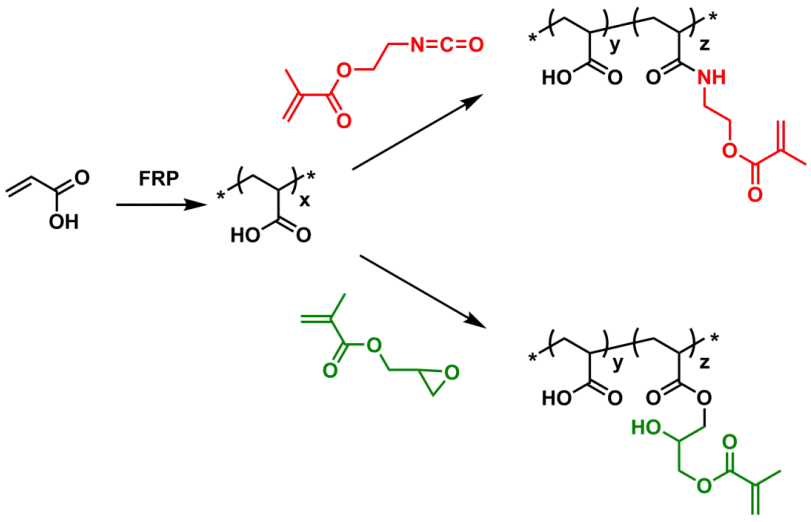


**Figure 1.24: IEM and GMA modification of polyacrylic acid with polymerizable methacrylate groups.[224]**

The first monomer introduced was HEMA, which acts as both a monomer and a solvent or compatibilizer.[224] However, recently RMGICs have used difunctional monomers in order to give a greater extent of crosslinking and reduce shrinkage during polymerization. The most significant of these is a dimethacrylate monomer based on bisphenol A, commonly known as bis-GMA, which is often diluted with TEGDMA.[194, 241] Bis-GMA provides desirable properties, such as excellent mechanical strength after curing, high molecular weight/low volatility and low polymerization shrinkage. However, the monomer often shows relatively low conversions and has an undesirably high viscosity[242], leading to the use of PEGDMAs with short spacers as dilutants. Bis-GMA has been found to be clinically safe for dental applications.[243]

RMGICs have been reported to absorb more fluoride than conventional ionomer systems from solutions containing high levels of fluoride, such as mouthwash, leading to more long term anti-cariogenic properties.[244] Cements based on this chemistry also show an increased working time and allow greater control over the setting of the final cement, as well as decreasing moisture sensitivity and enhancing mechanical properties (especially in the early stages of setting). However, while this chemistry has been hugely successful and has largely revolutionized glass ionomer chemistry, it has several clear problems:

Many polymers that find use in GICs – such as acrylic acid/itaconic acid copolymers - are synthesized in one simple polymerization process that can often be carried out in aqueous media. However, the methacrylate-modified polyacids used in many RMGICs require two synthetic steps (i.e. polymerization and modification) and additional purification.[224] In many cases, traditional polyelectrolyte solutions can be formulated immediately after polymerization, whereas the methacrylate coupling step requires the use of relatively toxic organic solvents (such as THF),[224] and very toxic isocyanate- and epoxy-methacrylates. This means that polymers prepared in this fashion will have to be extensively purified before use in clinically relevant cements. Additionally, the two step synthesis also represents a significant increase in the cost of the material. Ideally, a simple polymerization process requiring no specialist monomer synthesis could be used to provide a polyacid capable of undergoing a dual cure process in one step.

Other disadvantages of RMGICs include their complex setting chemistry, which is relatively poorly understood. Major drawbacks also include shrinkage during polymerization[245] – which has been remedied by use of higher MW difunctional monomer systems (such as bis-GMA and

TEGDMA)[234, 243, 246-247] – and the presence of cytotoxic un-cured monomer in the part of the cement closest to the pulp of the tooth.[186, 203] The problem of incomplete monomer cure has been resolved to some extent with the combination of photo-initiating systems with redox polymerization initiating systems, which will allow a high extent of cure independent of depth of irradiation. Despite the presence of cytotoxic monomers, commercial RMGICs have been shown to display acceptable biocompatibility.[248]

### *Recent advances in glass powder modification*

Modern powder components used in RMGICs will contain several components other than the calcium fluoroaluminosilicate glass. In many cases photo-initiating systems have been mixed into the powder component, and in some cases monomers have been added to the glass powder or have been tethered to the glass using silane monomers, as has been used in Fuji LC II photo-curable GICs.[249] This covalent linking of radical polymerizable groups to the glass powder represents something of an alternative to the methacrylate-modified polyacid strategy, with both used in current commercial materials. In order to increase the homogeneity of the final cement and aid efficient mixing of the powder and liquid components, manufacturers have started mixing dried PAA into the glass powder.[219, 250] This has been labelled an important modification in glass-ionomer systems.[186]

### *Non-linear polymers in RMGICs*

The research group of Dong Xie has explored the use of non-linear polymer architectures in the polyelectrolyte component of RMGICs. In 2006[251] the researchers used ATRP of *tert*-butyl acrylate to synthesize core-first 4-arm PAA stars, before using the IEM and GMA chemistry first reported by Mitra[224-225] (Figure 1.24) to tether polymerizable methacrylates to a portion of the carboxyl groups. The authors aimed to optimize the mechanical properties of the final cement by exploiting the lower viscosity of a branched system, allowing the use of higher molecular weight polymers while maintaining a workable paste. The cements synthesized show increased tensile and flexural strengths relative to commercially available photo-curable GIC Fuji II LC, but a less significant increase in compressive strength. While this work shows some success in improving aspects of the mechanical properties, compared to linear systems, the star copolymers require several synthetic steps, including core-initiator synthesis, polymerization of protected monomer, deprotection and methacrylate tethering. This process

amounts to a large increase in cost and laborious purification at several points, rendering it commercially not viable.

Further work by Xie and co-workers adapted this system to formulate a co-monomer free RMGIC, reducing the cytotoxicity of the material and apparently increasing the compressive strength relative to their previous study.[252] The researchers also found that increasing the number of arms of the star polymers from 4 to 8 gave fracture toughness and wear resistance in excess of commercial glass-ionomers,[253] possibly yielding a restorative capable of filling demanding class I and II restorations – an area where properties of previous GICs have been deemed insufficient.

Later work by Xie and co-workers reports the synthesis of hyper-branched poly(acrylic acid)s using an ATRP-SCVP[144, 149] or "inimer" strategy.[158] Cements formulated using these polymers show significantly higher mechanical properties (including compressive strength, tensile strength, flexural strength, fracture toughness and hardness) than commercial materials. However, the synthetic route again requires inimer synthesis, removal of protecting groups and vinyl tethering. While this work has clearly demonstrated the potential benefit of non-linear structures in RMGICs, it still remains highly unlikely such a system could be commercialized. An elegant method of synthesizing a branched polyacid bearing polymerizable groups in fewer steps would clearly be highly desirable.

## *1.7 Aims*

The work undertaken sets out to investigate the CCTP of water soluble, acidic monomers to create non-linear structures for use in dental composites. Homopolymerization of MAA under CCT conditions has been reported previously under monomer/CCTA feed conditions[62], and this will serve as a starting point. The efficiency of this approach will be investigated and PMAA of a range of molecular weights synthesized in order to test the applicability of $BF_2$-bridged cobaloxime CCTAs to acidic conditions. The incorporation of acrylic functionality will then be investigated and the structure of the copolymers obtained elucidated, as some CCT copolymerizations of acrylic and methacrylic species have been reported to lead to non-linear grafted structures.

In order to synthesize highly branched polymer structures, MAA will be copolymerized with difunctional EGDMA before analysis using multi detector SEC techniques to verify formation

branched polymer architectures. This methodology should lead to the efficient synthesis of branched polyacids containing a number of vinyl groups capable of undergoing further reaction. With this in mind, the materials will be applied to photo-curable resin modifed glass ionomer cements.

In order to test the effect of the polymers on the curing and properties of the final material, a model system must be developed. This will involve optimization of the photo-initiation system as well as investigation of the effect of varying the concentration of various key components, such as polymer, comonomer, additives and the powder to liquid ratio of the cement. These systems will be characterized using a variety of online techniques during irradiation, including differential scanning calorimetry, oscillatory rheology and FTIR. The mechanical properties of the final materials will also be evaluated and compared to those of commercial cements.

## *1.8 References*


1. P. J. Flory, *J. Am. Chem. Soc.* **1937**, *59*, 241.
2. G. Odian, *Principles of Polymerisation*, 4th ed., John Wiley & Sons, Hoboken, **2004**.
3. P. C. Hiemenz, T. P. Lodge, *Polymer Chemistry*, 2 ed., CRC Press: Taylor & Francis Group, **2007**.
4. A. T. Slark, D. C. Sherrington, A. Titterton, I. K. Martin, *J. Mater. Chem.* **2003**, *13*, 2711.
5. P. A. Costello, I. K. Martin, A. T. Slark, D. C. Sherrington, A. Titterton, *Polymer* **2002**, *43*, 245.
6. F. Isaure, P. A. G. Cormack, D. C. Sherrington, *J. Mater. Chem.* **2003**, *13*, 2701.
7. N. O'Brien, A. McKee, D. C. Sherrington, A. T. Slark, A. Titterton, *Polymer* **2000**, *41*, 6027.
8. F. Isaure, P. A. G. Cormack, D. C. Sherrington, *Macromolecules* **2004**, *37*, 2096.
9. D. M. Haddleton, D. Kukulj, T. P. Davis, D. R. Maloney, *Cobalt-Mediated Free-Radical Polymerization Of Acrylic-Monomers* in *Trends In Polymer Science, Vol. 3*, Elsevier Science, Oxford, **1995**, pp. 365.
10. J. P. A. Heuts, G. E. Roberts, J. D. Biasutti, *Aust. J. Chem.* **2002**, *55*, 381.
11. A. Gridnev, *J. Polym. Sci., Part A: Polym. Chem.* **2000**, *38*, 1753.
12. N. S. Enikolopyan, B. R. Smirnov, G. V. Ponomarev, I. M. Belgovskii, *J. Polym. Sci., Part A: Polym. Chem.* **1981**, *19*, 879.
13. A. Anastasaki, C. Waldron, V. Nikolaou, P. Wilson, R. McHale, T. Smith, D. M. Haddleton, *Polym. Chem.* **2013**, *4*, 4113.
14. D. R. Maloney, K. H. Hunt, P. M. Lloyd, A. V. G. Muir, S. N. Richards, P. J. Derrick, D. M. Haddleton, *Chem. Commun.* **1995**, 561.
15. B. R. Smirnov, I. M. Belgovskii, G. V. Ponomarev, A. P. Marchenko, N. S. Enikolopyan, *Dokl. Akad. Nauk. SSSR* **1980**, *254*, 127.
16. B. R. Smirnov, I. S. Morozova, A. P. Marchenko, M. A. Markevich, L. M. Pushchaeva, N. S. Enikolopyan, *Dokl. Akad. Nauk. SSSR* **1980**, *253*, 891.
17. B. R. Smirnov, I. S. Morozova, L. M. Pushchaeva, A. P. Marchenko, N. S. Enikolopyan, *Dokl. Akad. Nauk. SSSR* **1980**, *255*, 609.
18. B. R. Smirnov, A. P. Marchenko, G. V. Korolev, I. M. Belgovskii, N. S. Enikolopyan, *Vysokomol. Soedin. A* **1981**, *23*, 1042.
19. J. C. Lin, K. J. Abbey, US 4680354, **1987**.

20. K. J. Abbey, D. L. Trumbo, G. M. Carlson, M. J. Masola, R. A. Zander, *J. Polym. Sci., Part A: Polym. Chem.* **1993**, *31*, 3417.
21. G. M. Carlson, K. J. Abbey, US 4526945, **1985**.
22. M. J. Darmon, C. T. Berge, J. A. Antonelli, US 5362826, **1993**.
23. A. H. Janowicz, EP 222619, **1987**.
24. D. M. Haddleton, A. V. G. Muir, S. W. Leeming, J. P. O'Donnell, S. N. Richards, WO 9613527, **1996**.
25. D. M. Haddleton, A. V. G. Muir, S. W. Leeming, WO 9517435, **1995**.
26. D. M. Haddleton, J. C. Padget, G. C. Overbeek, WO9504767A1, **1995**.
27. J. Krstina, G. Moad, E. Rizzardo, C. L. Winzor, C. T. Berge, M. Fryd, *Macromolecules* **1995**, *28*, 5381.
28. S. Slavin, K. A. McEwan, D. M. Hadddleton, *Cobalt Catalysed Chain Transfer Polymerization: A Review* in *Polymer Science: A Comprehensive Reference, Vol. 3*, Elsevier, Oxford, **2012**, pp. 249.
29. D. G. Hawthorne, WO 8703605, **1987**.
30. D. M. Haddleton, A. V. G. Muir, WO 9504759, **1995**.
31. D. M. Haddleton, J. C. Padget, G. C. Overbeek, **1995**.
32. N. M. B. Smeets, T. G. T. Jansen, T. J. J. Sciarone, J. P. A. Heuts, J. Meuldijk, A. M. Van Herk, *Journal of Polymer Science Part a-Polymer Chemistry* **2010**, *48*, 1038.
33. N. M. B. Smeets, M. W. Freeman, T. F. L. McKenna, *Macromolecules* **2011**, *44*, 6701.
34. N. M. B. Smeets, R. W. K. Lam, R. P. Moraes, T. F. L. McKenna, *Polym. Chem.* **2012**, *3*, 514.
35. N. M. B. Smeets, T. G. T. Jansen, J. P. A. Heuts, A. M. van Herk, J. Meuldijk, *Macromolecular Reaction Engineering* **2012**, *6*, 110.
36. K. G. Suddaby, D. M. Haddleton, J. J. Hastings, S. N. Richards, J. P. O'Donnell, *Macromolecules* **1996**, *29*, 8083.
37. D. M. Haddleton, D. R. Morsley, J. P. O'Donnell, S. N. Richards, *J. Polym. Sci., Part A: Polym. Chem.* **1999**, *37*, 3549.
38. A. A. Gridnev, A. V. Goncharov, *Kinet. Katal.* **1989**, *30*, 767.
39. B. R. Smirnov, V. D. Plotnikov, B. V. Ozerkovskii, V. P. Roshchupkin, N. S. Enikolopyan, *Vysokomol. Soedin. A* **1981**, *23*, 2588.
40. J. P. A. Heuts, D. J. Forster, T. P. Davis, *Macromol. Rapid Commun.* **1999**, *20*, 299.

41. V. Y. Mironychev, M. M. Mogilevich, B. R. Smirnov, Y. Y. Shapiro, I. V. Golikov, *Polymer Science U.S.S.R.* **1986**, *28*, 2103.
42. A. A. Gridnev, *Polym J* **1992**, *24*, 613.
43. A. A. Gridnev, S. D. Ittel, *Chem. Rev.* **2001**, *101*, 3611.
44. G. E. Roberts, T. P. Davis, J. P. A. Heuts, G. E. Ball, *Macromolecules* **2002**, *35*, 9954.
45. G. E. Roberts, J. P. A. Heuts, T. P. Davis, *Macromolecules* **2000**, *33*, 7765.
46. C. Kowollik, T. P. Davis, *J. Polym. Sci., Part A: Polym. Chem.* **2000**, *38*, 3303.
47. E. F. McCord, W. L. Anton, L. Wilczek, S. D. Ittel, L. T. J. Nelson, K. D. Raffell, J. E. Hansen, C. Berge, *Macromol. Symp.* **1994**, *86*, 47.
48. A. Gridnev, *Polym. J.* **1992**, *24*, 613.
49. A. A. Gridnev, S. D. Ittel, M. Fryd, B. B. Wayland, *Organometallics* **1993**, *12*, 4871.
50. D. M. Haddleton, D. R. Maloney, K. G. Suddaby, A. V. G. Muir, S. N. Richards, *Macromol. Symp.* **1996**, *111*, 37.
51. R. A. Sanayei, K. F. O'Driscoll, *J. Macromol. Sci. Chem.* **1989**, *26*, 1137.
52. D. M. Hadddleton, S. Slavin, K. A. McEwan, *Comprehensive Polymer Science*, 2nd ed.
53. K. G. Suddaby, D. R. Maloney, D. M. Haddleton, *Macromolecules* **1997**, *30*, 702.
54. J. P. A. Heuts, T. P. Davis, G. T. Russell, *Macromolecules* **1999**, *32*, 6019.
55. J. P. A. Heuts, D. J. Forster, T. P. Davis, B. Yamada, H. Yamazoe, M. Azukizawa, *Macromolecules* **1999**, *32*, 2511.
56. D. A. Morrison, T. P. Davis, J. P. A. Heuts, B. Messerle, A. A. Gridnev, *J. Polym. Sci., Part A: Polym. Chem.* **2006**, *44*, 6171.
57. A. A. Gridnev, *Polym. Sci. USSR* **1989**, *31*, 2369.
58. L. Nurmi, J. Lindqvist, R. Randev, J. Syrett, D. M. Haddleton, *Chem. Commun.* **2009**, 2727.
59. S. Slavin, E. Khoshdel, D. M. Haddleton, *Polym. Chem.* **2012**, *3*, 1461.
60. Q. Zhang, S. Slavin, M. W. Jones, A. J. Haddleton, D. M. Haddleton, *Polym. Chem.* **2012**, *3*, 1016.
61. K. A. McEwan, S. Slavin, E. Tunnah, D. M. Haddleton, *Polym. Chem.* **2013**, *4*, 2608.
62. D. M. Haddleton, E. Depaquis, E. J. Kelly, D. Kukulj, S. R. Morsley, S. A. F. Bon, M. D. Eason, A. G. Steward, *J. Polym. Sci., Part A: Polym. Chem.* **2001**, *39*, 2378.
63. G.-Z. Li, R. K. Randev, A. H. Soeriyadi, G. Rees, C. Boyer, Z. Tong, T. P. Davis, C. R. Becer, D. M. Haddleton, *Polym. Chem.* **2010**, *1*, 1196.
64. K. A. McEwan, D. M. Haddleton, *Polym. Chem.* **2011**, *2*, 1992.

65. N. M. B. Smeets, *Eur. Polym. J.* **2013**, *49*, 2528.
66. A. H. Soeriyadi, G.-Z. Li, S. Slavin, M. W. Jones, C. M. Amos, C. R. Becer, M. R. Whittaker, D. M. Haddleton, C. Boyer, T. P. Davis, *Polym. Chem.* **2011**, *2*, 815.
67. B. Pierik, D. Masclee, A. van Herk, *Macromol. Symp.* **2001**, *165*, 19.
68. J. Chiefari, J. Jeffery, R. T. A. Mayadunne, G. Moad, E. Rizzardo, S. H. Thang, *Macromolecules* **1999**, *32*, 7700.
69. A. A. Gridnev, S. D. Ittel, C. L. Moad, G. Moad, E. Rizzardo, L. Wilczek, WO1997031030 A1, **1997**.
70. S. C. J. Pierik, A. M. van Herk, *Macromol. Chem. Phys.* **2003**, *204*, 1406.
71. P. Cacioli, D. G. Hawthorne, R. L. Laslett, E. Rizzardo, D. H. Solomon, *J. Macromol. Sci. Chem.* **1986**, *23*, 839.
72. D. M. Haddleton, D. R. Maloney, K. G. Suddaby Adam Clarke, S. N. Richards, *Polymer* **1997**, *38*, 6207.
73. C. L. Moad, G. Moad, E. Rizzardo, S. H. Thang, *Macromolecules* **1996**, *29*, 7717.
74. H. Ishigaki, H. Okada, S. Suyama, JP03212402A, **1991**.
75. M. Nagashima, H. Kazama, JP11071220A, **1999**.
76. D. M. Haddleton, C. Topping, J. J. Hastings, K. G. Suddaby, *Macromol. Chem. Phys.* **1996**, *197*, 3027.
77. D. M. Haddleton, D. R. Maloney, K. G. Suddaby, *Macromolecules* **1996**, *29*, 481.
78. D. M. Haddleton, C. Topping, D. Kukulj, D. Irvine, *Polymer* **1998**, *39*, 3119.
79. A. H. Soeriyadi, C. Boyer, J. Burns, C. R. Becer, M. R. Whittaker, D. M. Haddleton, T. P. Davis, *Chem. Commun.* **2010**, *46*, 6338.
80. J. A. Antonelli, C. Scopazzi, US 5310807, **1994**.
81. T. Pintauer, K. Matyjaszewski, *Chem. Soc. Rev.* **2008**, *37*, 1087.
82. B. M. Rosen, V. Percec, *Chem. Rev.* **2009**, *109*, 5069.
83. M. K. Georges, R. P. N. Veregin, P. M. Kazmaier, G. K. Hamer, *Macromolecules* **1993**, *26*, 2987.
84. C. J. Hawker, *Acc. Chem. Res.* **1997**, *30*, 373.
85. D. H. Solomon, E. Rizzardo, P. Cacioli, EP135280A2, **1985**.
86. C. J. Hawker, A. W. Bosman, E. Harth, *Chem. Rev.* **2001**, *101*, 3661.
87. D. Benoit, V. Chaplinski, R. Braslau, C. J. Hawker, *J. Am. Chem. Soc.* **1999**, *121*, 3904.
88. D. Benoit, S. Grimaldi, S. Robin, J.-P. Finet, P. Tordo, Y. Gnanou, *J. Am. Chem. Soc.* **2000**, *122*, 5929.

89. M. Kato, M. Kamigaito, M. Sawamoto, T. Higashimura, *Macromolecules* **1995**, *28*, 1721.
90. J.-S. Wang, K. Matyjaszewski, *J. Am. Chem. Soc.* **1995**, *117*, 5614.
91. M. Kamigaito, T. Ando, M. Sawamoto, *Chem. Rev.* **2001**, *101*, 3689.
92. K. Matyjaszewski, J. Xia, *Chem. Rev.* **2001**, *101*, 2921.
93. D. M. Haddleton, C. B. Jasieczek, M. J. Hannon, A. J. Shooter, *Macromolecules* **1997**, *30*, 2190.
94. J. Xia, K. Matyjaszewski, *Macromolecules* **1999**, *32*, 2434.
95. J. Xia, S. G. Gaynor, K. Matyjaszewski, *Macromolecules* **1998**, *31*, 5958.
96. V. Percec, T. Guliashvili, J. S. Ladislaw, A. Wistrand, A. Stjerndahl, M. J. Sienkowska, M. J. Monteiro, S. Sahoo, *J. Am. Chem. Soc.* **2006**, *128*, 14156.
97. D. Konkolewicz, Y. Wang, P. Krys, M. Zhong, A. A. Isse, A. Gennaro, K. Matyjaszewski, *Polym. Chem.* **2014**, *5*, 4396.
98. D. Konkolewicz, Y. Wang, M. Zhong, P. Krys, A. A. Isse, A. Gennaro, K. Matyjaszewski, *Macromolecules* **2013**, *46*, 8749.
99. A. H. Soeriyadi, C. Boyer, F. Nyström, P. B. Zetterlund, M. R. Whittaker, *J. Am. Chem. Soc.* **2011**, *133*, 11128.
100. A. Anastasaki, C. Waldron, P. Wilson, C. Boyer, P. B. Zetterlund, M. R. Whittaker, D. Haddleton, *ACS Macro Lett.* **2013**, *2*, 896.
101. A. Anastasaki, V. Nikolaou, G. S. Pappas, Q. Zhang, C. Wan, P. Wilson, T. P. Davis, M. R. Whittaker, D. M. Haddleton, *Chem. Sci.* **2014**.
102. Q. Zhang, P. Wilson, Z. Li, R. McHale, J. Godfrey, A. Anastasaki, C. Waldron, D. M. Haddleton, *J. Am. Chem. Soc.* **2013**, *135*, 7355.
103. J. Chiefari, Y. K. Chong, F. Ercole, J. Krstina, J. Jeffery, T. P. T. Le, R. T. A. Mayadunne, G. F. Meijs, C. L. Moad, G. Moad, E. Rizzardo, S. H. Thang, *Macromolecules* **1998**, *31*, 5559.
104. D. J. Keddie, G. Moad, E. Rizzardo, S. H. Thang, *Macromolecules* **2012**, *45*, 5321.
105. D. J. Keddie, *Chem. Soc. Rev.* **2014**, *43*, 496.
106. M. Benaglia, J. Chiefari, Y. K. Chong, G. Moad, E. Rizzardo, S. H. Thang, *J. Am. Chem. Soc.* **2009**, *131*, 6914.
107. D. J. Keddie, C. Guerrero-Sanchez, G. Moad, R. J. Mulder, E. Rizzardo, S. H. Thang, *Macromolecules* **2012**, *45*, 4205.
108. G. Gody, T. Maschmeyer, P. B. Zetterlund, S. Perrier, *Macromolecules* **2014**, *47*, 3451.
109. B. I. Voit, A. Lederer, *Chem. Rev.* **2009**, *109*, 5924.
110. R. M. England, S. Rimmer, *Polym. Chem.* **2010**, *1*, 1533.

111. S. Chen, X.-Z. Zhang, S.-X. Cheng, R.-X. Zhuo, Z.-W. Gu, *Biomacromolecules* **2008**, *9*, 2578.
112. Y. Wang, S. M. Grayson, *Adv. Drug Deliver. Rev.* **2012**, *64*, 852.
113. P. J. Flory, *J. Am. Chem. Soc.* **1952**, *74*, 2718.
114. H. Komber, A. Ziemer, B. Voit, *Macromolecules* **2002**, *35*, 3514.
115. Y. Segawa, T. Higashihara, M. Ueda, *Polym. Chem.* **2013**, *4*, 1746.
116. A. Carlmark, E. Malmstroem, M. Malkoch, *Chem. Soc. Rev.* **2013**, *42*, 5858.
117. D. Konkolewicz, M. J. Monteiro, S. Perrier, *Macromolecules* **2011**, *44*, 7067.
118. R. Hoogenboom, *Angew. Chem., Int. Ed.* **2010**, *49*, 3415.
119. S. Peleshanko, V. V. Tsukruk, *Prog. Polym. Sci.* **2008**, *33*, 523.
120. H. R. Kricheldorf, *Macromol. Rapid Commun.* **2007**, *28*, 1839.
121. C. R. Yates, W. Hayes, *Eur. Polym. J.* **2004**, *40*, 1257.
122. C. Gao, D. Yan, *Prog. Polym. Sci.* **2004**, *29*, 183.
123. M. Jikei, M.-a. Kakimoto, *Prog. Polym. Sci.* **2001**, *26*, 1233.
124. B. Voit, *J. Polym. Sci., Part A: Polym. Chem.* **2000**, *38*, 2505.
125. Y. H. Kim, *J. Polym. Sci., Part A: Polym. Chem.* **1998**, *36*, 1685.
126. P. J. Flory, *J. Am. Chem. Soc.* **1939**, *61*, 3334.
127. P. J. Flory, *J. Am. Chem. Soc.* **1940**, *62*, 2261.
128. P. J. Flory, *J. Am. Chem. Soc.* **1941**, *63*, 3083.
129. H. Jacobson, C. O. Beckmann, W. H. Stockmayer, *J. Chem. Phys.* **1950**, *18*, 1607.
130. D. T. Landin, C. W. Macosko, *Macromolecules* **1988**, *21*, 846.
131. W. H. Li, A. E. Hamielec, C. M. Crowe, *Polymer* **1989**, *30*, 1513.
132. B. T. Storey, *J. Poly. Sci. A* **1965**, *3*, 265.
133. C. Walling, *J. Am. Chem. Soc.* **1949**, *71*, 1930.
134. M. Yoshimura, H. Mikawa, Y. Shirota, *Macromolecules* **1978**, *11*, 1085.
135. G. Hild, R. Okasha, *Makromol. Chem.* **1985**, *186*, 389.
136. D. J. Cutler, P. J. Hendra, M. E. A. Cudby, H. A. Willis, *Polymer* **1977**, *18*, 1005.
137. P. E. Gloor, Y. Tang, A. E. Kostanska, A. E. Hamielec, *Polymer* **1994**, *35*, 1012.
138. N. M. Ahmad, B. Charleux, C. Farcet, C. J. Ferguson, S. G. Gaynor, B. S. Hawkett, F. Heatley, B. Klumperman, D. Konkolewicz, P. A. Lovell, K. Matyjaszewski, R. Venkatesh, *Macromol. Rapid Commun.* **2009**, *30*, 2002.
139. J. Liu, Y. Wang, Q. Fu, X. Zhu, W. Shi, *J. Polym. Sci., Part A: Polym. Chem.* **2008**, *46*, 1449.

140. S. Rimmer, S. Collins, P. Sarker, *Chem. Commun.* **2005**, 6029.
141. P. Sarker, J. R. Ebdon, S. Rimmer, *Macromol. Rapid Commun.* **2006**, *27*, 2007.
142. R. Baudry, D. C. Sherrington, *Macromolecules* **2006**, *39*, 5230.
143. Y. Liu, J. C. Haley, K. Deng, W. Lau, M. A. Winnik, *Macromolecules* **2008**, *41*, 4220.
144. J. M. J. Fréchet, M. Henmi, I. Gitsov, S. Aoshima, M. R. Leduc, R. B. Grubbs, *Science* **1995**, *269*, 1080.
145. C. J. Hawker, J. M. J. Frechet, R. B. Grubbs, J. Dao, *J. Am. Chem. Soc.* **1995**, *117*, 10763.
146. Y. Tao, J. He, Z. Wang, J. Pan, H. Jiang, S. Chen, Y. Yang, *Macromolecules* **2001**, *34*, 4742.
147. A. Niu, C. Li, Y. Zhao, J. He, Y. Yang, C. Wu, *Macromolecules* **2001**, *34*, 460.
148. C. Li, J. He, Li, J. Cao, Y. Yang, *Macromolecules* **1999**, *32*, 7012.
149. S. G. Gaynor, S. Edelman, K. Matyjaszewski, *Macromolecules* **1996**, *29*, 1079.
150. M. W. Weimer, J. M. J. Fréchet, I. Gitsov, *J. Polym. Sci., Part A: Polym. Chem.* **1998**, *36*, 955.
151. K. Matyjaszewski, S. G. Gaynor, A. Kulfan, M. Podwika, *Macromolecules* **1997**, *30*, 5192.
152. C. Cheng, K. L. Wooley, E. Khoshdel, *J. Polym. Sci., Part A: Polym. Chem.* **2005**, *43*, 4754.
153. K. T. Powell, C. Cheng, K. L. Wooley, *Macromolecules* **2007**, *40*, 4509.
154. W. Du, A. M. Nyström, L. Zhang, K. T. Powell, Y. Li, C. Cheng, S. A. Wickline, K. L. Wooley, *Biomacromolecules* **2008**, *9*, 2826.
155. H. Mori, A. Walther, X. André, M. G. Lanzendörfer, A. H. E. Müller, *Macromolecules* **2004**, *37*, 2054.
156. S. Muthukrishnan, G. Jutz, X. André, H. Mori, A. H. E. Müller, *Macromolecules* **2004**, *38*, 9.
157. S. Muthukrishnan, H. Mori, A. H. E. Müller, *Macromolecules* **2005**, *38*, 3108.
158. J. Zhao, D. Xie, *Dent. Mater.* **2011**, *27*, 478.
159. Z. Wang, J. He, Y. Tao, L. Yang, H. Jiang, Y. Yang, *Macromolecules* **2003**, *36*, 7446.
160. S. Carter, B. Hunt, S. Rimmer, *Macromolecules* **2005**, *38*, 4595.
161. S. Rimmer, S. Carter, R. Rutkaite, J. W. Haycock, L. Swanson, *Soft Matter* **2007**, *3*, 971.
162. S. Carter, S. Rimmer, A. Sturdy, M. Webb, *Macromolecular Bioscience* **2005**, *5*, 373.
163. A. P. Vogt, B. S. Sumerlin, *Macromolecules* **2008**, *41*, 7368.
164. S. Perrier, P. Takolpuckdee, C. A. Mars, *Macromolecules* **2005**, *38*, 2033.
165. I. V. Golokov, V. A. Semyannikov, M. M. Mogilevich, *Vysokomol. Soedin. A* **1985**, *27*, 304.

166. K. J. Abbey, US 4608423, **1986**.
167. Z. Guan, *US5767211* **1998**.
168. Z. Guan, *J. Am. Chem. Soc.* **2002**, *124*, 5616.
169. Z. Guan, *J. Polym. Sci., Part A: Polym. Chem.* **2003**, *41*, 3680.
170. J. Brandrup, I. E. H., *Polymer Handbook*, 3rd Ed ed., Wiley Interscience, Chichester, **1989**.
171. S. Kurmaz, E. O. Perepelitsina, M. L. Bubnova, G. A. Estrina, V. P. Roshchupkin, *Mendeleev Commun.* **2002**, *12*, 21.
172. S. Kurmaz, E. O. Perepelitsina, M. L. Bubnova, G. A. Estrina, *Mendeleev Commun.* **2004**, *14*, 125.
173. S. Camerlynck, P. A. G. Cormack, D. C. Sherrington, G. Saunders, *J. Macromol. Sci. Phys.* **2005**, *44*, 881.
174. S. Kurmaz, E. O. Perepelitsina, *Russ. Chem. Bull.* **2006**, *55*, 835.
175. D. J. Krasznai, T. F. L. McKenna, M. F. Cunningham, P. Champagne, N. M. B. Smeets, *Polym. Chem.* **2012**, *3*, 992.
176. A. D. Wilson, S. Crisp, DE2319715A1, **1973**.
177. A. D. Wilson, B. E. Kent, US3814717A, **1974**.
178. S. Crisp, A. D. Wilson, DE2439882A1, **1975**.
179. S. Crisp, A. D. Wilson, DE2547744A1, **1976**.
180. A. D. Wilson, B. E. Kent, DE2061513B2, **1976**.
181. A. D. Wilson, B. E. Kent, D. Clinton, R. P. Miller, *J. Mater. Sci.* **1972**, *7*, 220.
182. S. Crisp, A. J. Ferner, B. G. Lewis, A. D. Wilson, *J. Dent.* **1975**, *3*, 125.
183. S. Crisp, B. G. Lewis, A. D. Wilson, *J. Dent. Res.* **1975**, *54*, 1173.
184. N. Moszner, U. Salz, *Prog. Polym. Sci.* **2001**, *26*, 535.
185. J. W. McLean, *Clin. Mater.* **1991**, *7*, 283.
186. J. W. Nicholson, *Biomaterials* **1998**, *19*, 485.
187. B. M. Culbertson, *Prog. Polym. Sci.* **2001**, *26*, 577.
188. A. D. Wilson, *Clin. Mater.* **1991**, *7*, 275.
189. J. F. McCabe, *Biomaterials* **1998**, *19*, 521.
190. U. Lohbauer, *Materials* **2009**, *3*, 76.
191. J. W. Nicholson, *Materials Technology* **2010**, *25*, 8.
192. A. Moshaverinia, N. Roohpour, W. W. L. Chee, S. R. Schricker, *J. Mater. Chem.* **2011**, *21*, 1319.

193. S. K. Sidhu, *Australian Dental Journal* **2011**, *56*, 23.
194. A. Moshaverinia, N. Roohpour, W. W. L. Chee, S. R. Schricker, *J. Mater. Chem.* **2012**, *22*, 2824.
195. N. Suzuki, Y. Morino, Y. Hashiguchi, T. Segawa, US3962267A, **1976**.
196. C. Tezuka, Y. Karasawa, DE2651316A1, **1977**.
197. S. Crisp, A. D. Wilson, K. A. Hodd, GB1507981A, **1978**.
198. J. W. Nicholson, B. Czarnecka, *J. Biomater. Appl.* **2009**, *24*, 293.
199. R. A. Pires, I. Abrahams, T. G. Nunes, G. E. Hawkes, *J. Mater. Chem.* **2009**, *19*, 3652.
200. S. Crisp, M. A. Pringuer, D. Wardleworth, A. D. Wilson, *J. Dent. Res.* **1974**, *53*, 1414.
201. S. Crisp, H. J. Prosser, A. D. Wilson, *J. Mater. Sci.* **1976**, *11*, 36.
202. J. W. Nicholson, P. J. Brookman, O. M. Lacy, A. D. Wilson, *J. Dent. Res.* **1988**, *67*, 1451.
203. A. Kakaboura, G. Eliades, G. Palaghias, *Dent. Mater.* **1996**, *12*, 173.
204. S. Matsuya, T. Maeda, M. Ohta, *J. Dent. Res.* **1996**, *75*, 1920.
205. A. M. Young, *Biomaterials* **2002**, *23*, 3289.
206. A. M. Young, S. A. Rafeeka, J. A. Howlett, *Biomaterials* **2004**, *25*, 823.
207. H. T. Cheng, H. X. Liu, Q. Xiao, *Spectrosc. Spect. Anal.* **2005**, *25*, 1237.
208. W. D. Cook, *J. Biomed. Mater. Res.* **1983**, *17*, 1015.
209. E. A. Wasson, J. W. Nicholson, *Brit. Polym. J.* **1990**, *23*, 179.
210. A. D. Wilson, *J. Mater. Sci. Lett.* **1996**, *15*, 275.
211. E. A. Wasson, J. W. Nicholson, *Clin. Mater.* **1991**, *7*, 289.
212. A. D. Wilson, S. Crisp, G. Abel, *J. Dent.* **1977**, *5*, 117.
213. H. J. Prosser, D. R. Powis, A. D. Wilson, *J. Dent. Res.* **1986**, *65*, 146.
214. A. D. Wilson, *Chem. Soc. Rev.* **1978**, *7*, 265.
215. S. Crisp, B. G. Lewis, A. D. Wilson, *J. Dent.* **1977**, *5*, 51.
216. A. Wilson, S. Crisp, A. Ferner, *J. Dent. Res.* **1976**, *55*, 489.
217. W. D. Cook, *Biomaterials* **1983**, *4*, 85.
218. J. W. Nicholson, *J. Mater. Sci. - Mater. M.* **1996**, *7*, 241.
219. D. C. Smith, *Biomaterials* **1998**, *19*, 467.
220. S. Crisp, B. E. Kent, B. G. Lewis, A. J. Ferner, A. D. Wilson, *J. Dent. Res.* **1980**, *59*, 1055.
221. S. Crisp, B. G. Lewis, A. D. Wilson, *J. Dent. Res.* **1976**, *55*, 1032.
222. W. Schmitt, R. Purrmann, P. Jochum, O. Gasser, EP24056A2, **1981**.
223. A. Jurecic, DE2110665, **1971**.
224. S. B. Mitra, EP323120A2, **1989**.

225. S. B. Mitra, *J. Dent. Res.* **1991**, *70*, 72.
226. N. Suzuki, Y. Morino, Y. Hashiguchi, T. Segawa, US3962267A, **1976**.
227. ISO 4049.2009, *Dentistry - Polymer-based restorative materials.*
228. R. Guggenberger, R. May, K. P. Stefan, *Biomaterials* **1998**, *19*, 479.
229. S. F. Rosenstiel, W. M. Johnston, *J. Prosthet. Dent.* **1988**, *60*, 297.
230. P. Sasanaluckit, K. R. Albustany, P. J. Doherty, D. F. Williams, *Biomaterials* **1993**, *14*, 906.
231. H. Kawahara, Y. Imanishi, H. Oshima, *J. Dent. Res.* **1979**, *58*, 1080.
232. D. R. Powis, T. Follerås, S. A. Merson, A. D. Wilson, *J. Dent. Res.* **1982**, *61*, 1416.
233. A. D. Wilson, H. J. Prosser, D. M. Powis, *J. Dent. Res.* **1983**, *62*, 590.
234. A. Peutzfeldt, *Eur. J. Oral. Sci.* **1997**, *105*, 97.
235. J. L. Ferracane, *Dent. Mater.* **2011**, *27*, 29.
236. F. A. Rueggeberg, *Dent. Mater.* **2011**, *27*, 39.
237. J. E. McKinney, J. M. Antonucci, N. W. Rupp, *J. Dent. Res.* **1987**, *66*, 1134.
238. J. M. Antonucci, J. E. McKinney, J. W. Stansbury, US160856A0, **1988**.
239. S. B. Mitra, S. Mitra, US5154762A, **1992**.
240. J. W. Mays, D. Xie, A. D. Puckett, Jr., WO2003061606A1, **2003**.
241. R. L. Brown, US3066112, **1962**.
242. O. Karahan, K. Aydin, S. Edizer, N. Odabasi, D. Avci, *J. Polym. Sci., Part A: Polym. Chem.* **2010**, *48*, 3787.
243. K. J. Soderholm, A. Mariotti, *J. Am. Dent. Assoc.* **1999**, *130*, 201.
244. R. W. Billington, G. J. Pearson, J. A. Williams, *J. Dent.* **2007**, *35*, 452.
245. C. L. Davidson, A. J. Feilzer, *J. Dent.* **1997**, *25*, 435.
246. H. R. Dewji, J. L. Drummond, S. Fadavi, I. Punwani, *Eur. J. Oral. Sci.* **1998**, *106*, 594.
247. C. A. Khatri, J. W. Stansbury, C. R. Schultheisz, J. M. Antonucci, *Dent. Mater.* **2003**, *19*, 584.
248. C. A. d. S. Costa, A. P. D. Ribeiro, E. M. A. Giro, R. C. Randall, J. Hebling, *Dent. Mater.* **2011**, *27*, e158.
249. S. Akahane, S. Tosaki, Y. Kusayanagi, S. Kusakai, K. Hirota, K. Tomioka, DE3941629A1, **1990**.
250. H. J. Prosser, D. R. Powis, P. Brant, A. D. Wilson, *J. Dent.* **1984**, *12*, 231.
251. D. Xie, J.-G. Park, J. Zhao, *Dent. Mater.* **2007**, *23*, 395.
252. D. Xie, Y. Yang, J. Zhao, J.-G. Park, J.-T. Zhang, *Dent. Mater.* **2007**, *23*, 994.

253. J. Zhao, Y. Weng, D. Xie, *Dent. Mater.* **2009**, *25*, 526.

# 2 Synthesis of linear & branched polyacids via CCTP

This chapter relates to the synthesis of linear and branched polymers based on MAA. Firstly, to aid understanding of multi-detector SEC analysis of non-linear architectures, some theory relating to the coupling of refractive index and viscometry detectors, and the subsequent Universal Calibration, is presented.

The robustness of CCTP involving acidic monomers was investigated, with feed and batch polymerizations conducted in order to ascertain the optimal conditions for the synthesis of low MW PMAAs. This was used as a starting point for studying the CCT copolymerization of PMAA with other monomers. As work then moved toward copolymerization of MAA with AA, some previously published work on the copolymerization of active and non-active CCT monomers is discussed. The copolymers formed were analysed using multi-detector SEC techniques, as non-linear polymer structures have been reported for such systems.

Branched structures were then synthesized *via* the CCT copolymerization of MAA with difunctional EGDMA. The effect of two solvent systems on both the kinetics and the final polymer structure was investigated. The resulting structures were again studied using multi-detector SEC, and their highly-branched structures confirmed. As the levels of vinyl functionality will be key for the photo-curing application described in chapter 3, the numbers of vinyl groups were quantified using a bromine titration methodology.

## 2.1 Characterization techniques for branched polymers

### 2.1.1 Use and limitations of conventional SEC

Conventional size exclusion chromatography (SEC) relies upon the use of calibration standards of peak molecular weight ($M_p$), which are used to produce a plot of log molecular weight (MW) versus retention volume ($V_R$)[1-2]. This is fitted with a polynomial function that can be used to assign a MW to any retention volume within the range of the calibrants used. Due to its simplicity, this is by far the most commonly used form of SEC calibration, but conventional calibration has several limitations that will affect its application to analysis of more complex architectures, particularly copolymers and non-linear structures.

Separation is based on the hydrodynamic volume ($V_h$) of the polymer molecule, rather than its molecular weight.[3] Therefore, in order for an accurate MW to be calculated, the calibration standards should be of the same topology and repeat unit as the analyte, since any change in functionality or architecture would be expected to have some effect on the hydrodynamic volume.[1] Clearly, even if only a few samples of different monomers or architecture are synthesized, a specific calibration for each system would require an extensive set of known MW standards, which may or may not be commercially available, or well defined enough to accurately be used as a calibrant. Therefore, the majority of molecular weight averages quoted in literature will be an apparent value, based on PS, PMMA or PEO standards, giving an approximation of the real MW for the polymers analysed.

Crucially, for the work presented here, different non-linear structures of identical molecular weight and repeat unit will have different hydrodynamic volumes, and therefore different retention volumes[3-6]. The same will also be true for polymers with differing degrees of branching or different types of branching (for example, a star polymer compared to a long chain branched polymer). Therefore a different approach to calibration utilizing two or more detectors, which will be relevant for a larger number of cases, is often necessary for polymers with non-linear structures. Two widely used multi-detector calibrations strategies are Universal Calibration[6-7], which combines a concentration-sensitive detector with a viscometry detector, and Triple Detection[2, 4, 8], which uses concentration, viscometry and light scattering detectors. Due to the insensitivity of light scattering detectors to low molecular weight polymers[9-10], applicability of triple detection to such species is limited. For this reason triple detection will not be discussed in relation to this work.

### *2.1.2 Universal Calibration*

Universal calibration uses a viscometry (VISC) detector along with a concentration-sensitive detector (usually a differential-refractive index, DRI) to give a calibration that is more relevant for a range of topologies, architectures and repeat unit functionality. This method assumes that separation in SEC is dependent only on hydrodynamic volume, which is related to intrinsic viscosity (IV, [η]) and molecular weight by the Einstein viscosity law (Equation 2.1):

$$[\eta] = K\frac{V_h}{M}$$

**Equation 2.1: Where [η] is intrinsic viscosity, $V_h$ is hydrodynamic volume, M is molecular weight and K is a constant whose value is independent of polymer structure.[6]**

This relationship, and the assumption that SEC separates molecules only by their hydrodynamic volume, suggests that plotting log [η].M versus elution volume will be equivalent to a plot of log $V_h$ versus $V_R$, and the calibration curve obtained will be relevant for polymers of different architecture and functionality. The success of universal calibration (while still far from being universal) can be seen in Figure 2.1, showing a plot of log [η].M against $V_R$, in which samples of differing composition, architecture and degrees of branching are fitted well by a single calibration. This technique has proved valid for non-linear polymer topologies ranging from long chain branching seen in polyethylene[11] to hyper-branched poly(methyl methacrylate)[12].

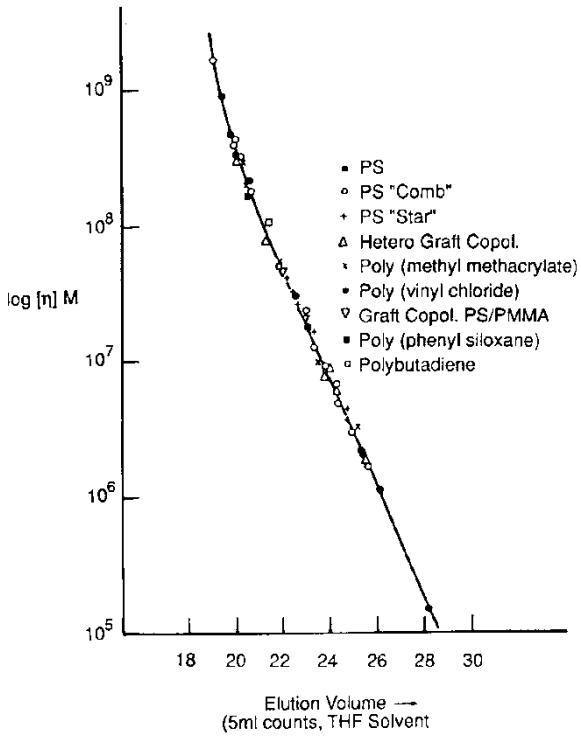


**Figure 2.1: An example of universal calibration, plotting the product of intrinsic viscosity and molecular weight against retention volume for polymer samples of various architectures. Adapted from reference.[6]**

In addition to giving a calibration more relevant to branched structures, viscometry detection can be used to generate Mark-Houwink plots. The Mark-Houwink-Sakurada equation is shown in Equation 2.2:

$$M = K[\eta]^{\alpha}$$

**Equation 2.2: Where M is molecular weight, [η] is intrinsic viscosity and K and α are the Mark-Houwink constants (note that K is not the same constant as appears in Equation 2.1).[2]**

A Mark-Houwink plot is constructed by plotting intrinsic viscosity against MW, on logarithmic scales. This provides a comparison of the intrinsic viscosity across the entire molecular weight distribution (MWD) of the polymer sample. This results in a simple but qualitative method for judging the extent of branching in polymer systems, if a linear standard of similar MW can be used for comparison: a branched polymer will have smaller hydrodynamic volume, and a lower IV than a linear polymer of the same MW, therefore a polymer with consistent branching would be expected to have a lower IV across its entire molecular weight distribution than its linear counterpart.

The slope, α (commonly known as the Mark-Houwink exponent), of a Mark-Houwink plot will give some information on the conformation of the polymer in dilute solution, with Mark-Houwink theory linking α values to different architectures in solution.[2] These are tabulated in Table 2.1, with the relationship between slope of the Mark-Houwink plot and polymer architecture demonstrated in Figure 2.2.

| Architecture | α |
|---|---|
| Rigid rod | - |
| Linear random coil (good solvent) | $0.5 < \alpha < 0.8$ |
| Linear random coil (θ conditions) | 0.5 |
| Random branching (good solvent) | $0.33 < \alpha < 0.5$ |
| Random branching (θ conditions) | 0.33 |
| Hard sphere | 0 |

**Table 2.1: Relationship between fractal dimension, Mark-Houwink exponent *α* and polymer architecture.[2]**

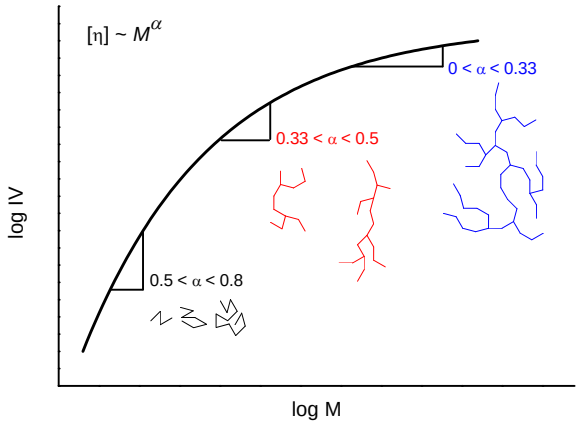


**Figure 2.2: The relationship between the slope of a plot of intrinsic viscosity (IV) against molecular weight (M) to polymer architecture. Adapted from reference.[2]**

The conformation a polymer assumes in dilute solution will be linked to its degree of branching. Linear polymers would be expected to exist as random coils in good solvents, which is indicated by an α value greater than 0.5, implying a constant increase in intrinsic viscosity with molecular weight. With increasing branching in polymer samples with the same molecular weight distribution, the value of α would be expected to decrease, as increasing molecular weight has less influence on hydrodynamic volume, and therefore IV. If branching increases to the point that a polymer system becomes crosslinked, α values tending to zero would be expected, as the molecule becomes more similar to a hard sphere. Generally speaking, a reduction in α for a given molecular weight is indicative of a decrease in the intrinsic viscosity and hydrodynamic volume.

### *2.1.3 Semi-quantitative descriptions of branching by SEC with viscometry detection*

Zimm and Stockmayer used the theory that mean-squared radius of gyration ($R_g^2$) will be decreased as a result of branching[13-14] – a theory that provides the basis for the triple detection method of column calibration – and defined this reduction with the contraction factor, g (Equation 2.3):

$$g = \left[\frac{\left(R_g^2\right)_B}{\left(R_g^2\right)_L}\right]_M$$

**Equation 2.3: The contraction factor g, where subscripts B and L denote the mean-square radius of gyration for branched and linear samples, respectively. Subscript M refers to values of the same molecular weight.[13]**

Since the radius of gyration can only be measured using a multi-angle light scattering (MALS) experiment, which will be difficult to measure at low MWs, a contraction factor can also be measured using viscometry detection. This is defined by the ratios of intrinic viscosities of linear and branched samples, and denoted *g'* (Equation 2.4):

$$g \neq g' = \left[\frac{[\eta]_B}{[\eta]_L}\right]_M \neq \left[\frac{[\eta]_B}{[\eta]_L}\right]_{V_R}$$

**Equation 2.4: The contraction factor *g'*. Note that the ratio of intrinsic viscosities of linear and branched samples with the same molecular weight (subscript M) is *not* equal to the ratio of intrinsic viscosities of linear and branched samples with the same retention volume (subscript $V_R$).[15]**

This method gives an indication of the extent of branching through comparison of a range of polymers to a linear standard, rather than an absolute branching number. While linear polymers should have a *g'* of 1, increasing branching will lead to greater deviation from the viscosity of the linear standard, and therefore a lower *g'* value.

## *2.2 Homopolymerization of methacrylic acid via CCTP*

Catalytic chain transfer polymerization (CCTP) of methacrylic acid (MAA) is not well reported in the academic literature. One article from this research group describes CCTP of various hydrophilic monomers (including MAA, 2-aminoethyl methacrylate hydrochloride, 2-methacryloxyethyl phosphoryl choline and a glyco-monomer) in aqueous solutions and aqueous/alcoholic mixtures[16]. However, this work calculates molecular weights of PMAAs by $^1$H-NMR, with no SEC results, and uses a monomer/CTA feed. Work conducted in this paper was used as a starting point for an investigation into the synthesis of polyacids *via* CCTP.

### *2.2.1 Measurement of $C_s$ for MAA/CoBF*

The paper cited above reports an apparent chain transfer constant ($C_s$), calculated using the Mayo method[17-19], since reactions were performed used a feed of CoBF and monomer.

Therefore, the chain transfer constant for this reaction (Figure 2.4) was measured using the Mayo method in a batch process, in order to measure its true value in our systems. Briefly, polymerizations with four [MAA]/[CoBF] ratios were stopped at very low conversions, in order to minimise termination and keep [monomer]/[CTA] ratios relatively consistent, and the molecular weight measured by SEC (Table 2.2). SEC measured $M_n$ was used to calculate the reciprocal of the degree of polymerization (1/DP).

| Reaction | [CoBF] ($gmol^{-1}$) | [CoBF]/[MAA] | Conversion[a] (%) | $M_n$[b] ($gmol^{-1}$) | 1/DP |
|---|---|---|---|---|---|
| **1A** | $6.06 \times 10^{-7}$ | $5.14 \times 10^{-6}$ | 4.8 | 22,100 | 0.004 |
| **1B** | $1.21 \times 10^{-6}$ | $1.03 \times 10^{-5}$ | 3.3 | 7,200 | 0.012 |
| **1C** | $2.42 \times 10^{-6}$ | $2.06 \times 10^{-5}$ | 2.0 | 2,530 | 0.034 |
| **1D** | $3.03 \times 10^{-6}$ | $2.57 \times 10^{-5}$ | 1.7 | 2,010 | 0.043 |

**Table 2.2: Data for PMAA homopolymerizations 1A-D, with varying [CobF]/[MAA] ratios used to construct Mayo plot (Figure 2.3). [a] Calculated from $^1$H-NMR. [b] Measured by conventional SEC-DRI, with 2 x PLgel mixed D columns, calibrated with PMMA standards, with DMF (1 mM $NH_4BF_4$) as eluent.**

Using the Mayo equation (Equation 2.5), plotting 1/DP against [CoBF]/[MAA] gives a straight line with slope $C_s$ = 1,900 (Figure 2.3). This is greater than the apparent chain transfer constant measured by Haddleton *et al* in 2001, and shows the catalytic CTA used in this work attains the expected reactivity. However, the fitted line shows a y intercept suggesting 1/DP < 0 for low [CoBF]/[MAA] ratios, which is impossible. This could perhaps be explained by error in the $M_n^{SEC}$ used to construct the plot, as the instrument will be calibrated with PMMA, not PMAA.

$$\frac{1}{DP_n} = \frac{1}{DP_n^0} + C_s \frac{[S]}{[M]}$$

**Equation 2.5: The Mayo equation, where $DP_n$ is the degree of polymerization, $DP_n^0$ is the degree of polymerization in the absence of CTA, $C_s$ is the chain transfer constant for transfer to CTA, and [S] and [M] are the concentrations of CTA and monomer, respectively.[18, 20]**

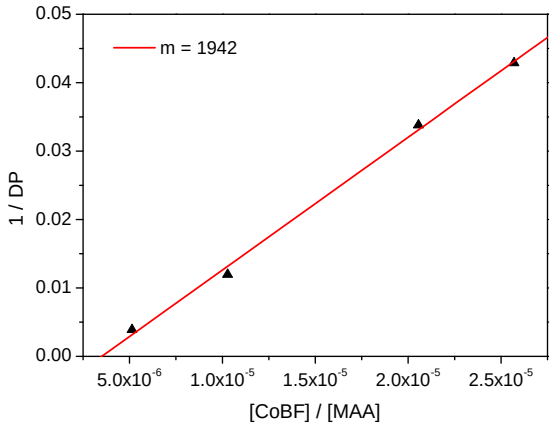


**Figure 2.3: Mayo plot of 1/DP against [CoBF]/[MAA] ratios for PMAA homopolymers 1A-1D (Table 2.2).**

## *2.2.2 Homopolymerization of MAA using CoBF/monomer feed*

Initially, work aimed to synthesize low molecular weight linear poly(methacrylic acid) by varying the ratio of monomer to chain transfer agent (Figure 2.4).

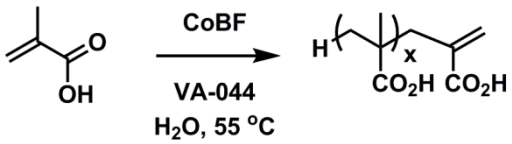


**Figure 2.4: Catalytic chain transfer polymerization of MAA in the presence of CoBF, initiated by VA-044.**

An azo initiator (2,2'-azobis[2-(2-imidazolin-2-yl)propane]dihydrochloride, VA-044) with a relatively low 10 h half-life of decomposition temperature was chosen, in order to give an acceptable rate of conversion at lower temperatures, reducing the rate of hydrolysis of the cobaloxime: it has previously been reported that low pH combined with elevated temperatures can cause hydrolysis at an appreciable rate,[21-22] although the difluoride boron bridging groups do impart some hydrolytic stability[16, 20, 22-24]. Polymerizations were conducted using a feed of monomer and CoBF, as reported previously for emulsion systems.[16] The feed of monomer will replace CoBF destroyed by hydrolysis, as the solution being fed into the reaction will not be at elevated temperature, reducing rate of CoBF hydrolysis. A schematic for the reaction set up utilizing a monomer/CoBF feed is shown in Figure 2.5.

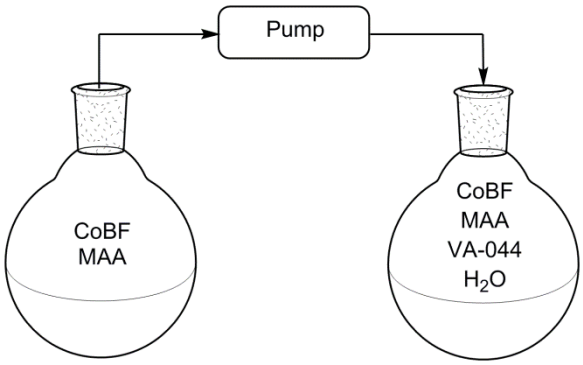


**Figure 2.5: Schematic of the reaction set up for the monomer/CTA feed polymerizaton of methacrylic acid *via* CCTP. The contents of the left-hand flask are fed into the reaction vessel (right-hand flask) over a period of several hours (see Table 2.3).**

All reactions reach high conversion (> 95 %) but give relatively broad dispersities and asymmetric MWDs (Table 2.3). The effect of increasing the concentration of CoBF is as expected, reducing the molecular weight of the final polymer in a controlled fashion. The SEC traces (Figure 2.6) show some tailing to low molecular weight, indicating a significant change in CoBF concentration (relative to monomer) during the polymerization, likely due to the unoptimised feed conditions.

| Reaction | [MAA]/[CoBF] | Feed time (h) | $M_w$ [a] ($gmol^{-1}$) | $Đ$ [a] | Conversion [b] (%) | Time (h) |
|---|---|---|---|---|---|---|
| **2** | 99,000 | 1.5 | 14,000 | 2.02 | > 99 | 24 |
| **3** | 62,700 | 2.5 | 8,900 | 2.32 | 98.5 | 24 |
| **4** | 31,000 | 2.5 | 6,240 | 2.03 | 96.9 | 22 |
| **5** | 16,000 | 2.5 | 3,540 | 1.54 | 97.6 | 22 |

**Table 2.3: Data for MAA homopolymerizations 2-5 utilizing a monomer/CTA feed, with varying [MAA]/[CoBF] ratio. [a] Measured by conventional SEC-DRI, with 2 x PLgel mixed D columns, calibrated with PMMA standards, with DMF (1 mM $NH_4BF_4$) as eluent. [b] Measured by GC-FID.**

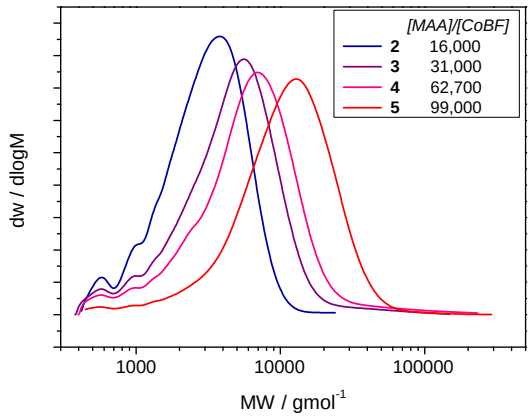


**Figure 2.6: SEC molecular weight distributions for MAA homopolymers 2-5, with [MAA]/[CoBF] ratios between 16,000 and 99,000, prepared under feed conditions (Table 2.3).**

It was thought that some drift in molecular weight throughout the polymerization, due to the change in [CoBF]/[MAA] ratio during and after the feed, could be the cause of the low molecular weight tailing, as explained by the second term on the RHS of Mayo equation (Equation 2.5) – MW will be controlled by the ratio of [monomer] to [CTA]. Therefore, the molecular weight was monitored by SEC at various points over the course of the polymerization. The evolution of the molecular weight distribution (Figure 2.7) shows a clear drift in the molecular weight, with a bimodal MWD during the 3 hour feed, with the final molecular weight distribution mono-modal but with considerable tailing to low MW.

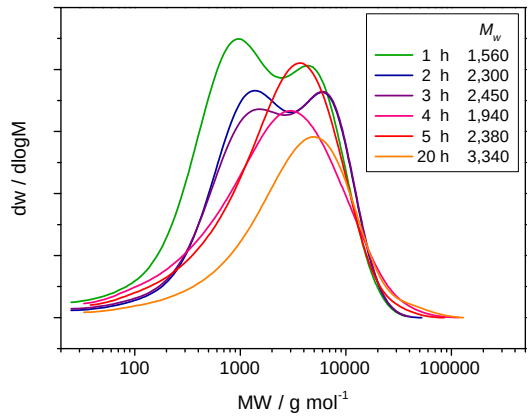


**Figure 2.7: Evolution of SEC molecular weight distribution throughout polymerization 6 of MAA, utilizing a 3 h monomer/CoBF feed.**

It was decided that polymerizations under batch conditions may lead to less drift in molecular weight and yield more well-defined polymers, without the need to optimize feed conditions.

### *2.2.3 Batch homopolymerization of MAA by CCTP*

Homopolymerizations of methacrylic acid using similar [CoBF] to [monomer] ratios as the feed reactions (as detailed in section 2.2.2) were carried out in batch conditions, and show a consistent molecular weight over the course of the polymerizations (Figure 2.8-2.12). As can be seen in the SEC traces, very little drift in MW occurs, with the $M_w$ of polymer produced at each sample time being within 10 % of the MW of the final polymer in all cases except reaction **11** (Figure 2.12), with [monomer] to [CoBF] ratio of 16,000. The production of polymer with very consistent molecular weight over the course of the reaction can be understood by the fact that the molecular weight of the polymer produced throughout the reaction is controlled by [CoBF]/[monomer]. Serendipitously, it appears that the acidic conditions cause degradation of the CTA at a similar rate to the consumption of the monomer, resulting in a constant ratio of reagents.

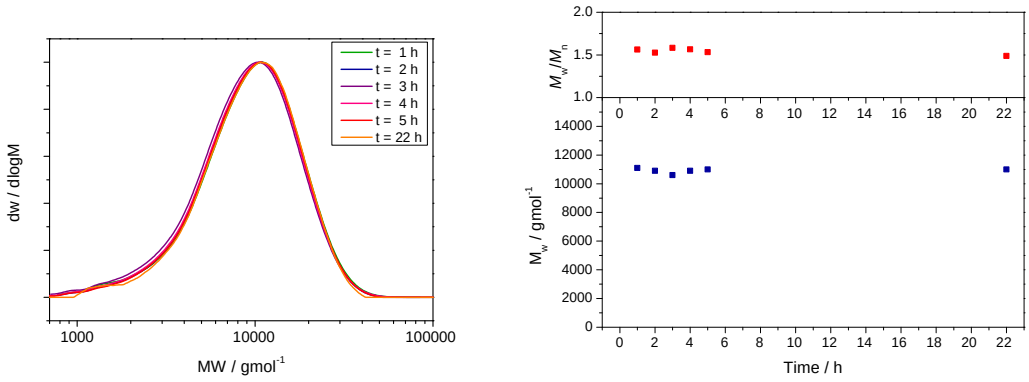


**Figure 2.8: Evolution of molecular weight distributions throughout MAA homopolymerization 7, with [MAA]/[CoBF] ratio = 100,000 (left). Evolution of $M_w$ and dispersity, measured by conventional SEC, throughout homopolymerization 7 (right).**

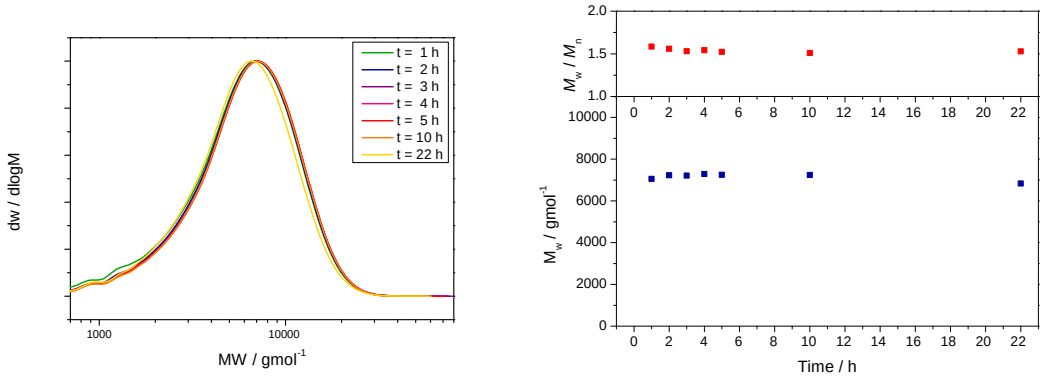


**Figure 2.9: Evolution of molecular weight distributions throughout MAA homopolymerization 8, with [MAA]/[CoBF] ratio = 50,000 (left). Evolution of $M_w$ and dispersity, measured by conventional SEC, throughout homopolymerization 8 (right).**

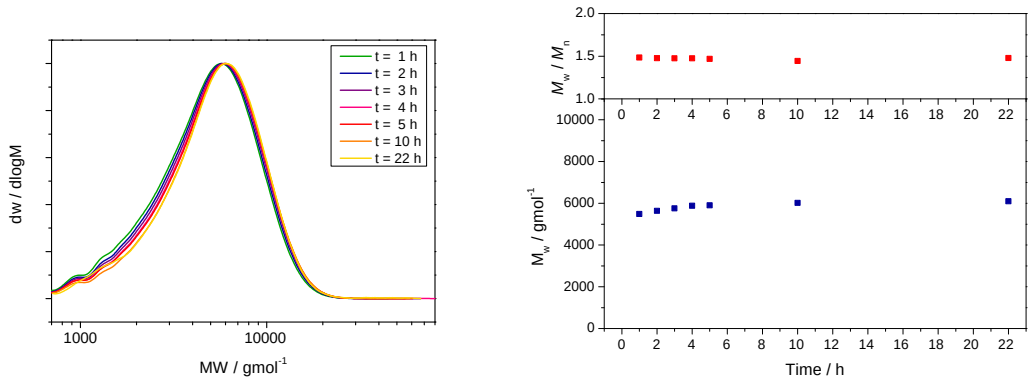


**Figure 2.10: Evolution of molecular weight distributions throughout MAA homopolymerization 9, with [MAA]/[CoBF] ratio = 32,000 (left). Evolution of $M_w$ and dispersity, measured by conventional SEC, throughout homopolymerization 9 (right).**

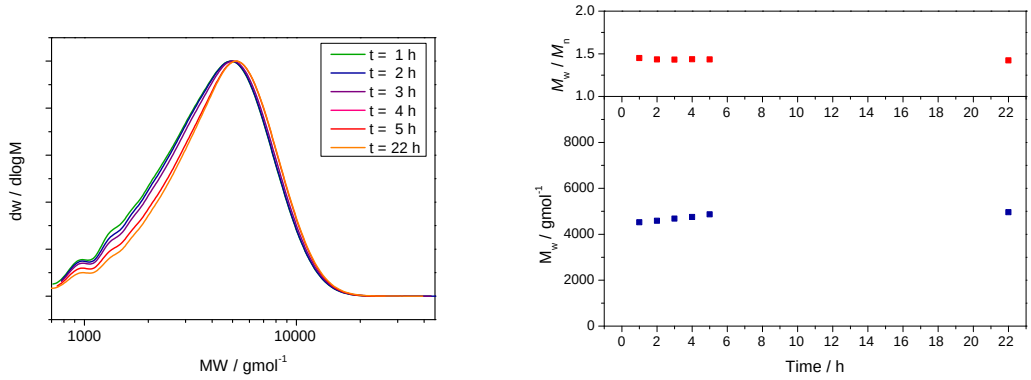


**Figure 2.11: Evolution of molecular weight distributions throughout MAA homopolymerization 10, with [MAA]/[CoBF] ratio = 25,000 (left). Evolution of $M_w$ and dispersity, measured by conventional SEC, throughout homopolymerization 10 (right).**

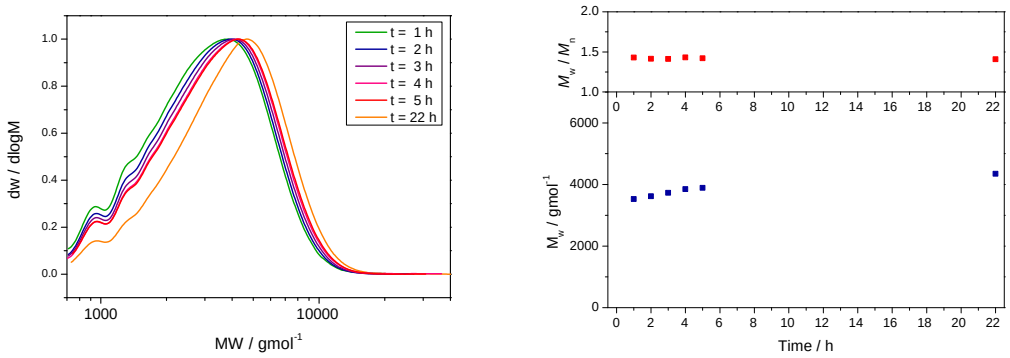


**Figure 2.12: Evolution of molecular weight distributions throughout MAA homopolymerization 11, with [MAA]/[CoBF] ratio = 16,000 (left). Evolution of $M_w$ and dispersity, measured by conventional SEC, throughout homopolymerization 11 (right).**

Data comparing all [MAA]/[CoBF] ratios is shown in Figure 2.13, with data summarized in Table 2.4. Increasing the CoBF concentration has the expected effect of decreasing molecular weight, providing a reliable means of controlling the molecular weight of the polymer produced. Increasing the concentration of CoBF causes a small increase in the dispersity of the final polymer, although all products show a narrower dispersity than would be expected for a free radical polymerization.

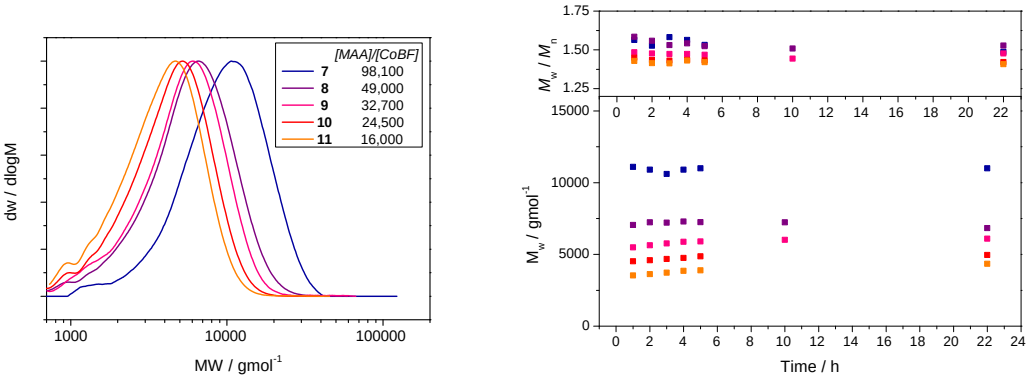


**Figure 2.13: Comparison of SEC molecular weight distributions for MAA homopolymerizations 7-11, varying [MAA]/[CoBF] ratio (left). Comparison of $M_w$ and dispersity, measured by conventional SEC, throughout homopolymerizations 7-11 (right).**

| Reaction | [MAA]/[CoBF] | $M_w$ [a] ($gmol^{-1}$) | $Đ$ [a] | Conversion [b] (%) | Time (h) |
|---|---|---|---|---|---|
| **7** | 98,100 | 11,000 | 1.49 | 99.6 | 22 |
| **8** | 49,000 | 6,840 | 1.53 | 99.1 | 22 |
| **9** | 32,700 | 6,100 | 1.48 | 98.9 | 22 |
| **10** | 24,500 | 4,960 | 1.42 | 97.5 | 22 |
| **11** | 16,000 | 4,350 | 1.41 | 97.5 | 22 |

**Table 2.4: Data for batch MAA homopolymerizations 7-10, with variation of [MAA]/[CoBF] ratio. [a] Measured by conventional SEC-DRI, with 2 x PLgel mixed D columns, calibrated with PMMA standards, with DMF (1 mM $NH_4BF_4$) as eluent. [b] Measured by GC-FID.**

The concentration of CoBF shows no significant effect on the final conversion of the polymerizations, with all reactions reaching conversions above 97 % in 22 h (Figure 2.14). The polymerization with the highest concentration of CoBF (**11**) does show slightly slower conversion than the other polymerizations. This is unexpected since concentration of a CTA should in theory have no effect on the rate of propagation, and this trend is not seen throughout the polymerizations with varying [MAA]/[CoBF] ratios.

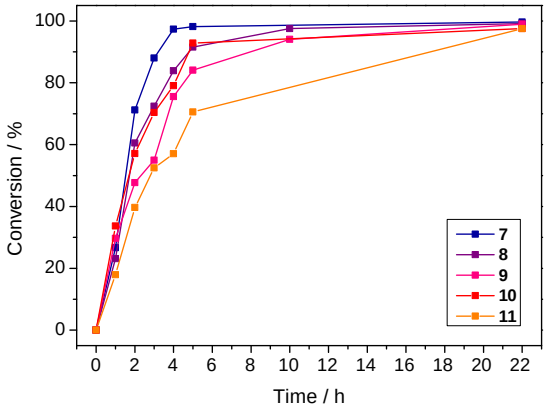


**Figure 2.14: Conversion, measured by GC-FID, throughout MAA homopolymerizations 7-11.**

Data for feed and batch type polymerizations with similar monomer to CoBF ratios are shown in Table 2.5. The batch polymers show lower dispersity in all cases, due to a reduced drift in the molecular weight throughout the process. These results show that batch polymerization is indeed the optimal process for synthesis of low molecular weight PMAA *via* CCTP.

| Reaction | Type (Feed time) | [MAA]/[CoBF] | $M_n$ [a] ($gmol^{-1}$) | $M_w$ [a] ($gmol^{-1}$) | $Đ$ [a] | Conversion [b] (%) |
|---|---|---|---|---|---|---|
| **2** | Feed (1.5 h) | 98,500 | 6,940 | 14,000 | 2.02 | > 99 |
| **7** | Batch | 99,000 | 7,450 | 11,100 | 1.49 | > 99 |
| **4** | Feed (2.5 h) | 32,100 | 3,080 | 6,240 | 2.03 | 96.9 |
| **9** | Batch | 32,700 | 4,120 | 6,100 | 1.48 | 98.9 |
| **5** | Feed (2.5 h) | 16,000 | 2,300 | 3,540 | 1.54 | 97.6 |
| **11** | Batch | 16,000 | 3,090 | 4,350 | 1.41 | 97.5 |

**Table 2.5: Comparison of data for monomer/CTA feed and batch homopolymerizations of MAA, with similar [CoBF]/[MAA] ratios between polymers 2 and 7, 4 and 9, 5 and 11. [a] Measured by conventional SEC-DRI, with 2 x PLgel mixed D columns, calibrated with PMMA standards, with DMF (1 mM $NH_4BF_4$) as eluent. [b] Measured by GC-FID.**

The structure of the PMAAs synthesized by CCTP were investigated with NMR and soft-ionization mass spectrometry (MS). $^1$H-NMR analysis (Figure 2.15) confirms the expected structure for linear PMAA, with the peaks at 6.2 and 5.6 ppm revealing a high level of vinyl functionality at the chain ends.

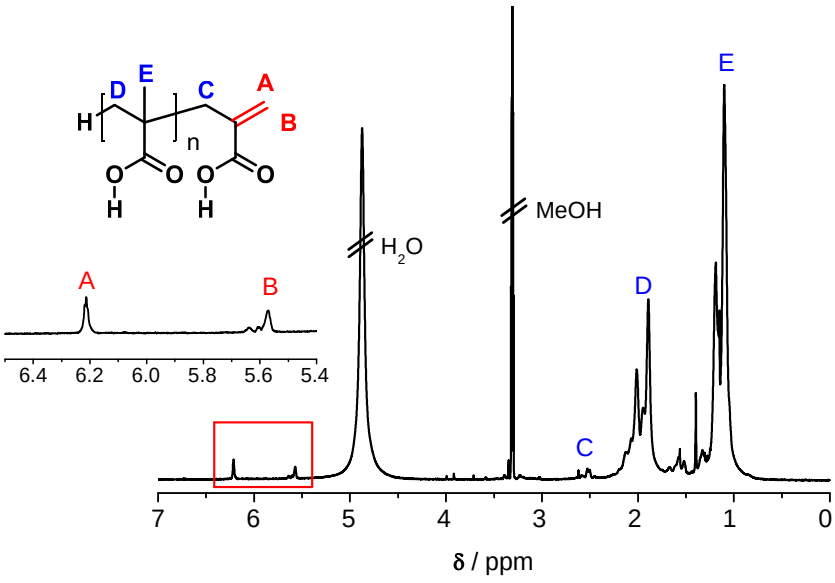


**Figure 2.15: Typical $^1$H-NMR spectrum of PMAA synthesized by CCTP, with characteristic vinyl signals at 6.20 and 5.58 ppm shown in expansion (NMR solvent - methanol-$d_4$).**

Mass spectrometry using soft ionization techniques, such as MALDI- (matrix-assisted laser desorption/ionization) or ESI-TOF (electrospray ionization, time of flight detection), will often give information about the molecular weight distribution. However, for CCTP systems quantitative informtion can rarely be obtained, even for relatively simple homopolymer systems, due to the broad dispersities encountered. MALDI and ESI are both subject to high molecular weight discrimination, with a large bias toward detection of low molecular weight species. The ESI-TOF-MS spectrum of **10** (Figure 2.17) shows the decay in number average MWD expected for chain transfer dominated reactions with broad dispersity (rather than the Gaussian distributions expected for controlled or living techniques), suggesting that chain transfer is the prevalent mode of chain termination[17, 19]. Despite the very low molecular weights (up to around 8 monomer units) detected, the spectrum will give some information about the molecular structure of the polymer formed.

As decribed in Chapter 1, initiation of polymer chains in CCTP can occur *via* two processes; either conventional free radical initiation from an azo initiator derived fragment, or a second initiation process from a cobalt(III) hydride subsequent to chain transfer (Figure 2.16).

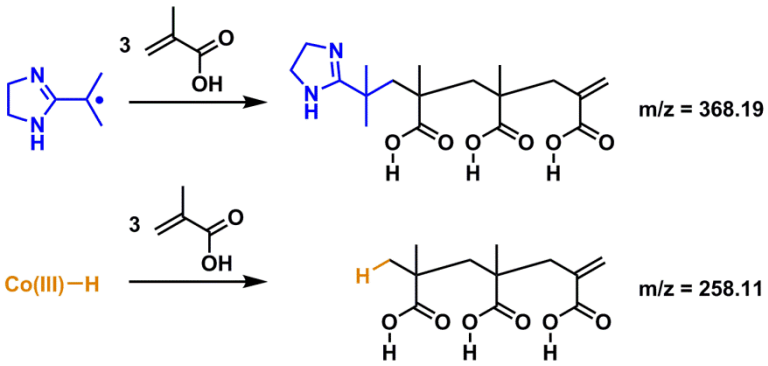


**Figure 2.16: Azo intiator (VA-044) fragment initiated MAA trimer, terminated by CCT (top) and cobalt(III) hydride initiated MAA trimer, terminated by CCT (bottom).**

The ESI-TOF-MS spectrum of **10** (Figure 2.17) shows no clear evidence of a polymeric distribution initiated by a VA-044 fragment, with the main distribution showing Co(III)-H initiation and the CCT vinyl group at all DPs. However, it should be noted that due to the semi-quantitative nature of ESI, this should not be interpreted as 100 % of polymer chains being initiated by cobalt hydride. The main distribution in the spectrum corresponds well with the calculated m/z values for each DP (Table 2.6) with ionization *via* loss of a proton (ESI experiment conducted in negative mode). Calculating theoretical isotopic abundances for each peak series in this distribution reveals high levels of vinyl functionality, with the

abundance of the saturated peak (m/z + 2) within experimental error of those calculated for the unsaturated, CCT derived vinyl end group indicating near perfect end group fidelity. While this does suggest the expected high levels of vinyl functionality associated with CCTP, it is very likely that this technique has underestimated the number of polymer end groups saturated by radical termination reactions, and such high end group fidelity would certainly not be expected for a free radical system.

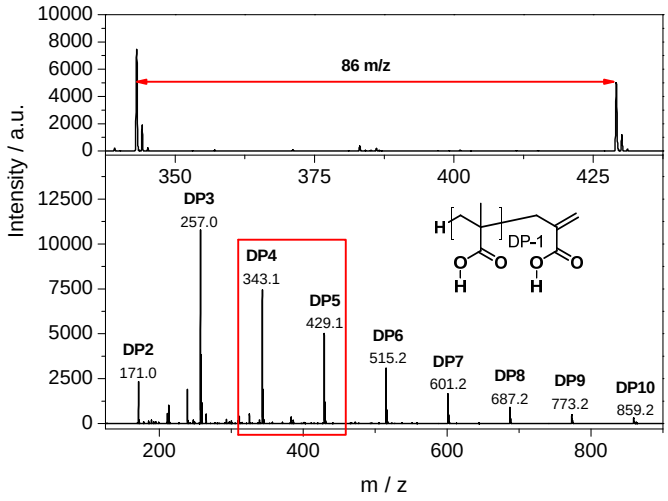


**Figure 2.17: ESI-TOF (negative mode) mass spectrum of PMAA homopolymer 10, with main peak distribution corresponding to the MAA repeat unit (86.09, Table 2.6).**

| Calc. mass $[M\text{-}H]^-$ | Obs. m/z | Assignment |
|---|---|---|
| **171.07** | 171.0 | Co(III)-H initiated, CCT end group - **DP2**, $C_4H_7O_2\,C_4H_5O_2$ |
| **257.10** | 257.0 | Co(III)-H initiated, CCT end group - **DP3**, $C_4H_7O_2\,C_4H_6O_2\,C_4H_5O_2$ |
| **343.14** | 343.1 | Co(III)-H initiated, CCT end group - **DP4**, $C_4H_7O_2\,(C_4H_6O_2)_2\,C_4H_5O_2$ |
| **429.18** | 429.1 | Co(III)-H initiated, CCT end group - **DP5**, $C_4H_7O_2\,(C_4H_6O_2)_3\,C_4H_5O_2$ |
| **515.21** | 515.2 | Co(III)-H initiated, CCT end group - **DP6**, $C_4H_7O_2\,(C_4H_6O_2)_4\,C_4H_5O_2$ |
| **601.25** | 601.2 | Co(III)-H initiated, CCT end group - **DP7**, $C_4H_7O_2\,(C_4H_6O_2)_5\,C_4H_5O_2$ |
| **687.29** | 687.2 | Co(III)-H initiated, CCT end group - **DP8**, $C_4H_7O_2\,(C_4H_6O_2)_6\,C_4H_5O_2$ |
| **773.32** | 773.2 | Co(III)-H initiated, CCT end group - **DP9**, $C_4H_7O_2\,(C_4H_6O_2)_7\,C_4H_5O_2$ |
| **859.34** | 859.2 | Co(III)-H initiated, CCT end group - **DP10**, $C_4H_7O_2\,(C_4H_6O_2)_8\,C_4H_5O_2$ |

**Table 2.6: Calculated mass and observed m/z values (assumed z = 1) for major peak series in MAA homopolymerization up to DP 10, initiated with Co(III)-H and terminated by CoBF mediated CCT, yielding unsaturated vinyl end group.**

## *2.3 Copolymerization of methacrylic acid with acrylic acid*

Since acrylic acid is less expensive than methacrylic acid, it would be favourable for an industrially relevant process to incorporate this monomer in as high a content as possible. Acrylates give poor activity in the CCTP process[20], with the Co-C bond formed at the end of the propagating chain, prior to chain transfer, far stronger than in the case of methacrylic monomers due to reduced steric hindrance with the secondary carbon[25-26]. This has the effect of temporarily reducing the concentration of the Co(II) catalyst in the cycle, reducing the frequency of chain transfer and lowering the chain transfer constant by several orders of magnitude.[27] Several methods have been developed, particularly by Moad, Rizzardo and Thang, requiring elevated temperatures to facilitate breaking of the Co-C bond, leading to an increased rate of β-scission and subsequent molecular weight reduction.[28-29] Homopolymerization of acrylic acid to form relatively low MW species *via* CCTP will be un-desirable, since molecular weight control of this system would likely require unfavourably high concentrations of CTA, which would prove expensive and leave higher levels of metallic residues. Additionally, the unsaturated terminal groups resulting from chain transfer would be internal, rather than the external double bonds produced when methacrylates are used. Formation of internal double bonds will be less favourable and the resulting groups will be much less reactive for steric and electronic reasons. This would lead to polymers without the reactive vinyl functionality CCTP of α-methyl monomer affords, reducing their potential for post-polymerization modification.

It has been shown that acrylic monomers can be copolymerized with CCT-active α-methyl monomers, with an associated decrease in the chain transfer constant[30], with the resulting macromolecules pre-dominantly terminated with a methacrylate-derived vinyl end group (since chain transfer is orders of magnitude faster in methacrylic species). However, studies of methacrylic acid/acrylic acid free radical copolymerization in polar solvents give unfavourable reactivity ratios, with $r_{MAA} > 1$ and $r_{AA} << 1$.[31-32] This suggests that if the system behaves as a free radical system, methacrylic acid homopolymers will be formed initially, with a compositional drift towards polyacrylic acid when conversion of methacrylic acid is high.[33]

Key to an efficient CCTP process forming linear structures is that propagating radicals do not react with the chain transfer derived vinyl end group, as this would lead to a graft-like morphology.[20] This will be the case for the more sterically hindered methacrylate-derived tertiary radical, but acrylate-derived secondary radicals are capable of propagating with

acrylate, methacrylate and alkacrylate double bonds[20, 25, 34], suggesting that CCT copolymerization of methacrylic acid with acrylic acid may lead to non-linear structures under some conditions (Figure 2.18). Indeed, many polymerizations involving both active (tertiary radical generating, generally) and inactive (secondary radical generating) CCT monomers result in complex systems, often giving a range of linear and grafted/branched products.

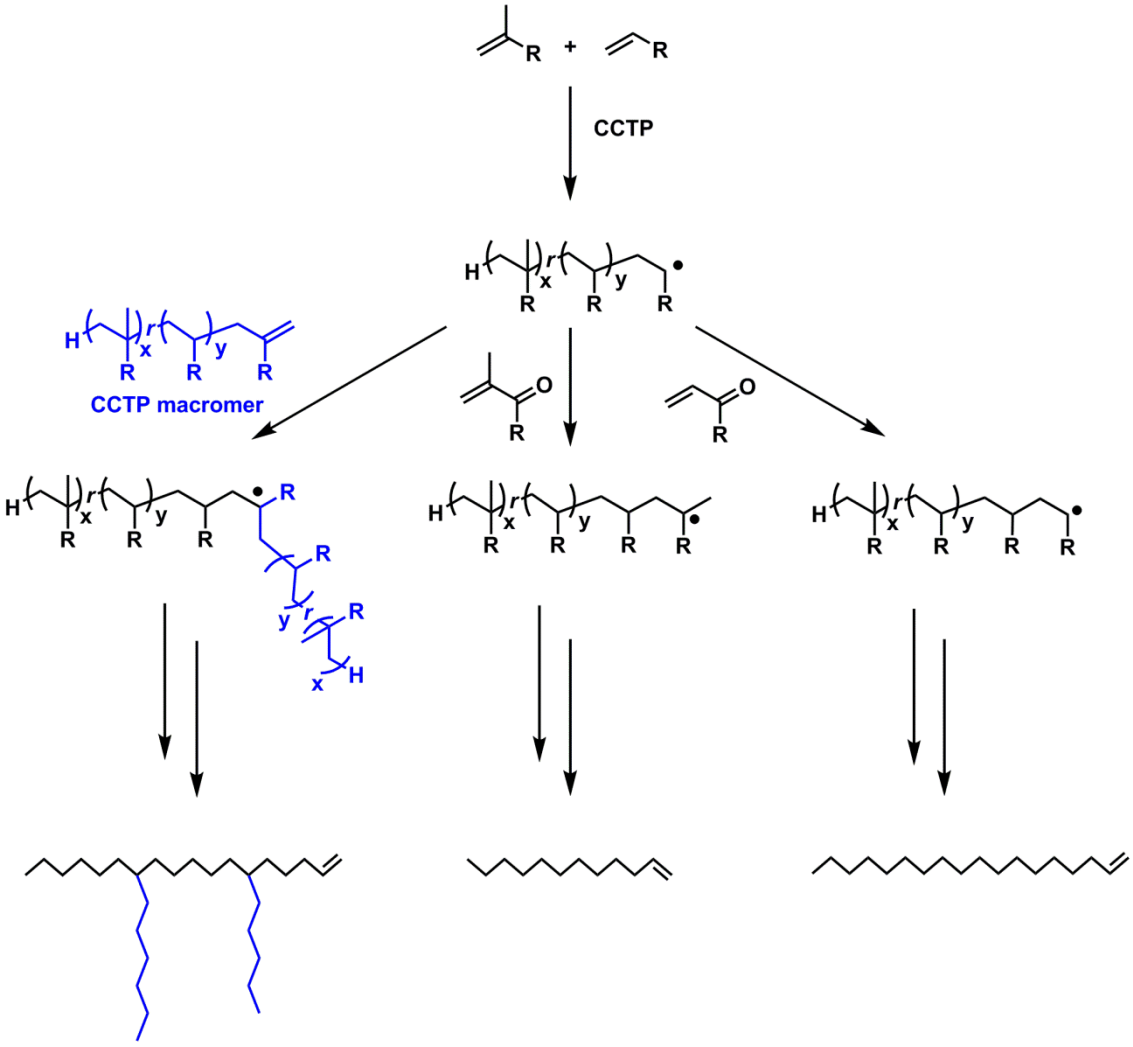


**Figure 2.18: Outcomes of acrylate-derived radicals propagating with macro-monomers, methacrylates and acrylates: Propagation of macro-monomer leads to grafting (left), low incorporation of acrylic species will give lower DP (middle) and high incorporation of acrylic species will lead to higher DP (right).**

In order to investigate the efficiency of CCTP copolymerization incorporating a less CCT active monomer, polymerizations of methacrylic acid with 10, 20 and 30 w. % acrylic acid (Figure 2.19, Table 2.7) were performed with consistent monomer to CoBF ratios. The corresponding SEC molecular weight evolutions are shown in Figure 2.20-Figure 2.22.

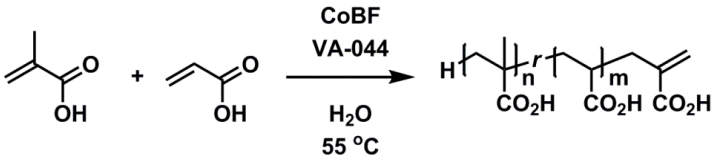


**Figure 2.19: Copolymerization of methacrylic acid and acrylic acid *via* CCTP, initated by VA-044.**

| Reaction | [MAA]/[CoBF] | [acrylic acid] (w. %) | $M_w$ [a] ($g\ mol^{-1}$) | $Đ$ [a] | Conversion [b] (%) | Reaction time (h) |
|---|---|---|---|---|---|---|
| **10** | 25,500 | 0 | 4,960 | 1.42 | > 99 | 22 |
| **12** | 25,500 | 10 | 8,840 | 1.51 | > 99 | 22 |
| **13** | 25,500 | 20 | 32,200 | 2.22 | 98.9 | 22 |
| **14** | 25,500 | 30 | 90,000 | 5.29 | 97.5 | 22 |

**Table 2.7: Data for MAA homopolymerizations and MAA/AA copolymerizations conducted with constant monomer to CoBF ratio, varying AA concentration. [a] Measured by conventional SEC-DRI, with 2 x PLgel mixed D columns, calibrated with PMMA standards, with DMF (1 mM $NH_4BF_4$) as eluent. [b] Measured by GC-FID.**

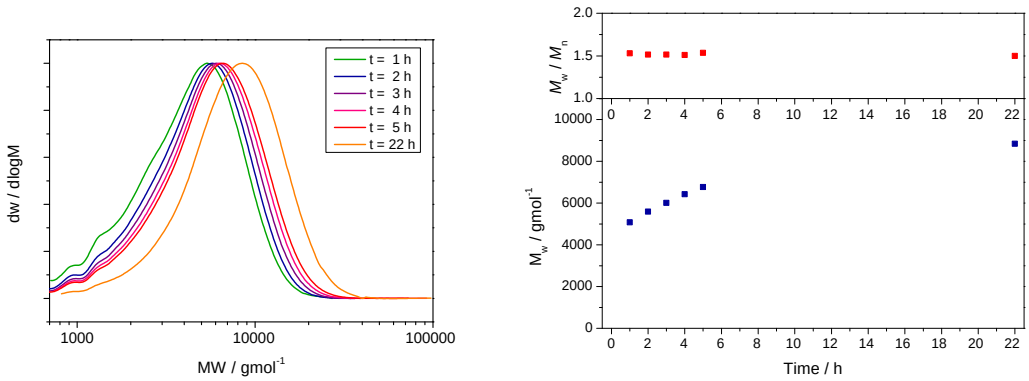


**Figure 2.20: Evolution of molecular weight distributions throughout copolymerization 12, with 10 w. % AA and [monomer]/[CoBF] ratio = 25,500 (left). Evolution of $M_w$ and dispersity, measured by conventional SEC, throughout copolymerization 12 (right).**

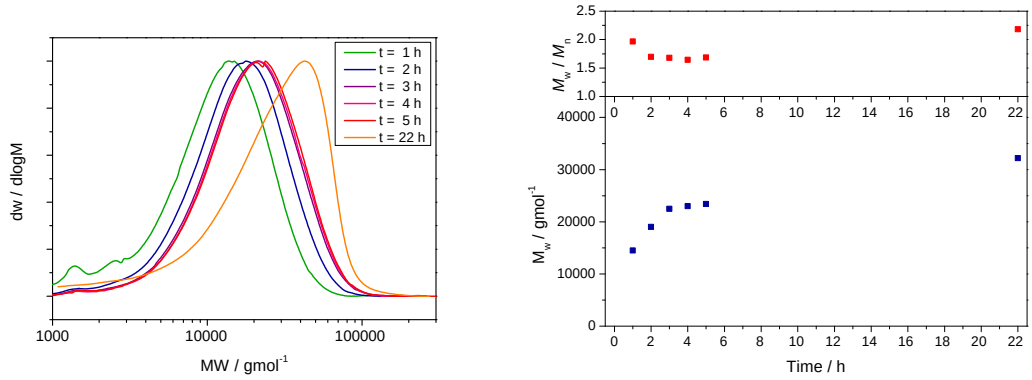


**Figure 2.21: Evolution of molecular weight distributions throughout copolymerization 13, with 20 w. % AA and [monomer]/[CoBF] ratio = 25,500 (left). Evolution of $M_w$ and dispersity, measured by conventional SEC, throughout copolymerization 13 (right).**

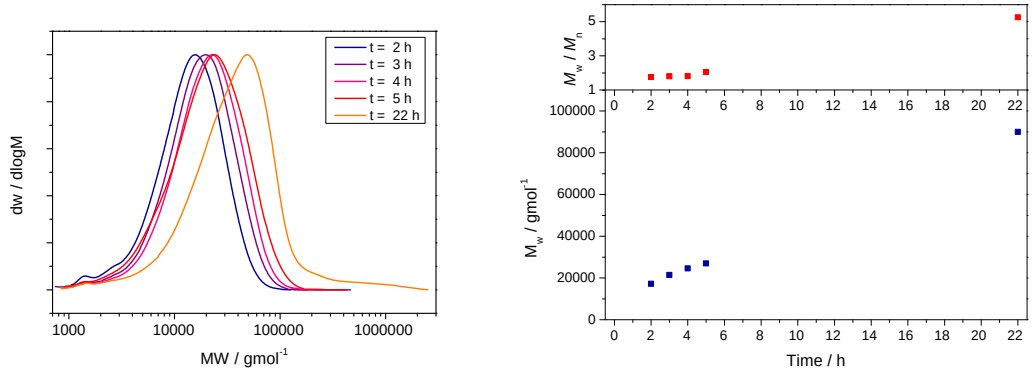


**Figure 2.22: Evolution of molecular weight distributions throughout copolymerization 14, with 30 w. % AA and [monomer]/[CoBF] ratio = 25,500 (left). Evolution of $M_w$ and dispersity, measured by conventional SEC, throughout copolymerization 14 (right).**

Comparison of the final polymers produced with 0-30 w. % AA (Figure 2.23) clearly shows the effect of increasing acrylic acid concentration is to increase the molecular weight and broaden the dispersity.

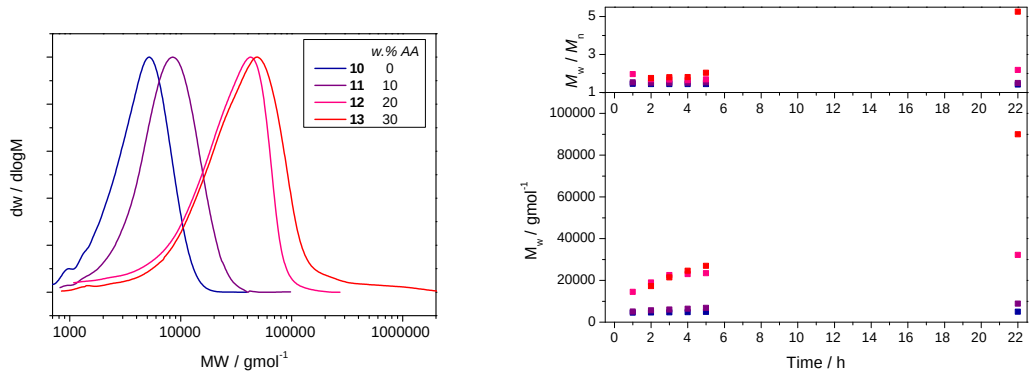


**Figure 2.23: Comparison of molecular weight distributions for MAA homopolymerization 10 and MAA/AA copolymers 12-14, increasing AA concentration from 0 – 30 w. % (left). Comparison of $M_w$ and dispersity throughout homopolymerization 9 and copolymerizations 12-14 (right).**

In contrast to homopolymerization of PMAA (**9**), the molecular weight of the polymer formed throughout the copolymerizations increases over time in all cases. This can be attributed to several factors: firstly, conversion data (Figure 2.24 and Figure 2.26) for the two monomers shows that nearly all of the methacrylic acid is consumed early in the reaction, whilst acrylic acid conversion remains very low until methacrylic acid concentration is considerably reduced. This suggests that the previously quoted free radical reactivity ratios do hold under CCT conditions, in accordance with CCTP being a free radical process. Since lower chain transfer frequency is expected for acrylic acid, if MAA homopolymerization dominates the early stages of the polymerization, the molecular weight would be expected to be low, with molecular weight increasing as more acrylic acid propagates and chain transfer frequency is reduced. Conversions also show that acrylic acid consumption largely occurs after approximately 5 hours, which would explain the relatively large increase the molecular weight seen after this time. Secondly, it would be expected that as more AA is incorporated into the polymer chains produced, the likelihood of propagating acrylate radicals reacting with alkacrylate end groups will increase, resulting in the formation of some grafted structures. This may explain the high molecular weight (> 90 $kgmol^{-1}$, with $Đ$ > 5) polymer produced in reaction **14**, containing 30 w. % AA. This possibility has been investigated by SEC-DRI-VISC analysis in the next section.

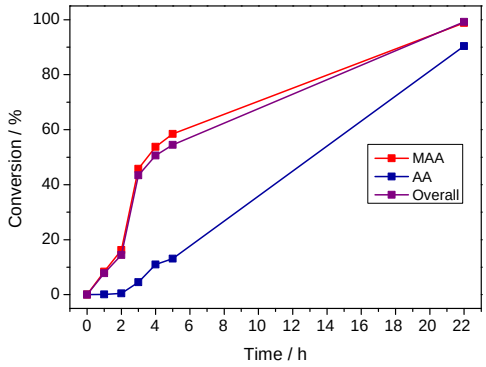


**Figure 2.24: Conversion, measured by GC-FID, throughout copolymerization 12 with 10 w. % AA and monomer to CoBF ratio 25,500.**

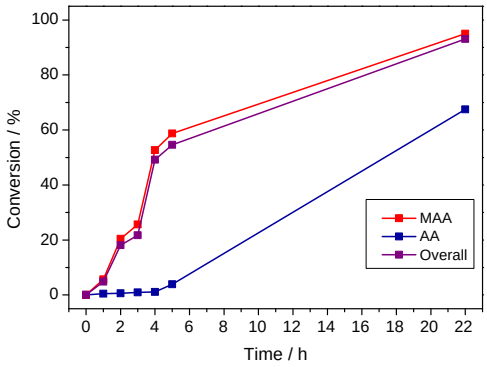


**Figure 2.25: Conversion, measured by GC-FID, throughout copolymerization 13 with 20 w. % AA and monomer to CoBF ratio 25,500.**

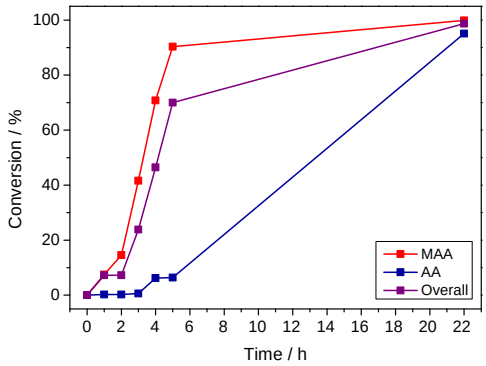


**Figure 2.26: Conversion, measured by GC-FID, throughout copolymerization 14 with 30 w. % AA and monomer to CoBF ratio 25,500.**

Conversion for copolymerization **14** with 30 w. % acrylic acid shows a significantly increased rate of monomer consumption relative to copolymerizations **12** and **13**. This could be attributed to the viscosity of the reaction mixture, which increases with increasing AA concentration, due to rate acceleration and the Tromsdorff effect.[35]

### *2.3.1 Multi-detector SEC analysis of copolymers with acrylic acid*

P(MAA-*co*-AA) copolymers **12** and **13** were analysed by SEC-RI-VISC, along with PMAA **7**, using universal calibration, in order to generate Mark-Houwink plots (Figure 2.27).

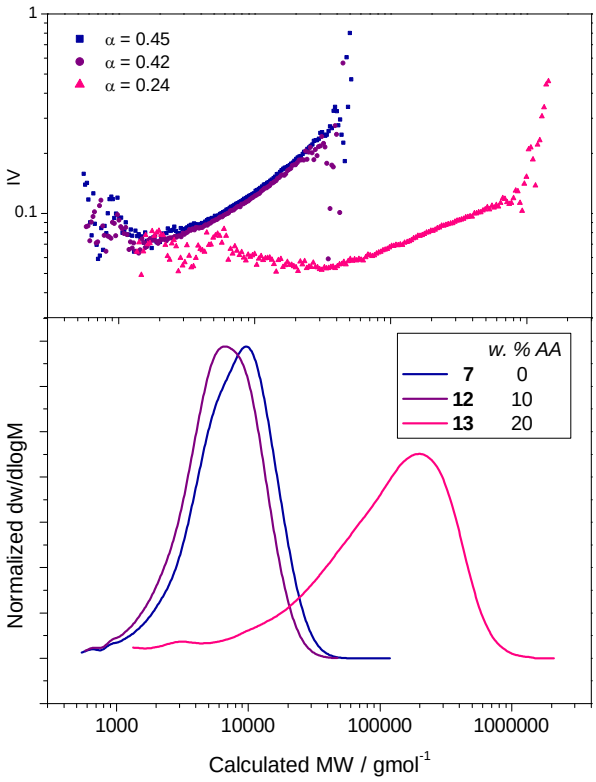


**Figure 2.27: SEC-DRI-VISC calculated molecular weight distributions (lower pane) and Mark-Houwink plots of IV vs MW (upper pane) for P(MAA-*co*-AA) copolymers 12-13, compared to PMAA homopolymer 7.**

The PMAA homopolymer and copolymer **12** (with 10 w. % AA) have very similar IV values throughout the MWDs, whereas copolymer **13** clearly shows a far lower IV in the region of overlapping MWs (ideally, polymers compared would have the same $M_w$, and overlap near the centre of the distributions). This suggests a reduced hydrodynamic volume across the molecular weight distribution of copolymer **13** relative to the linear homopolymer, indicative of branching and non-linear architecture. Comparison of α values mirrors this trend, with **7**

and **12** showing values close to those expected for linear polymers. Conversely, the α value obtained for copolymer **13** shows a clear decrease from linear PMAA **7**, again suggesting a decrease in hydrodynamic volume caused by branching.[1-2, 6-7, 13, 15]

| Reaction | [M]/[CoBF] | [AA] (mol. %) | $M_w$ [a] ($gmol^{-1}$) | $Đ$ [a] | α [a] | $g'$ [a] |
|---|---|---|---|---|---|---|
| **7** | 98,100 | 0 | 9,170 | 1.67 | 0.45 | 0.95 |
| **12** | 25,500 | 11.8 | 20,400 | 5.39 | 0.40 | 0.92 |
| **13** | 25,500 | 23.2 | 108,000 | 30.18 | 0.24 | 0.16 |

**Table 2.8: Compositions, monomer/CTA ratios and SEC-DRI-VISC data for PMAA homopolymer 7 and P(MAA-*co*-AA) copolymers 12 and 13.**

It should be noted that the α value for PMAA **7** differs from the expected value. According to theory[1, 4, 36] α values of ≥ 0.5 should be expected for linear polymers, rather than the measured value of α = 0.45. This could be attributed to the limited applicability of universal calibration and Mark-Houwink theory to polymers of low molecular weight, as well as solvent effects. Examples of deviation from the linear relationship of log [η] and log M at molecular weights of < 10,000 g $mol^{-1}$ have been reported[7, 36-38], and several methods have been used to correct the relationship between intrinsic viscosity and molecular weight in order to increase its relevance at low molecular weights. These include equations developed by Benoit and Dondos (Equation 2.6)[7], Sadron and Rempp (Equation 2.7)[38] and Stockmayer and Fixman (Equation 2.8)[39]. However, the equations used in these methods require knowledge of a range of constants relating to polymer-solvent interactions. These values are quoted in the literature for very few systems and are non-trivial to measure. While α values calculated in this work do show some deviation from theory, it is still expected that a trend of decreasing α values with decrease in hydrodynamic volume, indicative of increased branching, would be apparent and relevant.

$$\frac{1}{[\eta]} = -A_2 + \frac{A_1}{M^{1/2}}$$

**Equation 2.6: Benoit-Dondos equation, where $A_1$ and $A_2$ are constants relating to the polymer-solvent system.** [7]

$$[\eta] = A_1 + A_2 M^{\alpha}$$

**Equation 2.7: Sadron-Rempp equation, where $A_1$ and $A_2$ are constants relating to the polymer solvent system.** [38]

$$[\eta] = K_\theta M^{1/2} + K'M$$

**Equation 2.8: Stockmayer-FIxman equations, where $K_\theta$ is a universal constant regardless of solvent and temperature, and K' is a constant relating to the polymer-solvent system.** [39]

Plots of the contraction factor *g'* were also constructed (Figure 2.28) and *g'* values calcuated (Table 2.8). Clear trends are again observed, with linear polymer **7** and the copolymer with 10 w. % AA showing *g'* values close to 1, suggesting a similar IV, and therefore hydrodynamic volume, to a linear polymer of the same MW. Copolymer **13**, with 20 % AA, shows a large decrease in *g'*, indicating a large difference in hydrodynamic volume to the linear standard. This data, along with the Mark-Houwink plots above, show clear evidence that polymer **13** has a non-linear architecture. This strongly suggests a graft type morphology, as discussed above. Agreement between data for PMAA **7** and copolymer **12** suggests that grafting does not occur to an observable extent below a certain concentration of the acrylic monomer.

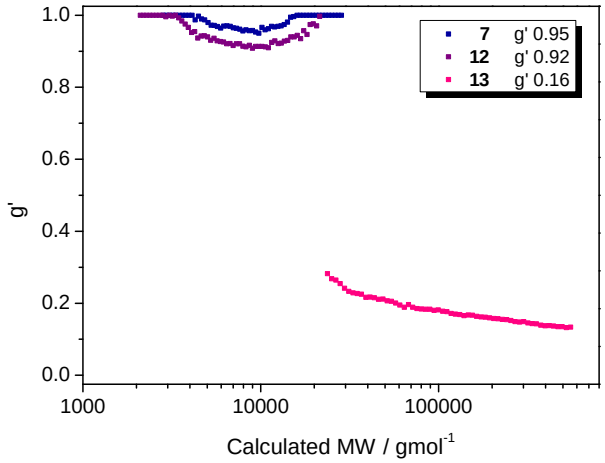


**Figure 2.28: SEC-DRI-VISC derived *g'* plots for P(MAA-*co*-AA) copolymers 12 and 13, comprising 10 and 20 w. % AA, compared to linear PMAA 7.**

These experiments show that efficient incorporation of acrylic acid into the CCTP of methacrylic acid is problematic, both in terms of reactivity ratios – which lead to substantial compositional drift and possible formation of homopolymers of the two monomers – and the associated loss of control with acrylic species, which leads to both high molecular weights and a non-linear, likely grafted, architecture at higher concentrations of AA. It is possible that combining higher concentrations of CoBF with a feed of monomers could overcome some of these issues, but optimization of such a process was expected to be non-trivial and not

pursued, as incorporation of considerable concentrations of AA would be expected to reduce the vinyl functionality of the resulting polymer, which is highly desirable for post-polymerization applications explored in chapter 3.

## *2.4 Synthesis of branched polyacids via CCTP*

Copolymerization of multi-functional monomers (usually containing two polymerizable groups) with mono-functional monomers will lead to structures with varying degrees of branching. Under free radical conditions, these systems will crosslink at low conversions, leading to a macroscopic insoluble gel within minutes, even with relatively low amounts of difunctional monomer[25, 40-41]. However, it has been shown that these systems can be controlled, and gelation prevented, using relatively small amounts of catalytic chain transfer agents.[40-41] This often allows higher degrees of branching and higher conversions than can be achieved by competing radical approaches[42-45], such as the "*Strathclyde route"* using thiols as conventional chain transfer systems in FRP[46-49] and SCVP relying on CRP chemistries[43, 50-52] (see chapter 1). Additionally, preparation of highly branched materials *via* CCTP uses very low levels of a relatively non-toxic CTA, unlike the stoichiometric amount of toxic and malodorous thiols used in conventional chain transfer approaches, and requires no specialist monomer synthesis (as is necessary for SCVP). Indeed, it has been shown that dimethacrylates such as ethylene glycol dimethacrylate (EGDMA) can be homopolymerized by CCTP and taken to > 95 % monomer conversion without crosslinking, yielding truly hyperbranched structures from commercially available monomers in an industrially viable process. This gives a facile route to dendrimer-like structures, and has the additional advantage of providing excellent handles for post-polymerization functionalization[53-56], in the form of vinyl groups from chain-transfer and EGDMA derived pendant vinyl groups[40, 56].

This work aims to combine the branching chemistry and associated high levels of vinyl functionality with the acidic monomer systems described previously, to give branched polyacids with groups for post-polymerization modification and curing application, which will be exploited in chapter 3.

### *2.4.1 Copolymerization of MAA and EGDMA via CCTP*

The copolymerization of MAA with EGDMA under CCT conditions has been reported in the patent literature by Guan[41], in which the copolymer contains nearly 40 mol. % of the

dimethacrylate. This example would give a lower degree of water solubility than is desired for this work, with the polymerization being conducted in relatively hydrophobic THF. The patent reports a weight average molecular weight of only 4,270 g $mol^{-1}$ and a narrow $Đ$ (1.4) which is uncharacteristic of a highly branched CCTP system.

In this work the monomer system was adapted to a water-based solvent system, targeting higher molecular weights with lower levels of crosslinking monomer, so as to maximize post-polymerizable functionality, number of acid groups and water-solubility. EGDMA was added in relatively low amounts (7 – 20 w. %) to the polymerization of MAA described above (Figure 2.29). However, EGDMA is only sparingly soluble in water, leading to a biphasic mixture in the form of an unstable emulsion. This could perhaps be eliminated by increasing the length of the ethylene glycol spacer in the crosslinker molecule, but it was thought that this would too greatly reduce the acidic functionality of the final polymer, which would be required for the application envisaged for the product (see chapter 3), as well as reducing the degree of branching possible.

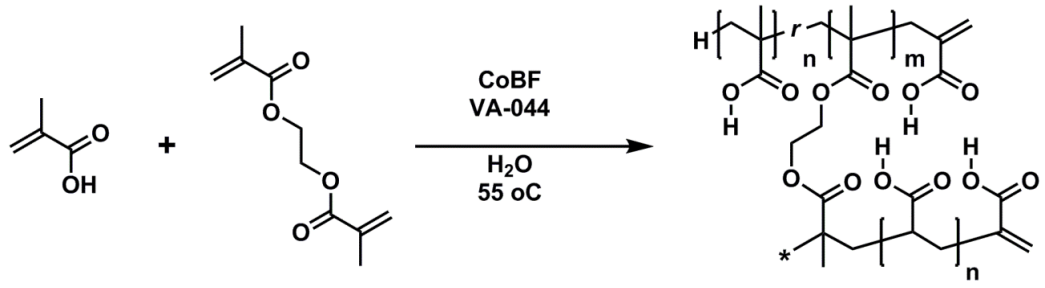


**Figure 2.29: Catalytic chain transfer copolymerization of MAA and EGDMA, in the presence of CoBF and initated by VA-044, to give branched copolymer.**

Polymerizations with 7 and 10 w. % EGDMA (**15**,**16**) gave biphasic emulsions at the start of the reaction, but became homogenous after 5 h, presumably when most of the EGDMA had been consumed, yielding relatively high MW polymers with the broad dispersities expected from branched radical polymerizations[33, 40, 54, 56-57]. It should be noted that conventional SEC is expected to give underestimation of the MW of branched polymers due to the difference in $V_h$ of linear and non-linear structures. Attempts to increase the level of dimethacrylate in the system were unsuccessful, with reactions incorporating 15 and 20 w. % EGDMA (**17**, **18**) leading to insoluble hydrogels. Data for these polymerizations are shown in Table 2.9, with SEC molecular weight distributions shown in Figure 2.30 and Figure 2.31.

| Reaction | [M]/[CoBF] | [EGMDA] (w. %) | [EGDMA] (mol. %) | $M_w$ [a] ($gmol^{-1}$) | $Đ$ [a] | Conversion [b] (%) | Time (h) |
|---|---|---|---|---|---|---|---|
| **15** | 29,100 | 7 | 3.2 | 23,600 | 3.53 | 97.2 | 7 h |
| **16** | 29,500 | 10 | 4.7 | 62,200 | 8.4 | 97.7 | 5 h |
| **17** | 28,700 | 15 | 7.2 | gel | - | - | 2 h |
| **18** | 28,000 | 20 | 9.9 | gel | - | - | 1 h |

**Table 2.9: Data for P(MAA-*co*-EGDMA) copolymerizations 15-18, synthesized in water with monomer/CTA ratios between 28,000-29,500, incorporating varying amounts of EGDMA. [a] Measured by conventional SEC-DRI, with 2 x PLgel mixed D columns, calibrated with PMMA standards, with DMF (1 mM $NH_4BF_4$) as eluent. [b] Measured by GC-FID.**

There are two possible reasons for the gelation of the aqueous copolymerizations of MAA with EGDMA: firstly, if an insufficient concentration of CoBF was used, extensive crosslinking would occur and lead to an insoluble macroscopic gel. Secondly, since EGDMA is sparingly water-soluble, high incorporation of this monomer may lead to the resulting polymer being insoluble in the reaction medium, and would also likely result in gelation. However, subsequent experiments below appear to disprove the latter possibility.

In order to improve the control of the reactions and be sure to delay gelation, the reactions were repeated with an increased concentration of CoBF (Table 2.10), giving a [monomer]/[CoBF] ratio = 21,400 (c.f. 28,000-29,500 in reactions **15**-**18**). A relatively small reduction in molecular weight is seen for polymer **19** (7 w. % EGDMA) with increased CTA concentration, also giving a similarly broad dispersity to **15**. Importantly, the viscosity of these reactions remained lower than those with reduced [CoBF], and reactions could be left for 24 hours - reaching conversion > 95 % - without gelation, giving a more reliable method for the synthesis of branched MAA copolymers.

| Reaction | [M]/[CoBF] | [EGMDA] (w. %) | [EGDMA] (mol. %) | $M_w$ [a] ($gmol^{-1}$) | $Đ$ [a] | Conversion [b] (%) | Time (h) |
|---|---|---|---|---|---|---|---|
| **19** | 21,400 | 7 | 3.2 | 18,400 | 3.41 | 98.0 | 24 h |
| **20** | 21,700 | 10 | 4.7 | 25,200 | 5.12 | 94.9 | 24 h |

**Table 2.10: Data for P(MAA-*co*-EGDMA)s copolymerizations 19-20, synthesized in water with monomer/CTA ratio 21,400. [a] Measured by conventional SEC-DRI, with 2 x PLgel mixed D columns, calibrated with PMMA standards, with DMF (1 mM $NH_4BF_4$) as eluent. [b]Measured by GC-FID.**

The SEC traces (Figure 2.30 and Figure 2.31) show an increase in $M_w$ over the course of the reactions, as expected for branched systems. Low molecular weight species are produced

early in the reaction and persist in the final products, giving a final polymer with a broad dispersity. The relatively small increase in the concentration of EGDMA in reaction **20** gives a significantly higher molecular weight and dispersity, which may indicate that the system is on the verge of crosslinking, with gelation of the reactions with increased crosslinker concentrations also suggesting this is the case.

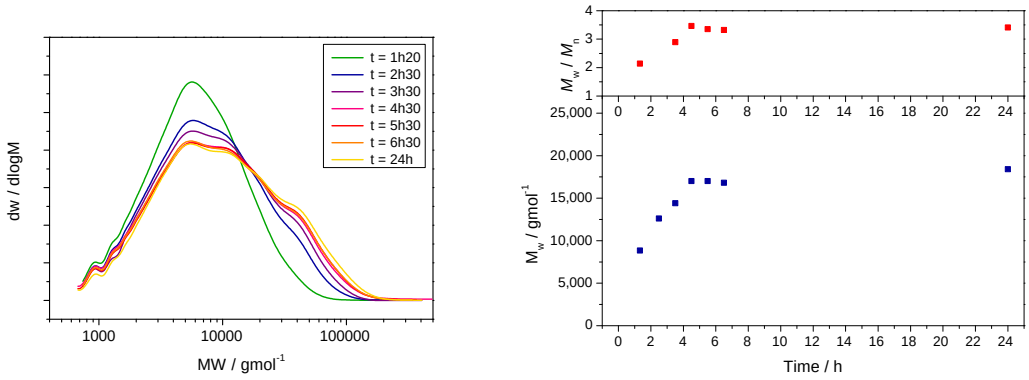


**Figure 2.30: Evolution of SEC molecular weight distributions throughout copolymerization 19, with 7 w. % EGDMA and [monomer]/[CoBF] ratio = 21,400 (left). Evolution of $M_w$ and dispersity, measured by conventional SEC, throughout copolymerization 19 (right).**

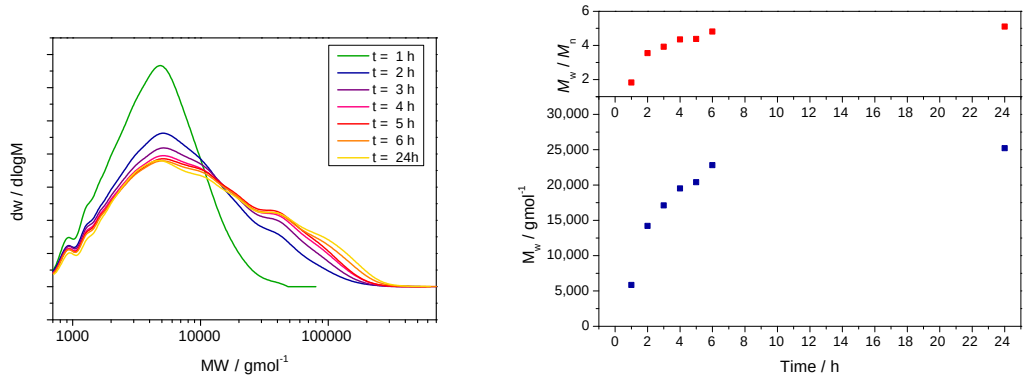


**Figure 2.31: Evolution of SEC molecular weight distributions throughout copolymerization 20, with 10 w. % EGDMA and [monomer]/[CoBF] ratio = 21,400 (left). Evolution of $M_w$ and dispersity, measured by conventional SEC, throughout copolymerization 20 (right).**

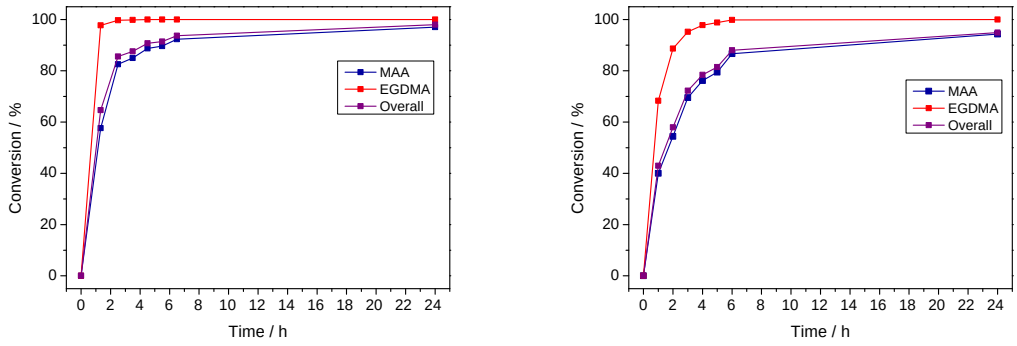


**Figure 2.32: GC-FID measured conversion for MAA-EGDMA copolymerization 19, containing 7 w. % EGDMA (left) and MAA-EGDMA copolymerization 20, containing 10 w. % EGDMA (right).**

Conversion of both monomers is shown in Figure 2.32. EGDMA is consumed far more rapidly than the MAA co-monomer, with the majority of the crosslinker consumed within 2 hours. This can be explained by the fact that a di-functional molecule is inherently more likely to react than a mono-functional equivalent, but may also be due to the EGDMA existing as droplets at the outset of the reactions, leading to localized high concentrations of crosslinker. This suggests that propagation occurring in or around an EGDMA-rich droplet may to a hyperbranched core containing predominantly the difunctional monomer, with MAA incorporation increased toward the corona of the branched structure. This will be explored in depth using SEC-DRI-VISC analysis (section 2.4.2).

In order to address the issue of EGDMA solubility, polymerizations were carried out in binary mixtures of water/2-isopropyl alcohol (IPA), which gave homogenous solutions at all points in the reactions. Polymerizations of MAA were carried out with 10 (**21**) and 20 (**22**) w. % EGDMA, with the conversion and molecular weight measured throughout (Figure 2.33 and Figure 2.34).

| Reaction | [M]/[CoBF] | [EGDMA] (w. %) | [EGDMA] (mol. %) | $M_w$ [a] ($gmol^{-1}$) | $Đ$ [a] | Conversion [b] (%) | Time (h) |
|---|---|---|---|---|---|---|---|
| **21** | 29,500 | 10 | 4.7 | 7,260 | 2.72 | 92.1 | 24 h |
| **22** | 27,800 | 20 | 9.9 | 21,100 | 4.51 | 94.3 | 22 h |

**Table 2.11: Data for P(MAA-*co*-EGDMA) copolymers 21 and 22, with 10 and 20 wt. % EGDMA, synthesized in a 1 to 1 mixture of water and IPA. [a] Measured by conventional SEC-DRI, with 2 x PLgel mixed D columns, calibrated with PMMA standards, with DMF (1 mM $NH_4BF_4$) as eluent. [b] Measured by GC-FID**

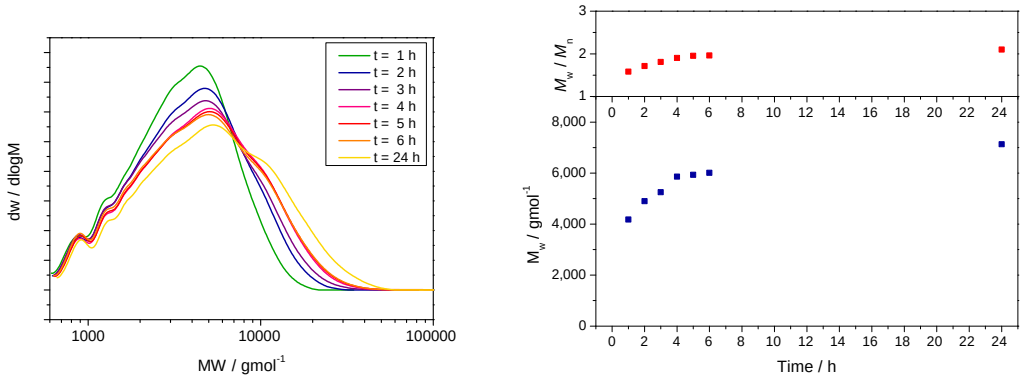


**Figure 2.33: Evolution of SEC molecular weight distributions throughout copolymerization 21, in water-IPA with 10 w. % EGDMA and [monomer]/[CoBF] ratio = 21,400 (left). Evolution of $M_w$ and dispersity, measured by conventional SEC, throughout copolymerization 21 (right).**

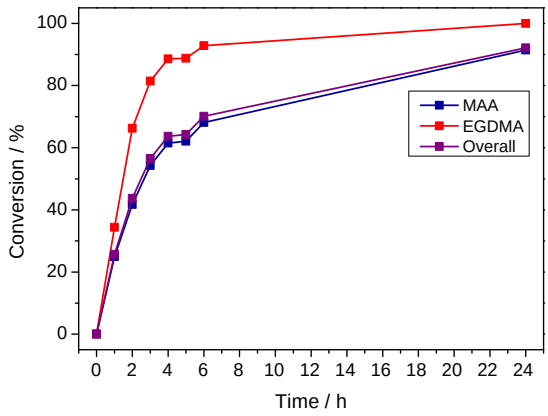


**Figure 2.34: Conversion, measured by GC-FID, throughout P(MAA-*co*-EGDMA) copolymerization 21.**

It can immediately be seen that the change of solvent increases the control over the reaction, with lower molecular weight polymers and lower dispersities obtained. This may be due to chain transfer to IPA, which would lead to a reduction of the molecular weight, despite having a far lower $C_s$ value than the CCTA. The water-IPA solvent system also allowed significantly more crosslinker to be incorporated without gelation occurring, at lower CoBF concentrations compared to the water-based system (for example, copolymerization **18**, with the same concentration of CoBF and EGDMA as **22**, gelled within 1 hour). It should be noted that these polymers are all water soluble after work-up, indicating that polymer insolubility in the water system above is unlikely to have been a contributing factor to gelation.

Comparing reactions incorporating 10 w. % EGDMA performed in water (**20**) and water-IPA (**21**), clear differences can be seen in both the evolution of the molecular weight and the

conversion (Figure 2.35). Overall conversion is more rapid in the water solvent system, with MW and dispersity also increasing at a higher rate, likely due to the increases viscosity of the reaction mixtures.

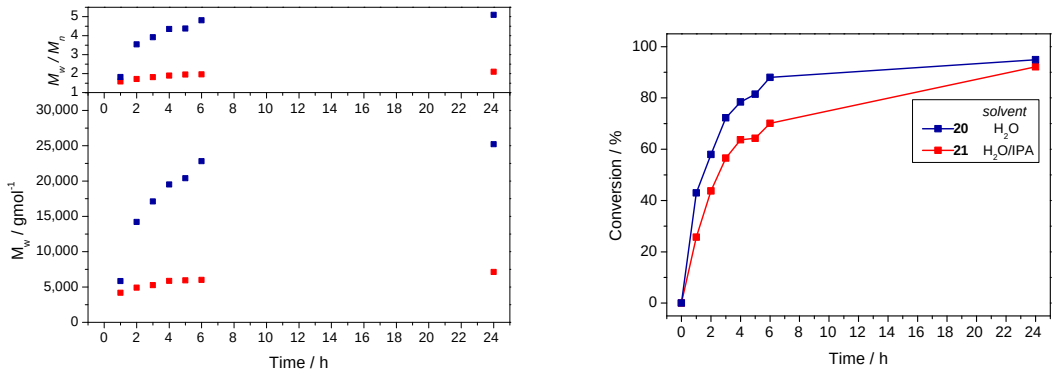


**Figure 2.35: Comparison of evolution of $M_w$ and dispersity throughout P(MAA-*co*-EGDMA) copolymers 20 and 21 (left) and overall conversion throughout copolymers 20 and 21 (right).**

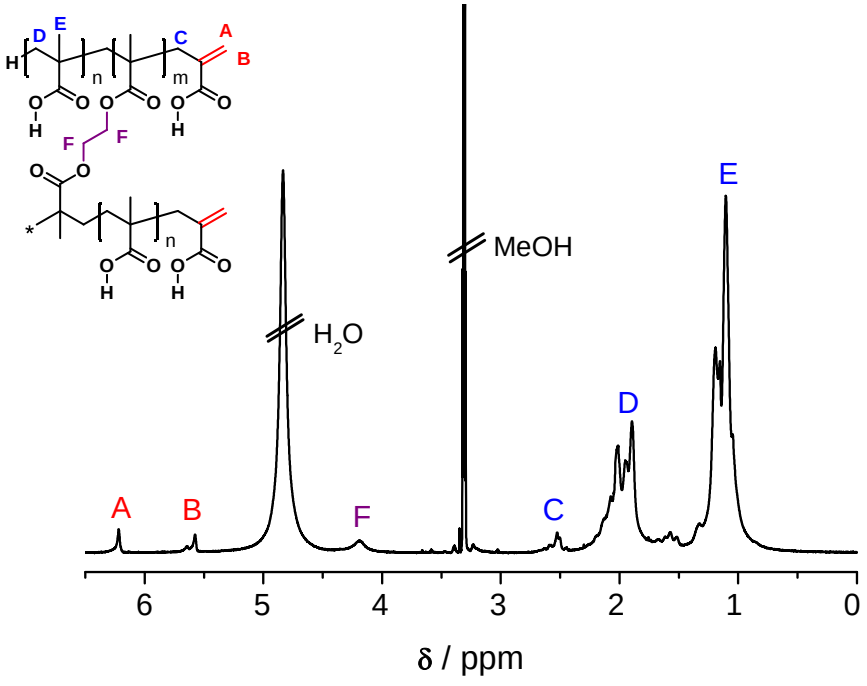


**Figure 2.36: Typical $^1$H-NMR spectrum of P(MAA-*co*-EGDMA) synthesized by CCTP, with characteristic vinyl signals and ethylene glycol proton signals (NMR solvent - methanol-$d_4$).**

$^1$H-NMR analysis of the branched MAA/EGDMA copolymers reveals characteristic peaks for the expected polymer structure (Figure 2.36), with vinyl functionality revealed by the peaks at 6.2 and 5.6 ppm, and the broad signal at 4.2 ppm due to the EGDMA $CH_2$ groups.

### *2.4.2 Quantifying number of vinyl groups in branched polyacids*

The number of vinyl groups per mass of branched copolymer can be calculated using bromination of the double bonds and titration techniques. A procedure for calculating the Bromine Index (BI) – the amount of bromine (in mg, readily converted to moles) consumed by the double bonds of 100 g of substrate – was adapted from work conducted by Ling-Shu Wan and co-workers, who used this technique to quantify the number of residual vinyl groups in crosslinked polystyrene microspheres.[58]

Molecular bromine was generated *in situ* by the reaction of potassium bromate with potassium bromide, in the presence of acetic acid; addition across double bonds will remove bromine from the solution (Figure 2.37). Potassium iodide and hydrochloric acid are then added, and will react with the excess bromate, producing iodine which can be titrated against sodium thiosulfate. The end point is further elucidated by using starch as an indicator for iodine toward the end of the titration.

$$KBrO_3 + 5KBr + 6AcOH \rightleftharpoons 3Br_2 + 6AcOK + 3H_2O$$

**Equation 2.9: Equilibrium between potassium bromate and potassium bromide forming molecular bromine.**

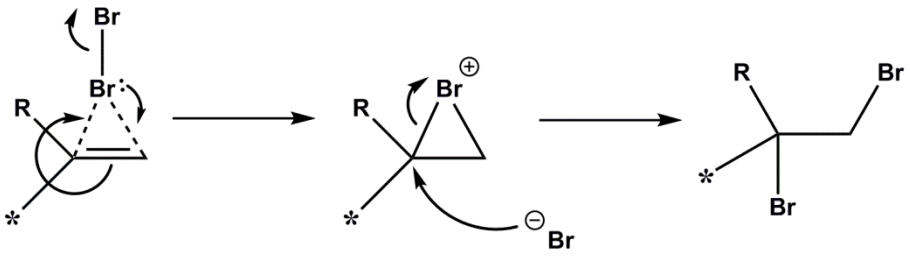


**Figure 2.37: Mechanism of bromination of vinyl groups.**

$$6KI + KBrO_3 + 6HCl \rightleftharpoons 3I_2 + KBr + 6KCl + 3H_2O$$

$$I_2 + 2Na_2S_2O_3 \rightleftharpoons 2NaI + Na_2S_4O_6$$

**Equation 2.10: Reaction between potassium iodide, hydrochloric acid and excess potassium bromate, forming iodine (top) and reaction between iodine and sodium thiosulphate used in titration step (bottom).**

Vinyl groups are quantified using the Bromine Index (Equation 2.11), which can be converted to moles of vinyl groups per gram.

$$BI = \frac{7990.(V_1 - V_2).c}{m}$$

**Equation 2.11: Bromine Index (BI), where $V_1$ and $V_2$ are the volumes (in mL) of $Na_2S_2O_3$ titrated in the blank and sample solutions, repectively, $c$ is the concentration of the $Na_2S_2O_3$ solution (in mol.dm$^{-3}$) and $m$ is the mass of particles.**

The BI and mmol of vinyl groups per gram of the branched P(MAA-*co*-EGDMA)s are shown in Table 2.12. The number of vinyl groups would be expected to increase with increasing concentration of EGDMA crosslinker, as incorporation of an EGDMA unit during propagation should give a branch-point and an additional chain end to be terminated *via* CCT. No dependence of BI on concentration of EGDMA is observed, which could be due to incomplete conversion and subsequent wastage of the difunctional monomer, which should be responsible for all branch-points. However, this technique verifies that the polymers synthesized do contain considerable quantities of reactive vinyl functionality, which will be important for work undertaken in the following chapter.

| Reaction | $M_w$ (g mol$^{-1}$) | [EGDMA] (mol %) | BI (mg / 100 g) | Vinyl groups (mmol/g) |
|---|---|---|---|---|
| **19** | 18,400 | 3.2 | 16,400 | 1.03 |
| **20** | 25,200 | 4.7 | 13,600 | 0.85 |
| **21** | 7,260 | 4.7 | 9,300 | 0.58 |
| **22** | 21,100 | 9.9 | 17,500 | 1.09 |

**Table 2.12: Bromine Index and subsequent calculation of number of vinyl groups per gram of polymers 19-22.**

### *2.4.3 Multi-detector SEC characterization of branched polyacids*

Purified samples of **19-22** were analysed by SEC-RI-VISC with universal calibration, from which Mark-Houwink plots can be generated (Figure 2.38). Linear PMAA homopolymer **7** was employed as a linear standard for comparison, in order to compare intrinsic viscosity values across the MWD and α values derived from the Mark-Houwink data (Table 2.13).

| Reaction | [M]/[CoBF] | Reaction solvent | [EGDMA] (mol. %) | $M_w$ [a] ($gmol^{-1}$) | $Đ$ [a] | α [a] | $g'$ [a] |
|---|---|---|---|---|---|---|---|
| **7** | 98,100 | water | 0 | 9,170 | 1.67 | 0.45 | 0.94 |
| **19** | 21,400 | water | 3.2 | 20,400 | 5.39 | 0.29 | 0.52 |
| **20** | 21,700 | water | 4.7 | 108,000 | 30.18 | 0.28 | 0.42 |
| **21** | 29,500 | water-IPA | 4.7 | 8,510 | 2.93 | 0.25 | 0.67 |
| **22** | 27,800 | water-IPA | 9.9 | 32,000 | 9.30 | 0.29 | 0.60 |

**Table 2.13: Molecular weight, dispersity, α and *g'* for linear PMAA 7 and P(MAA-*co*-EGDMA)s synthesized in water (19-20) and water-IPA (21-22). [a] Derived from SEC-DRI-VISC and universal calibration.**

As discussed in section 2.3.1, the value of α obtained for the linear standard shows some deviations from theory. It is still expected that a trend of decreasing α values with decrease in hydrodynamic volume, indicative of increased branching, would be apparent and relevant.

It can be seen from the Mark-Houwink plots (Figure 2.38) that the EGDMA copolymers have lower intrinsic viscosities at all points in the molecular weight range than the linear standard, indicating a smaller hydrodynamic volume for a comparable MW. This is echoed in the α values calculated for the branched copolymers which range from 0.25 to 0.29, and show considerably lower values than that of the linear homopolymer. The α values and intrinsic viscosities suggest a similar degree of branching for all samples, despite the mol. % of difunctional monomer ranging from 3.2 to 9.9. The α value obtained for copolymer **21** is unexpected, since it does not contain the highest level of difunctional monomer, nor is it of high molecular weight (branching would be expected to increase with MW). However, this may be explained by the relatively low molecular weight of the product compared with other polymers synthesized – ideally, comparisons would be made between polymers of identical MW.

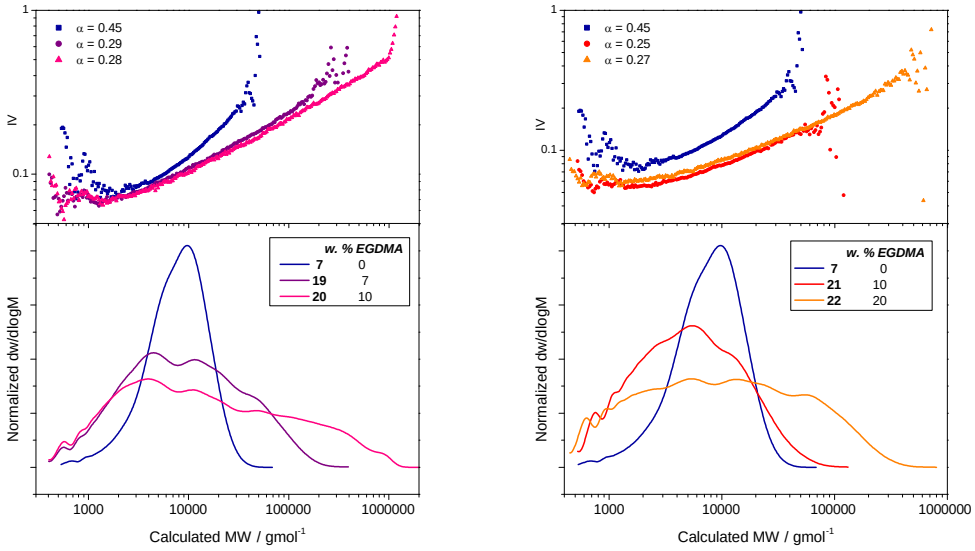


**Figure 2.38: SEC-DRI-VISC calculated molecular weight distributions (lower pane) and Mark-Houwink plots of IV vs MW (upper pane) for P(MAA-*co*-EGDMA) copolymers 21-22 synthesized in water-IPA (right), and P(MAA-*co*-EGDMA) copolymers 19-20 synthesized in water (left).**

A Mark-Houwink plot was constructed for copolymers **20** and **21** (Figure 2.39), which both contain 10 w. % EGDMA, but were synthesized in either water (giving unstable emulsion due to low solubility of EGDMA) or water-IPA (1:1, homogeneous solution), respectively.

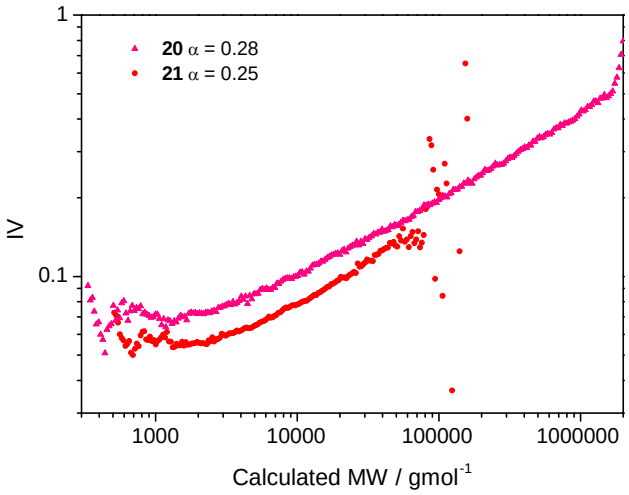


**Figure 2.39: Mark-Houwink plot of instrinsic viscosity versus molecular weight for P(MAA-*co*-EGDMA) copolymers 20 and 19 both with 10 w. % EGDMA, synthesized in water-IPA (1:1) and water, respectively.**

The polymer synthesized in water (**20)** shows a more consistent slope across the molecular weight range, whereas the polymer synthesized in water/IPA (**21)** shows an increasing gradient

with molecular weight. This is consistent with a higher degree of branching at low molecular weight (where the gradient, α, is lower), suggesting a more star-like structure, with a more highly branched core and more linear chains at the periphery, as seen in the left-hand schematic in Figure 2.40. This postulated change in EGDMA incorporation could be explained by the biphasic nature of the polymerization when carried out in water. It is probable that the majority of initiation and propagation takes place in the aqueous phase, with EGDMA incorporation controlled by its partitioning between the aqueous phase and EGDMA droplets. This could lead to more consistent branching throughout the polymer chain, as EGDMA partitions into the aqueous phase at a steady rate. Indeed, work previously published by this research group, in collaboration with Davis and Boyer, attributed the formation of unusually well-defined arm-first stars to a similar effect, with a sparingly soluble crosslinker resulting in consistent formation of the nano-gels used to link the arms.[59]

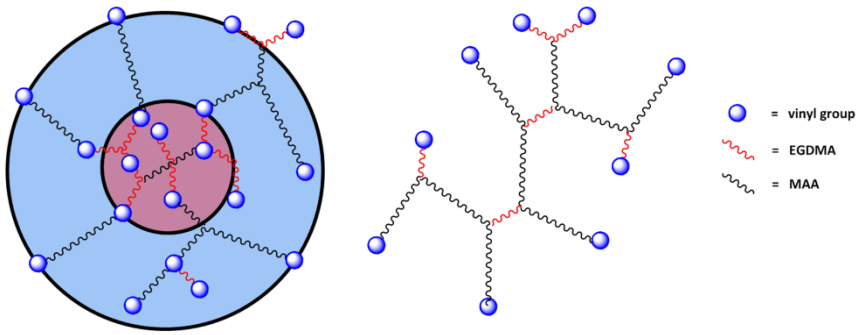


**Figure 2.40: Cartoon showing branched polymers with more star-like highly branched core (left) and branched polymer with evenly distributed branching (right).**

The *g'* plots for the branched P(MAA-*co*-EGDMA) copolymers **19**-**22**, compared to linear PMAA **7**, provide further evidence for branching. MAA-EGDMA copolymers show an increase in contraction across the molecular weight range in all cases, with the difference between the IVs of the linear standard and branched sample increasing with MW. The *g'* values (Table 2.13) show a reduction with increasing EGDMA composition across both solvent systems, also indicating a reduced IV relative to the linear standard and a decreased hydrodynamic volume. It should be noted that this trend, indicative of the expected increase in branching with increasing concentration of difunctional monomer, is not seen in the α values calculated for the same systems. Due to the semi-quantitative nature of values calculated here, the clearest indication of branching is expected to be the IV across the molecular weight range, shown in

the Mark-Houwink plots above (Figure 2.38), which reveals a relatively similar reduction in IV for all samples. As the branched polymers synthesized contain similar, relatively low levels of EGDMA (between 3.2 and 9.9 mol. %), this is not unexpected.

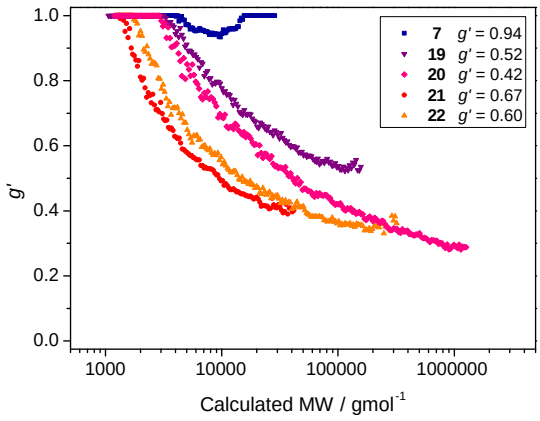


**Figure 2.41: SEC-DRI-VISC derived *g'* plots for P(MAA-*co*-EGDMA) copolymers 19-22, compared to linear PMAA 7.**

## *Methylation of branched polyacids and SEC analysis*

There are several examples in the literature of using diazomethane-generating[60] reagents to efficiently methylate PAA and PMAA, giving poly(methyl acrylate) (PMA) and poly(methyl methacrylate) (PMMA), respectively. This has been used particularly to aid with MS analysis of acidic polymer products and to allow for SEC in commonly used organic solvents against narrow molecular weight distribution standards[61-62] (rather than using the relatively uncommon DMF eluent). In order to provide more evidence for the branching of the polymers synthesized, a range of linear and branched samples were methylated with trimethylsilyl diazomethane and analysed by SEC-DRI-VISC in THF. The data collected using a more "ideal" and commonly investigated solvation system should allow verification of the data obtained using DMF as eluent.

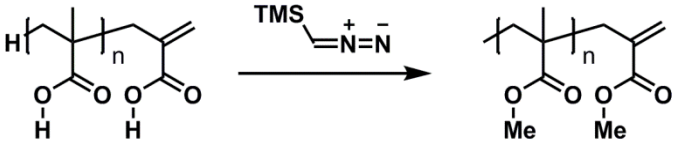


**Figure 2.42: Methylation of CCTP derived PMAA with TMS-diazomethane, producing PMMA.**

Molecular weight averages and dispersities calculated for the methylated products (Table 2.14) show moderate agreement with the values calculated for the native acidic polymers in

DMF, with differences in MWs within around 20 %. Dispersity values show more deviation, which can be explained by the more robust nature of calculation of weight average MW, compared to the number average, which will be more sensitive to very low MW species and changes in baseline.[17, 19] The difference in values calculated for the two systems highlights that SEC-DRI-VISC cannot provide a truly 'universal calibration', and that polymer functionality and the chosen solvent system will always have some affect on the values calculated.

| Reaction | [M]/[CoBF] | [EGDMA] (mol. %) | $M_w$ [a] ($gmol^{-1}$) | $Đ$ [a] | α [a] | $g'$ [a] |
|---|---|---|---|---|---|---|
| **7-Me** | 98,100 | 0 | 6,800 | 1.59 | 0.42 | 0.96 |
| **19-Me** | 21,400 | 3.2 | 18,700 | 5.03 | 0.26 | 0.49 |
| **20-Me** | 21,700 | 4.7 | 141,000 | 24.42 | 0.25 | 0.31 |
| **21-Me** | 29,500 | 4.7 | 6,600 | 3.32 | 0.18 | 0.33 |
| **22-Me** | 27,800 | 9.9 | 33,500 | 6.58 | 0.27 | 0.51 |

**Table 2.14: Molecular weight, dispersity, α and *g'* for linear PMAA 7 and P(MAA-*co*-EGDMA)s synthesized in water (19-20) and water-IPA (21-22). [a] Derived from SEC-DRI-VISC and universal calibration**

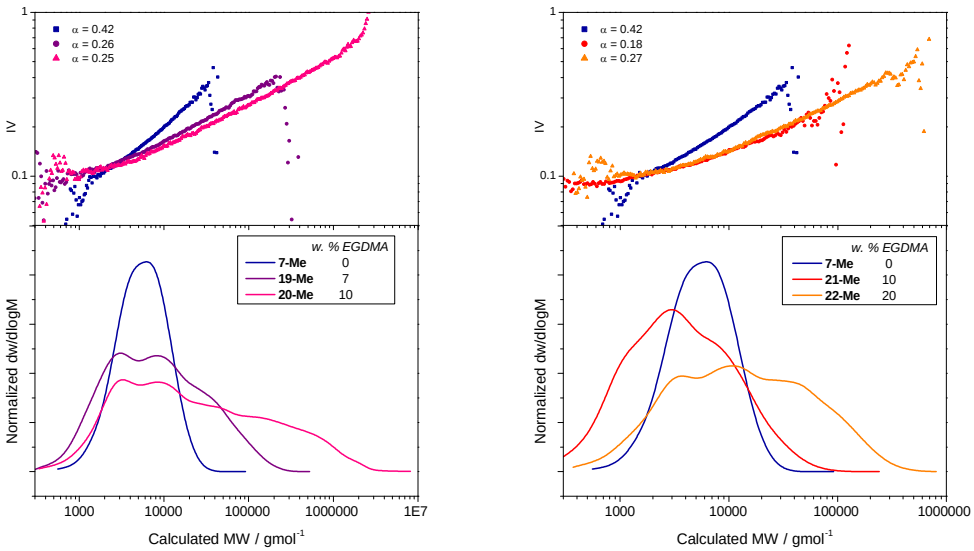


**Figure 2.43: SEC-DRI-VISC calculated molecular weight distributions (lower pane) and Mark-Houwink plots of IV vs MW (upper pane) for methylated P(MMA-*co*-EGDMA) copolymers 21-Me – 22-Me, originally synthesized in water-IPA (right), and P(MMA-*co*-EGDMA) copolymers 19-Me – 20-Me originally synthesized in water (left).**

The SEC-MWDs and Mark-Houwink plots (Figure 2.43) for the methylated polymers show similar trends to those observed above for the polymers before methylation. The linear

homopolymer sample (**7-Me**) again shows a greater intrinsic viscosity across the molecular weight range than the copolymers with EGDMA (**19-Me – 22-Me)**. However, the α value of 0.42 for the linear PMMA sample again shows some deviation from the theoretical value of ≥ 0.5. The α values for EGDMA copolymers (Table 2.14) range from 0.18 to 0.27 (c.f. 0.25-0.29 for the same polymers before methylation), indicating reduced hydrodynamic volume and increased branching. The expected trend of decreasing α value with increasing EGDMA concentration is still not observed, suggesting a similar degree of branching under all conditions.

*g'* plots for the methylated polymers were also constructed (Figure 2.44) and *g'* values calculated (Table 2.14). The *g'* plot shows an increase in contraction throughout the molecular weight range for all branched samples, with *g'* values echoing this trend. As above, little agreement between trends in *g'* and α values is seen, however, comparison to the linear standard for IV, *g'* and α all clearly suggest the reduction in hydrodynamic volume associated with branching for all P(MAA-*co*-EGDMA)s synthesized and methylated.

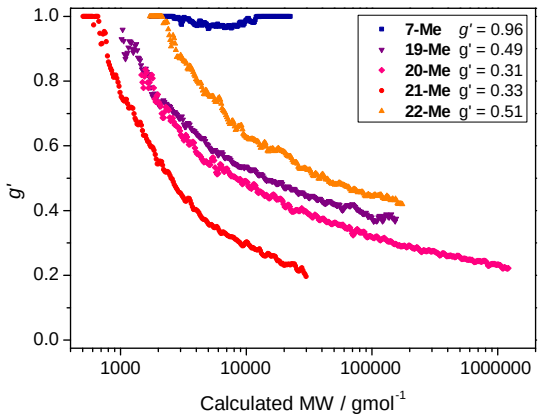


**Figure 2.44: *g'* plots for methylated PMAA 7-Me and methylated P(MAA-*co*-EGDMA)s 18-22-Me.**

Multidetector analysis using universal calibration shows clear evidence for the formation of the expected branched structures, with similar results obtained even when polymer functionality and solvent were changed. Both factors would be expected to change the solvation, and therefore hydrodynamic volume, of the polymer samples in solution, so observation of similar trends between the two analysis methods provides further evidence of the branching.

## *2.5 Conclusions*

A range of linear MAA homopolymers were synthesized *via* CCTP with a monomer/CTA feed. However, some compositional drift was observed, leading to a broadening of the molecular weight distribution. This was addressed by switching to a batch polymerization method, which yielded polymers of consistent molecular weight throughout the polymerization across a range of [monomer]/ [CTA] ratios. The dominant mode of initiation of polymer chains was identified as re-initiation by Co(III)-H hydride complexes following chain transfer *via* ESI-TOF mass spectrometry, while ESI-TOF combined with $^{1}$H-NMR reveals the expected vinyl functionality as the polymer end-group. This post-polymerizable functionality will be important for the application investigated in chapter 3.

Copolymerization of MAA with AA under CCT conditions was attempted but proved problematic. While addition of the less CCT active acrylic monomer lead to the expected increase in molecular weight and dispersity, a large extent of compositional drift was observed due to unfavourable reactivity ratios. At relatively low concentrations of AA the molecular weight was well controlled, but on addition of 20 w. % AA and above very high MW products were formed, with SEC-DRI-VISC suggesting a non-linear architecture.

Branched copolymers of MAA and EGDMA were also synthesized *via* CCTP, with copolymers containing up to 20 w. % EGDMA synthesized at high conversions without gelation. Two solvent systems for this copolymerization were investigated; water and a mixture of water and IPA. It was found that the poor water solubility of EGDMA led to an unstable emulsion in water, and a higher molecular weight product with greater dispersity. In contrast, the water/IPA solvent system led to more control of the polymerization, with lower molecular weights obtained and greater levels of EGDMA incorporation possible without gelation occurring. SEC-DRI-VISC analysis revealed lower intrinsic viscosities for the copolymers synthesized and provides evidence for the formation of branched architectures. Furthermore, the vinyl end groups were verified by $^{1}$H-NMR and quantified using a bromination titration method.

## 2.6 Experimental

### 2.6.1 Materials

All reagents were purchased from Aldrich and used as received, unless otherwise stated. 2,2'-azobis[2-(2-imidazolin-2-yl)propane]dihydrochloride (VA-044) was purchased from Alpha Labs and used as received. (Trimethylsilyl)diazomethane ($TMSCHN_2$) was purchased from Acros as a 2M solution in diethyl ether, and used as received. CoBF was synthesised as previously reported.[22]

### 2.6.2 Instruments

**$^{1}$H- and $^{13}$C-NMR spectroscopy**

All NMR spectra were recorded on Bruker DPX-400, DPX-300 and Bruker AC-250 spectrometers as solutions in $D_2O$, $CD_3OD$ or $CDCl_3$ (with TMS), as indicated. Chemical shifts were calibrated using the solvent residual peaks in the case of $D_2O$ and $CD_3OD$, or with TMS for $CDCl_3$.

**Fourier Transform Infrared (FT-IR) spectroscopy**

FT-IR was carried out on a Bruker Vector 22 using a Golden Gate diamond attenuated flow cell and analysed using Opus software.

**Size Exclusion Chromatography/Gel Permeation Chromatography (SEC/SEC)**

All SEC experiments were performed on Agilent 390-LC multi-detector suites equipped with a PL-AS RT/MT autosampler, fitted with a PLgel 5 µm guard column and two PLgel 5 µm Mixed D columns (with an exclusion limit of $2.0 \times 10^6$ $gmol^{-1}$). All data was collected and analysed using Agilent GPC software. Mobile phases were DMF and THF with a flow rate of 1 $mL.min^{-1}$ and an injection volume of 100 µL. The column sets were maintained at ambient temperature and 50 $^{o}C$ for THF and DMF, respectively.

***Conventional SEC***

A DRI detector was used for conventional calibration. Calibrations were created using PMMA EasiVial standards (690-1,944,000 g $mol^{-1}$) purchased from Agilent, with a minimum of 9 points fitted with a third order calibration curve. Points with an error greater than 10 % were not included in the final calibration.

***SEC-DRI-VISC (universal calibration)***

Final polymers were purified by precipitation and dried under vacuum prior to analysis in DMF and THF, in order to ensure accurate sample concentrations. An RI and a 4 capillary viscometer were used as detectors, with inter-detector delay calibrated using a single PMMA narrow standard ($M_p$ 90,250 g $mol^{-1}$) of known concentration. Column calibrations were created using PMMA EasiVial standards (690-1,944,000 g $mol^{-1}$), analysed at known concentrations, purchased from Agilent, with a minimum of 9 points fitted with a third order calibration curve. g' values were calculated using linear PMAA **7** (for analysis in DMF) and linear PMMA **7-Me** (for analysis in THF) as standards.

**Electrospray Ionization Time-of-Flight mass spectrometry (ESI-ToF)**

ESI-ToF was carried out on a Bruker MicroTOF instrument in negative mode.

**Gas Chromatography – Flame Ionization detector (GC-FID)**

GC-FID was performed using a Varian 450 fitted with a FactorFour™ capillary column VF-1ms, of 15 m x 0.25 mm I.D. and film thickness 0.25 µm. Oven temperature was programmed as follows: 40 °C (hold for 1 min) at 25 °C $min^{-1}$ to 200 °C. The injector was operated at 200 °C with the FID at 220 °C. Nitrogen was used as the carrier gas at a flow rate of 1 mL $min^{-1}$ and a split ratio of 1:100 was applied. Data were processed using Galaxie software (version 1.9.302.530).

## *2.6.3 General Procedures*

### *Homopolymerizations of MAA*

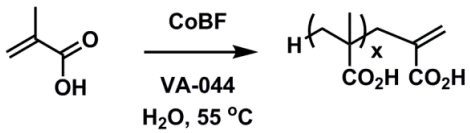


**A typical feed-type homopolymerization was carried out as follows:**

To prepare the monomer/CTA feed solution, a solution of 90 mL $H_2O$ and 75 g MAA (0.87 mol) was deoxygenated *via* bubbling with a stream of nitrogen for 1 hour and added to a flask containing CoBF (35 % of total) *via* cannular.

A 500 mL round bottom flask was charged with 90 mL $H_2O$ and deoxygenated *via* bubbling with a stream of nitrogen for 1 hour. A 3-neck round bottom flask, equipped with nitrogen inlet, septum and stirring bar, containing CoBF (65 % of total) and 0.3 g VA-044 (0.95 mmol), was degassed with three vacuum/nitrogen-backfill cycles before the deoxygenated water was added *via* cannular and stirred under positive pressure of nitrogen at ambient temperature until all solids were dissolved. This flask was placed in an oil bath at 55 $^{o}$C and the feed of monomer/CTA solution prepared above was added over a period of several hours using an FMI pump. After the indicated reaction time, the volume of reaction mixture was reduced under reduced pressure and the water removed by freeze-drying.

| Reaction | [MAA]/[CoBF] | CoBF (mg) | CoBF (mmol) | Feed time | Reaction time |
|---|---|---|---|---|---|
| **2** | 99,000 | 4 | 0.010 | 1.5 h | 24 h |
| **3** | 62,700 | 7 | 0.018 | 2.5 h | 24 h |
| **4** | 31,000 | 11 | 0.028 | 2.5 h | 22 h |
| **5** | 16,000 | 22 | 0.055 | 2.5 h | 22 h |
| **6** | 31,000 | 11 | 0.028 | 3 h | 20 h |

**A typical batch-type homopolymerization was carried out as follows:**

A 500 mL round bottom flask was charged with 150 g MAA (1.72 mol), 350 mL $H_2O$ and 5 mL diethylene glycol (DEG, for use as an internal standard for GC-FID) and equipped with a stirring bar and septum. This mixture was deoxygenated *via* bubbling with a stream of nitrogen for a minimum of 1 hour. A 3-neck round bottom flask, equipped with nitrogen inlet, septum and stirring bar, containing CoBF and 0.6 g VA-044 (1.86 mmol), was degassed with three vacuum/nitrogen-backfill cycles before the monomer/solvent mixture was added *via* cannular. The resulting reaction mixture was allowed to stir under a positive pressure of nitrogen at ambient temperature until all solids were dissolved, yielding a homogenous solution, at which point the vessel was placed in an oil bath at 55 $^{O}$C. After the indicated reaction time, the volume of reaction mixture was reduced under reduced pressure and the water removed by freeze-drying.

| Reaction | [MAA]/[CoBF] | CoBF (mg) | CoBF (mmol) | Reaction time |
|---|---|---|---|---|
| **7** | 98,100 | 3 | $7.5 \times 10^{-3}$ | 22 h |
| **8** | 49,000 | 6 | 0.015 | 22 h |
| **9** | 32,700 | 9 | 0.023 | 22 h |
| **10** | 24,500 | 12 | 0.030 | 22 h |
| **11** | 16,000 | 18 | 0.045 | 22 h |

## *Copolymerization of MAA with AA*

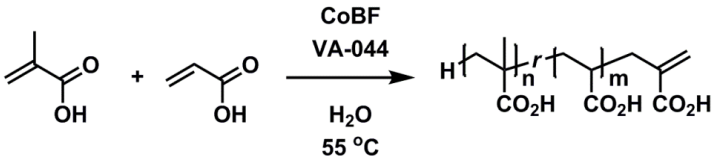


A typical copolymerization was adapted from the batch procedure above, with varying w. % AA at constant ratio of [monomer]/[CoBF].

| Reaction | [MAA]/[CoBF] | [acrylic acid] (w. %) | [acrylic acid] (mol %) | Reaction time |
|---|---|---|---|---|
| **12** | 25,500 | 10 | 11.8 | 22 h |
| **13** | 25,500 | 20 | 23.2 | 22 h |
| **14** | 25,500 | 30 | 34.1 | 22 h |

## *Copolymerization of MAA with EGDMA*

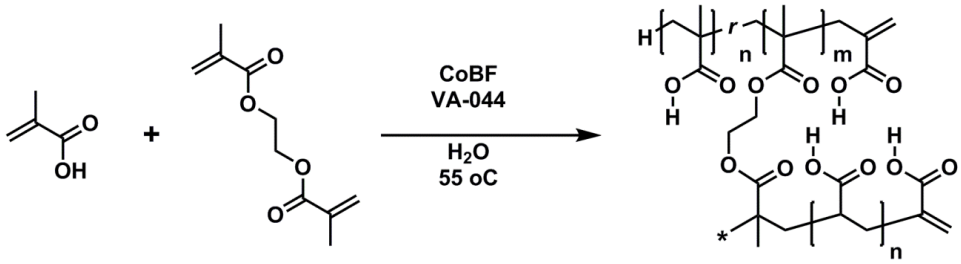


**Polymerizations conducted in water**

A 500 mL round bottom flask was charged with MAA, 350 mL $H_2O$ and 5 mL diethylene glycol (DEG, for use as an internal standard for GC-FID) and equipped with a stirring bar and septum.

This mixture was deoxygenated *via* bubbling with a stream of nitrogen for a minimum of 1 hour. A separate vessel was charged with EGDMA and deoxygenated *via* bubbling with a stream of nitrogen for 20 min. A 3-neck roundbottom flask, equipped with nitrogen inlet, septum and stirring bar, containing CoBF and 0.6 g VA-044 (1.86 mmol), was degassed with three vacuum/nitrogen-backfill cycles before the monomer/solvent mixture was added *via* cannular and EGDMA added *via* degassed syringe. The resulting reaction mixture was allowed to stir under a positive pressure of nitrogen at ambient temperature until all solids were dissolved, yielding a biphasic solution, at which point the vessel was placed in an oil bath at 55 $^{o}$C. After the indicated reaction time, the volume of reaction mixture was reduced under reduced pressure and water removed by freeze-drying.

**Polymerizations conducted in water-IPA**

A typical copolymerization in water-IPA was adapted from the PMAA batch procedure above, with varying w. % EGDMA at constant ratio of [monomer]:[CoBF]. Unlike MAA-EGDMA copolymerizations conducted in water, this system give homogenous solutions throughout polymerization.

[Monomer]/[CoBF] ratios and concentrations of EGDMA are shown below.

| Reaction | [MAA]/[CoBF] | Solvent | [EGDMA] (w. %) | [EGDMA] (mol %) | Reaction time |
|---|---|---|---|---|---|
| **15** | 29,100 | water | 7 | 3.2 | 7 h |
| **16** | 29,500 | water | 10 | 4.7 | 5 h |
| **17** | 28,700 | water | 15 | 7.2 | 2 h (gel) |
| **18** | 28,000 | water | 20 | 9.9 | 1 h (gel) |
| **19** | 21,400 | water | 7 | 3.2 | 24 h |
| **20** | 21,700 | water | 10 | 4.7 | 24 h |
| **21** | 29,500 | water-IPA | 10 | 4.7 | 24 h |
| **22** | 27,800 | water-IPA | 20 | 9.9 | 22 h |

## *Quantification of vinyl groups in branched P(MAA-co-EGDMA)s*

Bromination-titration to yield bromine index (BI) was carried out as follows:

P(MAA-*co*-EGDMA) copolymer (0.2 g) was added to a solution of 9 mL water, 0.5 mL methanol and 0.5 mL glacial acetic acid in a Erlenmeyer flask. The solution was stirred until dissolution of the copolymer before 50 mL of a solution containing $KBrO_3$ (0.1392 g, 0.834 mmol) and KBr (0.4960 g, 4.165 mmol) in a ratio of 1:5 (total salt concentration 0.1 M) was added. The mixture was stirred in the dark at room temperature for up to 6 hours, at which point the bromination of vinyl groups was confirmed by $^1$H-NMR.

When bromination was complete the solution was cooled in an ice-water bath, 2 mL concentrated HCl added and the solution stirred for 30 minutes. Potassium iodide (1.5 g) was added and the solution stirred until homogeneous. This solution was titrated with a 0.1 M sodium thiosulfate solution until pale yellow, at which point 0.5 mL of 1 % solution of starch in water was added to give a black solution. Further sodium thiosulfate solution was added, with the end point a colourless solution.

A "blank" titration, containing no polymer but identical solutions, was also carried out for use in calculation of BI.

Number of vinyl groups per gram was calculated using Bromine Index:

$$BI = \frac{7990.(V_1 - V_2).c}{m}$$

Where *BI* is the amount of bromine (mg) consumed by 100 g of polymer, $V_1$ and $V_2$ are the volume of $Na_2S_2O_3$ titrated in the blank and sample solutions, respectively; *c* is the concentration of $Na_2S_2O_3$ in mol.dm$^{-3}$ and *m* is the mass of polymer in grams.

| Reaction | [MAA]/[CoBF] | [EGDMA] (mol %) | BI | Vinyl groups (mol/g) |
|---|---|---|---|---|
| **19** | 21,400 | 3.2 | 16,400 | 1.03 |
| **20** | 21,700 | 4.7 | 13,600 | 0.85 |
| **21** | 29,500 | 4.7 | 9,300 | 0.58 |
| **22** | 27,800 | 9.9 | 17,500 | 1.09 |

## *Methylation of PMAA, P(MAA-co-AA) and P(MAA-co-EGDMA) using trimethylsilyl diazomethane in methanol.*

Methylation of polyacids was carried out as follows:

A glass vial, equipped with a stirring bar and septum, was charged with 50 mg polyacid dissolved in 1 mL MeOH and 0.3 mL TMS-diazomethane solution (2 M in diethyl ether) was added drop-wise *via* syringe. At this point 1 mL toluene was added to keep the methylated product soluble, before further TMS-diazomethane solution was added drop-wise until its yellow colour persisted for more than 30 minutes, indicating no further reaction. Nitrogen was blown over the open vial to remove volatiles and the concentrated polymer solution was precipitated from hexanes. Solid was recovered *via* centrifugation and dried at 40 $^{0}$C under vacuum.

### *2.6.4 Characterization*

**Characterization of 2-11** (**2**: linear PMAA prepared with 1.5 h feed of MAA and CoBF, [MAA]/[CoBF] 99,000. **3**: linear PMAA with 2.5 h feed of MAA and CoBF, [MAA]/[CoBF] 62,700. **4**: linear PMAA with 2.5 h feed of MAA and CoBF, [MAA]/[CoBF] 31,000. **5**: linear PMAA with 2.5 h feed of MAA and CoBF, [MAA]/[CoBF] 16,100. **6**: linear PMAA prepared with 3 h feed of MAA and CoBF, [MAA]/[CoBF] 31,000. **7**: linear PMAA batch polymerization, [MAA]/[CoBF] 98,100. **8**: linear PMAA batch polymerization, [MAA]/[CoBF] 49,100. **9**: linear PMAA batch polymerization, [MAA]/[CoBF] 32,200. **10**: linear PMAA batch polymerization, [MAA]/[CoBF] 24,500. **11**: linear PMAA batch polymerization, [MAA]/[CoBF] 16,000)

$^{1}$H-NMR (300 MHz, $CD_3OD$ at 25 $^{o}$C): δ 0.80-1.65 (backbone $CH_3$), 1.75-2.30 (backbone $CH_2$), 2.35-2.70 (terminal backbone $C\underline{H}_2$=C), 5.55-5.75 (cis to terminal $CO_2H$ C=C$\underline{H}_a\underline{H}_b$), 6.20-6.25 (*trans* to terminal $CO_2H$ C=C$H_a\underline{H}_b$).

FT-IR: $\nu_{max}$/cm$^{-1}$ 3500-2500 (b, $CO_2H$, various bands), 2988 (m, CH sp$^3$), 1693 (s, C=O), 1480 (w, $CH_2$/$CH_3$), 1449 (w, $CH_2$/$CH_3$), .

Conventional SEC (g mol$^{-1}$): **2**: $M_n$ 6930, $M_w$ 14000, Đ 2.02. **3**: $M_n$ 3840, $M_w$ 8900, Đ 2.32. **4**: $M_n$ 3070, $M_w$ 6240, Đ 2.03. **5**: $M_n$ 2230, $M_w$ 3540, Đ 1.54. **6**: $M_n$ 3350, $M_w$ 7040, Đ 2.10. **7**: $M_n$ 7380, $M_w$ 11000, Đ 1.49. **8**: $M_n$ 4470, $M_w$ 6840, Đ 1.53. **9**: $M_n$ 4120, $M_w$ 6100, Đ 1.48. **10**: $M_n$ 3490, $M_w$ 4960, Đ 1.42. **11**: $M_n$ 3090, $M_w$ 4350, Đ 1.41.

SEC-DRI-VISC Universal Calibration (g mol$^{-1}$): **7**: $M_n$ 5490, $M_w$ 9170, Đ 1.67.

GC-FID (final conversion, %): **2**: > 99. **3**: 98.5. **4**: 96.9. **5**: 97.6. **6**: X. **7**: > 99. **8**: > 99. **9**: 98.9. **10**: 97.5. **11**: 97.5.

**Characterization of 12-14** (**12**: P(MAA-*co*-AA) 90/10 w. % MAA/AA, [monomer]/[CoBF] 25,500. **13**: P(MAA-*co*-AA) 80/20 w. % MAA/AA, [monomer]/[CoBF] 25,500. 14: P(MAA-*co*-AA) 70/30 w. % MAA/AA, [monomer]/[CoBF] 25,500.)

$^1$H-NMR (250 MHz, $CD_3OD$ at 25 $^oC$): δ 0.80-1.45 (backbone $CH_3$), 1.55-2.30 (backbone $CH_2$, CH), 2.35-2.65 (terminal backbone $C\underline{H}_2$=C), 5.55-5.65 (cis to terminal $CO_2H$ C=C$\underline{H}_a$H$_b$), 6.15-6.25 (*trans* to terminal $CO_2H$ C=CH$_a\underline{H}_b$).

FT-IR: $\nu_{max}/cm^{-1}$ 3500-2400 (b, $CO_2H$, various bands), 2987 (m, CH $sp^3$), 2900 (m, CH $sp^3$), 1694 (s, C=O), 1474 (w, $CH_2/CH_3$), 1451 (w, $CH_2/CH_3$).

Conventional SEC (g $mol^{-1}$): **12**: $M_n$ 4590, $M_w$ 8840, Đ 1.51. **13**: $M_n$ 14500, $M_w$ 32200, Đ 2.22. **14**: $M_n$ 17000, $M_w$ 90000, Đ 5.29.

SEC-DRI-VISC Universal Calibration (g $mol^{-1}$): **12**: $M_n$ 3780, $M_w$ 20400, Đ 5.39. **14**: $M_n$ 3580, $M_w$ 108000, Đ 30.18.

GC-FID (final conversion, %): **12**: MAA 98.8, AA 90.4, total 99.0. **13** MAA 95.0, AA 67.5, total 93.1. **14**: MAA > 99, AA 95.1, total 98.7.

**Characterization of 15-22** (**15**: P(MAA-*co*-EGDMA) 93/7 w. % MAA/EGDMA, [monomer]/[CoBF] 29,100. **16**: P(MAA-*co*-EGDMA) 90/10 w. % MAA/EGDMA, [monomer]/[CoBF] 29,500. **17** and **18** gave insoluble gels, no characterization obtained. **19**: P(MAA-*co*-EGDMA) 93/7 w. % MAA/EGDMA, [monomer]/[CoBF] 21,400. **20**: P(MAA-*co*-EGDMA) 90/10 w. % MAA/EGDMA, [monomer]/[CoBF] 21,700.)

$^1$H-NMR (400 MHz, $CD_3OD$ at 25 $^oC$): δ δ 0.80-1.65 (backbone $CH_3$), 1.70-2.35 (backbone $CH_2$), 2.40-2.70 (terminal backbone $C\underline{H}_2$=C), 4.05-4.35 (O$C\underline{H}_2C\underline{H}_2$O) 5.55-5.75 (cis to terminal $CO_2H$ C=C$\underline{H}_a$H$_b$), 6.20-6.25 (*trans* to terminal $CO_2H$ C=CH$_a\underline{H}_b$).

FT-IR: $\nu_{max}/cm^{-1}$ 3500-2400 (b, $CO_2H$, various bands), 2984 (m, CH $sp^3$), 2930 (m, CH $sp^3$), 1688 (s, C=O), 1632 (m, C=$CH_2$), 1478 (w, $CH_2/CH_3$), 1452 (w, $CH_2/CH_3$).

Conventional SEC (g $mol^{-1}$): **15**: $M_n$ 6690, $M_w$ 23600, Đ 3.53. **16**: $M_n$ 7400, $M_w$ 62200, Đ 8.41. **19**: $M_n$ 5400, $M_w$ 18400, Đ 3.41. **20**: $M_n$ 4920, $M_w$ 25200, Đ 5.12. **21**: $M_n$ 2670, $M_w$ 7260, Đ 2.72. **22**: $M_n$ 4680, $M_w$ 21100, Đ 4.51.

SEC-DRI-VISC Universal Calibration (g $mol^{-1}$): **19**: $M_n$ 3780, $M_w$ 20400, Đ 5.39. **20**: $M_n$ 3580, $M_w$ 108000, Đ 30.18. **21**: $M_n$ 2900, $M_w$ 8510, Đ 2.93. **22**: $M_n$ 3440, $M_w$ 32000, Đ 9.30.

GC-FID (final conversion, %): **15**: MAA 96.5, EGDMA > 99, total 97.2. **16**: MAA 96.7, EGDMA > 99, total 97.7. **19**: MAA 97.0, EGDMA > 99, total 98.0. **20**: MAA 94.3, EGDMA > 99, total 94.9 **21**: MAA 91.4, EGDMA > 99, total 92.1. **22**: MAA 92.3, EGDMA > 99, 9, total 94.3.

**Characterization of 19-Me – 22-Me**

$^1$H-NMR (250 MHz, $CD_3OD$ at 25 $^oC$): δ δ 0.70-1.50 (backbone $CH_3$), 1.35-1.55 (terminal $CH_3$), 1.55-2.25 (backbone $CH_2$), 3.40-3.80 ($OCH_3$), 4.05-4.30 ($OC\underline{H}_2C\underline{H}_2O$) 6.2 (cis to terminal $CO_2H$ $C=C\underline{H}_aH_b$), 6.6 (*trans* to terminal $CO_2H$ $C=CH_a\underline{H}_b$).

SEC-DRI-VISC Universal Calibration (g $mol^{-1}$): **7-Me**: $M_n$ 4,270, $M_w$ 7,800, Đ 1.59. **19-Me**: $M_n$ 3,720, $M_w$ 18,700, Đ 5.03. **20-Me**: $M_n$ 5,770, $M_w$ 141,000, Đ 24.42. **21-Me**: $M_n$ 1,990, $M_w$ 6,600, Đ 3.32. **22-Me**: $M_n$ 5,090, $M_w$ 33,500, Đ 6.58.

## *2.7 References*


1. P. C. Hiemenz, T. P. Lodge, *Polymer Chemistry*, 2 ed., CRC Press: Taylor & Francis Group, **2007**.
2. A. Streigel, W. Yau, J. Kirkland, D. Bly, *Modern Size-Exclusion Liquid Chromatography: Practice of Gel Permeation and Gel Filtration Chromatography. 2nd Ed.; Wiley.* **2009**.
3. M. Gaborieau, J. Nicolas, M. Save, B. Charleux, J.-P. Vairon, R. G. Gilbert, P. Castignolles, *J. Chromatogr. A* **2008**, *1190*, 215.
4. L. K. Kostanski, D. M. Keller, A. E. Hamielec, *J. Biochem. Bioph. Methods* **2004**, *58*, 159.
5. A. M. Striegel, *Anal. Chem.* **2005**, *77*, 104 A.
6. Z. Grubisic, P. Rempp, H. Benoit, *Journal of Polymer Science Part B: Polymer Letters* **1967**, *5*, 753.
7. A. Dondos, H. Benoit, *Polymer* **1977**, *18*, 1161.
8. G. Saunders, P. A. G. Cormack, S. Graham, D. C. Sherrington, *Macromolecules* **2005**, *38*, 6418.
9. O. Procházka, P. Kratochvíl, *J. Appl. Polym. Sci.* **1987**, *34*, 2325.
10. M. Netopilík, J. Podešva, J. Lokaj, P. Kratochvíl, *Polym. Int.* **2008**, *57*, 1152.
11. E. E. Drott, R. A. Mendelson, *Journal of Polymer Science Part A-2: Polymer Physics* **1970**, *8*, 1373.
12. P. F. W. Simon, A. H. E. Müller, T. Pakula, *Macromolecules* **2001**, *34*, 1677.
13. B. H. Zimm, W. H. Stockmayer, *J. Chem. Phys.* **1949**, *17*, 1301.
14. B. H. Zimm, *J. Chem. Phys.* **1948**, *16*, 1093.
15. B. H. Zimm, R. W. Kilb, *Journal of Polymer Science* **1959**, *37*, 19.
16. D. M. Haddleton, E. Depaquis, E. J. Kelly, D. Kukulj, S. R. Morsley, S. A. F. Bon, M. D. Eason, A. G. Steward, *J. Polym. Sci., Part A: Polym. Chem.* **2001**, *39*, 2378.
17. G. Moad, C. L. Moad, *Macromolecules* **1996**, *29*, 7727.
18. F. R. Mayo, *J. Am. Chem. Soc.* **1943**, *65*, 2324.
19. J. P. A. Heuts, T. P. Davis, G. T. Russell, *Macromolecules* **1999**, *32*, 6019.
20. J. P. A. Heuts, N. M. B. Smeets, *Polym. Chem.* **2011**.
21. A. Gridnev, *Polym. J.* **1992**, *24*, 613.
22. A. Bakac, J. H. Espenson, *J. Am. Chem. Soc.* **1984**, *106*, 5197.
23. H. B. Gjerde, J. H. Espenson, *Organometallics* **1982**, *1*, 435.
24. D. M. Haddleton, D. R. Morsley, J. P. O'Donnell, S. N. Richards, *J. Polym. Sci., Part A: Polym. Chem.* **1999**, *37*, 3549.

25. A. A. Gridnev, S. D. Ittel, *Chem. Rev.* **2001**, *101*, 3611.
26. D. C. Woska, Z. D. Xie, A. A. Gridnev, S. D. Ittel, M. Fryd, B. B. Wayland, *J. Am. Chem. Soc.* **1996**, *118*, 9102.
27. S. Slavin, K. A. McEwan, D. M. Hadddleton, *Cobalt Catalysed Chain Transfer Polymerization: A Review* in *Polymer Science: A Comprehensive Reference, Vol. 3*, Elsevier, Oxford, **2012**, pp. 249.
28. J. Chiefari, J. Jeffery, R. T. A. Mayadunne, G. Moad, E. Rizzardo, S. H. Thang, *Macromolecules* **1999**, *32*, 7700.
29. A. A. Gridnev, S. D. Ittel, C. L. Moad, G. Moad, E. Rizzardo, L. Wilczek, WO1997031030 A1, **1997**.
30. J. C. Lin, K. J. Abbey, US4680354 A, **1987**.
31. S. Ali-Miraftab, M. Ansarian, A. Chapiro, Z. Mankowski, *Eur. Polym. J.* **1981**, *17*, 947.
32. A. Chapiro, L. D. Trung, *Eur. Polym. J.* **1978**, *14*, 393.
33. K. G. Suddaby, K. H. Hunt, D. M. Haddleton, *Macromolecules* **1996**, *29*, 8642.
34. A. Gridnev, *J. Polym. Sci., Part A: Polym. Chem.* **2000**, *38*, 1753.
35. G. Odian, *Principles of Polymerisation*, 4th ed., John Wiley & Sons, Hoboken, **2004**.
36. T. Gruendling, T. Junkers, M. Guilhaus, C. Barner-Kowollik, *Macromol. Chem. Phys.* **2010**, *211*, 520.
37. A. Dondos, V. Skordilis, *Journal of Polymer Science: Polymer Physics Edition* **1985**, *23*, 615.
38. L. Mrkvičková, *J. Liq. Chromatogr. R. T.* **1997**, *20*, 403.
39. W. H. Stockmayer, M. Fixman, *Journal of Polymer Science Part C: Polymer Symposia* **1963**, *1*, 137.
40. Z. Guan, *J. Am. Chem. Soc.* **2002**, *124*, 5616.
41. Z. Guan, *US5767211* **1998**.
42. C. Gao, D. Yan, *Prog. Polym. Sci.* **2004**, *29*, 183.
43. S. G. Gaynor, S. Edelman, K. Matyjaszewski, *Macromolecules* **1996**, *29*, 1079.
44. Y. H. Kim, *J. Polym. Sci., Part A: Polym. Chem.* **1998**, *36*, 1685.
45. B. Voit, *J. Polym. Sci., Part A: Polym. Chem.* **2000**, *38*, 2505.
46. P. A. Costello, I. K. Martin, A. T. Slark, D. C. Sherrington, A. Titterton, *Polymer* **2002**, *43*, 245.
47. F. Isaure, P. A. G. Cormack, D. C. Sherrington, *J. Mater. Chem.* **2003**, *13*, 2701.
48. F. Isaure, P. A. G. Cormack, D. C. Sherrington, *Macromolecules* **2004**, *37*, 2096.
49. A. T. Slark, D. C. Sherrington, A. Titterton, I. K. Martin, *J. Mater. Chem.* **2003**, *13*, 2711.

50. J. M. J. Fréchet, M. Henmi, I. Gitsov, S. Aoshima, M. R. Leduc, R. B. Grubbs, *Science* **1995**, *269*, 1080.
51. S. Li, J. Han, C. Gao, *Polym. Chem.* **2013**, *4*, 1774.
52. T. Zhao, Y. Zheng, J. Poly, W. Wang, *Nat Commun* **2013**, *4*, 1873.
53. Q. Zhang, S. Slavin, M. W. Jones, A. J. Haddleton, D. M. Haddleton, *Polym. Chem.* **2012**, *3*, 1016.
54. D. J. Krasznai, T. F. L. McKenna, M. F. Cunningham, P. Champagne, N. M. B. Smeets, *Polym. Chem.* **2012**, *3*, 992.
55. A. H. Soeriyadi, G.-Z. Li, S. Slavin, M. W. Jones, C. M. Amos, C. R. Becer, M. R. Whittaker, D. M. Haddleton, C. Boyer, T. P. Davis, *Polym. Chem.* **2011**, *2*, 815.
56. K. A. McEwan, D. M. Haddleton, *Polym. Chem.* **2011**, *2*, 1992.
57. Z. Guan, *J. Polym. Sci., Part A: Polym. Chem.* **2003**, *41*, 3680.
58. X. Yang, L.-W. Zhu, L.-S. Wan, J. Zhang, Z.-K. Xu, *J. Mater. Res.* **2013**, *28*, 642.
59. J. Ferreira, J. Syrett, M. Whittaker, D. Haddleton, T. P. Davis, C. Boyer, *Polym. Chem.* **2011**, *2*, 1671.
60. E. Kühnel, D. D. P. Laffan, G. C. Lloyd-Jones, T. Martínez del Campo, I. R. Shepperson, J. L. Slaughter, *Angew. Chem. Int. Ed.* **2007**, *46*, 7075.
61. B. P. Fors, C. J. Hawker, *Angew. Chem. Int. Ed.* **2012**, *51*, 8850.
62. S. Graham, P. A. G. Cormack, D. C. Sherrington, *Macromolecules* **2004**, *38*, 86.

# 3 Application of branched, vinyl functional polyacids to dental composites

Herein the highly branched polymers synthesized in Chapter 2 are applied to a dual-cure polymer-inorganic composite material for dental applications – namely resin-modified glass ionomer cements. Some materials characterization techniques employed in this chapter will be introduced, particularly photo-coupled oscillatory rheometry and differential scanning calorimetry.

It was envisaged that the branched polyacids containing multiple vinyl end groups synthesized previously may provide an alternative to the methacrylate-tethered poly(acrylic acids) used in current photo-curable glass ionomer restoratives. With this in mind, a model photo-curable glass ionomer system was developed, in order to allow testing and comparison of different polymer components. This involved testing of a multi-component photo-initiating system and the effects of additives and polymer concentration on the cement. The curing of the materials was studied using a variety of online monitoring techniques, including photo-DSC, photo-rheology and series-mode FTIR. The compressive strengths of the final cements were also evaluated.

Additionally, a range of linear PAAs were synthesized *via* CRP and a portion of the groups modified with photo-polymerizable methacrylate groups. This allowed investigation of the effects of molecular weight and polymerizable functionality on the curing and mechanical properties of the resulting materials. These were compared to cements based on the linear and branched PMAAs, as well as commercial materials.

## 3.1 Introducing CCTP-derived branched PMAAs to GICs

The work cited in the introduction chapter demonstrates the desirability of non-linear, polymerizable polyacids for use in dental resins: such polymers would allow increased MW materials to be incorporated into the cement without compromising the workability of the material. This should allow greater mechanical properties – particularly strength and toughness – and facile mixing of the restorative before application. An added motivation for

this work is provided by economic factors, in that a cost-effective synthesis of such a polymer would be invaluable to a commercially viable process.

With this in mind, it appears that branched P(MAA-*co*-EGDMA) synthesized in the previous chapter may represent an efficient, one step route to polyacids containing multiple vinyl groups able to participate in photo-polymerization.

## 3.2 Characterization methods for photo-curable composites

### 3.2.1 Photo-DSC

Differential scanning calorimetry (DSC) measures the difference in the heat required to increase or maintain the temperature of a sample and reference, giving the difference in energy required as heat flow or heat flux. Chemical reactions and many physical transitions (for example, melting or crystallization) will be exothermic or endothermic. Such transitions will show as either peaks or troughs when heat flow is plotted against temperature (for dynamic experiments over a range of temperatures) or time (for isothermal studies), as more or less heat will be required to maintain sample temperature. DSC can be adapted so that the sample and reference cells are irradiated with a light-source split by a bifurcated light guide, allowing accurate monitoring of exothermic photo-polymerization reactions, which will have a negative heat flow. Integration of the curve can be used to calculate the enthalpy of polymerization and related to overall conversion of monomer vinyl groups.[1] DSC can also be used to monitor the acid-base neutralization component of the setting in glass-ionomer cements (which will also be exothermic), with the time taken for the heat flow to return to the baseline being a measure of the total time for the cement to fully set.[2] It should be noted that the polymerization and ionic setting reactions will occur concurrently, and will be indistinguishable by DSC.

### 3.2.2 Photo-Rheology

Rheology is the study of deformation of a material upon the application of a force, with the type of deformation depending on the state of material the force acts on. For example, a liquid would be expected to flow when a force is applied with the energy dissipated as heat, displaying viscous properties, whereas many solids will deform before regaining their shape when the force is removed, showing elastic properties. However, some solutions and materials, especially those containing polymers, show viscoelasticity – that is, they display

properties somewhere between those of a solid (elastic) and a liquid (viscous). In order to present and discuss measurements relating to such properties, some treatment of the theory of viscoelastic behaviour and oscillatory rheology measurements is necessary.[3-5]

## *Stress and Strain*

An oscillating rotational rheometer will subject the sample to a displacement and measure the resulting force. A diagram for this deformation, called simple shear, is shown in Figure 3.1: if one plate moves a distance d*x*, the sample has been subjected to a strain, $\gamma = dx/dy$, which is dimensionless and usually expressed as a percentage. The velocity of the plate $V_X = dx/dt$ and the shear rate can be written as $d(dx/dy)/dt = \dot{\gamma}$. While it takes the exertion of a force to affect this deformation on the material, alternatively it can be thought of as the material exerting a force on the moving plate. Total force will depend on the area of the plate in contact with the sample (A), and is thus considered as force per unit area, or stress, σ.

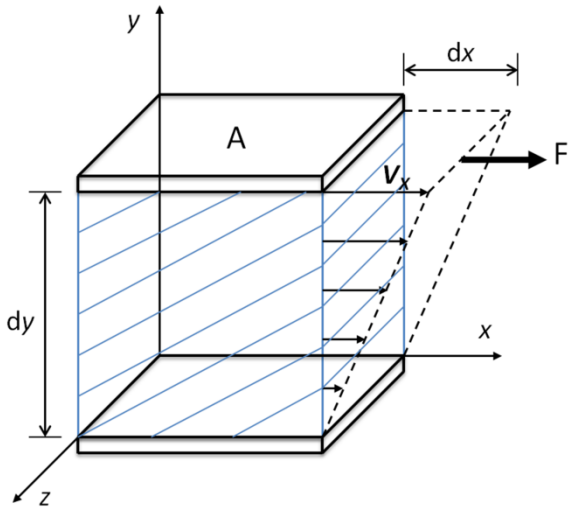


**Figure 3.1: Diagram of simple shear flow between two parallel plates.**

## *Viscosity and moduli*

The viscosity of a liquid can be defined as the ratio of stress to strain rate, as in Newton's relation (Equation 3.1) and, similarly, the modulus of a solid is defined as the ratio of stress to strain (Equation 3.2):

$$\sigma = \eta \dot{\gamma}$$

**Equation 3.1: Newton's relation, where η = viscosity.**

$$G = \sigma / \gamma$$

**Equation 3.2: The relationship between (shear) modulus, G, stress and strain.**

Measurements of moduli and viscosity should always be performed in the linear viscoelastic region of the material, when G is independent of the magnitude of strain – that is, the response is linear. This will generally be true as γ tends to 0, but obviously a finite strain is necessary to give a measurable stress.

## *Viscous and elastic response*

As mentioned above, the limiting cases in the rheology of polymeric materials are viscous and elastic response. Viscous flow requires *loss* of energy due to friction and heat, whereas elasticity reflects the storage of energy, allowing the material to recover after the deforming force is removed. Viscoelastic materials will show a combination of these, with the contribution of each determining its properties. A rotational rheometer in oscillatory mode will apply a sinusoidal time-varying strain at a certain frequency (ω), with the resulting stress also varying sinusoidally, but out of phase with the strain if the material shows some viscous properties (Figure 3.2). The resulting complex dynamic modulus (G*) is resolved into a real and imaginary modulus, as represented mathematically in Equation 3.3:

$$G^*(\omega) = \frac{\sigma^*(\omega)}{\gamma^*(\omega)} = G'(\omega) + iG''(\omega)$$

**Equation 3.3: Complex dynamic modulus resolved to (real) dynamic storage and (imaginary) loss modulus.**

The modulus in-phase with the applied strain, that is, relating to the instantaneous response of the material, will reflect the elastic component of the total modulus, and is called the (dynamic) storage modulus, G'. The modulus that is in-phase with the stress, and out of phase with the applied strain, reflects the viscous component of the response, and is called the (dynamic) loss modulus, G''. We can say that when G' >> G'' the material is solid-like, and when G'' >> G' the material is liquid-like.

Additionally, the complex viscosity of the fluid can be resolved in into a real and an imaginary component, as shown in Equation 3.4:

$$\eta^*(i\omega) = \frac{\sigma^*(i\omega)}{\gamma^*(i\omega)} = \eta'(\omega) - i\,\eta''(\omega)$$

**Equation 3.4: Complex viscosity resolved into real and imaginary components.**

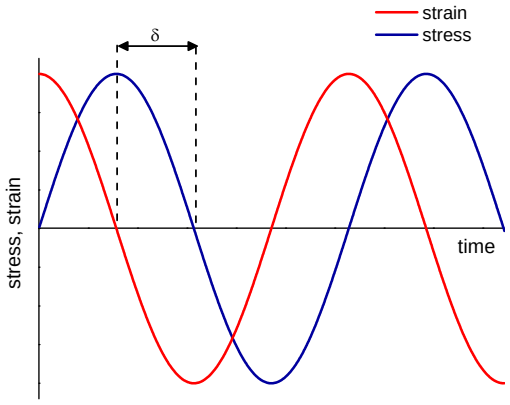


**Figure 3.2: Sinusoidally applied strain and resulting out of phase stress of a linear viscoelastic fluid, with the phase angle, δ, labelled.**

Inspection of the diagram of stress and strain in an oscillatory system (Figure 3.2) reveals another important quantity, the phase angle, δ. A phase angle of 90° suggests a purely viscous material, with the material flowing and the stress out of phase with the applied strain. A phase angle of 0° would be expected for an elastic solid, with the stress independent of frequency and in phase with strain. Alternatively, these observations can also be discussed in terms of the loss tangent, tan δ, which is defined as the ratio of viscous and elastic parts (Equation 3.5). A material behaving as a liquid will have tan δ >> 1, with tan δ << 1 for a solid.

$$\tan \partial = \frac{G''}{G'}$$

**Equation 3.5: The *loss tangent*, where δ is the phase angle and G'' and G' and the dynamic loss and storage moduli, respectively.**

Calculation of these quantities throughout the photo-curing of RMGIC type materials will allow monitoring of important aspects of the system. For example, monitoring the viscosity of the paste prior to photo-polymerization will give a measure of the workability of the cement and working time. Most critically, plotting G' and G'' as a function of time throughout photo-curing will give important information on the state of the material, providing a measure of the elastic, solid-like properties of the end product, and therefore the extent of curing.

## 3.3 Components of a photo-curable glass-ionomer system

### 3.3.1 Photo-polymerization system

Photo-curable dental restorations are highly desirable due to their "cure on demand" nature and the spatial control a light source provides. Much commercial and industrial photo-polymerization relies on UV wavelength curing, due to its higher energy relative to visible light. For dental applications, this is undesirable as the cost of UV lamps is higher compared to visible LEDs and the damaging effects of UV radiation on living tissue.[6] Therefore, the favoured light source for photo-polymerizable dental composites is in the visible range, typically with blue LEDs centred around 470 nm. Many visible light photo-initiation systems rely on a light absorbing ketone – typically camphorquinone (CQ) – as a photo-oxidizer, and indeed CQ-based systems have been extensively reported in dental systems.[7-10]

As visible light absorbed rarely exceeds the bond dissociation energy of organic molecules, the light absorbing molecule is usually combined with one or more additives in order to generate a species capable of initiating polymerization.[11-15] This leads to increased rate of photo-polymerization and in many cases enhances spectral sensitivity. Traditionally, these two component visible light systems can be separated into two distinct classes of system – those in which the photo-sensitizer is reduced, and those where the photo-sensitizer is oxidized.

Many common photo-initiating systems use CQ as a photo-oxidizer in conjunction with an amine acting as a photo-reducer. A mechanism proposed by Cook[1, 14] (Figure 3.3), based on photo-DSC and UV-vis experiments suggests excitation of CQ to a singlet state after absorbance of 470 nm radiation, which rapidly forms a more stable triplet state. This excited species and the tertiary amine then form an exciplex which, after electron and proton transfer, gives an aminoalkyl radical capable of initiating polymerization, in addition to a ketyl radical (which will not be capable of initiation). This system has been reported to give a large increase in rate of photo-polymerization, but consumes CQ.

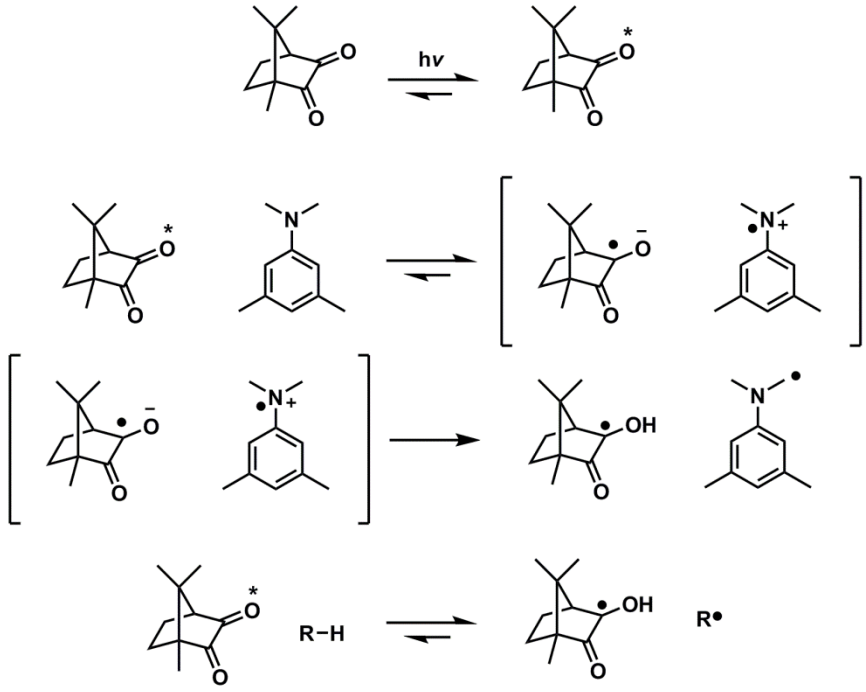


**Figure 3.3: Proposed mechanism for generation of propagating radicals by irradiation of CQ and TMA with visible light.[1]**

Some cationic initiating systems have used ketones as light absorbing reducers and onium salts as oxidizers, although it has been reported that some radicals capable of initiating radical polymerization will be formed, in addition to cations.[16] Cook postulates[1] that if no amine (or similar species capable of reducing the excited CQ state) is present, the excited CQ species can only be reduced in a slow process mediated by monomer. This would lead to slow photo-polymerization, as the DPI cation can only generate initiating radicals subsequent to the slow reduction of the excited CQ molecule (Figure 3.4). The authors find a relatively slow curing rate compared to the amine-system *via* photo-DSC. The results suggest that, despite being reported in patent[9, 17] and academic literature[6, 18-21] (which all describe satisfactory curing), the CQ/DPI initiating system would lead to slow initiation and slow curing rate.

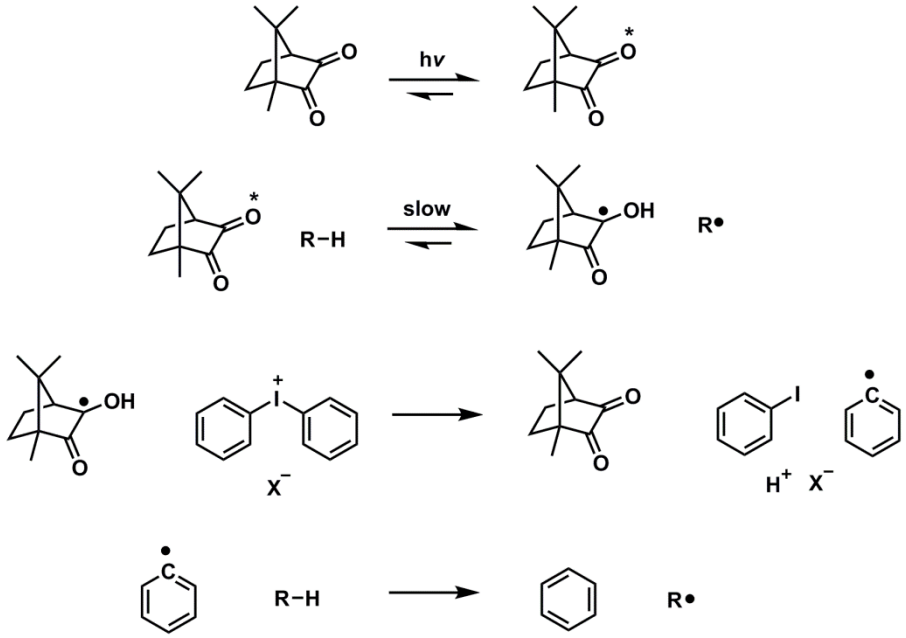


**Figure 3.4: Proposed mechanism for generation of propagating radicals (R˙) by irradiation of CQ and DPI with visible light.[1]**

Cook and Chen also investigated a relatively novel 3 component initiating system, using CQ in conjunction with a tertiary amine and an iodinium salt.[1] Photo-DSC experiments revealed that using this three component system led to a 5-fold increase in photo-polymerization rate (relative to CQ/amine systems), as well as rapid photo-bleaching of the CQ photo-sensitizer, which would be expected to allow greater depth of cure, which would have the additional benefit of removing the yellow colour of CQ from the material. The authors propose that the mechanism shown in Figure 3.3 will still occur, with reduction of the excited CQ molecule by the amine resulting in an active aminoalkyl radical and a ketyl radical. However, in the presence of the strongly oxidizing DPI cation, electron transfer to the ketyl radical will allow regeneration of CQ and production of a propagating phenyl radical (scheme). If this mechanism is correct, it will increase photo-initiation efficiency by converting terminating radicals to initiating radicals.

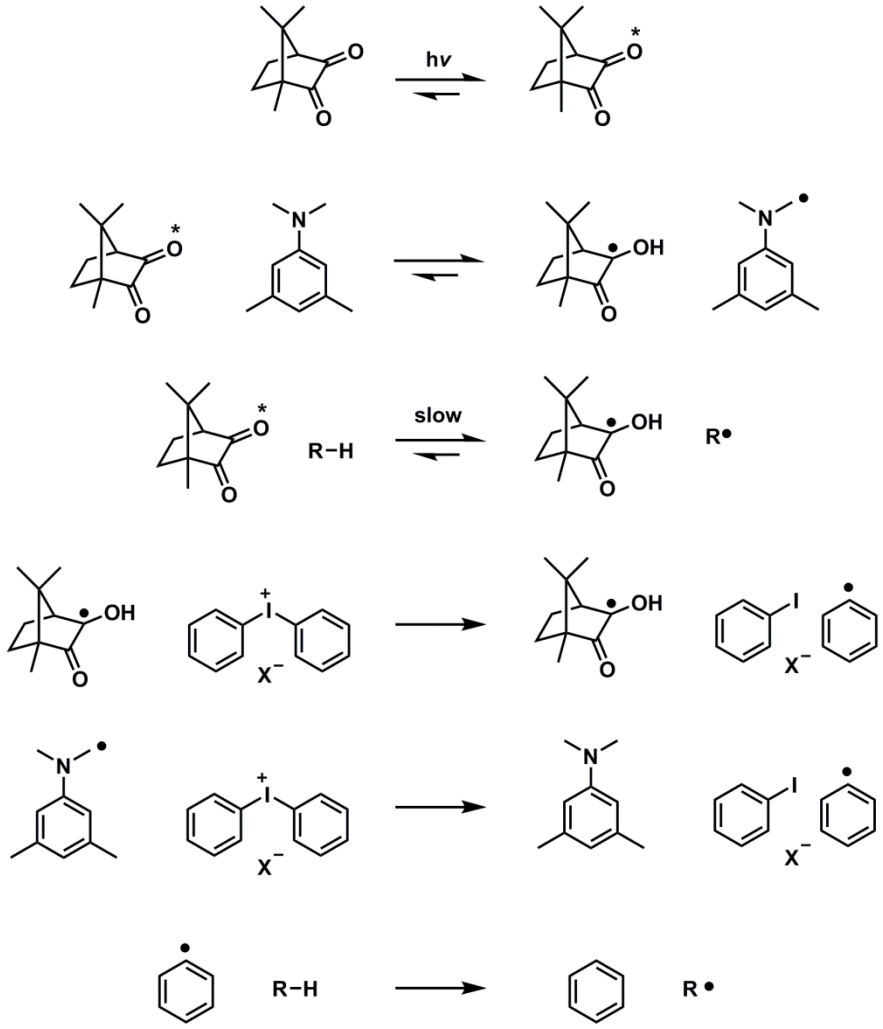


**Figure 3.5: Proposed mechanism for generation of propagating radicals in a 3 component system, comprising CQ, TMA and DPIX, irradiated with visible light.[1]**

Despite many mechanisms having been proposed for these systems, it is highly likely that several mechanisms occur simultaneously, and that monomer, solvent and other factors will influence the various pathways of photo-initiation. Regardless of the mechanism, the reported increase in rate of photo-polymerization warrants further investigation, as it may lead to increased rates of curing in the dental composites formulated in this work.

The two- and three-component CQ initiating systems will be investigated in formulations relevant to glass-ionomers, using diphenyl iodinium chloride (DPIC) and 3,5,*N,N*-tetramethylaniline (TMA). The monomer used will be HEMA, as it has been used extensively in RMGICs since their introduction,[8-9] along with the highly-branched, vinyl functional polyacids synthesized in Chapter 2.

## *3.4 Optimization of photo-polymerization initiating system*

As described in section 3.3.1, three component initiating systems based on CQ with a tertiary amine and a diphenyl iodinium salt have been shown to give more rapid curing than two component visible light initiating systems.[1, 14] However, these results relate to the homopolymerization of several dimethacrylates in bulk, rather than the more complex glass-ionomer systems; which will contain acidic polymer, one or more monomers, water and a reactive glass powder. Therefore, the three component visible photo initiating system was applied to a glass-ionomer type monomer system.

A simple photo-polymerizable ionomer solution – containing branched P(MAA-*co*-EGDMA) **15**, HEMA and water – was used to prepare three solutions containing both two component CQ initiating systems and the three component CQ/TMA/DPIC system (Table 3.1). These solutions were irradiated with visible light and analysed using photo-DSC. The photo-DSC experiment will give an indication of the rate of polymerization and allows for the calculation of the total change in enthalpy of the photo-polymerization, which can be linked to conversion using the heat of polymerization of HEMA and the theoretical enthalpy of polymerization.

| Solution | Ionomer Composition (w. %) | [CQ] (w. %) | [TMA] (w. %) | [DPIC] (w. %) | $-\Delta H$ [a] (J/g) | Conversion [b] (%) |
|---|---|---|---|---|---|---|
| **I-1** | polymer **15** - 33<br>HEMA - 33<br>water – 33 | 0.25 | 0.3 | 1 | 225 | 57 |
| **I-2** | polymer **15** - 33<br>HEMA - 33<br>water - 33 | 0.25 | - | 1 | 255 | 65 |
| **I-3** | polymer **15** - 33<br>HEMA - 33<br>water - 33 | 0.25 | 0.3 | - | 7 | 2 |

**Table 3.1: Data and compostion of ionomer solutions I-1 – 1-3, with various photo-initiator components.**
**[a]Measured by integration of DSC trace. [b] Calculated from enthalpy of polymerization.**

The calculated enthalpies suggest that both systems containing CQ and the DPI salt show moderate curing (**I-1** and **I-2**), with monomer conversion around 60 %. It is clear from the photo-DSC traces (Figure 3.6) that the CQ/TMA/DPIC system cures rapidly, with the CQ/DPIC system showing a slower rate of conversion and lower maximum heat flux. However, calculated enthalpies of polymerization show that the extent of reaction in two component system **I-2** is greater than the three component system. This may be due to vitrification of the solution at modest conversion to polymer reducing the mobility of the sample and preventing

further reaction. An alternative explanation for the rapid curing at the outset of experiment **I-1** leading to only around 60 % conversion to polymer could be that the rapid generation of radicals upon irradiation leads to increased termination and decreasing radical concentration after several minutes. The relatively similar values for conversion suggest the photo-initiating system and rate of cure of the two solutions have little effect on the final structure. In contrast to the two DPIC containing systems, solution **I-3** showed almost no evidence for photopolymerization. This may be due to the low pH of the ionomer solution, as the tertiary amine would be expected to be protonated, preventing it from reducing the excited CQ species and producing radicals. Interestingly, this effect is not seen in the CQ/TMA/DPIC three component system, which clearly shows an increased rate of conversion compared to the CQ/DPIC system.

These results conclusively show that the most rapid photo-initiation systems for curing of polyacid and HEMA containing ionomer solutions is the three component system described previously by Cook and Chen. However, Cook and Chen found the CQ/amine system to give a moderate cure, albeit relatively slowly.[1] This was not observed in the solutions investigated.

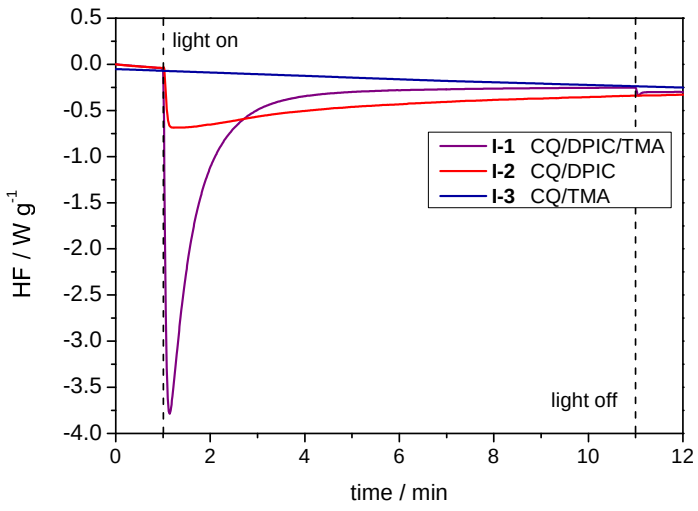


**Figure 3.6: Photo-DSC trace of ionomer solutions I-1 – I-3, with various photo-initiator components.**

The photo-polymerization activity of the three CQ containing systems was also investigated by online FTIR spectroscopy. Solutions **I-1** – **I-3** were cast as a 1 mm film on the ATR crystal of the spectrometer and the spectrum collected continuously as the sample was irradiated with visible light.

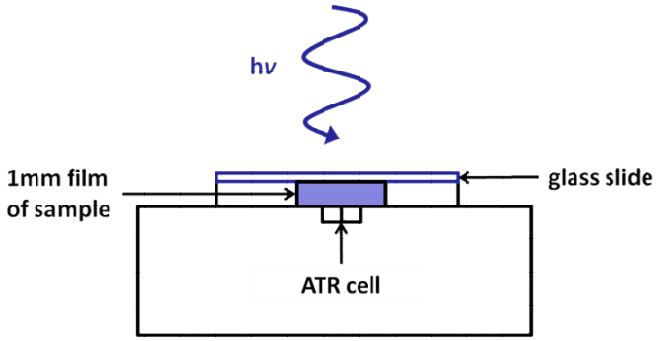


**Figure 3.7: Schematic of the set-up for online FTIR monitoring of photo-curing. A 1 mm film of the ionomer solution was cast on the ATR cell of the spectrometer and the spectra recorded as the sample was irradiated with visible light.**

Consumption of the vinyl groups could not be monitored directly using the vinylic C=C absorbance at around 1640 $cm^{-1}$, as this signal is obscured by water in the sample. However, the methacrylic C-O stretch has characteristic signals at 1325 and 1300 $cm^{-1}$ which shift to lower wavenumbers of 1275 and 1250 $cm^{-1}$ respectively upon saturation of the C=C double bond during polymerization.

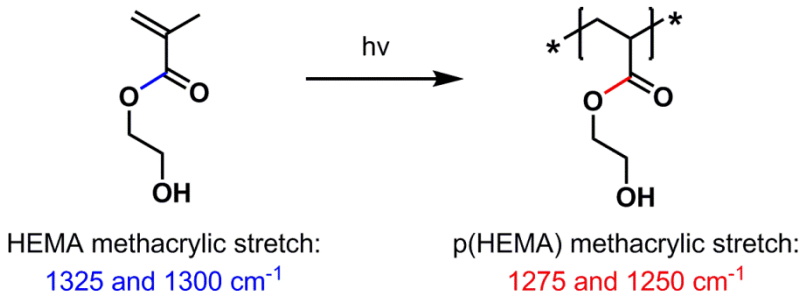


**Figure 3.8: HEMA and P(HEMA) with methacrylic stretch frequencies labelled.**

Analysis of the spectra collected throughout irradiation of ionomer solution **I-1** (Figure 3.9) reveals an isosbestic point due to the shift in the methacrylic C-O. A clear isosbestic point suggests that the change in the spectrum is due to a single transformation, indicating that these signals can be used to monitor the photo-polymerization of HEMA in these systems.

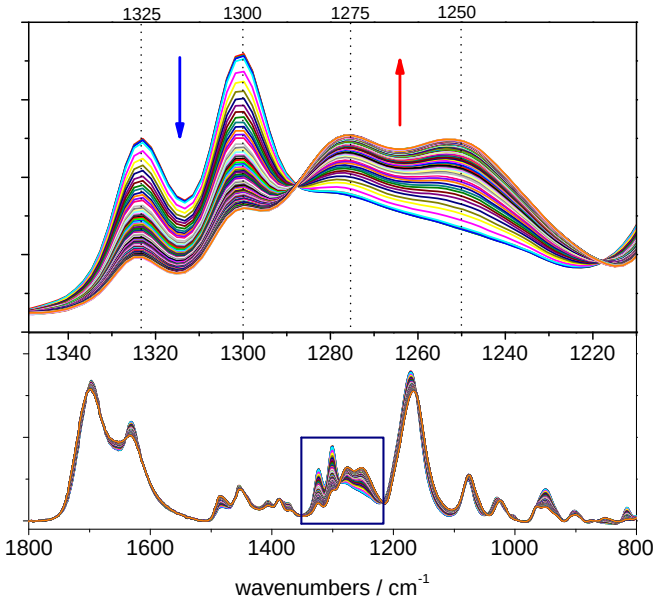


**Figure 3.9: Series mode online-FTIR spectra of ionomer solution I-1 during irradiation with visible light for 30 min, with expansion of isosbestic point at approximately 1290 $cm^{-1}$.**

Plotting the absorbance at these wavelengths against reaction time shows the disappearance of the monomer peaks and appearance of the polymer signals (Figure 3.10). This method allows comparison of the three initiating systems investigated by photo-DSC previously. The absorbances at these four key wavenumbers were plotted against time for ionomer solutions **I-1 – 1-3** (Figure 3.11). Unfortunately, the spectra could not be corrected for deviations in baseline sufficiently to be used to obtain absolute conversion data, but useful qualitative information can still be extracted.

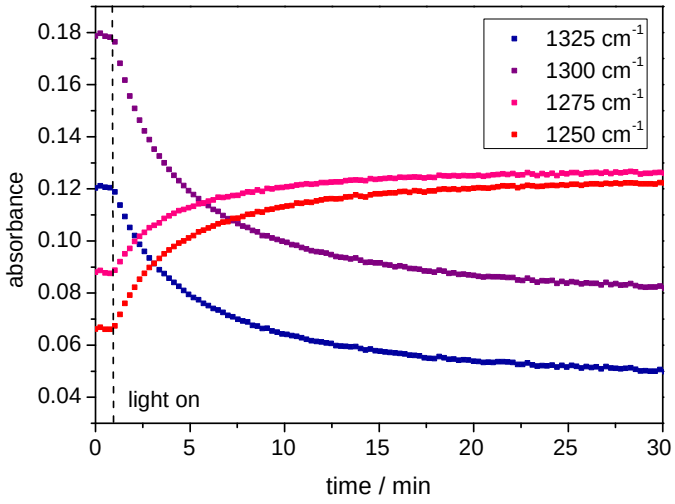


**Figure 3.10: FTIR absorbances at 1325 and 1300 $cm^{-1}$ due to the methacrylic stretch of HEMA and absorbances at 1275 and 1250 $cm^{-1}$ due to the methacrylic stretch of P(HEMA), plotted against time during irradtiation of the sample with visible light for 30 minutes.**

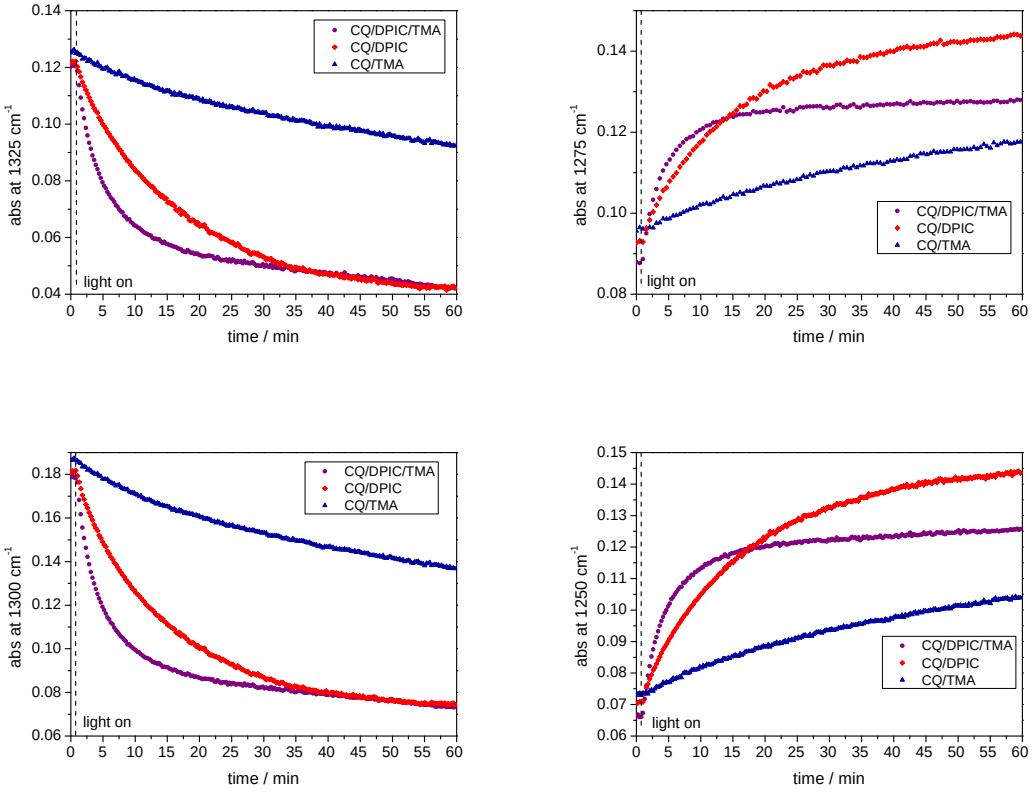


**Figure 3.11: FTIR absorbances due to HEMA (1325 and 1300 $cm^{-1}$, left) and P(HEMA) (1275 and 1250 $cm^{-1}$, right) for ionomer solutions I-1 (purple), I-2 (red) and I-3 (blue); plotted against time during irradtiation of the sample with visible light for 30 minutes.**

FTIR monitoring of the shift in methacrylic peaks during photo-polymerizations confirm that the CQ/TMA initiating system shows the least polymerization activity. This is seen in both the disappearance of the monomer peaks and the appearance of the peaks relating to polymer. The FTIR study also shows good agreement with the photo-DSC analysis of the rate of conversion, with CQ/TMA/DPIC system (**I-1**) showing the most rapid cure. Monitoring of the appearance of polymer peaks reveals that the CQ/DPIC system reaches a higher conversion at a slower rate, as previously shown by calculation of enthalpies of polymerization for photo-cure of ionomer solutions **I-1** and **I-3**. This provides further evidence that the rapid curing of the three component system may limit polymer mobility or lead to diminished concentration of radical generating species, thus preventing further curing of the material over on the time-scales measured.[1]

While these studies show conclusively that the three component initiating system provides the most rapid photo-initiation (if not the most complete curing), the solutions tested are not glass-ionomers systems. Therefore, these initiating systems were investigated in glass ionomer systems containing reactive glass powder, as well as the photo-curable monomer system. Ionomer solutions containing the same polymer, monomer and photo-initiator components as the ionomer solutions **I-1 - 1-3** above (Table 3.1) were prepared and mixed with reactive dental glass, in a 2:1 powder to liquid ratio, prior to irradiation with visible light and monitored by photo-DSC (Table 3.2). It should be noted that quantitative calculation of the enthalpy of polymerization will not be possible in these dual-cure systems, as the acid-base neutralization reaction between the polyacid and glass powder will also be exothermic. For this reason the DSC curve would not be expected to return to the baseline. Nonetheless, integration of the area of the DSC trace will give some information about the extent of cure in each system.

| Glass ionomer | Ionomer Composition (w. %) | [FAS glass] (w. %) | [CQ] (w. %) | [TMA] (w. %) | [DPIC] (w. %) | $-\Delta H$ [a] (J/g) |
|---|---|---|---|---|---|---|
| **GI-1** | polymer **15** - 33<br>HEMA - 33<br>water – 33 | 100 | 0.25 | 0.3 | 1 | 428 |
| **GI-2** | polymer **15** - 33<br>HEMA - 33<br>water - 33 | 100 | 0.25 | - | 1 | 620 |
| **GI-3** | polymer **15** - 33<br>HEMA - 33<br>water - 33 | 100 | 0.25 | 0.3 | - | 321 |

**Table 3.2: Composition and enthalpies of reaction for glass ionomers GI-1 – GI -3. [a] Measured by integration of DSC trace.**

Photo-DSC traces for curing of glass ionomers **GI-1 - 3** (Figure 3.12) show that while the two component and three component systems (**GI-1, GI-2**) containing CQ and DPIC show a similar maximum heat flow, the enthalpy of curing (which will have contributions from the photo-polymerization and acid-base setting reaction) is different for the two systems. The two component system shows an enthalpy of curing nearly 1.5 times greater than the three component system. It is possible that vitrification of the cement, due to the more rapid photo-polymerization expected for the CQ/TMA/DPIC system, may prevent further setting occurring during the time-scale of the experiment.

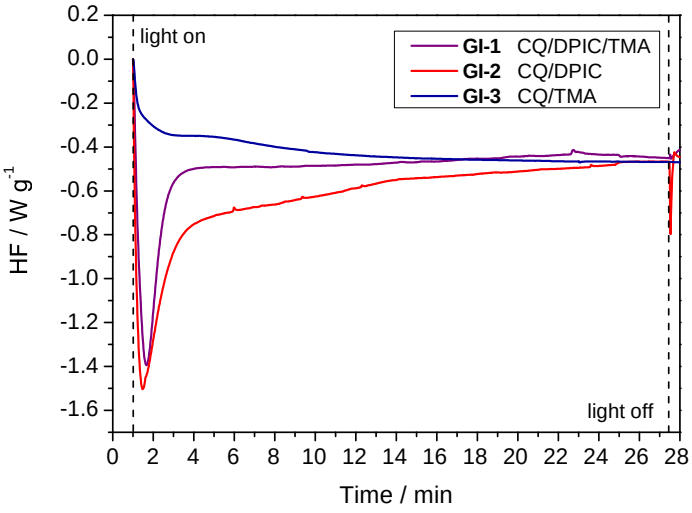


**Figure 3.12: Photo-DSC traces for glass ionomers GI-1 – GI -3, with varying concentrations of photo-initiator components.**

The two component system with CQ/TMA (**GI-2**) shows a relatively low extent of curing. This is due to the inefficiency of the photo-initiator used, as previously demonstrated. It is likely that the heat flux observed for this reaction is largely due to the ionic setting reaction.

The same glass ionomer cements were also analysed by oscillatory photo-rheology. This technique provides little information about the extent of polymerization or acid-base setting in the material, but will show the change in material properties throughout the curing process. The storage modulus, loss modulus and intrinsic viscosity were recorded throughout the curing process. The storage modulus (G') will give a measure of the elastic, solid-like properties of the material, and therefore can be used to monitor the degree of curing.

For viscous liquids, the loss modulus (G'') would be expected to dominate, as it relates to the loss of energy and delayed response to deformation: properties associated with liquid-like materials. However, the glass ionomers have G' and G'' values of similar magnitude during the early stages of curing, with G' quickly increasing during curing, Figure 3.13. These data suggest that the cements are near the gel point immediately after mixing, and behave primarily as elastic materials after a short time of irradiation or the "dark" ionic setting reaction. Figure 3.14 plots the calculated tan δ values, revealing that all cements exhibit primarily elastic properties within 1 min of irradiation, as indicated by tan $\delta << 1$.

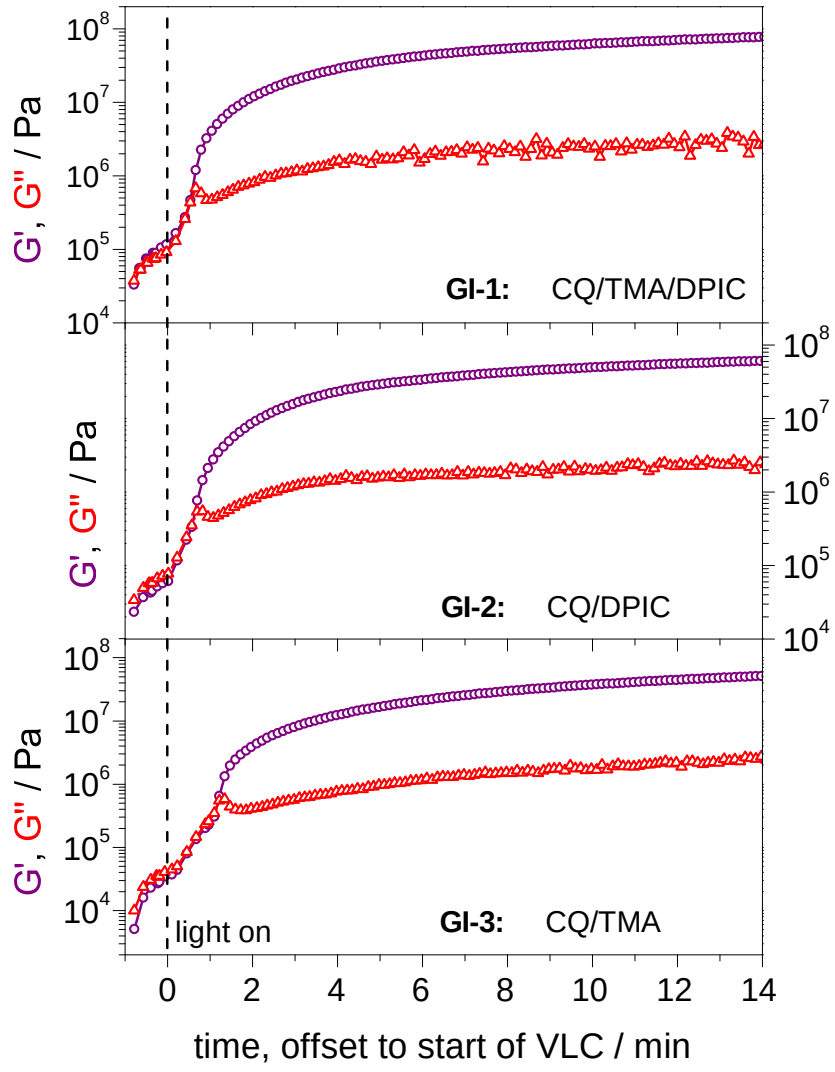


**Figure 3.13: Photo-rheology measurement of storage modulus (G') and loss modulus (G'') vs. time for irradiation of glass ionomers GI-1 (top), GI-2 (middle) and GI-3 (bottom).**

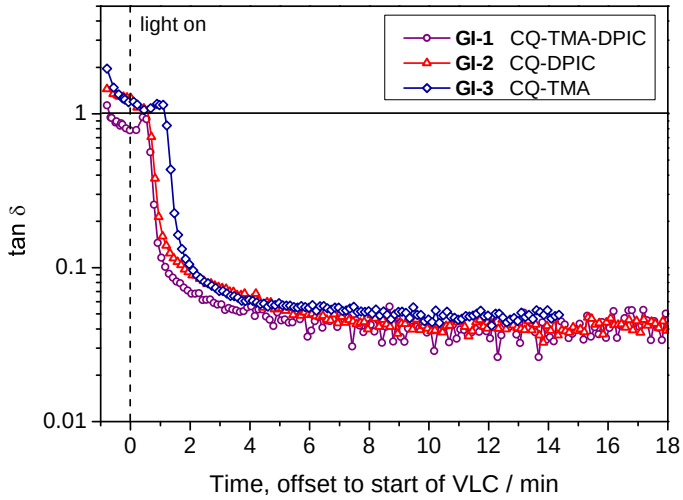


**Figure 3.14: Photo-rheology measurement of tan δ during irradiation of glass ionomers GI-1, GI-2 and GI-3, with varying concentrations of photo-inititor components.**

Figure 3.15 shows a plot of the storage modulus and complex viscosity of the three samples with the two and three component photo-initiating systems, allowing comparison of the curing time across the samples. As expected, the three component CQ/TMA/DPIC system (**GI-1**) shows the fastest increase in both G' and viscosity, reaching close to its final values within around 6 minutes. However, in contradiction of results obtained using photo-DSC, the rheology experiments for the CQ/TMA (**GI-3**) and CQ/DPIC (**GI-2**) systems suggest that the curing of the amine containing system is more rapid than that of the iodinium system. Nonetheless, these results clearly show the three component initiator to be the system of choice. It should be noted that while photo-DSC of the three component system appears to show a lesser extent of reaction than the CQ-TMA material, the rheology shows no such inhibition of curing (although, as stated previously, neither technique will provide any information on whether the change is due to the ionic or photo-polymerization reaction).

It should be noted that the deviations in baseline of the three materials prior to irradiation may be effects of the photo-initiation additives TMA and DPIC, which will both form salts in the ionomer solutions that could effect on the ionic setting of the cements.

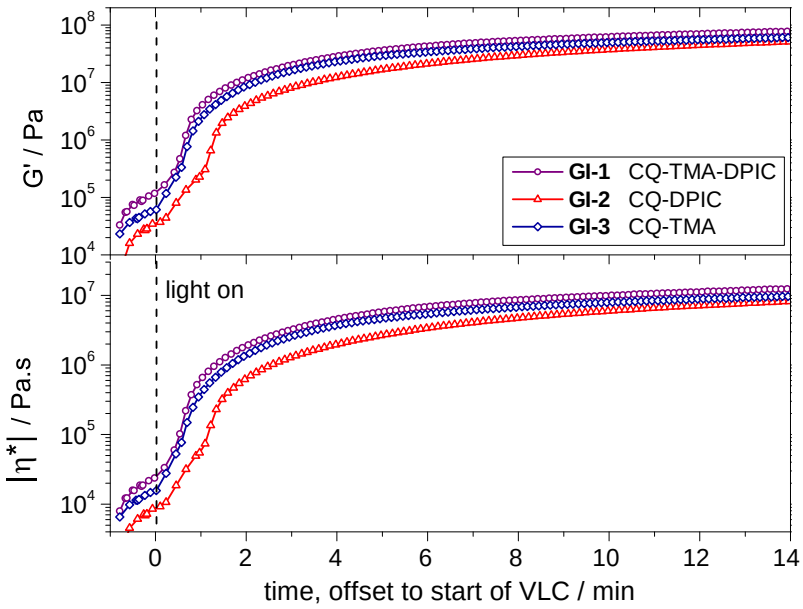


**Figure 3.15: Photo-rheology measurement of the storage modulus (G') and complex viscosity (|η*|) during irradiation of glass ionomers GI-1, GI-2 and GI-3, with varying concentrations of photo-inititor components.**

## *3.5 Optimization of polymer composite materials*

With an efficient photo-initiation system established, work moved toward improving the properties of the materials, in order to produce a model glass ionomer system.

As discussed previously (section 1.6.1), by far the most important additive in glass ionomer materials is (+)-TA, which is reported to have the two-fold effect of delaying the initial setting reaction (increasing working time) and sharpening the acid-base setting reaction after onset (leading to a stronger material).[22-24]

Generally speaking, increasing both the amount of glass powder in the final cement and the concentration of polymer in the liquid component will be expected to increase the mechanical strength of the material.[25-28] However, both will also lead to a very viscous mixture, which may be too viscous to work or have a very short working time. Additionally, such cements will often be difficult to mix efficiently, reducing the mechanical properties as the material will not be homogenous.

The effect of (+)-TA on glass ionomers formulated in this work will be studied as it is considered to be an essential additive for an acceptable cement to be obtained.[24, 29] As this work aims to focus on the polymeric components of these materials, the concentration of the

polymer in the ionomer solutions will be investigated, but the powder to liquid ratio of the materials will not be studied.

### *3.5.1 Effect of (+)-tartaric acid*

Ionomer solutions containing branched P(MAA-*co*-EGDMA) **19**, HEMA, water and the photo-initiating system were prepared with 0, 5 and 10 w. % (+)-TA (Table 3.3) and their curing upon irradiation with visible light monitored by photo-rheology (Figure 3.16).

| Glass ionomer | Sol$^{n}$. Composition (w. %) | $M_w$ of PMAA (g mol$^{-1}$) | [Fuji II LC glass] (w. %) | [CQ]:[TMA]:[DPIC] (w. %) | [(+)-TA] (w. %) | CS ± σ (MPa) |
|---|---|---|---|---|---|---|
| **GI-1** | polymer **19** - 33<br>HEMA - 33<br>water – 33 | 18,400 | 200 | 0.25 : 0.3 : 1 | 0 | < 1* |
| **GI-4** | polymer **19** - 33<br>HEMA - 33<br>water – 33 | 18,400 | 200 | 0.25 : 0.3 : 1 | 5 | 24.0 ± 2 |
| **GI-5** | polymer **19** - 33<br>HEMA - 33<br>water - 33 | 18,400 | 200 | 0.25 : 0.3 : 1 | 10 | 27.9 ± 3 |

**Table 3.3: Compositions and compressive strength of glass ionomers GI-1, GI-4 and GI-5, with varying concentration of (+)-TA. * Material gave CS outside of the range of the 10 kN load cell.**

The cement with 10 % (+)-TA (**GI-5**) clearly shows the fastest curing and reaches a greater G' than those containing 0 and 5 % of the additive. However, the material shows substantial setting even before the start of irradiation, with the viscosity and storage modulus considerably greater than the other samples. In contrast, **GI-4** with 5 % (+)-TA, shows a lower viscosity and modulus before irradiation than the sample without (+)-TA. This is indicative of the reported effect of the additive to delay the initial setting, and it should be noted that the viscosity and modulus of the material then increase to values larger than those of the additive free cement. The fact that this effect is not seen in the system with higher [(+)-TA] likely suggests that too high a concentration of the additive may lead to crosslinking of the cement by a different mechanism, which would involve (+)-TA not chelating cations but linking them together.

Both cements containing (+)-TA show an increase in the storage modulus throughout the 20 min experiment, in contrast to the additive free cement. This suggests that (+)-TA also has a beneficial effect on the properties of the cement over a longer time-scale.

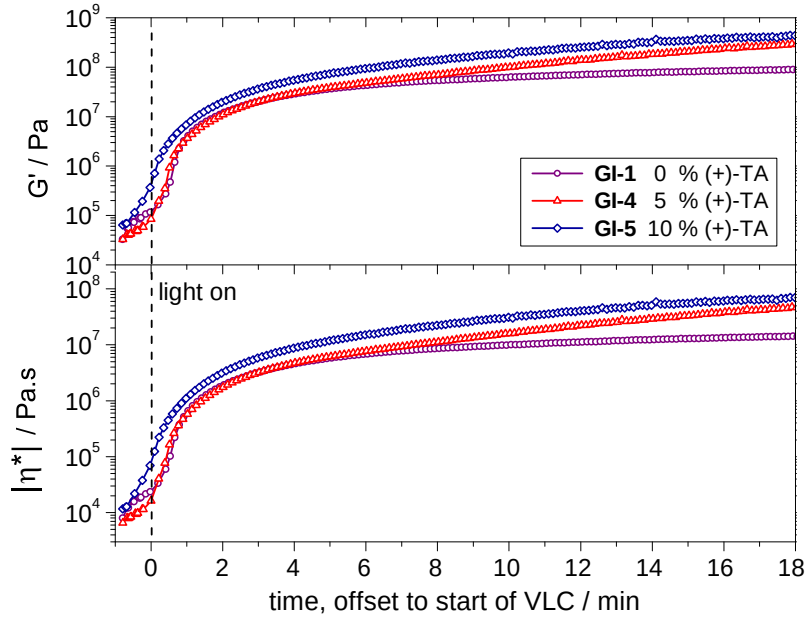


**Figure 3.16: Photo-rheology measurement of the storage modulus (G') and complex viscosity (|η*|) during irradiation of glass ionomers GI-1, GI-4 and GI-5, with varying concentrations of (+)-TA.**

In order to further study the effect of (+)-TA on the ionic setting reaction, the same rheology experiments were performed without irradiation (Figure 3.17). These "dark" experiments show an even more pronounced effect of the additive, with the cement containing 0 % of the additive (**GI-1**) taking around 30 minutes to reach its final G' value. The cements with 5 (**GI-4**) and 10 % (+)-TA (**GI-5**) show both sharper setting and reach higher G' values, indicating a more elastic material and a more complete cure. It should be noted, however, that overall extent of curing is still relatively slow, and that without polymerization of the vinylic monomer these would always provide unsatisfactory cements, as demonstrated by the lower G' values obtained compared to the photo-cured materials.

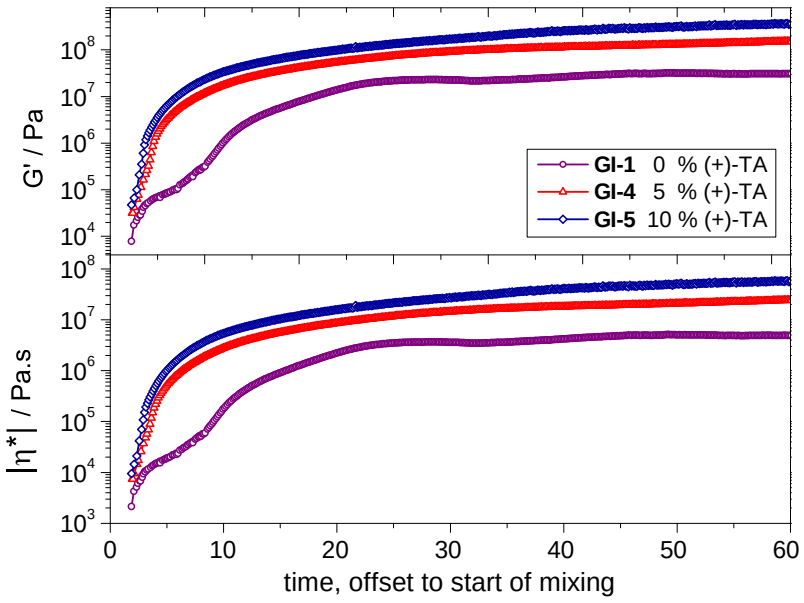


**Figure 3.17: "Dark"-rheology measurement of the storage modulus (G') and complex viscosity (|η*|) during the setting of glass ionomers GI-1, GI-4 and GI-5 in the absence of visible light, with varying concentrations (+)-TA.**

In order to evaluate the properties of the final cement, the fully-cured materials containing varying concentrations of (+)-TA were subjected to compressive strength (CS) testing. The mean CS values and range of the data is plotted in Figure 3.18. The composite with 0 % (+)-TA added showed a very low compressive strength, with the instrument's 10 kN load cell unable to provide an accurate measurement. The addition of 5 % (+)-TA (**GI-4**) gave a far stronger material with a CS value of 24.0 MPa, with the cement containing 10 % of the additive (**GI-5**) showing a more modest increase in strength to 27.9 MPa. However, the 10 % (+)-TA system shows an increased range and standard deviation (SD) of results than the material containing 5 %. This may be due to the increased viscosity of the material in the early stages of mixing preventing efficient mixing and the formation of a homogenous material.

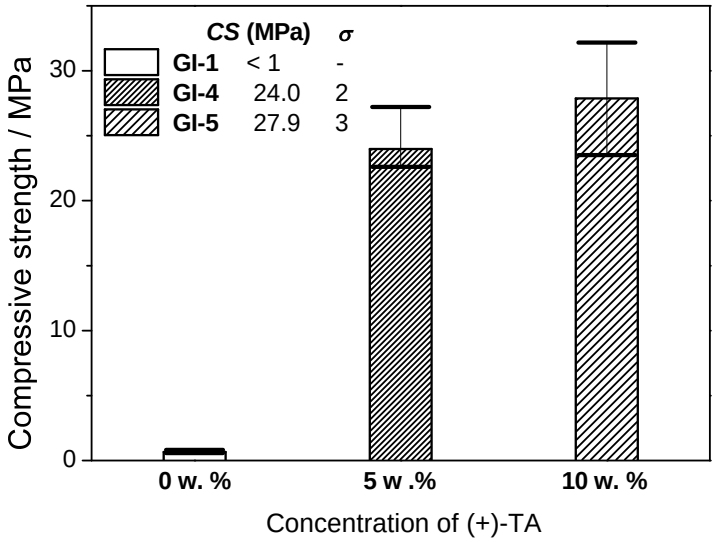


**Figure 3.18: Mean compressive strengths and standard deviations for glass ionomers GI-1 (0 % (+)-TA), GI-4 (5 % (+)-TA) and GI-5 (10 % (+)-TA). The range of values is represented by the whiskers.**

As this increased viscosity during mixing may limit the concentration and MW of the polymer incorporated into the cement, it was decided that further experiments would be conducted with 5 % (+)-TA, which would allow facile mixing while still providing a decrease of curing time and increase in the mechanical strength of the polymer.

### *3.5.2 Investigation of polymer concentration in liquid component of RMGICs*

It is desirable to increase the percentage of polymer in the liquid component not only for the increase in mechanical properties,[24-25, 29-30] but also as it will allow reduction of the concentration of monomer present in the cement. This will give a reduction in both shrinkage during polymerization – which can lead to poor restoration of a cavity – and the amount of residual monomer in the material – which could trigger an allergic reaction or sensitivity in the patient. However, as many monomers used in powder-liquid type RMGICs play an important role in solubilizing/compatibilizing the various components, the level of monomer present will usually not be below around 30 %.[6, 8, 17, 24, 29, 31-33] Ionomer solutions with concentrations of polymer from 33 to 50 w. % were prepared, mixed with Fuji II LC glass powder (Table 3.4) and their curing monitored by photo-rheology.

| Glass ionomer | Sol$^{n}$. Composition (w. %) | $M_w$ of PMAA (g mol$^{-1}$) | Powder : liquid ratio | [CQ]:[TMA]:[DPIC]:[(+)-TA] (w. %) | CS ± σ (MPa) |
|---|---|---|---|---|---|
| **GI-4** | polymer **19** - 33<br>HEMA - 33<br>water – 33 | 18,400 | 2 : 1 | 0.25 : 0.3 : 1 : 5 | 24.0 ± 2 |
| **GI-6** | polymer **19** - 40<br>HEMA - 27<br>water – 33 | 18,400 | 2 : 1 | 0.25 : 0.3 : 1 : 5 | 32.7 ± 3 |
| **GI-7** | polymer **19** - 50<br>HEMA - 17<br>water - 33 | 18,400 | 2 :1 | 0.25 : 0.3 : 1 : 5 | 28.8 ± 8 |

**Table 3.4: Composition and compressive strength values for glass ionomers GI-5 – GI-7, with varying concentration of polymer in ionomer solutions.**

As expected, the ionomer system with the lowest concentration of polymer shows (**GI-4**, with 33 % polymer) a greatly reduced storage modulus and viscosity immediately after mixing. However, the expected trend of increasing modulus and viscosity with increasing polymer concentration in the cement is not observed for the cements containing 40 % (**GI-6**) and 50 % (**GI-7**) polymer in the liquid component. The cement containing 40 % polymer reaches the highest storage modulus, despite having a similar viscosity and storage modulus to the material with 50 % polymer. This may be due to the reduced concentration of photo-polymerizable groups in cements with higher polymer concentration, as more polymer is incorporated at the expense of HEMA.

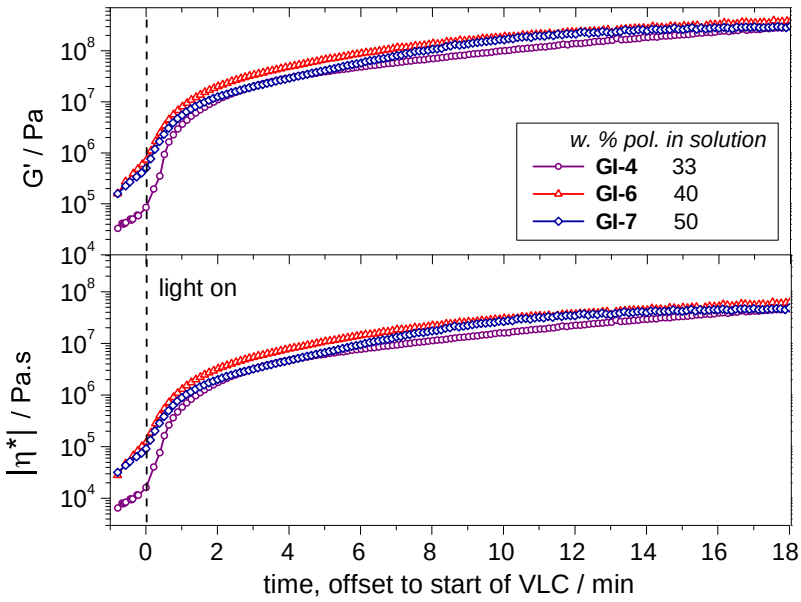


**Figure 3.19: Photo-rheology measurement of the storage modulus (G') and complex viscosity (|η*|) during irradiation of glass ionomers GI-4, GI-6 and GI-7, with varying concentrations of polymer in ionomer solutions.**

The compressive strengths of the cements with varying concentration of the polyacid were also evaluated, and results are shown in Figure 3.20. The increase in polymer concentration from 33 to 40 % yields the expected increase in the strength of the material, with the mean CS value increasing from 24.0 to 32.7 MPa. However, further increasing the polymer concentration to 50 % gives a lower CS value of 28.8 MPa (for **GI-6**). The range of the data presented (represented by the whiskers in Figure 3.20) shows that the maximum CS value for the three sets of tests is for the cement containing 50 % polymer, in a value far higher than the mean value for that system. This, coupled with the substantially greater standard deviation of the results for the most concentrated solution, suggests that the expected trend of increasing CS with polymer concentration may be followed if mixing and curing of the cements were identical between samples. From these results it is clear that the ionomer solutions containing 40 % polymer will give the most reliable and robust materials while maintaining good mechanical properties.

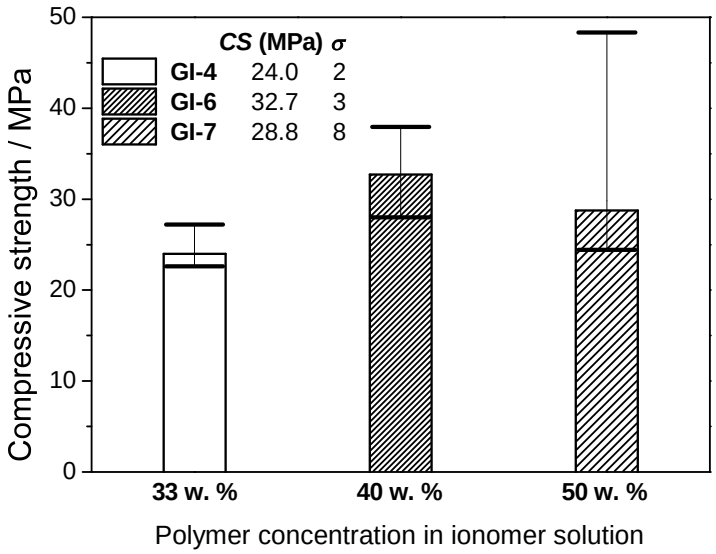


**Figure 3.20: Mean compressive strengths and standard deviations for glass ionomers GI-4 (33 w. % polymer in ionomer solution), GI-6 (40 w. % polymer in ionomer solution) and GI-7 (50 % polymer in ionomer solution). The range of values is represented by the whiskers.**

## *3.6 Variation of polymer materials*

### *3.6.1 Effect of molecular weight – PMAA*

In order to investigate the effects of changing the MW of the polyacid component on the curing and properties of the resulting glass-ionomer material, three ionomer solutions containing PMAAs of differing molecular weights were studied (Table 3.5). Photo-rheology (Figure 3.21) of the ionomer materials confirms the expected trend of increasing viscosity with MW, as can be seen before irradiation of the samples. Ionomer **GI-10**, containing the highest MW PMAA, also reaches the greatest G' value during the 18 min irradiation. However, the material containing a lower MW polymer (**GI-9**) does show an increased rate of curing in the early stages of irradiation, despite not reaching the G' value of **GI-10**.

| Glass ionomer | Ionomer Composition (w. %) | $M_w$ of PMAA (g $mol^{-1}$) | Powder : liquid ratio | [CQ]:[TMA]:[DPIC]:[(+)-TA] (w. %) | CS ± σ (MPa) |
|---|---|---|---|---|---|
| **GI-8** | polymer **10** - 40<br>HEMA - 27<br>water – 33 | 4,960 | 2:1 | 0.25 : 0.3 : 1 : 5 | 17.4 ± 7 |
| **GI-9** | polymer **7** - 40<br>HEMA - 27<br>water – 33 | 11,100 | 2:1 | 0.25 : 0.3 : 1 : 5 | 24.7 ± 4 |
| **GI-10** | polymer **2**- 40<br>HEMA - 27<br>water - 33 | 14,200 | 2:1 | 0.25 : 0.3 : 1 : 5 | 26.5 ± 6 |

**Table 3.5: Composition and compressive strength values for glass ionomers GI-8 – GI-10, with varying MW of PMAA in ionomer solutions.**

The CS of the cements were also evaluated, and are shown in Figure 3.22. The ionomer formulated with the lowest MW PMAA has the lowest mean CS, while there is little difference between **GI-9** and **GI-10**, containing PMAAs of 11,100 and 14,200 g $mol^{-1}$, respectively.

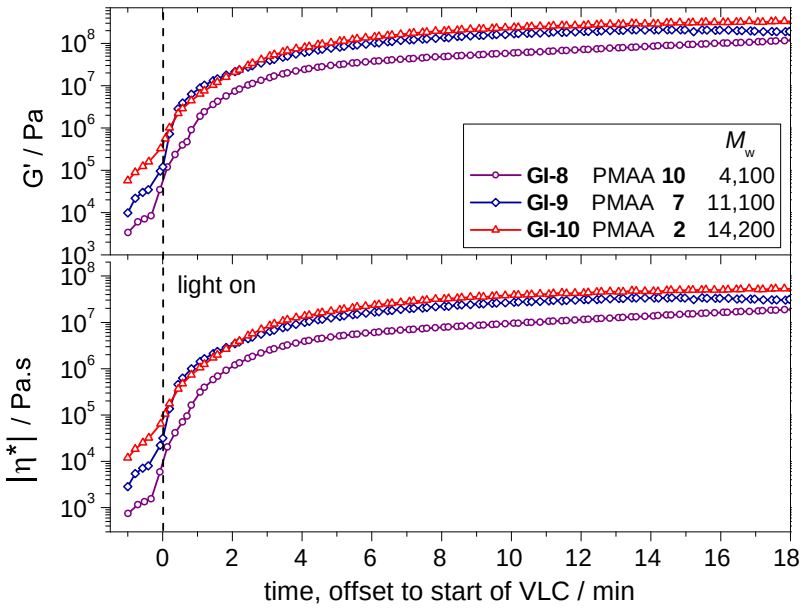


**Figure 3.21: Photo-rheology measurement of the storage modulus (G') and complex viscosity (|η*|) during irradiation of glass ionomers GI-8, GI-9 and GI-10, with varying MW of PMAA in ionomer solutions.**

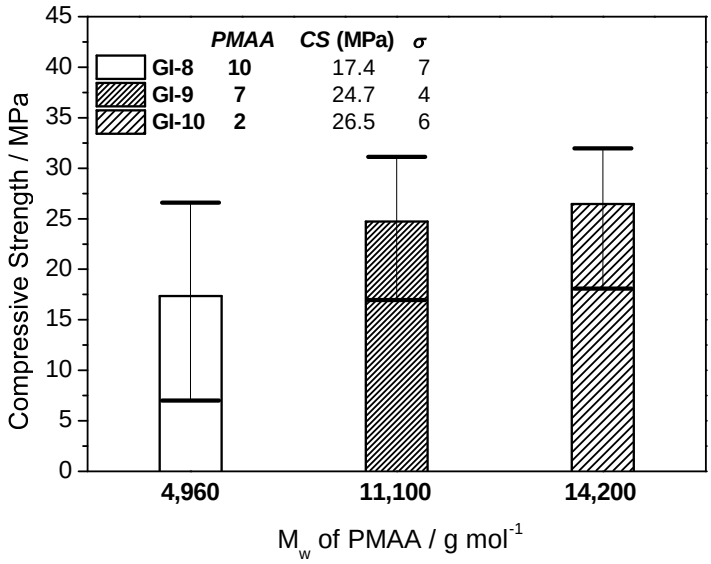


**Figure 3.22: Mean compressive strengths and standard deviations for glass ionomers GI-8 (containing PMAA 10 with $M_w$ 4,960 g mol$^{-1}$), GI-9 (containing PMAA 7 with $M_w$ 11,100 g mol$^{-1}$) and GI-10 (containing PMAA 2 with $M_w$ 14,200 g mol$^{-1}$). The range of values is represented by the whiskers.**

## *3.6.2 Synthesis and testing of methacrylate-tethered poly(acrylic acid)*

A major difference in the polymer component of cements investigated up to this point and the polymers used in commercial glass ionomers (and indeed those reported in the academic and patent literature) is that the commercial systems are nearly always based on PAA, rather than PMAA. Therefore, in order to evaluate the performance of the cements based on branched P(MAA-*co*-EGDMA) and linear PMAA, well defined PAAs were synthesized and modified with methacrylate groups by reported methods, Figure 3.23.[9, 17-18]

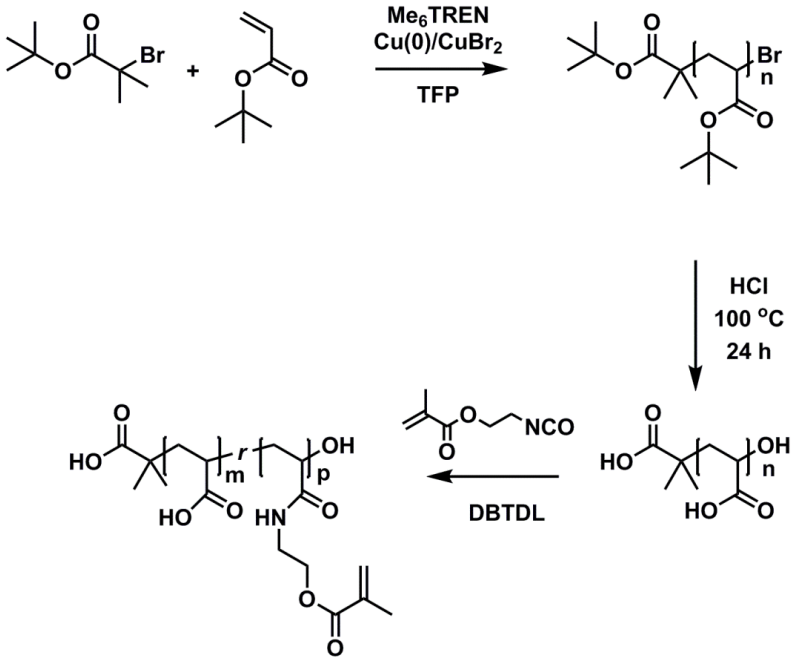


**Figure 3.23: Synthesis of methacrylate-tethered poly(acrylic acid) *via* Cu(0)-mediated CRP of *tert*-butyl acrylate, deprotection of *tert*-butyl groups under acid hydrolysis and coupling of carboxylic acids with 2-isocyanatoethyl methacrylate.**

Briefly, *tert*-butyl acrylate was polymerized *via* Cu(0)/Cu(II)/$Me_6$Tren-mediated CRP in 2,2,3,3-tetrafluoropropan-1-ol (TFP).[34-35] The *tert*-butyl protecting group was then removed by acid hydrolysis and a portion of the acrylic acid units modified with methacrylate groups using tin (dibutyltin dilaurate)-catalysed addition of 2-isocyanatoethyl methacrylate (IEM).

The Cu(0)-mediated polymerization afforded well-defined, low dispersity P(*t*-BA) products with $M_n$ close to the theoretical value (DPs of 70, 130 and 200 were targeted, Table 3.6), although induction periods were often observed. (It should be noted that the number average molecular weight is the more appropriate average for CRP processes, as opposed to the

transfer-dominated FRP processes which are best described by the weight average, and will be used throughout these sections).

| Polymer | [*t*BA]:[I]:[$Me_6$Tren]:[Cu(0)]:[$CuBr_2$] (eq.) | $M_n$ [th] (g $mol^{-1}$) | $M_n$ [a] (g $mol^{-1}$) | $Đ$ [a] | Conversion [b] (%) | Time (h) |
|---|---|---|---|---|---|---|
| **23** | 70 : 1 : 0.18 : 0.4 : 0.05 | 8,960 | 8,070 | 1.06 | 97.3 | 48 |
| **24** | 130 : 1 : 0.18 : 0.4 : 0.05 | 16,600 | 14,800 | 1.08 | 94.0 | 48 |
| **25** | 200 : 1 : 0.18 : 0.4 : 0.05 | 25,600 | 25,100 | 1.04 | 92.6 | 48 |

**Table 3.6: Equivalents of reagents and data for *t*BA homopolymerizations 23- 25 in TFP, with targeted DPs 70, 130 and 200. [a] Measured by conventional SEC-DRI, with 2 x PLgel mixed D columns, calibrated with PMMA standards, with $CHCl_3$ (1 % TEA) as eluent. [b] Measured by GC-FID with anisole internal standard.**

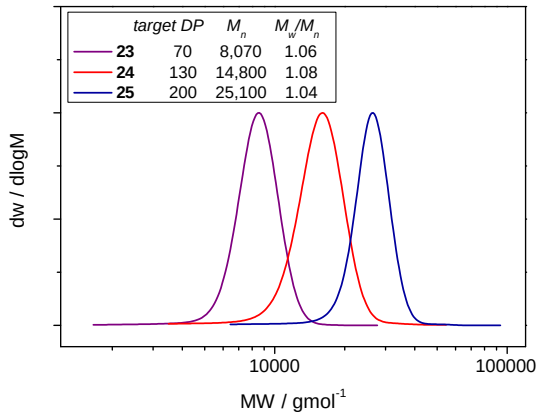


**Figure 3.24: SEC molecular weight distributions for *t*-BA homopolymers 23-25, with targeted DPs 70, 130 and 200.**

The synthesis of p(*t*BA) gave excellent control over the MW and gave access to PAAs of varying molecular weight. Removal of the *tert*-butyl group was achieved by heating the polymer to 100 °C for 24 h in concentrated HCl/dioxane.[18, 36-37] The successful deprotection was verified by the lack of signals for the *tert*-butyl methyl groups (at 1.36 ppm) in the $^1$H-NMR spectrum after precipitation of the product from acetonitrile (Figure 3.25). SEC revealed the polymer chains remained largely intact and with MW close to the theoretical values, although the deprotected polymers exhibited broader MWDs and significant tailing to low MW, which may indicate some degradation (Figure 3.26). However, as the SEC for the p(*t*BA) and PAA were performed using different eluents (chloroform and DMF, respectively) it is also possible that differing interactions between the polymer and solvent are responsible for this broadening of the distribution.

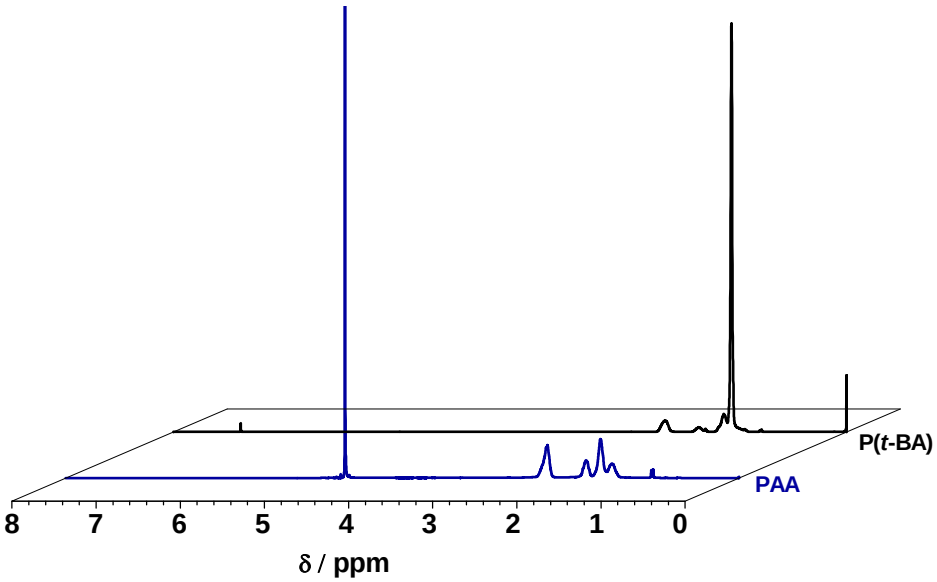


**Figure 3.25: $^{1}$H-NMR spectra of P(*t*-BA) 24 in $CDCl_3$ prior to deprotection (black) and PAA 27 in $D_2O$ after hydrolysis and precipitation (blue).**

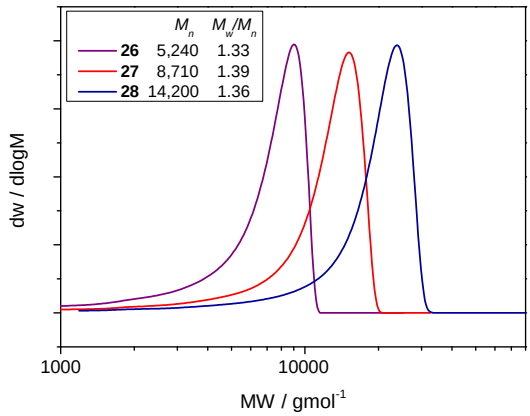


**Figure 3.26: SEC molecular weight distributions of PAA 26 – 28, derived from hydrolysis of P(*t*-BA)s 23 -25.**

Data for the deprotected PAAs are shown in Table 3.7. The MWs show good agreement with the theoretical values (calculated from the SEC-$M_n$ of the P(*t*BA)s), providing further evidence that deprotection has been successful and PAAs of the desired MW have been produced.

| Polymer | $M_n$ of P(*t*-BA) prior to hydrolysis (g mol$^{-1}$) | $M_n^{th}$ (g mol$^{-1}$) | $M_n$ [a] (g mol$^{-1}$) | $Đ$ [a] |
|---|---|---|---|---|
| **26** | 8,070 | 5,020 | 5,240 | 1.33 |
| **27** | 14,800 | 8,290 | 8,710 | 1.39 |
| **28** | 25,100 | 14,100 | 14,200 | 1.36 |

**Table 3.7: Molecular weight and dispersity of PAAs 26 – 28 dervived from the hydrolysis of P*t*BAs 23 - 25. Theoretical $M_n$ calculated from the loss of the *tert*-butyl protecting group. [a] Measured by conventional SEC-DRI, with 2 x PLgel mixed D columns, calibrated with PMMA standards, with DMF (1 mM $NH_4BF_4$) as eluent.**

The PAAs synthesized were then incorporated into glass ionomer systems analogous to those containing PMAA (Table 3.8) and analysed by photo-rheology and compressive strength testing.

| Glass ionomer | Ionomer Composition (w. %) | $M_n$ of PAA (g mol$^{-1}$) | Powder : liquid ratio | [CQ]:[TMA]:[DPIC]:[(+)-TA] (w. %) | CS ± σ (MPa) |
|---|---|---|---|---|---|
| **GI-11** | polymer **26** - 40<br>HEMA - 27<br>water – 33 | 5,240 | 2:1 | 0.25 : 0.3 : 1 : 5 | 32.2 ± 5 |
| **GI-12** | polymer **27** - 40<br>HEMA - 27<br>water – 33 | 8,710 | 2:1 | 0.25 : 0.3 : 1 : 5 | 55.1 ± 16 |
| **GI-13** | polymer **28**- 40<br>HEMA - 27<br>water - 33 | 14,200 | 2:1 | 0.25 : 0.3 : 1 : 5 | 56.6 ± 8 |

**Table 3.8: Compositions of glass ionomer cements GI-11 – GI-13, based on PAAs 26-28, with MWs from 5,240 – 14,200 g mol$^{-1}$.**

Photo-rheology reveals that the sharpest cure is achieved for the system containing the polymer with the lowest MW, **GI-11** (Figure 3.27). This is contrary to results obtained for the PMAA systems of similar MWs, in which both G' and the viscosity increased with MW, but little effect on the sharpness of the curing time was observed. The viscosities of the materials immediately after mixing also show little dependence on MW of the polymer. This somewhat anomalous data may perhaps be due to the increased viscosities of the ionomer solutions, relative to the linear PMAA analogues.

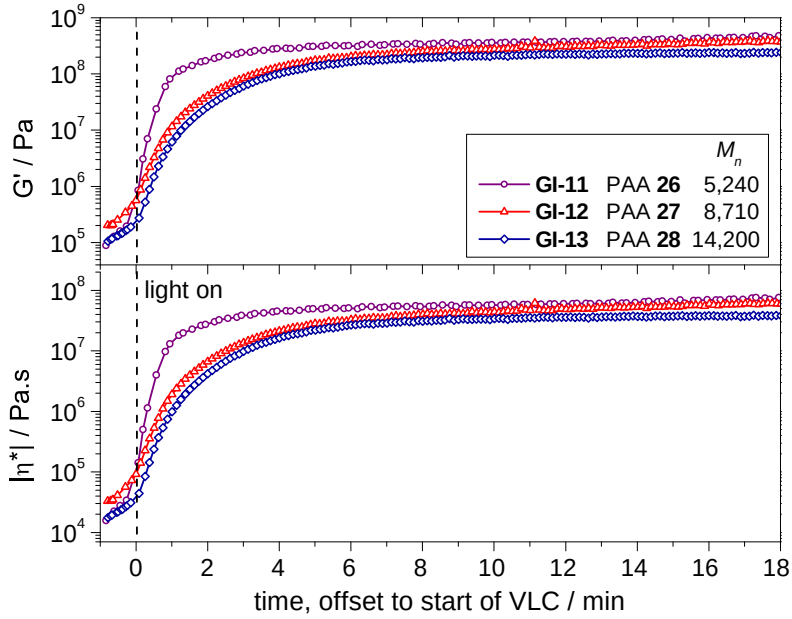


**Figure 3.27: Photo-rheology measurement of the storage modulus (G') and complex viscosity (|η*|) during irradiation of glass ionomers GI-11, GI-12 and GI-13, with varying MW of PAA in ionomer solutions.**

The CS values of cements based on PAA were also measured. Figure 3.28 shows the trend of increasing CS with increasing MW, although the cements with PAAs of 8,710 (**GI-12**) and 14,200 g $mol^{-1}$ (**GI-13**) have relatively similar values. Results for PAA- and PMAA-based systems containing polymers of similar MW are compared in Figure 3.29. CS values for the acrylic materials are approximately double those of the methacrylic materials, suggesting that PMAA-based systems provide inferior cements in the case of linear polymers. This could be due to the poor flexibility of the methacrylic polymer chains, relative to the acrylic chain, due to the backbone methyl group. This rigidity could hinder the efficient chelation of cations in the cement, as well as increasing the overall rigidity of the cement, leading to brittleness and a lack of mechanical strength. Conversely, the more flexible acrylic polymers may be expected to show more elastic properties, reducing fracturing of the material.

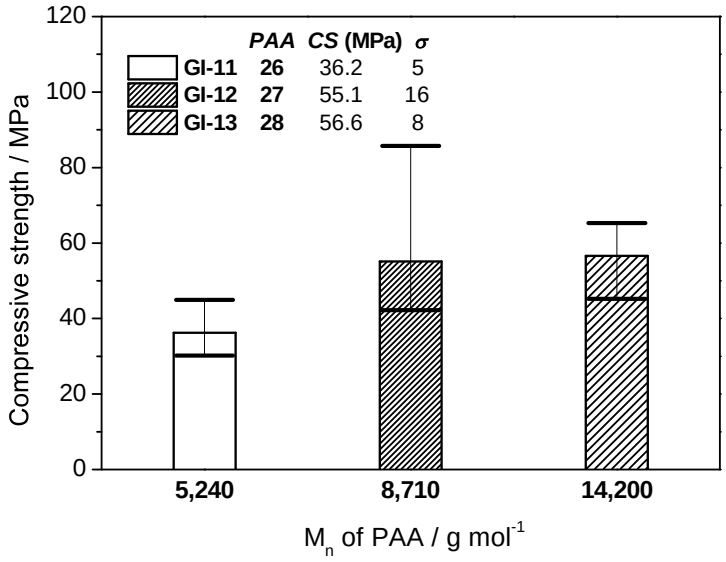


**Figure 3.28: Mean compressive strengths and standard deviations for glass ionomers GI-11 (containing PAA 26 with $M_w$ 5,240 g mol$^{-1}$), GI-12 (containing PAA 27 with $M_w$ 8,710 g mol$^{-1}$) and GI-28 (containing PAA 28 with $M_w$ 14,200 g mol$^{-1}$). The range of values is represented by the whiskers.**

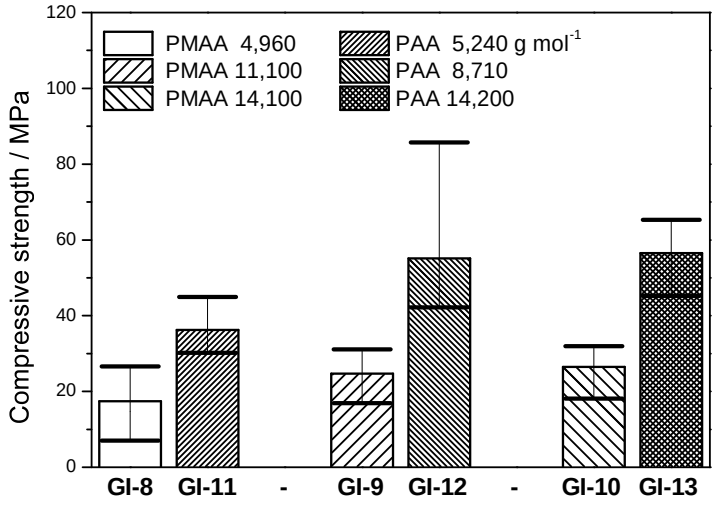


**Figure 3.29: Mean compressive strengths and standard deviations for glass ionomers GI-8 – GI-13, with varying molecular weights of PAA and PMAA in the ionomer solutions. The range of values is represented by the whiskers.**

Mitra[9, 17] and others[8, 18-19] have utilized the efficient coupling of isocyanates with carboxylic acids to functionalize the polyacid chains with polymerizable methacrylate groups (Figure 3.30).

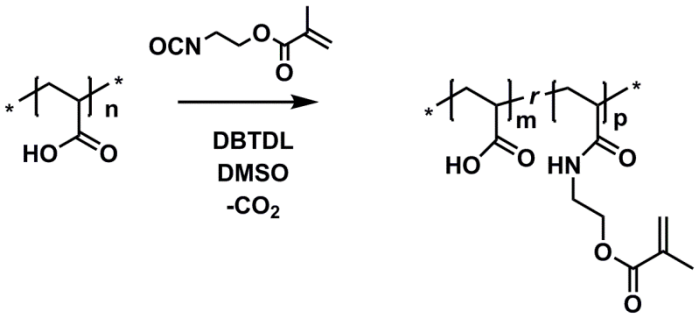


**Figure 3.30: Dibutyltin dilaurate catalysed coupling of the carboxylic acid of poly(acrylic acid) with 2-isocyanatoethyl methacrylate, with loss of $CO_2$.**

Using this method, the PAAs synthesized were functionalized with 25 w. % IEM (Table 3.9). The theoretical $M_n$ values calculated for the modified polymers correspond well to those measured by SEC, with the SEC-MWDs (Figure 3.31) narrowing significantly with respect to the native PAAs. This indicates the relatively broad MWDs for polymers **26 – 28** may be in part due to column interactions and differing $V_h$ of the native and hydrophobically modified PAAs in the DMF eluent.

| Polymer | $M_n$ of PAA prior to modification (g $mol^{-1}$) | $M_n$ $^{th}$ (g $mol^{-1}$) | $M_n$ $^{a}$ (g $mol^{-1}$) | $Đ$ $^{a}$ |
|---|---|---|---|---|
| **29** | 5,240 | 7,280 | 7,380 | 1.12 |
| **30** | 8,710 | 12,100 | 12,100 | 1.16 |
| **31** | 14,200 | 19,700 | 22,400 | 1.19 |

**Table 3.9: Molecular weight and dispersity of methacrylate-modifed PAAs 29 – 31 dervived from reaction of 25 w. % IEM with PAAs 26 - 28. Theoretical $M_n$ calculated from the addition of 25 w. % IEM. [a] Measured by conventional SEC-DRI, with 2 x PLgel mixed D columns, calibrated with PMMA standards, with DMF (1 mM $NH_4BF_4$) as eluent.**

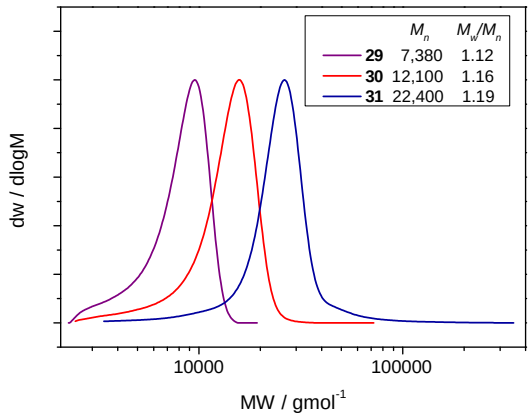


**Figure 3.31: SEC molecular weight distributions of methacrylate-modifed PAAs 29 – 31, derived from reaction 25 w. % IEM with PAAs 26 - 28.**

As discussed in section 1.6.2, methacrylate-tethered "resin modified" polymers have found extensive use in dental glass ionomer restoratives, as the polymerizable group should allow the polyacid to participate in both the acid-base setting and radical polymerization during curing, leading to the formation of a stronger network. With this in mind, photo-rheology and CS values for cements containing native PAAs and the methacrylate-modified analogues were compared.

| Glass ionomer | Ionomer Composition (w. %) | $M_n$ of PAA-*g*-IEM (g mol$^{-1}$) | IEM tethered (w. %) | [CQ]:[TMA]:[DPIC]:[(+)-TA] (w. %) | CS ± σ (MPa) |
|---|---|---|---|---|---|
| **GI-14** | polymer **29** - 40<br>HEMA - 27<br>water – 33<br>Fuji II LC glass - 200 | 7,380 | 25 | 0.25 : 0.3 : 1 : 5 | 89.9 ± 7 |
| **GI-15** | polymer **30**- 40<br>HEMA - 27<br>water – 33<br>Fuji II LC glass - 200 | 12,100 | 25 | 0.25 : 0.3 : 1 : 5 | 96.5 ± 8 |
| **GI-16** | polymer **31** - 40<br>HEMA - 27<br>water – 33<br>Fuji II LC glass - 200 | 22,400 | 25 | 0.25 : 0.3 : 1 : 5 | 110.5 ± 15 |

**Table 3.10: Compositions of glass ionomer cements GI-14 – GI-16, based on PAAs 29-31 modifed with 25 w. % , with MWs from 5,240 – 14,200 g mol$^{-1}$.**

Rheology (Figure 3.32) shows similar results across the three methacrylate-modified systems, with the polymer of lowest MW yielding the cement (**GI-14**) with the lowest viscosity after mixing. In order to judge the effect of the tethered photo-polymerizable groups, these results were overlayed with the results obtained for the native-PAAs with no polymerizable groups

(Figure 3.33). The methacrylate-modifed systems exhibit lower G' immediately after mixing, suggesting that the decrease in the number of acid groups able to participate in the ionic setting reaction in the early stages of curing provides a less elastic material prior to irradiation, despite the increase in MW due to addition of the methacrylate groups. The tethered photo-polymerizable groups appear to provide a sharper cure in the systems containing polymers of 14,200 (**GI-13**, **GI-16**) and 8,710 g $mol^{-1}$ (**GI-12**, **GI-15**), although this effect is not observed for the lower molecular weight cements (**GI-11**, **GI-14**). However, the G' values achieved after irradiation show little dependence on the presence of tethered-methacrylate groups, with the native PAAs showing similar G' values after approximately 18 min of curing.

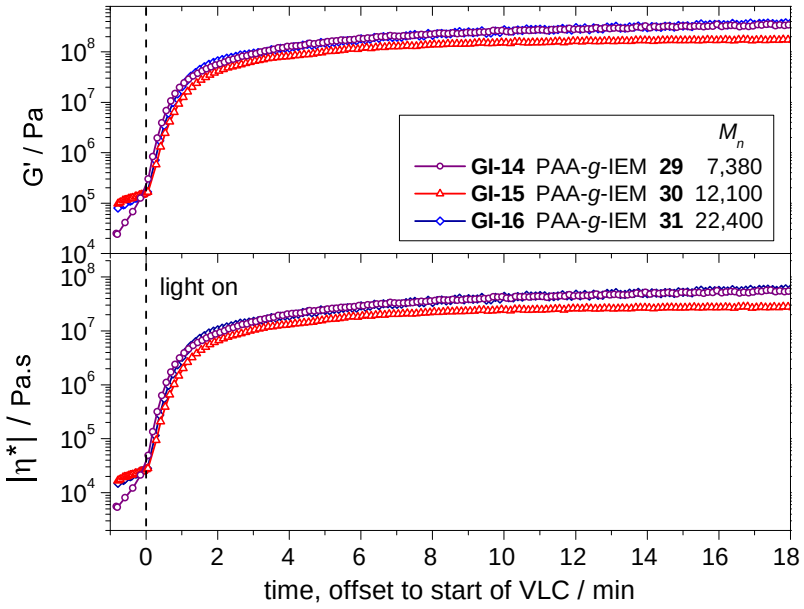


**Figure 3.32: Photo-rheology measurement of the storage modulus (G') and complex viscosity (|η*|) during irradiation of glass ionomers GI-14, GI-15 and GI-16, with varying MW of PAA modified with 25 % methacrylate groups.**

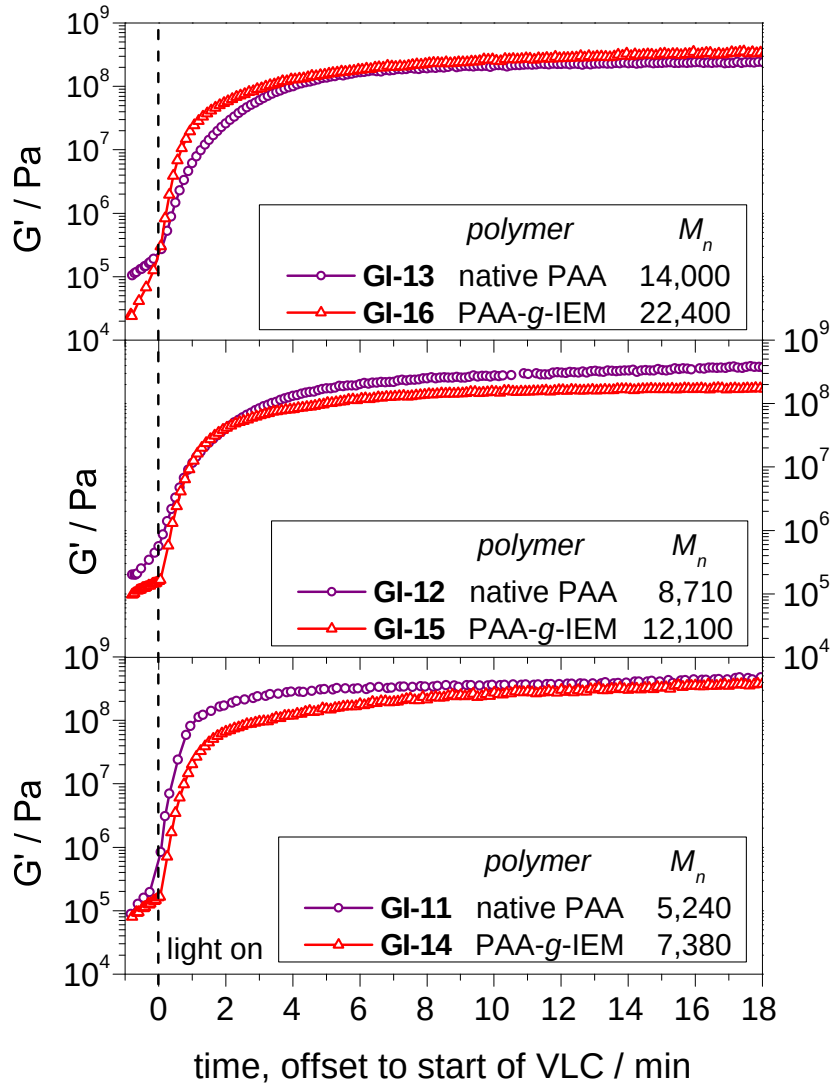


**Figure 3.33: Photo-rheology measurement of the storage modulus (G') during irradiation of glass ionomers GI-11 – GI-16, with varying MW of native PAA and PAA modfied with 25 % methacrylate groups.**

The CS testing of the native and methacrylate-modifed cements reveals a large increase in the strengths of the methacrylate-modifed materials (Figure 3.34 and Figure 3.35). Tethering 25 w. % of methacrylate groups has the effect of increasing the CS by approximately 100 % in all cases, and verifies this prominant strategy for improving the mechanical properties of photo-curable cements. The IEM-modified material containing the polymer of $M_n$ 22,400 g $mol^{-1}$ (**GI-16**) in fact surpases the minimum CS requirement of 100 MPa set out by the American Dental Association and International Standards Organisation for glass-polyalkenoates in restorative applications.[38-39]

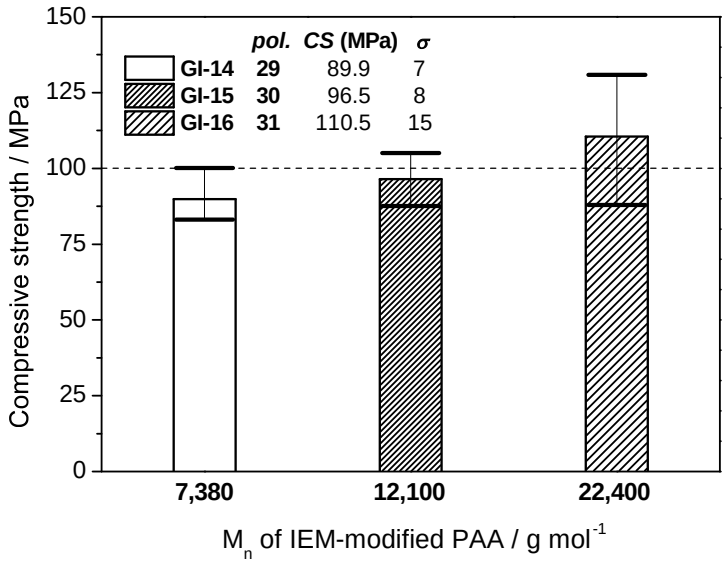


**Figure 3.34: Mean compressive strengths and standard deviations for glass ionomers GI-14 (containing IEM modified PAA 29, with $M_w$ 5,240 g mol$^{-1}$), GI-15 (containing IEM-modifed PAA 30, with $M_w$ 8,710 g mol$^{-1}$) and GI-16 (containing IEM-modified PAA 31, with $M_w$ 14,200 g mol$^{-1}$). The range of values is represented by the whiskers and the 100 MPa CS required by the American Dental Association for restorative applciations is marked by the dashed line.**

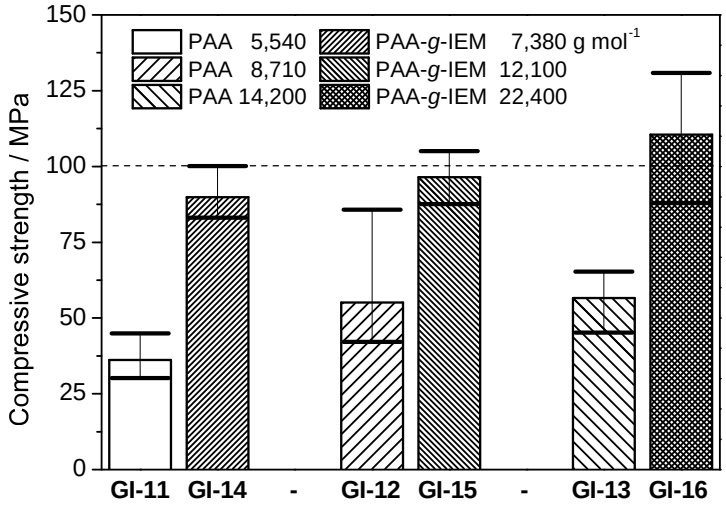


**Figure 3.35: Mean compressive strengths and standard deviations for glass ionomers GI-11 – GI-16, with varying molecular weights of PAA and IEM-modifed PAA in the ionomer solutions. The range of values is represented by the whiskers and the 100 MPa CS required by the American Dental Association for restorative applciations is marked by the dashed line.**

### *3.6.3 Evaluation of branched P(MAA-co-EGDMA)-based cements*

Testing and comparison of linear PMAAs, PAAs and IEM-modified PAAs has shown that the acrylic polymers give the optimal properties when used in GICs, providing a reduced curing time and greater compressive strength in the final material, especially in the case of the methacrylate modified materials. However, it was thought that branching in PMAA-based samples may allow polymers of increased MW to be incorporated without yielding an unworkable cement, potentially increasing the strength of the final cement. Branched PMAA copolymers **19 – 22** were incorporated into ionomer solutions with 40 w. % polymer and mixed with Fuji II LC glass powder in a 1 : 2 liquid to powder ratio and the CS of the final cement after curing measured.

| Glass ionomer | Ionomer Composition (w. %) | $M_w$ of pol. (g $mol^{-1}$) | % EGDMA (w. %) | [CQ]:[TMA]:[DPIC]:[(+)-TA] (w. %) | CS ± σ (MPa) |
|---|---|---|---|---|---|
| **GI-6** | polymer **19** - 40<br>HEMA - 27<br>water - 33<br>glass powder - 200 | 18,400 | 7 | 0.25 : 0.3 : 1 : 5 | 32.7 ± 3 |
| **GI-17** | polymer **20** - 40<br>HEMA - 27<br>water - 33<br>glass powder - 200 | 25,200 | 10 | 0.25 : 0.3 : 1 : 5 | 30.6 ± 2 |
| **GI-18** | polymer **21**- 40<br>HEMA - 27<br>water - 33<br>glass powder - 200 | 7,260 | 10 | 0.25 : 0.3 : 1 : 5 | 30.1 ± 5 |
| **GI-19** | polymer **22**- 40<br>HEMA - 27<br>water - 33<br>glass powder - 200 | 21,100 | 20 | 0.25 : 0.3 : 1 : 5 | 32.4 ± 6 |

**Table 3.11: Compositions and compressive strengths of glass inomer cements GI-17 – GI-1, based on P(MAA-*co*-EGMDA) branched copolymers 19 – 22.**

The CS values measured for the branched systems are relatively similar, showing little dependence on MW or the amount of crosslinking monomer used (which should be related to the number of branch points). While the branched polymers tested provided workable cements in all cases, the increase in mechanical properties compared to the linear PMAAs tested was found to be modest – **GI-10** with a PMAA of 14,200 g $mol^{-1}$ gave a cement with a CS value of 26.5 MPa, while the cement containing a branched P(MAA-*co*-EGDMA) with a $M_w$ 18,400 g $mol^{-1}$ (**GI-6**) increased the mean CS value to 32.7 MPa.

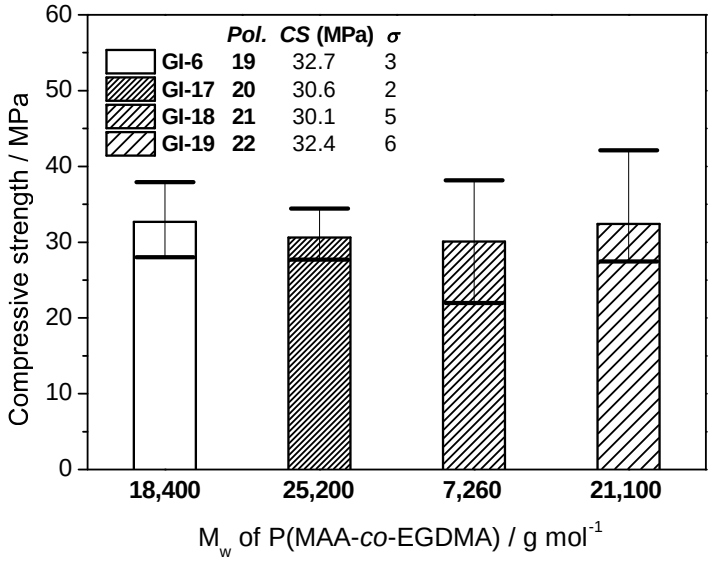


**Figure 3.36: Mean compressive strengths and standard deviations for glass ionomers GI-6 and GI-17 – GI-19, with varying molecular weights of branched P(MAA-*co*-EGDMA) in the ionomer solutions. The range of values is represented by the whiskers.**

It should be noted that the International Standards Organisation's requirements for dental cements (also referenced in the American Dental Association's standard procedures for testing dental materials) requires a minimum CS of 50.0 MPa for glass ionomers used in luting applications and a minimum of 100.0 MPa for glass ionomers used in restoration.[38-39] Clearly, the materials based on branched polyacids synthesized in this thesis fall somewhat short of this requirement. The linear PAAs based cements tested do show CS values in excess of the requirements for luting applications in the case of the polymers of 8,800 and 14,200 g $mol^{-1}$, with the methacrylate-modified PAA-based materials giving compressive strengths close to the 100 MPa required for restorative applications. These results show that the very basic glass ionomer compositions tested do provide cements with mechanical properties close to those required commercially, and suggest that an appropriate model system has been developed.

The relatively high standard deviations and range of results obtained for several CS tests in this thesis suggests that the mixing of cements and sample preparation may not consistently provide uniform materials (although this is analogous to the error associated with dental workers mixing such materials). In order to evaluate the sample preparation and mechanical testing carried out, two commercial dual-cure GICs were tested: Fuji II LC improved (GC), a cement for restorative applications, and RelyX luting cement (3M ESPE). Results for the CS testing are shown in Figure 3.37. The commericial materials show CS values above the 50 and

100 MPa required values for their luting and restorative applications, respectively. The Fuji material shows a higher CS value than any of the systems formulated in this work, but is only around 8 MPa greater than the best IEM-modified PAA tested. The luting cement showed moderate strength but had a very low range of results and standard deviation. This is likely due to the lower powder to liquid ratio of this material allowing facile mixing to a homogeneous state.

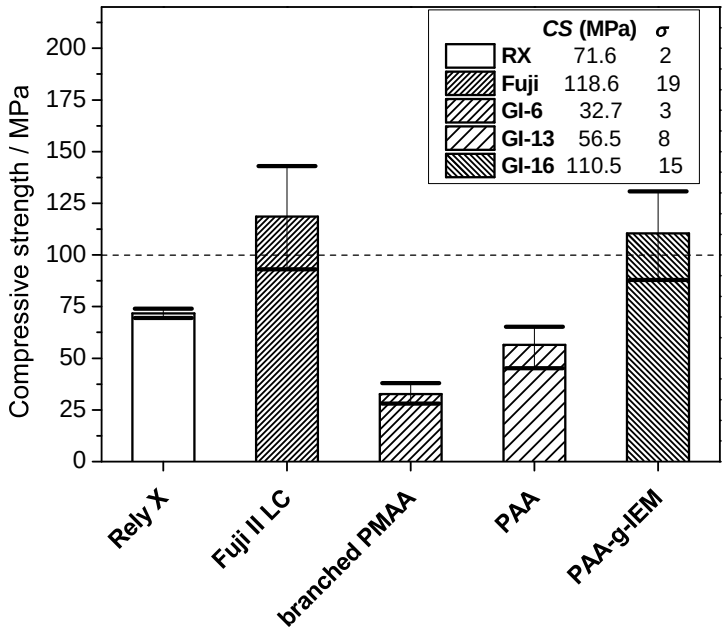


**Figure 3.37: Mean compressive strengths and standard deviations for commerical materials RelyX and Fuji II LC and glass ionomers GI-6, GI-13 and GI-16. The range of values is represented by the whiskers and the 100 MPa CS required by the American Dental Association for restorative applciations is marked by the dashed line.**

The relatively similar mechanical properties of the linear and branched PMAA cements suggest that the CCT-derived vinyl end groups have relatively little effect on the properties of the final cement. It is known that the more sterically hindered alkacrylate vinyl groups will react only very slowly with methacrylic monomers that propagate with tertiary radicals, instead favouring an addition-fragmentation chain transfer mechanism[40-46], and this would be likely to limit the crosslinking possible by the photo-polymerization mechanism, leading to incomplete network formation.

## *3.7 Conclusions*

This work set out to utilize the branched P(MAA-*co*-EGDMA)s synthesized in the previous chapter in photo-curable GICs for dental applications. A three component CQ-based photo-

initiator system was investigated both in solution and in glass ionomer systems mixed with reactive FAS glass. The effect of an important additive, (+)-TA, was also investigated and led to further optimization of the composite material: it was found that the polymer concentration of the ionomer solution should be increased to 40 %, in order to give the optimal setting time and mechanical properties.

This early work allowed the design of a model glass ionomer system which could be used for further investigation into the polymer component of the cements. Linear PMAAs were incorporated into the model glass ionomer system, revealing the expected effect of increasing MW increasing the viscosity of the cement after mixing and increasing the CS of the final material.

PAAs of a range of MWs were synthesized *via* Cu(0)-mediated CRP of *t*-BA, followed by deprotection. These acrylic polymers were found to reduce the curing time and increase the CS of the glass ionomers formulated, relative to the methacrylic systems studied. Furthermore, modification of these with polymerizable methacrylate groups yielded further increases in the mechanical properties of the cements.

Finally, a range of branched P(MAA-*co*-EGDMA)s incorporated into glass ionomer materials and their compressive strengths tested. It was found that these cements provided lower CS values than both the linear PAAs and the methacrylate-modified PAAs, which have previously found use in commercial systems. Unfortunately, the cements based on the branched polyacids did not provide high enough CS values to satisfy ISO requirements for either luting or restorative dental applications.

## *3.8 Outlook*

Although this study revealed that the methacrylic polymer materials detailed in this thesis failed to show sufficient mechanical properties for use in the class of materials studied, several aspects covered would warrant further investigation. It should also be noted that a very simple glass ionomer system was developed and used as a model to test the polymer components. As such, several components of the cement were not investigated or optimized. For example, the co-monomer – which in leading cements is often difunctional, and should give more complete network formation – or the glass powder. Therefore, it is possible that if

the investigation were expanded to optimize these components, a cement of superior mechanical properties would be obtained.

The most likely reason for the decreased mechanical strength of the cements based on both linear and branched methacrylic acid, rather than acrylic acid, is the reduced chain flexibility due to the backbone methyl groups. This may prevent the polyacid efficiently chelating metal cations in the cement, as the polymer is unable to reach the optimal conformation, as well as increasing the rigidity of the sample and increasing likelihood of fracture. It would be desirable to incorporate some acrylic units into the branched PMAA copolymers, in order to increase the chain flexibility and decrease rigidity while retaining the desired effects of branching. However, the CCT copolymerization of MAA with AA has been investigated in the previous chapter, and found to be somewhat problematic, with appreciable incorporations of AA giving side reactions and complex mixtures of linear and non-linear structures. Such graft-like structures may provide interesting properties if applied to GICs, and would certainly merit further investigation as a facile route to branched polymers. Furthermore, utilizing a blend of methacrylic and acrylic polyacids may also have the effect of decreasing the rigidity of the structure, thereby reducing likelihood of fracture and increasing mechanical strength.

CCTP has also been shown to be a simple, cost effective route to polymer structures with higher levels of difunctional monomer than those presented in this thesis.[47-49] Such polymers have been found to possess high levels of methacrylic functionality, with a portion of the vinyl groups derived from crosslinker units in which only one vinyl group has taken part in propagation, as well as the more sterically hindered vinyl polymer chain ends imparted by CCT.[48, 50-51] Such systems may provide polymers that could be incorporated more fully into the photo-polymerized networks studied. However, increased concentrations of commercially available crosslinkers, such as EGDMA or PEGDMA, in the final polymer will lead to a reduction in both the water solubility of the polymer and the number of acid groups available for the ionic setting. Ideally, a crosslinking agent containing an acid or salt group would be used, as a means to increase branching and numbers of reactive polymerizable functionality while maintaining water solubility. This increase in rapidly photo-polymerizable functionality, coupled with a large increase in number of branch-points, would be likely to yield a stronger material than those studied herein.

## 3.9 Experimental

### 3.9.1 Materials

All reagents were purchased from Aldrich and used as received, unless otherwise stated. *N,N,'N,'N*-tetramethyl aniline (TMA) was purchased from Fisher. RelyX (3M ESPE) dental restorative was purchased as a complete kit including powder and liquid from Kent Express Ltd. Dental Supplies. Fuji II LC improved powder (A1 shade) and liquid components were also purchased from Kent Express Ltd. Dental Supplies. 1,1,2,2-tetrafluoropropan-1-ol (TFP) was purchased from Apollo Scientific Ltd. and used as received. Tris[2-(dimethylamino)ethyl]amine ($Me_6$Tren) was synthesized by previously reported methods.

### 3.9.2 Preparation of glass ionomer cements

Glass ionomer cements used in this work consist of a powder and a liquid component. In the case of a commercial product (Fuji II LC or RelyX) the material was prepared according to the manufacturer's instruction. In the case of non-commercial materials (i.e. formulations described in this thesis), a liquid component of the indicated composition was hand-mixed with Fuji II LC glass powder in a 1:2 (liquid to powder, by weight) ratio for approximately 90 seconds using a plastic spatula on a Pyrex glass plate. In the case of very viscous cements that proved difficult to mix efficiently, a drop of distilled water was added to the paste to aid mixing. Where appropriate, the time between the start of mixing and the start of data collection was recorded and used to offset the time of the experiment.

#### *Photo-curing*

Where applicable, GICs were photo-initiated by irradiation with an Omnicure S2000 unit from Lumen Dynamics, equipped with an internal 320-500 nm filter, an external 400-500 nm filter and a liquid light guide. The power output was found to be 380 mW $cm^{-2}$ (the American Dental Association requires a minimum output of 300 W/$cm^2$, although some dental light sources will have reported outputs > 400 W/$cm^2$)[38]. The spectrum the light emitted by this set-up is shown below. This light source was used for online-curing during DSC, rheometry and series mode FTIR experiments.

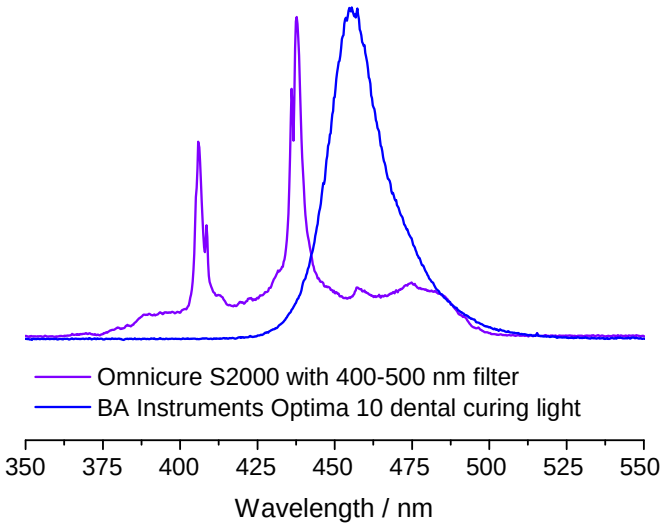


### *Sample preparation for compressive strength testing*

Cylindrical samples with height of 6 mm and diameter of 4 mm were prepared using a stainless steel split mould with internal dimensions of 6 ± 0.1 mm height and 4 ± 0.1 mm diameter. The internal surface of the mould was coated with a thin film of silicon grease and one side of the mould was covered a glass slide, with a sheet of acetate film between the mould and slide. The samples of specified compositions were prepared as described above and used to fill the mould and the mould was covered with an acetate sheet and glass slide. The mould was clamped between the two slides, in order to displace any excess material, and each face of each sample was irradiated for 120 seconds using the Omnicure S200 set-up described above. After irradiation the mould, slides and clamp were immersed in a water bath maintained at 37 ± 1 $^{o}$C. After 1 hour, the clamp, slides and acetate sheets were removed from the mould and the faces of the cylindrical samples ground flat using ANSI/CAMI grit number 600 abrasive paper. At this point the samples were visually inspected, and any samples with obvious defects (such as cracks or air-voids) were discarded. Samples to be tested were stored in distilled water at ambient temperature for at least 24 hours. The diameter of samples was measured with a micrometer accurate to 0.01 mm, taking two measurements at right angles to each other and the mean diameter recorded to an accuracy of 0.01 mm.

### *3.9.3 Instruments*

**Differential Scanning Calorimetry (DSC) with *in situ* irradiation**

DSC experiments were performed isothermally in a Perkin-Elmer DSC-7 equipped with an Intracooler. The instrument was calibrated for temperature and enthalpy using high purity Indium and Zinc standards supplied by Perkin-Elmer. The instrument was modified with a PMMA lid containing holes centred above the sample and reference pan holders, to allow irradiation of both the sample and reference pans using a 2-leg bifurcated liquid light guide attached to the Omnicure S2000 unit described above. The sample holders were covered with 0.05 mm poly(ethylene terephthalate) discs in order to minimise baseline deviation All experiments were performed at 50 $^{o}$C under an atmosphere of $N_2$ at a flow rate of 20 mL min$^{-1}$. Sample mass was approximately 5 mg, in order to obtain a film thickness < 0.5 mm. A baseline measurement was obtained by irradiating the fully cured sample and subtracted from the DSC trace for the photo-curing sample using Microcal Origin software (version 8.5). Data was divided by the sample mass to give heat flux in W g$^{-1}$ and the traces integrated using Origin software to give enthalpy of reaction.

**Fourier Transform Infrared (FTIR) spectroscopy**

FTIR to obtain a single spectrum was carried out on a Bruker Vector-22 using a Golden Gate diamond attenuated total reflection (ATR) cell at a resolution of 4 cm$^{-1}$ for 32 scans and analysed using Opus software.

Series mode measurements were carried out on a Thermo-Nicolet 6700 spectrometer equipped with a Nicolet Smart Orbit single bounce and a Thermo Electron Corp diamond ATR cell. Samples were cast as a 1 mm film on the ATR cell using a silicone-rubber mould and covered with a glass slide to prevent dehydration. The light guide connected to the Omnicure S2000 unit was positioned directly on top of the glass slide. The instrument was programmed using Thermo Omnic software to continuously scan for 30 minutes in series mode, at a resolution of 4 cm$^{-1}$. A spectrum was recorded every 16 scans.

The series data was then split into single spectra using Omnic software and baseline corrected using Opus software. Further processing (such as transposition to obtain plots of absorbance vs. time across many spectra) was performed using Microcal Origin software (version 8.5).

**Rheology**

Rheology experiments were performed on a HAAKE MARS III rheometer equipped with an air cooled temperature control chamber and a glass lower plate, in order to allow irradiation of the sample *in situ* using the Omnicure S2000 unit described above. A stainless steel upper plate of 8 mm diameter was used with a gap between the plates of 0.5 mm. All experiments were performed at 37 $^{o}$C. The instrument was controlled in CS-autostrain mode (RheoWin Job Manager software, Thermo), with an initial strain of 0.5 % displacement and a frequency of 1 Hz. The strain decreased to approximately 0.002 % as the sample reached a high level of curing. Irradiation commenced 1 min after the start of the experiment.

For curing experiments a minimum of three runs for each system were recorded and the experiment best describing the average properties of the material across the runs was used for comparison with other systems. If one or more runs showed substantial deviation from trends observed in the other experiments, the run was repeated.

**Compressive Strength testing[39]**

Compressive strength testing was performed on a Shimadzu Autograph AGS-X universal mechanical tester equipped with a 10 kN load cell and compressive testing geometry consisting of two parallel stainless steel plates of 20 cm diameter. A compressive load was applied at a cross-head speed of 0.75 mm min$^{-1}$ along the long axis of the samples, and the maximum force at failure recorded. Any samples that showed clear signs of defects (such as jumps, local maxima or troughs before the sample reached its maximum force) were discarded.

Compressive strength was calculated using the formula:

$$CS = \frac{p}{\pi r^2}$$

Where p is the maximum force in Newtons, r is the mean diameter of the sample in mm and CS is the compressive strength of the sample in MPa.

A minimum of 6 samples were analysed and the mean compressive strength and standard deviation reported.

**$^{1}$H- and $^{13}$C-NMR spectroscopy**

All NMR spectra were recorded on Bruker DPX-400, DPX-300 and Bruker AC-250 spectrometers as solutions in $D_2O$, $CD_3OD$ or $CDCl_3$ (with TMS), as indicated. Chemical shifts were calibrated using the solvent residual peaks in the case of $D_2O$ and $CD_3OD$, or with TMS for $CDCl_3$.

**Size Exclusion Chromatography/Gel Permeation Chromatography (SEC/GPC)**

All SEC experiments were performed on Agilent 390-LC multi-detector suites equipped with a PL-AS RT/MT autosampler, fitted with a PLgel 5 µm guard column and two PLgel 5 µm Mixed D columns (with an exclusion limit of 2.0 x $10^6$ $gmol^{-1}$). All data was collected and analysed using Agilent GPC software. Mobile phases were DMF and $CHCl_3$ with a flow rate of 1 $mL.min^{-1}$ and an injection volume of 100 µL. The column sets were maintained at ambient temperature and 50 $^{o}$C for $CHCl_3$ and DMF, respectively. Calibrations were created using PMMA EasiVial standards (690-1,944,000 g $mol^{-1}$) purchased from Agilent, with a minimum of 9 points fitted with a third order calibration curve. Points with an error greater than 10 % were not included in the final calibration.

**Gas Chromatography – Flame Ionization detector (GC-FID)**

GC-FID was performed using a Varian 450 fitted with a FactorFour™ capillary column VF-1ms, of 15 m x 0.25 mm I.D. and film thickness 0.25 µm. Oven temperature was programmed as follows: 40 $^{o}$C (hold for 1 min) at 25 $^{o}$C $min^{-1}$ to 200 $^{o}$C. The injector was operated at 200 $^{o}$C with the FID at 220 $^{o}$C. Nitrogen was used as the carrier gas at a flow rate of 1 mL $min^{-1}$ and a split ratio of 1:100 was applied. Data were processed using Galaxie software (version 1.9.302.530). Anisole was used as an internal standard to calculate monomer conversion during polymerization.

### *3.9.4 General procedure for synthesis of methacrylate-modified PAAs*

#### *Synthesis of poly(tert-butyl acrylate)*

A Schlenk tube equipped with a septum was charged with 20 g *tert*-butyl acrylate (*t*-BA, 156.25 mmol), *tert*-butyl α-bromoisobutyrate (*t*-BBiB, 1 eq.), $Me_6$Tren (0.18 eq.), copper(II) bromide ($CuBr_2$, 0.05 eq.), 19.5 mL 2,2,3,3-tetrafluoropropan-1-ol (TFP) and 0.5 mL anisole (for use as an internal standard for GC-FID). The mixture was deoxygenated *via* bubbling with a stream of nitrogen for 20 min. Meanwhile, copper wire (0.4 eq.)was wrapped around a magnetic stirring

bar and stirred in 35 % HCl solution for 15 minutes before being washed with acetone and dried with a stream of compressed air. After 20 minutes of bubbling the reaction mixture the stirring bar was added to the Schlenk tube under a blanket of nitrogen and the vessel maintained at 25 $^{o}$C for 48 hours.

After this time the reaction mixture was exposed to air and diluted with 100 mL of chloroform before being passed through a short basic alumina column in order to remove the catalytic complexes. The solvents were then removed *in vacuo* and the resulting visocous material dried overnight in a vacuum oven at 60 $^{o}$C.

| Reaction | *t*-BBiB | | $CuBr_2$ | | Cu(0) | | $Me_6$Tren | |
|---|---|---|---|---|---|---|---|---|
| | (g) | (mmol) | (mg) | (mmol) | (mg) | (mmol) | (mL) | (mmol) |
| **23** | 0.5 | 2.23 | 25 | 0.112 | 57 | 0.898 | 0.11 | 0.399 |
| **24** | 0.27 | 1.2 | 13 | 0.058 | 31 | 0.488 | 0.06 | 0.217 |
| **25** | 0.17 | 0.78 | 9 | 0.040 | 16 | 0.252 | 0.037 | 0.139 |

## *Deprotection of poly(tert-butyl acrylate)*

A round bottom flask equipped with a water-cooled condenser and a stirring bar was charged with 10 g poly(*tert*-butyl acrylate), 20 mL 1,4-dioxane and 25 mL HCl (35 % solution) and heated at reflux for 24 hours. The solution was then allowed to cool to ambient temperature before being added dropwise to approximately 1 L acetonitrile to induce precipitation. The poly(acrylic acid) was collected *via* vacuum filtration and washed with acetonitrile to remove excess HCl and water. The white solid collected was dried overnight in a vacuum oven at 60 $^{o}$C.

## *Modification of of poly(acrylic acid) with IEM*

A Schlenk tube equipped with a stirring bar and rubber septum was charged with 1 g PAA and degassed with three vacuum/nitrogen-backfill cycles before 4 mL anhydrous DMSO was added *via* degassed syringe. The solution was stirred at 50 $^{o}$C for 30 minutes to aid dissolution of the polymer and allowed to cool to 30 $^{o}$C prior to the addition of 21 µL dibutyltin dilaurate (DBTDL) and the dropwise addition of 0.21 mL 2-isocyanatoethyl methacrylate (IEM, 25 w. % of acrylic acid units) *via* degassed syringe. The reaction mixed was allowed to stirred at 30 $^{o}$C for 20 minutes after formation of $CO_2$ bubbles ceased. The consumption of the –NCO group was

confirmed using FTIR and the solution diluted with water (20 mL) and dialysed against water for a minimum of 24 h. The white solid was collected by freeze drying.

### *3.9.5 Characterization*

**Characterization of 23-25** (**23**: linear P*t*BA with [*t*BA]/[*t*BBiB] 70. **24**: linear P*t*BA with [*t*BA]/[*t*BBiB] 130. **25**: linear P*t*BA with [*t*BA]/[*t*BBiB] 200).

$^1$H-NMR (400 MHz, $CDCl_3$ at 25 $^o$C): δ 1.10-1.75 (backbone $CH_2$), 1.36 (*tert*-butyl $CH_3$), 2.08-2.32 (backbone CH).

FTIR: $\nu_{max}/cm^{-1}$: 2976 (m, CH $sp^3$), 1722 (s, C=O).

Conventional SEC (g $mol^{-1}$): **23**: $M_n$ 8,070, $M_w$ 8,550, Đ 1.06. **24**: $M_n$ 14,800, $M_w$ 16,000, Đ 1.08. **25**: $M_n$ 25,100, $M_w$ 26,100, Đ 1.04.

GC-FID (final conversion, %): **23**: 97.3. **24**: 94.0. **25**: 92.6.

**Characterization of 26-28** (**26**: linear PAA derived from acid hydrolysis of **23**. **27**: linear PAA derived from acid hydrolysis of **24**. **28**: linear PAA derived from acid hydrolysis of **25**)

$^1$H-NMR (400 MHz, $CD_3OD$ at 25 $^o$C): δ 1.38-1.92 (backbone $CH_2$), 2.18-2.46 (backbone CH).

FTIR: $\nu_{max}/cm^{-1}$: 3500-2400 (b, $CO_2H$, various bands), 2988 (m, CH $sp^3$), 1699 (s, C=O).

Conventional SEC (g $mol^{-1}$): **26**: $M_n$ 5,020, $M_w$ 6,680, Đ 1.33. **27**: $M_n$ 8,290, $M_w$ 11,500, Đ 1.39. **28**: $M_n$ 14,100, $M_w$ 19,200, Đ 1.36.

**Characterization of 29-31** (**29**: linear PAA **26** coupled with 25 w. % IEM. **30**: linear PAA **27** coupled with 25 w. % IEM. **31**: linear PAA **28** coupled with 25 w. % IEM)

$^1$H-NMR (400 MHz, $CD_3OD$ at 25 $^o$C): δ 1.40-2.05 (backbone $CH_2$ + methacrylate $CH_3$), 2.25-2.65 (backbone CH), 3.5 (N-C$\underline{H_2}$-$CH_2$O), 4.25 (N$CH_2$-C$\underline{H_2}$-O), 5.66 (*cis* to methyl group C=C$\underline{H_a}H_b$), 6.17 (*trans* to methyl group C=C$H_a\underline{H_b}$).

FTIR: $\nu_{max}/cm^{-1}$: 3500-2400 (b, $CO_2H$, various bands), 2988 (m, CH $sp^3$), 1683 (s, C=O).

Conventional SEC (g $mol^{-1}$): **29**: $M_n$ 7,380, $M_w$ 8,270, Đ 1.12. **30**: $M_n$ 12,100, $M_w$ 14,000, Đ 1.16. **29**: $M_n$ 22,400, $M_w$ 26,700, Đ 1.19.

## *3.10 References*


1. W. D. Cook, F. Chen, *J. Polym. Sci., Part A: Polym. Chem.* **2011**, *49*, 5030.
2. S. K. H. Khalil, E. D. T. Atkins, *J. Mater. Sci. - Mater. M.* **1998**, *9*, 529.
3. P. C. Hiemenz, T. P. Lodge, *Polymer Chemistry*, 2 ed., CRC Press: Taylor & Francis Group, **2007**.
4. R. Hughes, *Practical Rheology* in *Colloid Science: Principles, methods and applications*, 2nd ed. (Ed.: T. Cosgrove), John Wiley & Sons, Chichester, **2010**.
5. C. D. Han, *Rheology and Processing of Polymeric Materials, Vol. 1*, 1st ed., Oxford University Press, Oxford, **2007**.
6. F. A. Rueggeberg, *Dent. Mater.* **2011**, *27*, 39.
7. S. H. Dickens, J. W. Stansbury, K. M. Choi, C. J. E. Floyd, *Macromolecules* **2003**, *36*, 6043.
8. J. M. Antonucci, J. E. McKinney, J. W. Stansbury, US160856A0, **1988**.
9. S. B. Mitra, EP323120A2, **1989**.
10. S. Akahane, S. Tosaki, Y. Kusayanagi, S. Kusakai, K. Hirota, K. Tomioka, DE3941629A1, **1990**.
11. W. D. Cook, *Polymer* **1992**, *33*, 600.
12. A. D. Jenkins, *Polym. Int.* **2000**, *49*, 1729.
13. D. Kim, A. Scranton, *J. Polym. Sci., Part A: Polym. Chem.* **2004**, *42*, 5863.
14. W. D. Cook, S. Chen, F. Chen, M. U. Kahveci, Y. Yagci, *J. Polym. Sci., Part A: Polym. Chem.* **2009**, *47*, 5474.
15. U. Bulut, G. E. Gunbas, L. Toppare, *J. Polym. Sci., Part A: Polym. Chem.* **2010**, *48*, 209.
16. J. V. Crivello, M. Sangermano, *J. Polym. Sci., Part A: Polym. Chem.* **2001**, *39*, 343.
17. S. B. Mitra, S. Mitra, US5154762A, **1992**.
18. D. Xie, J.-G. Park, J. Zhao, *Dent. Mater.* **2007**, *23*, 395.
19. D. Xie, Y. Yang, J. Zhao, J.-G. Park, J.-T. Zhang, *Dent. Mater.* **2007**, *23*, 994.
20. J. Zhao, Y. Weng, D. Xie, *Dent. Mater.* **2009**, *25*, 526.
21. T. Buruiana, M. Nechifor, V. Melinte, V. Podasca, E. C. Buruiana, *J. Biomater. Sci., Polym. Ed.* **2014**, Ahead of Print.
22. A. Wilson, S. Crisp, A. Ferner, *J. Dent. Res.* **1976**, *55*, 489.
23. W. D. Cook, *Biomaterials* **1983**, *4*, 85.
24. J. W. Nicholson, *Biomaterials* **1998**, *19*, 485.
25. S. Crisp, B. G. Lewis, A. D. Wilson, *J. Dent.* **1977**, *5*, 51.

26. A. D. Wilson, *Chem. Soc. Rev.* **1978**, *7*, 265.
27. W. D. Cook, *Biomaterials* **1983**, *4*, 21.
28. A. Moshaverinia, N. Roohpour, W. W. L. Chee, S. R. Schricker, *J. Mater. Chem.* **2012**, *22*, 2824.
29. J. F. McCabe, *Biomaterials* **1998**, *19*, 521.
30. W. D. Cook, P. Brockhurst, *J. Dent. Res.* **1980**, *59*, 795.
31. B. M. Culbertson, *Prog. Polym. Sci.* **2001**, *26*, 577.
32. K. D. Jandt, B. W. Sigusch, *Dent. Mater.* **2009**, *25*, 1001.
33. J. L. Ferracane, *Dent. Mater.* **2011**, *27*, 29.
34. S. R. Samanta, M. E. Levere, V. Percec, *Polym. Chem.* **2013**, *4*, 3212.
35. S. R. Samanta, H.-J. Sun, A. Anastasaki, D. M. Haddleton, V. Percec, *Polym. Chem.* **2014**, *5*, 89.
36. K. A. Davis, K. Matyjaszewski, *Macromolecules* **2000**, *33*, 4039.
37. J. Zhao, D. Xie, *Dent. Mater.* **2011**, *27*, 478.
38. *ADA Professional Product Review. Laboratory Testing Methods: Core Materials, Vol. 3*, **2008**.
39. ISO 4049.2009, *Dentistry - Polymer-based restorative materials.*
40. S. Slavin, K. A. McEwan, D. M. Hadddleton, *Cobalt Catalysed Chain Transfer Polymerization: A Review* in *Polymer Science: A Comprehensive Reference, Vol. 3*, Elsevier, Oxford, **2012**, pp. 249.
41. J. P. A. Heuts, N. M. B. Smeets, *Polym. Chem.* **2011**.
42. J. P. A. Heuts, G. E. Roberts, J. D. Biasutti, *Aust. J. Chem.* **2002**, *55*, 381.
43. A. A. Gridnev, S. D. Ittel, *Chem. Rev.* **2001**, *101*, 3611.
44. J. Krstina, G. Moad, E. Rizzardo, C. L. Winzor, C. T. Berge, M. Fryd, *Macromolecules* **1995**, *28*, 5381.
45. D. M. Haddleton, D. R. Maloney, K. G. Suddaby, *Macromolecules* **1996**, *29*, 481.
46. D. M. Haddleton, C. Topping, J. J. Hastings, K. G. Suddaby, *Macromol. Chem. Phys.* **1996**, *197*, 3027.
47. Z. Guan, *US5767211* **1998**.
48. Z. Guan, *J. Am. Chem. Soc.* **2002**, *124*, 5616.
49. K. A. McEwan, D. M. Haddleton, *Polym. Chem.* **2011**, *2*, 1992.
50. K. A. McEwan, S. Slavin, E. Tunnah, D. M. Haddleton, *Polym. Chem.* **2013**, *4*, 2608.
51. D. J. Krasznai, T. F. L. McKenna, M. F. Cunningham, P. Champagne, N. M. B. Smeets, *Polym. Chem.* **2012**, *3*, 992.